
Inverse modelling of the rainfall-runoff relation

A multi objective model calibration approach



Tom H.M. Rientjes



TR 4224
Bosson
1994

TR 4224

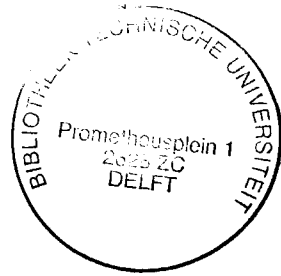
Inverse modelling of the rainfall-runoff relation

**A multi objective model
calibration approach**



Inverse modelling of the rainfall-runoff relation

A multi objective model calibration approach



PROEFSCHRIFT

ter verkrijging van de graad van doctor
aan de Technische Universiteit Delft,
op gezag van de Rector Magnificus prof.dr.ir. J.T. Fokkema,
voorzitter van het College van Promoties,
in het openbaar te verdedigen op maandag 10 mei 2004 om 13.00 uur

door

Thomas Henricus Maria RIENTJES

Hbo ingenieur Cultuurtechniek
Geboren te Hengelo (O)

Dit proefschrift is goedgekeurd door de promotoren:

Prof.dr.ir. P. van der Veer

Prof.dr.ir. H. Savenije

Samenstelling promotiecommissie:

Rector Magnificus,	voorzitter
Prof.dr.ir. P. van der Veer,	Technische Universiteit Delft, promotor
Prof.dr.ir. H. Savenije,	Technische Universiteit Delft, promotor
Prof.dr.ir. G. Stelling,	Technische Universiteit Delft
Prof. ir. E. van Beek,	Technische Universiteit Delft
Prof.dr.ir. M. Stive,	Technische Universiteit Delft
Prof.dr.ir. P. Troch,	Wageningen Universiteit
Dr.ir. C. te Stroet,	Nederlands Instituut voor Toegepaste Geowetenschappen TNO, Utrecht
Dr.ir. J. Boll,	Universiteit van Idaho, Idaho, USA

Published and distributed by: DUP Science

DUP Science is an imprint of
Delft University Press
P.O. Box 98
2600 MG Delft
The Netherlands
Telephone: +31 15 27 85 678
Telefax: + 31 15 27 85 706
E-mail: info@library.tudelft.nl

ISBN 90-407-2491-1

Keywords: physically based, rainfall-runoff modelling; automated calibration,

Copyright © 2004 by T.H.M. Rientjes

All rights reserved. No part of the material protected by this copyright notice may be reproduced or utilized in any form or by any means, electronic or mechanical, including photocopying, recording or by any information storage and retrieval system, without written permission from the publisher:
Delft University Press

Printed in The Netherlands

aan mijn ouders

Voorwoord

Promoveren is een job op zichzelf wordt wel eens gezegd. Nu mijn promotietraject is afgerond kan ik dit bevestigen en kan ik mijn bestaan als Promovendus "oude stijl" definitief vaarwel zeggen. Het schrijven van een proefschrift in deeltijd vraagt veel en misschien wel te veel van een mens. Promoveren laat je nooit los en gedurende het gehele promotietraject ben je bezig tijd te vinden. Als promovendus oude stijl had ik het voorrecht mijn onderzoeksonderwerp vrij te mogen kiezen. Na overleg met Prof.dr.ir. J.C. van Dam heb ik besloten mij te richten op de modellering van de neerslag-afvoer relatie op fysisch gebaseerde grondslag. Een onderwerp waarvoor in Nederland nog nauwelijks belangstelling bestond en waarover weinig expertise aanwezig was. Gedurende de eerste jaren van het promotietraject heb ik weinig vakinhoudelijke steun kunnen genieten van vakgenoten en heb ik al mijn autodidactische talenten aan moeten spreken om mij deze geheel nieuwe vakdiscipline eigen te maken. Gelukkig kreeg het onderwerp in de internationale onderzoekswereld wel steeds meer aandacht waardoor ik geïnspireerd bleef en met interesse aan dit onderwerp kon blijven werken.

Dat ik het proefschrift nu succesvol af kan ronden komt mede door niet nalatende steun van een groot aantal mensen. Zeer veel dank ben ik verschuldigd aan Prof.dr.ir. J.C. van Dam die mij, vlak voor zijn afscheid van de TUD, stimuleerde een proefschrift te gaan schrijven. Hij sprak zijn vertrouwen in mij uit en heeft mij, ook nadat hij met emeritaat is gegaan, nog lange tijd gesteund en met advies bijgestaan. Zijn kritische beschouwingen heb ik met veel waardering en respect ontvangen en zijn voor mijn functioneren nog steeds van grote waarde.

Ongeveer 5 jaar geleden is de rol van promotor overgenomen door Prof.dr.ir. Peter van der Veer, dit nadat wij een aantal persoonlijke gesprekken hadden gevoerd. Daarin werd mij wederom vertrouwen geschonken en hebben wij besloten het vervolgtraject in nauwe wisselwerking af te gaan leggen. Peter, jouw rol als promotor heb ik als zeer plezierig ervaren waarbij jouw positief kritische beschouwingen mijn werk naar een hoger niveau hebben getild. Na onze voortgangsgesprekken vond ik altijd weer nieuwe motivatie en stimulans. Voor het genoten vertrouwen en begeleiding ben ik je zeer veel dank verschuldigd. Verder ben ik je bijzonder erkentelijk voor jouw menselijke inbreng. Diverse keren heb je mij door vertroebeld vaarwater kunnen loodsen en heb je mij altijd onvoorwaardelijk gesteund. Zonder jouw persoonlijke

commitment was het voor mij denk ik niet mogelijk geweest het proefschrift af te ronden.

Een bijzonder woord van dank wil ik richten aan Prof.dr.ir. Majid Hassanizadeh. Majid, hoewel je niet direct inhoudelijk betrokken was bij mijn proefschrift heb ik ook bij jou altijd het gevoel van waardering en respect mogen ontvangen. Op gezamenlijk initiatief hebben wij diverse onderzoeksprojecten op kunnen zetten en uit kunnen voeren die in het verlengde van mijn proefschrift lagen. Op deze wijze heb je voor mij een belangrijker rol vervuld. Kenmerkend voor onze samenwerking is dat je ondanks je zeer drukke agenda toch altijd tijd vrij maakte om even persoonlijk en vakinhoudelijk bij te praten. Hiervoor spreek ik mijn waardering uit.

Prof.dr.ir Huub Savenije wil ik danken voor zijn rol als promotor die ongeveer een jaar geleden gestalte kreeg. De vakinhoudelijke discussies die wij sindsdien hebben gevoerd heb ik als constructief ervaren waarbij ik mijn waardering uitspreek voor de wijze waarop je aan mijn proefschrift hebt bijgedragen.

Andere collega's en oud-collega's die ik, in alfabetische volgorde, wil bedanken zijn Reinder Boekelman, Margreet Evertman, Gu Albert Oude Essink, Paolo Reggiani, Betty Rothfusz, Ruud Schotting, Chris te Stroet, Hans Vermeulen en Willem-Jan Zaadnoordijk. Een ieder van jullie heeft op eigen wijze bijgedragen maar gezamenlijk hebben jullie een belangrijke rol voor mij vervuld. Zonder jullie support was het voor mij ook heel moeilijk geworden het proefschrift op succesvolle wijze af te ronden.

Tot slot wil ik een woord van dank richten aan Jan Boll die mij de data set van de Troy-basin beschikbaar heeft gesteld. Zonder deze set had ik mijn berekening niet uit kunnen voeren. Oud-afstudeerders die op een of andere wijze hebben bijgedragen aan het proefschrift zijn Marcel Boomgaard, Edwin Dado, Guus Fransen, Neeltje Goorden, Robbert Petter, Arjen Pilot en Johan Valstar. De samenwerking met jullie heb ik zeer gewaardeerd en als heel plezierig ervaren.

Mijn allerlaatste en bijzonder woord van dank wil ik richten aan mijn ouders, familie en vrienden. Als een van jullie mij weer eens vroeg of "Promotieonderzoek doen" nu wel of niet leuk was zei ik altijd "Het is maar hoe je het bekijkt; jezelf gedurende langere tijd kunnen verdiepen in een onderwerp waarin je interesse hebt is een voorrecht, het feit dat je vele onvoorziene omstandigheden tegenkomt waar je eigenlijk helemaal niet op zit te wachten is niet leuk". Voordat ik bij de TU ging werken had ik eigenlijk nooit overwogen een proefschrift te gaan schrijven. Nu het werk af is heb ik er

een ambivalent gevoel aan overgehouden. Hoewel op dit moment het gevoel van tevredenheid overheerst zou ik promoveren op dezelfde manier niet over willen doen. Veel tijd is verloren gaan aan inefficiëntie als gevolg van mijn dubbele taakstelling en door werkperikelen als gevolg van het veranderde werkklimaat. Het zijn met name jullie en mijn oud-collega's die mijn gevoelens daarover kennen en daar begrip voor hebben.

Mijn allerlaatste woord van dank richt ik aan Marjolein. Jij hebt me altijd alle steun en ruimte gegeven mijn werk voort te kunnen zetten. Met jouw stimulans en positivisme gaf je me energie en schepte je vertrouwen voor een goede afloop. De tijd die nu vrijgekomen is hoop ik met jou door te brengen want het proefschrift is nu echt helemaal af.



Table of Contents

Table of Contents	xi
List of Symbols	xiv
List of Figures	xxiii
List of Tables	xxx
List of Definitions	xxxi
List of Abbreviations	xxxiv
1 Introduction	1
1.1 The rainfall-runoff relation and society	2
1.2 Background, problem definition and objectives	3
1.3 Outline	5
2 Rainfall-runoff modelling	9
2.1 Introduction	10
2.2 The catchment hydrologic cycle	11
2.3 Deterministic rainfall-runoff model approaches	15
3 Review of distributed physically based rainfall-runoff modelling	21
3.1 Historic perspective	22
3.2 Catchment runoff behaviour	24
3.2.1 Flow processes	24
3.2.2 Mechanisms of runoff generation	26
3.2.3 Runoff source areas	32
3.2.4 Characteristics of flow processes and scale issues	36

3.3 Research efforts in physically based rainfall-runoff simulation	39
3.3.1 Système Hydrologique Européen (SHE)	41
3.3.2 THALES	49
3.3.3 Institute of Hydrology Distributed Model (IHDM)	63
3.3.4 Distributed Basin Simulator (DBSIM)	74
3.4 Conclusions	89
3.4.1. Model concepts	90
3.4.2 Data requirements and model performance	97
3.5 Model parameterisation and model calibration	101
4 Model concept 'Flowsim'	105
4.1 Introduction	106
4.2 Rainfall	109
4.2.1 Spatial rainfall distribution	109
4.2.2 Temporal rainfall distribution	110
4.3 Evaporation	111
4.4 Overland flow	112
4.5 Unsaturated subsurface flow	117
4.6 Saturated subsurface flow	121
4.7 Channel flow	125
5 Model calibration	131
5.1 Introduction	132
5.2 Trial and Error procedure	140
5.3 Automated model calibration by the Generalised Likelihood Uncertainty Estimation (GLUE) procedure	142
5.4 Automated model calibration by evolutionary methods	148
5.5 Automated calibration by Maximum Likelihood Estimation (MLE)	162
5.6 Automated calibration by Artificial Neural Networks (ANN)	174
5.6.1 ANN model concept	175
5.6.2 Real world physics and ANN model concepts	180
5.6.3 Improved Physically Based Modelling by use of ANNs	184
5.7 Conclusions	187

6 Case study Troy catchment	193
6.1 Introduction	194
6.2 Data collected at the Troy catchment	196
6.2.1 Topography	196
6.2.2 Shallow Subsurface	199
6.2.3 Rainfall-Runoff relation	204
6.3 Model calibration	207
7 Summary and Conclusions	223
Appendix A: Mathematical model of Flowsim	239
I Rainfall and evaporation model	240
I.1 Random functions theory	241
I.2 Stationary semi-variogram models	245
I.3 Estimation techniques	246
II Overland flow model	252
III Unsaturated subsurface flow model	267
IV Saturated subsurface flow model	274
V Channel flow model	281
Appendix B: Analyses Troy data set	293
I Groundwater	294
II Rainfall-runoff	305
Appendix C: Initial Soil Moisture Content	311
Appendix D: Analyses of MLE estimation	325
Summary	339
Samenvatting	345
References	353
Curriculum Vitae	371

List of Symbols

Chapter 2

P_s	: precipitation on the land surface	$[L T^{-1}]$
P_w	: precipitation on open water bodies	$[L T^{-1}]$
E_s	: evaporation from the land surface	$[L T^{-1}]$
E_w	: evaporation from open water bodies	$[L T^{-1}]$
E_{uz}	: evaporation from the unsaturated zone	$[L T^{-1}]$
Q_{sf}	: runoff from the land surface	$[L T^{-1}]$
Q_{uz}	: runoff from the unsaturated zone	$[L T^{-1}]$
Q_{sz}	: runoff from the saturated zone	$[L T^{-1}]$
ΔC	: increase of the canopy interception	$[L]$
ΔS_s	: increase of water storage at the land surface zone	$[L]$
ΔS_{uz}	: increase of moisture storage in the unsaturated zone	$[L]$
ΔS_{sz}	: increase of water storage in the saturated zone	$[L]$
I_i	: infiltration at the land surface	$[L T^{-1}]$
I_e	: exfiltration at the land surface	$[L T^{-1}]$
Q_{gin}	: groundwater inflow	$[L T^{-1}]$
Q_{gout}	: groundwater outflow	$[L T^{-1}]$
CR	: capillary rise from the groundwater table	$[L T^{-1}]$
PR	: percolation to the groundwater table	$[L T^{-1}]$
R	: root water uptake	$[L T^{-1}]$
$Q_{(x,t)}$: discharge observation at location x for time instant t	$[L^3 T^{-1}]$
$Q_{(x,t,...)}$: discharge observations at location x	$[L^3 T^{-1}]$
$Q_{(y,t,...)}$: discharge observations at location y	$[L^3 T^{-1}]$
$P_{(m,t,...)}$: precipitation observations at location m	$[L T^{-1}]$
$P_{(n,t,...)}$: precipitation observation at location n	$[L T^{-1}]$
ϵ	: error term	$[-]$

Chapter 3

3.3.1 Système Hydrologique Européen (SHE)

A_{of}	: cross-sectional flow area overland flow	$[L^2]$
C	: specific water capacity	$[L^{-1}]$
h_s	: local water depth at the land surface	$[L]$
h_p	: hydraulic head of phreatic water table	$[L]$

H	: saturated thickness	[L]
i_x	: water surface gradient in the x direction	[-]
i_y	: water surface gradient in the y direction	[-]
$k_{m,x}$: the Strickler roughness coefficients	[L T ⁻¹]
$k_{m,y}$: the Strickler roughness coefficients	[L T ⁻¹]
$k_{(\theta)}$: hydraulic conductivity subject to θ	[L T ⁻¹]
k_x	: saturated hydraulic conductivity in x direction	[L T ⁻¹]
k_y	: saturated hydraulic conductivity in y direction	[L T ⁻¹]
Q_{of}	: overland flow discharge	[L ³ T ⁻¹]
R_{sz}	: recharge of saturated zone	[L T ⁻¹]
S_y	: specific yield	[-]
S_{fx}	: friction slopes in the x direction	[-]
S_{fy}	: friction slopes in the y direction	[-]
S_{ox}	: ground slopes in the x direction	[-]
S_{oy}	: ground slope in the y direction	[-]
S_{sf}	: sink/source term surface layer	[L ² T ⁻¹]
S_{uz}	: sink/source term for unsaturated subsurface	[T ⁻¹]
t	: time	[T]
v_x	: flow velocities in x-direction	[L T ⁻¹]
v_y	: flow velocities in y-direction	[L T ⁻¹]
x	: horizontal space co-ordinate	[L]
y	: horizontal space co-ordinate	[L]
z	: vertical space co-ordinate	[L]
θ	: soil water content	[-]
Ψ	: soil pressure head	[L]

3.3.2 THALES

A_e	: plan area of grid element	[L ²]
A_f	: cross-sectional flow area	[L ²]
A_{ch}	: cross-sectional flow area channel flow	[L ²]
A_{gf}	: cross-sectional flow area groundwater flow	[L ²]
A_{of}	: cross-sectional flow area overland flow	[L ²]
B	: $H_c (\theta_s - \theta_i)$	[L]
D	: thickness of hydrologic active soil profile	[L]
f	: the infiltration rate	[L T ⁻¹]
F	: volume of water infiltrated per area unit	[L]
F_d	: infiltration volume for an unit area at time t_d	[L]

F_m	: mean infiltration volume for a unit area between times t_d and t	[L]
H	: depth of flow above the impermeable layer	[L]
H_c	: effective capillary drive	[L]
i_n	: net rainfall intensity	[L T ⁻¹]
K_s	: saturated hydraulic conductivity	[L T ⁻¹]
$K_{s,r}$: re-saturated hydraulic conductivity	[L T ⁻¹]
K_θ	: hydraulic conductivity subject to soil water content θ	[L T ⁻¹]
$K_{\theta,d}$: hydraulic conductivity at time t_d and subject to θ	[L T ⁻¹]
m	: coefficient	[-]
Q_e	: discharge from grid element	[L ³ T ⁻¹]
Q_f	: flow discharge	[L ³ T ⁻¹]
Q_g	: rapid groundwater flow discharge of a grid element	[L ³ T ⁻¹]
Q_{of}	: overland flow discharge of a grid element	[L ³ T ⁻¹]
R_h	: hydraulic radius	[-]
s	: location along a stream line	[L]
s_e	: flow distance along a streamline in a grid element	[L]
t	: time instant	[T]
t_p	: time to ponding	[T]
α	: coefficient	[-]
β	: local slope of land surface	[-]
γ	: effective porosity	[-]
n	: Manning resistance coefficient	[T L ^{-1/3}]
θ	: soil water content	[-]
θ_i	: initial soil water content	[-]
θ_r	: residual soil water content	[-]
θ_s	: saturated soil water content	[-]
λ	: pore size index	[-]
μ	: $3 + 2/\lambda$	[-]
ν	: coefficient	[-]
ω	: width of grid element orthogonal to the streamline	[L]

3.3.3 Institute of Hydrology Distributed Model (IHDM)

A_{of}	: cross sectional flow area overland flow	[L ²]
b	: a constant	[-]
c_k	: kinematic wave velocity	[L T ⁻¹]
C_h	: Chézy overland flow roughness coefficient	[L ^{1/2} T ⁻¹]
$K_{x(\theta)}$: hydraulic conductivity in x direction subject to θ	[L T ⁻¹]

$K_{z(\theta)}$: hydraulic conductivity in z direction subject to θ	[L T ⁻¹]
l_d	: downslope distance	[L]
q_{lr}	: lateral inflow rate per unit downslope length	[L ² T ⁻¹]
Q_{of}	: overland flow discharge	[L ³ T ⁻¹]
s	: local slope angle	[-]
S_{SS}	: sink/source term subsurface	[L T ⁻¹]
t	: time	[T]
x_d	: horizontal downslope distance	[L]
z_d	: vertical distance from arbitrary stratum	[L]
θ	: soil moisture content	[-]
ϕ	: hydraulic head potential	[L]
ϖ	: variable slope width	[L]

3.3.4 Distributed Basin Simulator (DBSIM)

A_c	: size of catchment area	[L ²]
c_v	: coefficient	[-]
f	: parameter	[L ⁻¹]
$h_{(x,y,t-\tau)}$: instantaneous response function of a grid element	[T ⁻¹]
K_0	: the saturated hydraulic conductivity at the land surface	[L T ⁻¹]
$K_{s(z)}$: saturated hydraulic conductivity at depth z	[L T ⁻¹]
$K_{s(z)}$: the saturated hydraulic conductivity at depth z	[L T ⁻¹]
$K_{(\theta)}$: hydraulic conductivity at water content θ	[L T ⁻¹]
$K_{(\theta,z)}$: hydraulic conductivity water subject to θ at depth z	[L T ⁻¹]
l_h	: length of hill slope flow path	[L]
l_c	: length of channel flow path	[L]
M_t	: total water depth above the wetting front	[L]
$M_{in(R,K_0)}$: infiltration rate subject to R and K_0	[L ⁻¹ T]
$q_z(\theta)$: specific discharge at depth z and subject to θ	[L T ⁻¹]
Q_{base}	: observed base flow	[L ³ T ⁻¹]
Q_{out}	: groundwater discharge out of grid element	[L ³ T ⁻¹]
$Q_{Ac(t)}$: calculated surface runoff of the catchment	[L ³ T ⁻¹]
$Q_{\tau,o}(\tau)$: catchment discharge	[L ³ T ⁻¹]
Q_{ss}	: perched subsurface runoff	[L ³ T ⁻¹]
$Q_{ss,in}$: subsurface inflow of grid element	[L ³ T ⁻¹]
$Q_{ss,out}$: subsurface outflow of grid element	[L ³ T ⁻¹]
r	: calibration parameter	[-]
R	: actual rainfall rate	[L T ⁻¹]
R_i	: catchment recharge rate	[L T ⁻¹]

$R_{v(x,y,t)}$: rate of runoff generation per unit area	[L T ⁻¹]
t	: time instant	[T]
$v_{h(t)}$: average hill slope velocity value	[L T ⁻¹]
W	: width of flow perpendicular to the direction of flow	[L]
z	: depth below surface	[L]
z_f	: depth of infiltration front	[L]
z_{imp}	: depth of impervious base	[L]
z_t	: depth of top of a perched zone	[L]
(α)	: hill slope gradient	[-]
$(\alpha)_d$: lateral deflection angle of infiltration front with respect to the vertical direction	[-]
ξ	: ratio of hill slope and channel flow velocities	[-]
θ	: volumetric soil water content	[-]
θ_s	: saturated water content	[-]
θ_r	: residual water content	[-]
$\theta_{(R,z)}$: vol. soil water rainfall rate subject to R at depth z	[-]
$\theta_{(R_i,z)}$: vol. soil water rainfall rate subject to R_i at depth z	[-]
τ	: time instant	[T]
λ	: pore size distribution index	[-]
ϕ	: hydraulic head	[L]
$\Psi_{(\theta)}$: soil pressure head	[L]

Chapter 4

4.1 Rainfall

$h_{observed}$: observed rainfall depth	[L]
t_b	: begin time rain period	[-]
t_e	: end time rain period	[-]

4.2 Evaporation

$h_{observed}$: observed evaporation depth	[L]
t_b	: begin time evaporation period	[-]
t_e	: end time evaporation period	[-]

4.3 Overland flow

A	: surface area of grid element	[L ²]
A_{of}	: cross sectional flow area	[L ²]
b	: width of flow	[L]

g	: acceleration of gravity	[L T ⁻²]
h	: water depth	[L]
h_{of}	: overland flow water depth	[L]
$i_{sl,x}$: hydraulic gradient x-direction	[-]
k_m	: reciproke of the Manning resistance coefficient	[L ^{1/3} T ⁻¹]
Q	: discharge	[L ³]
$Q_{of,x}$: discharge overland flow in x direction	[L ² T ⁻¹]
$Q_{of,y}$: discharge overland flow in y direction	[L ² T ⁻¹]
$Q_{of,j-1/2,i}$: overland flow discharge at $j-1/2,i$	[L ³ T ⁻¹]
$Q_{of,j+1/2,i}$: overland flow discharge at $j+1/2,i$	[L ³ T ⁻¹]
$Q_{of,j,i-1/2}$: overland flow discharge at $j,i-1/2$	[L ³ T ⁻¹]
$Q_{of,j,i+1/2}$: overland flow discharge at $j,i+1/2$	[L ³ T ⁻¹]
S_f	: friction force slope	[-]
S_o	: bed slope	[-]
S_{of}	: sink/source term overland flow model	[L T ⁻¹]
t	: time	[T]
x,y	: horizontal Cartesian co-ordinates	[L]
Δt	: time increment	[T]

4.4 Unsaturated subsurface flow

$h(\theta)$: pressure head subject to θ	[L]
$k(\theta)$: hydraulic conductivity subject to θ	[L T ⁻¹]
m	: constant	[-]
n	: constant	[-]
$q_{n+1/2}^t$: specific discharge at point $n+1/2$ and time instant t	[L T ⁻¹]
$q_{n-1/2}^t$: specific discharge at point $n-1/2$ and time instant t	[L T ⁻¹]
$q_{sf,z}$: specific discharge unsaturated flow in z direction	[L T ⁻¹]
S_{sf}	: sink/source term subsurface flow model	[T ⁻¹]
t	: time instant	[T]
z	: elevation height	[L]
$z_{n+1/2}$: layer elevation at point $n+1/2$	[L]
$z_{n-1/2}$: layer elevation at point $n-1/2$	[L]
α	: constant	[L]
Δt	: time increment	[T]
η	: porosity	[-]

θ	: soil water content	[-]
θ_r	: residual soil water content	[-]
θ_e	: effective soil water content	[-]
θ_n^{t+1}	: soil water content at point n at time instant t+1	[-]
θ_n^t	: soil water content at point n at time instant t	[-]

4.5 Saturated subsurface flow

C	: hydraulic resistance at channel bottom	[T]
$h_{ch(j,i)}$: hydraulic head in channel flow model at element j,i	[L]
$h_h(j,i)$: hydraulic head of saturated flow model at cell j,i	[L]
$h_{h,wt}$: hydraulic head of groundwater table	[L]
$h_h^{t+1}(j,i)$: hydraulic head at grid element j,i and at time instant t+1	[L]
$h_h^t(j,i)$: hydraulic head at grid element j,i and at time instant t	[L]
h_{sat}	: thickness of saturated layer	[L]
k_s	: saturated hydraulic conductivity	[L T ⁻¹]
l	: distance in direction of flow	[L]
$q_{gf,x,y}^t$: specific discharge groundwater flow in x-y direction	[L ² T ⁻¹]
$q_{gf}^t(j+1/2,i)$: specific discharge groundwater flow at j+1/2,i	[L ² T ⁻¹]
$q_{gf}^t(j-1/2,i)$: specific discharge groundwater flow at j-1/2,i	[L ² T ⁻¹]
$q_{gf}^t(j,i+1/2)$: specific discharge groundwater flow at j,i+1/2	[L ² T ⁻¹]
$q_{gf}^t(j,i-1/2)$: specific discharge groundwater flow at j,i-1/2	[L ² T ⁻¹]
$q_{ch,gws}$: exchange flux channel - saturated subsurface	[L T ⁻¹]
S_{gf}	: sink/source term groundwater flow	[L T ⁻¹]
t	: time instant	[T]
x,y	: Cartesian space co-ordinates	[L]
S	: storage coefficient	[-]

4.6 Channel flow

A_{ch}	: wetted cross sectional area	[L ²]
b	: width of cross sectional flow area	[L]
h	: water depth	[L]
h_{ch}	: thickness of water layer in channel segment	[L]
$h_{ch,j}^{t+1}$: channel flow water depth at grid element j and time t+1	[L]
$h_{ch,j}^t$: channel flow water depth at grid element j and time t	[L]
i	: energy gradient line	[-]

k_m	: reciprocal of Manning resistance coefficient	$[L^{1/3} T^2]$
l	: spatial co-ordinate in flow direction	$[L]$
R	: hydraulic radius	$[L]$
S_{ch}	: sink/source term channel flow model	$[L T^{-1}]$
t	: time	$[T]$
q_{ch}	: specific channel flow discharge	$[L^2 T^{-1}]$
Q_{ch}	: discharge	$[L^3 T^{-1}]$
$q_{j-1/2}$: specific channel flow discharge at $j-1/2$	$[L^2 T^{-1}]$
$q_{j+1/2}$: specific channel flow discharge at $j+1/2$	$[L^2 T^{-1}]$
$Q_{j+1/2}$: Channel flow discharge at element boundary $j+1/2$	$[L^3 T^{-1}]$
Δt	: time increment	$[T]$
ξ	: upwind weighing factor	$[-]$

Chapter 5

5.1 Introduction

Q_c	= calculated channel flow discharge
Q_o	= observed channel flow discharge
$\overline{Q_o}$	= average of observed channel flow discharge
t	= index for time interval
T	= number of time intervals in the selected calibration period

5.3 GLUE- procedure

N	= likelihood shape factor
w	= likelihood weight
$\ell(\Theta_i M)$	= prior likelihood of parameter set i
$\ell(\Theta_i Y,M)$	= posterior likelihood of parameter set i
$\ell(Y \Theta_i,M)$	= likelihood calculated by use of additional time series Y
σ_e	= variance of residuals
σ_o	= variance of observations

5.4 Evolutionary methods

$e(\Theta)_{1..n}$	= residual error over time step $1..n$
$E(\Theta)$	= residual vector of model calculated and observed state variables
f	= function for linear or non linear transformation
$S_c(\Theta)$	= vector of model calculated state information
S_o	= vector of observed state information

- $U^f(\Theta)$ = uncertainty of the parameter space
 $U^o(\Theta)$ = prior uncertainty of parameter space
 Θ = parameter set
 Θ^* = Member of Pareto set
 $P(\Theta)$ = Pareto set
 $\theta_{1,2}$ = parameters

5.5 Maximum likelihood estimation

- e_m = residual error due to incompleteness of the model concept
 e_o = residual error due to inaccurate observations
 e_p = residual error due to parameter uncertainty
 $E[e]$ = expectation of the residual error
 h_{so} = observation of state variable
 h_{so} = observed state variable
 h_{sc} = calculated state variable
 i = iteration index
 m = number of observations
 w_i = weight for measurement number i
 C = covariance observation vector
 C_{cp} = model parameters covariance matrix
 C_{rp} = model parameter correlation matrix
 C_e = covariance matrix of head residuals
 $D(\lambda)$ = characteristic determinant
 h_{sc} = state vector
 h_{so} = observation state vector
 h_{sc} = calculated state vector
 I = unit matrix
 J = Jacobian matrix
 p = column matrix of estimated parameter set
 p_{true} = column matrix of statistical true parameter set
 P = parameter vector
 Z = matrix of eigen-vectors
 $p(h_o|p)$ = conditional probability density function
 ϑ = objective function value
 σ^2 = variance of the residuals
 λ = eigen-values

5.6 Artificial Neural Networks (ANN)

n	=	number of time instants
x_i	=	input from neuron I
Y_j	=	net input to neuron j
Y_o^t	=	observed state variable at time t
Y_c^t	=	calculated state variable at time t.
w_{ji}	=	weight of each input i to neuron j
$w_{i,j}^{t+1}$	=	optimised weight for input signal i at neuron j at time t+1
$w_{j,i}^t$	=	weight at neuron j for input signal i at time t
$\Delta w_{j,i}^{t+1}$	=	weight increment
μ	=	momentum parameter

List of Figures

Figure 2.1: Major processes of the schematised cycle at the catchment scale (modified after Chow et al., 1988).	12
Figure 2.2: Water balance components for specific catchment domains.	14
Figure 3.1: Cross-sectional presentation of hill slope flow processes.	27
Figure 3.2: Soil moisture contents versus depth profiles for a) Infiltration excess mechanism b) Saturation excess mechanism (Dunne, 1978).	30
Figure 3.3: Overland flow generation for a) Infiltration excess mechanism b) Saturation excess mechanism (Dunne, 1978).	30
Figure 3.4: Dynamic behaviour of the saturation overland flow source area during a storm event (Hewlett and Hibbert, 1967).	34
Figure 3.5: Diagram of the occurrence of various overland flow and subsurface storm flow processes in relation to their major controls (Dunne, 1978).	35

- Figure 3.6:** *Catchment responses by of Horton and saturation overland flow and aggregated subsurface storm flow processes in terms of a) lag times and b) specific peak runoff rates (modified after Kirkby, 1985).* 37
- Figure 3.7:** *Schematic of the SHE (Abbott et al, 1986a,b).* 42
- Figure 3.8:** *Hypothetical catchment showing elements shaped by intersections of adjacent streamlines and elevation lines (Brakensiek, 1968).* 50
- Figure 3.9:** *Schematic representation of the flow system being simulated by the saturation overland flow - groundwater flow model (Moore and Grayson, 1991).* 57
- Figure 3.10:** *Comparison of simulated and observed discharge for measured rainfall (Grayson et al., 1992a).* 60
- Figure 3.11:** *Comparison of simulated and observed discharge using $K_s = 1000 \text{ mm h}^{-1}$ (Grayson et al., 1992a).* 61
- Figure 3.12:** *Schematic of the model input zones (Beven et al., 1987).* 64
- Figure 3.13:** *Hill slope partitioning as applied in IHDM (Beven et al., 1987).* 65
- Figure 3.14:** *Cross-sectional presentation of hill slope finite element mesh with applied boundary conditions.* 70
- Figure 3.15:** *Dependency of actual evaporation, E_w on potential evaporation, E_p and capillary soil potential ψ (Feddes et al., 1976).* 71
- Figure 3.16:** *Best fit simulations for the storm event of 19 November 1977 on Tanllwyth catchment (Calver, 1988).* 72
- Figure 3.17:** *Sensitivity of model output to a) initial water potential (ψ_i), b) saturated hydraulic conductivity (K_s), c) porosity (P_o), and d) overland flow roughness coefficients (C_n) (Calver, 1988).* 73
- Figure 3.18:** *Soil water profile in a grid cell (Garrote and Bras, 1995a).* 78

Figure 3.19: Soil water profiles, $\theta_{(R,z)}$, for rainfall rates $R_{1..3} < K$, (Cabral, 1990).	79
Figure 3.20: Sensitivity of basin response to surface flow routing parameters (Garrote and Bras, 1995a).	85
Figure 3.21: Catchment response decomposed for different runoff contributions, antecedent catchment conditions with 0, 50 and 90% probability of exceedance (Garrote and Bras, 1995a).	87
Figure 3.22: Observed and predicted hydrographs for two storm events by considering the effect of the initial state of the catchment (Garrote and Bras, 1995a).	88
Figure 3.23: Data requirements, model performance and model complexity relations (Rientjes and Hassanizadeh, 1999).	100
Figure 4.1: Schematic of runoff model concept.	107
Figure 4.2: Schematic of rainfall model concept.	108
Figure 4.3: Schematic of temporal rainfall distribution.	110
Figure 4.4: Comparison of flow paths as modelled in the 2D overland flow model and real world flow paths.	115
Figure 4.5: Schematic of the finite difference scheme of the overland flow algorithm.	116
Figure 4.6: Schematic of the model concept for the unsaturated zone.	120
Figure 4.7: Schematic of the finite difference scheme for the saturated subsurface.	123
Figure 4.8: Schematic of the model concept to simulate mass exchange between the channel-subsurface flow models.	124
Figure 4.9: Schematic of Strahler ordering scheme.	126
Figure 4.10: Schematic of the channel flow algorithm.	127
Figure 5.1: Model calibration based on parameter estimation.	137

Figure 5.2: <i>Marginal likelihood distribution functions.</i>	145
Figure 5.3: <i>Contour lines of equal likelihood values for two parameter n and k (Werner, 2001).</i>	146
Figure 5.4: <i>Illustration of the evolution steps in each complex (Duan et al., 1994).</i>	152
Figure 5.5: <i>Illustration of the SCE-UA algorithm (Duan et al., 1994).</i>	153
Figure 5.6: <i>Reduction of the prior parameter space to Pareto space (Sorooshian, 1998).</i>	158
Figure 5.7: <i>Illustration of parameter and hydrograph estimates obtained using the multi objective calibration approach.</i>	159
Figure 5.8: <i>Iterative improvement of initial parameter values towards the global objective function minimum for a two parameter (p_1, p_2) estimation problem (Watermark, 1994).</i>	171
Figure 5.9: <i>Diagram of a feed forward ANN.</i>	176
Figure 5.10: <i>Sigmoidal function for re-scaling the net input.</i>	179
Figure 5.11: <i>Diagram of a recurrent ANN.</i>	182
Figure 6.1: <i>Location of the Troy-basin in Idaho, USA.</i>	194
Figure 6.2: <i>DEM of the surveyed area with elevation contour lines added.</i>	196
Figure 6.3: <i>DEM of the Troy catchment, local depressions are removed and elevation contour lines are added.</i>	197
Figure 6.4: <i>Hill slope gradient map.</i>	197
Figure 6.5: <i>Hill slope aspect indicating the flow direction of each element</i>	198
Figure 6.6: <i>Runoff contributing area map indicating the total up-slope area that drains through an element and serves to delineate the channel drainage system.</i>	198
Figure 6.7: <i>Soil depth of the Troy catchment for soil horizons A,B and E and total depth.</i>	200

Figure 6.8: <i>Map of piezometers situated in the catchment area. column and row numbers are added and serve as ID.</i>	201
Figure 6.9 <i>Groundwater table hydrographs of piezometers selected for model calibration.</i>	202
Figure 6.10: <i>Temperature-precipitation relation for the month February/March 1999.</i>	203
Figure 6.11: <i>Temperature graphs for Troy catchment. Ta(max) and Ta(min) are maximum and minimum day temperature respectively Tsoil is soil temperature at specified depths.</i>	204
Figure 6.12: <i>Channel flow hydrograph with precipitation depth and air temperature added.</i>	205
Figure 6.13: <i>Precipitation -runoff-temperature relation for March 1999. Precipitation depths are added for time intervals of 15 minutes.</i>	206
Figure 6.14: <i>Soil water retention curves for the three soil types of the Troy catchment. Curves are based on the Van Genuchten relation (Pilot, 2002).</i>	208
Figure 6.15: <i>Temporal rainfall distribution.</i>	209
Figure 6.16a: <i>Soil moisture distribution Case 1.</i>	210
Figure 6.16b: <i>Soil moisture distribution Case 2.</i>	210
Figure 6.17: <i>Selected piezometers for model calibration are indicated by red.</i>	212
Figure 6.18a: <i>Calculated and observed hydrographs for the non-calibrated cases Case_1 and Case_2.</i>	215
Figure 6.18b: <i>Calculated and observed hydrographs for the cases where channel flow data and channel flow data combined with piezometer data is used for automated calibration.</i>	216
Figure 6.18c: <i>Calculated and observed hydrographs for the cases where piezometer data is used for automated model calibration.</i>	216
Figure 7.1: <i>Data requirements, model performance and model complexity relations (Rientjes and Hassanizadeh, 1999).</i>	229

Figure A.1: <i>Simulation of the catchment shape by a raster grid.</i>	253
Figure A.2: <i>5-Point calculation scheme.</i>	253
Figure A.3: <i>Labelling of grid elements.</i>	263
Figure A.4: <i>Simulating overland flow runoff into the channel.</i>	265
Figure A.5: <i>Schematised representation of the unsaturated flow model.</i>	269
Figure A.6: <i>Schematic representation of the finite difference scheme of the saturated flow algorithm.</i>	277
Figure A.7: <i>Schematic of aggregated grid cells and saturated flow simulation.</i>	279
Figure A.8: <i>Schematic of mass exchange in the saturated subsurface by channel-groundwater system interaction.</i>	280
Figure A.9: <i>Schematic of mass exchange model in the unsaturated subsurface by channel groundwater system interaction.</i>	280
Figure A.10: <i>Geometric representation of channel network layout.</i>	283
Figure A.11: <i>3-Point calculation scheme.</i>	284
Figure A.12: <i>Schematic of perpendicular connected segments.</i>	288
Figure A.13: <i>Schematic of segment connectivity at confluences.</i>	288
Figure A.14: <i>Channel shape and geometry by the Strahler order network approximation.</i>	291
Figure B.1: <i>Piezometer network of the Troy area.</i>	295
Figure B.2: <i>Ground water table hydrographs for each grid column of piezometers.</i>	296
Figure B.3: <i>Selected cross sections of piezometers along the catchment.</i>	297
Figure B.4: <i>Graphs of cross section 1.</i>	299
Figure B5: <i>Graphs of cross section 2.</i>	300

Figure B.6: <i>Graphs of cross section 3.</i>	300
Figure B.7: <i>Graphs of cross section 4.</i>	300
Figure B.8: <i>Graphs of cross section 5.</i>	302
Figure B.9: <i>Graphs of cross section 6a.</i>	302
Figure B.10: <i>Graphs of cross section 6b.</i>	304
Figure B.11: <i>Graphs of cross section 7.</i>	304
Figure B.12: <i>Runoff records Troy catchment for the period January-May 1999.</i>	305
Figure B.13: <i>Temperature-precipitation relation for the month February/March 1999.</i>	305
Figure B.14: <i>Precipitation -runoff-temperature relation for the month of February and March 1999. Precipitation depths are added for time intervals of 15 minutes.</i>	307
Figure B.15: <i>Precipitation -runoff-temperature relation for the two isolated storm periods.</i>	307
Figure C.1: <i>Schematic of the ISMC model approach (Pilot, 2002).</i>	312
Figure C.2: <i>Schematic showing the saturated hydraulic conductivity and the transmissivity as function of the storage deficit (Ambroise et al., 1996).</i>	315
Figure C.3: <i>Schematic of the calculation of $S_{i,VG}$ in a subsurface Column. (Pilot, 2002).</i>	320
Figure C.4a: <i>Soil moisture distribution Case 1.</i>	323
Figure C.4b: <i>Soil moisture distribution Case 2.</i>	323

List of Tables

Table 3.1: <i>Spatial and temporal process scales of the rainfall-runoff processes.</i>	38
Table 3.2: <i>Soil hydraulic conductivity on the Wagga Wagga Catchment.</i>	59
Table 3.3: <i>Review of hydrologic processes simulated (Rientjes, 1999a).</i>	94
Table 3.4: <i>Model concept characteristics (Rientjes, 1999a).</i>	94
Table 3.5: <i>Required model parameters (Rientjes, 1999a).</i>	98
Table 4.1: <i>Sub-models in Flowsim and number of model layers required.</i>	108
Table 5.1: <i>Selection of objective functions used by the National Weather Service for calibrating the SAC-SMA model (modified after Basil et al., 1981).</i>	156
Table 6.1: <i>Soil physical properties of the Troy catchment (Boll, et al., 1998).</i>	199
Table 6.2: <i>Van Genuchten parameter sets for the three soil types of the Troy catchment.</i>	208
Table 6.3: <i>Automated model calibration cases; number and type of state observations selected.</i>	211
Table 6.4a: <i>Case a: Observation data for piezometers 1.4; -1.4; -3.6; 0.9; 4.8.</i>	212
Table 6.4b: <i>Case b: Observation data for piezometers 1.4; -1.6; -2.4; -5.10; 4.9.</i>	212
Table 6.5: <i>Selected channel flow discharges.</i>	213
Table 6.6: <i>Optimised model parameters.</i>	214
Table A.1: <i>Statistical parameters of process stationarity.</i>	243

List of Definitions

- **Calibration:** The fine-tuning of a hydrologic model. Such tuning can be achieved by optimising the model parameter values, modifying the model concept, improving the estimates of meteorological model inputs, modifying boundary conditions.
- **Catchment parameter:** A characteristics of a catchment that that remains constant in time but generally changes over the three dimensional space.
- **Computer code:** A computer code or computer programme is a listing of lines of a computer language that, when compiled by a software compiler, produces a computer programme that enables a modeller to create a hydrologic model.
- **Conceptual rainfall-runoff model:** At the core of the mathematical model a set of equations resides that is based on conservation equations of mass combined with equations that describe the hydrologic model behaviour by an empirical expressions.
- **Distributed model:** Model domains are discretised in space by use of uniform on non-uniform grid elements.
- **Empirical models:** At the core of the mathematical model a set of equations resides that only is able to simulate input-output patterns. Such models often are termed transfer models.
- **Equivalence:** Parameter sets are equivalent in such a manner that parameter sets gives equivalent model output within predefined limits.
- **Hydrology:** Hydrology is the science of the occurrence, the behaviour and the chemical and physical properties of water in all its phases on and under the surface of the earth, with the exception of water in the seas and oceans. [CHO-TNO, 1986].
- **Hydrologic model:** A hydrologic model or simply “model” is a simplified representation of a (part of a complex) hydrologic system by means of a mathematical model, model parameters, state-variables, meteorological stresses and possibly boundary conditions.

- **Hydrologic system:** a structure or volume in space, surrounded by a boundary, that accepts water and other inputs, operates on them internally, and produces them as output, [Ven Te Chow, Maidment & Mays, 1988].
- **Inverse Modelling:** the procedure in which measurements of state variables are used to calibrate a model.
- **Lumped:** the spatial distribution of model input data is averaged over the spatial model domains and expressed by single values.
- **Mathematical model:** A mathematical model is defined as a set of mathematical equations and logical statements that, when combined, allows the simulation of a hydrologic system.
- **Model error:** The cumulated calculation error due to insufficiencies in the model concept, incorrectness of parameter values and the erroneous modelling of meteorological and hydrologic influences.
- **Model concept:** Represents the concept a hydrologic model is based on and relates to the applied discretisation of the model domain, the selected mathematical equations, the allowed interchanges between sub-models, the manner distributions of parameter values are modelled and the manner meteorological stresses and external influences are modelled.
- **Model parameter:** Model input data that represents some catchment characteristic that remains constant in time.
- **Model parameterisation:** Assigning values to model parameters.
- **Non-uniqueness:** Within a parameter set many different combinations of parameter values can be defined that all give satisfactory simulation results. Although parameter values are optimised and uniquely defined, many different but yet optimised parameter values can be defined.
- **Over-parameterisation:** Effects of single parameters on calculated model output cannot be defined exclusively due to dependency relations between parameters.
- **Parameter set:** A set of model parameters for which parameter values are defined.

- **Parameter value:** A value of a parameter.
- **Physically Based Rainfall-Runoff model:** At the core of the mathematical model resides a set of equations that describe the “real world” physics that governs nature. Such a set of equations is based on conservation equations of mass and momentum and, in particular cases, also energy and entropy.
- **Residual error:** The difference between observed and model calculated state variables. The cumulated error due to insufficiencies in the model concept, incorrectness of parameter values and the erroneous modelling of meteorological and hydrologic influences and state observation error.
- **State variable:** A characteristic of a system that is measured and that can assume different values at different times.
- **Trial and Error:** Optimisation of parameter values by a manual procedure.

List of Abbreviations

ANN	: Artificial Neural Network
ABSERR	: Mean Absolute error
ABSMAX	: Maximum Absolute Error
AGNPS	: AGricultural Non-Point Source pollution
ANN	: Artificial Neural Networks
ANSWERS	: Areal Non-Point Source Watershed Environment Response Simulation
BB	: Black Box
BLUE	: Best Linear Unbiased Estimator
CCE	: Competitive Complex Evolution
cdf	: cumulative distribution function
CREAMS	: Chemicals, Runoff, and Erosion from Agricultural Management Systems
CRR	: Conceptual Rainfall-Runoff
DHI	: Danish Hydraulic Institute
DBSIM	: Distributed Basin SIMulator
DEM	: Digital Elevation Model
DRMS	: Daily Root Mean Squared Error
FLAWSIM	: FLOW SIMulation
GIS	: Geographic Information System
GLUE	: Generalised Likelihood Uncertainty Estimation
FFNN	: Feed Forward Neural Network
HMLE	: Heteroscedastic Maximum Likelihood Estimation
IHDM	: Institute of Hydrology Distributed Model
ISMC	: Initial Soil Moisture Content model
KINEROS	: KINematic runoff and EROsion
MLE	: Maximum Likelihood Estimation
MOCOM-UA	: Multi-Objective Complex Evolution-University of Arizona

NN	: Neural Network
RMSE	: Root Mean Square Error
(R ²)	: Nash-Sutcliffe efficiency
PBIAS	: Percent BIAS
PBRR	: Physically Based Rainfall-Runoff
REV	: REgionalized Variable
SCE-UA	: Shuffled Complex Evolution-University of Arizona
SHE	: Système Hydrologique Européen
SMA	: Sacramento soil Moisture Accounting
SLS	: Single Least Squares
THALES	: after THALES of Miletos' a Greek philosopher who revealed the influence of topography on runoff generation
TMVOL	: Total Mean Monthly Volume Squared Error
TOPMODEL	: Topography based hydrologic MODEL
UI	: University of Idaho
WEPP	: Water Erosion Prediction Project

1

Introduction



1.1 The rainfall-runoff relation and society

It is commonly known that the relation between rainfall and runoff plays an important role in many water related societal issues. Generally speaking, one can say these issues relate to a) the operational aspects of (real-time) water management practices such as high and low water forecasting b) the simulation of hydrologic processes and systems for defining design criteria for infra structural works and c) defining effects of land use and climate change on runoff processes. An example of the role of rainfall-runoff processes in operational water management is the optimal use of limited available water volumes for domestic and/or agricultural use. By quantifying the runoff volumes in a channel network system, a strategy can be developed to manage, redistribute and allocate the water spatially and temporally over the various water users. It is obvious that optimal water management becomes even more important under extreme meteorological conditions such as droughts where runoff volumes decrease over time. As a consequence, water availability is reduced and emphasis is laid on developing advanced water management and allocation strategies. Contrary to the drought conditions are the extreme meteorological conditions of rainfall that lead to high water levels in the catchment channel system. An understanding of the rainfall-runoff relation becomes very important when rainfall is expected to cause hazardous flooding conditions. Infra-structural works such as dikes and dams have to be designed, dimensioned and enforced to prevent floodings and thereby societal damage.

The unambiguous understanding of the relation between rainfall and runoff has been a subject of hydrologic research for many decades. Research focussed on various subjects such as an understanding of the meteorological processes, an understanding of the rainfall-runoff transformation process and, in particular, the modelling of this transformation process. Many modelling studies use computer codes which are selected and/or developed to model the transformation process. A computer code often is termed a computer programme and describes and solves a set of equations by means of numerical, analytical and/or statistical methods. By use of a computer code a hydrologic model of the area under study (often a catchment) can be built and the hydrologic behaviour and meteorological conditions of the system under study can be simulated. A hydrologic model here is interpreted as a

simplified representation of a (part of a complex) hydrologic system by means of a mathematical model, model parameters, (state)-variables and a predefined model concept.

A critical note on modelling studies however is that society only benefits from modelling when hydrologic models are reliable. A requirement of a 'good' hydrologic model for example must be that the model is able to simulate and possibly forecast runoff volumes and/or runoff stages as close as possible to the real world observations. Hydrologic models, however, in general have great difficulties in describing the very complex real world behaviour and models have shortcomings related to different aspects of the rainfall-runoff process.

Since their early development, frequently heard criticisms are that models are 'unreliable, uncertain, not trustworthy and that the performance of a model often is not sufficient'. Especially for the past decade, research in the field of rainfall-runoff modelling focussed on improving the modelling results by developing more sophisticated modelling approaches as compared to approaches that are developed in the seventies and eighties. An important research topic herewith deals with the calibration of a hydrologic model that also is the main topic of this thesis.

1.2 Background, problem definition and objectives

In December 1993, January 1995 and December 1998 the Dutch society was confronted with extreme high water levels in the transboundary rivers Meuse and Rhine. The river Meuse flooded 8% of the province of Limburg in December 1993. In January 1995 an even larger area flooded. In January 1995 the river Rhine flooded large areas of the province of Gelderland. Societal damages due to these floodings were enormous. The Ministry of Public Works [1994] reports that only the 1993 flood of the river Meuse caused material damage of Mƒ 254 to the province of Limburg.

During and after the floods many questions were posed in society such as

“where did the abundant amount of water come from”; “what caused the extremeness of the floods”; and “can we expect even higher water levels in the (near) future”.

It is obvious that a better understanding of the hydrologic catchment behaviour of the rivers Meuse and Rhine under conditions of heavy, prolonged rainfall is required. Runoff generation and contributions of various runoff processes therefore have to be quantified as a function of time and space. The size of the catchments of the rivers Meuse and Rhine, 33.000 km² and 185.000 km² respectively makes the modelling of the real world hydrologic behaviour virtually impossible. Large scale catchments of fluvial scale (10⁴ to 10⁷ km²) must be partitioned into smaller subcatchments of maximum regional scale (10² to 10³ km²) to be able to model the real world hydrologic runoff behaviour at, model wise, manageable space and time levels. Catchments of regional scale must be modelled by computer codes that, at the core of the computation algorithm, apply the physical laws of mass and momentum conservation. Such computer codes are termed 'physically-based' and enable the modelling of the real world runoff behaviour.

The first objective of this research is to improve the modelling of the hydrologic catchment behaviour under meteorological conditions that cause the generation of saturation overland flow. Runoff volumes from this process caused major contributions to the floods in 1995 and 1998 and, as such, a better understanding of the runoff production mechanism is required. By this requirement, the natural mechanisms for runoff generation and the various flow- and runoff processes in the catchment first must be identified and understood. A computer code must be applied for the modelling and model calculations must be 'as reliable as possible'. Such a code must be able to simulate the natural runoff generation mechanisms causing the development of extreme runoff volumes and the dominant flow processes underlying these runoff generation mechanisms. As such, the code must be based on physically-based flow equations and requires spatially distributed real world catchment data.

A second objective is to develop and apply a modelling framework for improved model calibration of physically-based rainfall-runoff models. This framework must be footed on the use of a distributed, physically-based rainfall-runoff model that, combined with an inverse modelling approach, must result in improved methodology for catchment parameterisation and consequently runoff modelling. The use of multiple state variables of a different nature, such as piezometer data and channel runoff data, is desired as part of model calibration. As part of the

research, a critical analysis will investigate whether physically-based rainfall-runoff modelling can be improved by implementing a multi-objective model calibration approach.

Other objectives of this study are:

- To present a review of the simulation of the hydrologic catchment behaviour with respect to the rainfall-runoff relation.
- To evaluate and analyse rainfall-runoff modelling approaches that are footed on a distributed model concept and physically-based flow equations.
- To develop a distributed Physically-Based Rainfall-Runoff (PBRR) computer code to simulate the saturation overland flow mechanism. This objective includes pre-processing and post-processing of model input and model output using a raster Geographical Information System (GIS).
- To review the issue of model performance and model reliability particularly when automated model calibration procedures are applied. Procedures will first be reviewed and conclusions will be drawn on usefulness.
- To develop and investigate the performance of a new modelling framework for improved model calibration based on the new PBRR computer code and selected procedure for automated model calibration.

1.3 Outline

The structure of this thesis is as follows. In Chapter 2, a short description of the catchment hydrologic cycle is presented since distributed modelling of rainfall-runoff processes is closely related to quantifying the various components of this cycle. In this chapter a brief description on common model concepts to model the rainfall-runoff relation is presented.

Chapter 3 reviews literature studies on the catchment rainfall-runoff behaviour and on PBRR modelling. To understand the relation between rainfall and runoff, an in-depth review of hydrologic catchment behaviour due to rainfall is presented in section 3.2. In section 3.3 modelling approaches, model concepts and some modelling results of

four distributed PBRR models are reviewed and model performance is evaluated. Analysis with respect to the model concept focuses on aspects like the applied model discretisation, selected mathematical models and how meteorological inputs are modelled. By comparing the approaches and the applied model concepts, it is shown that significant differences exist with respect to a) the applied spatial and temporal model discretisations, b) the number of flow processes simulated, c) how these processes are simulated, d) the applied flow equations and e) how meteorological inputs are simulated. By an evaluation of the simulation results it is shown that PBRR models perform poorly and that PBRR modelling suffers from major set-backs relating to the high data demand to create a model and the parameterisation of a hydrologic model. In section 3.4 summary remarks are presented on the model concept to be developed and the modelling approach to be implemented in order to fulfil the main objective of this study.

Chapter 4 presents the new computer code 'Flowsim'. Five sub-models are defined including rainfall and evaporation, overland flow, unsaturated subsurface flow, saturated subsurface flow and channel flow. The mathematical equations applied to each of these sub-models are presented and flux exchanges between the sub-models are described. In this chapter the applied spatial discretisation and required model input parameters and calculated state variables also are presented.

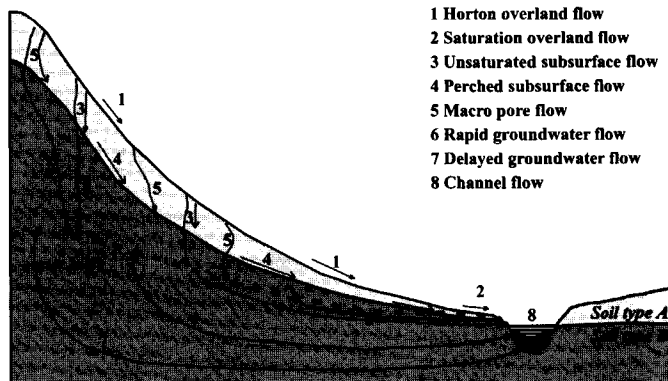
In Chapter 5 model calibration is reviewed and conclusions on suitability of calibration procedures to optimise model parameterisation are drawn. In section 5.1 the Trial and Error calibration procedure is presented. This procedure is a manual calibration procedure and is applied to all modelling studies that are described in section 3.3. In sections 5.2 through 5.5 four automated calibration procedures are described. In section 5.2 a Monte Carlo-based calibration procedure called Generalised Likelihood Uncertainty Estimation procedure is presented. In section 5.3 evolutionary procedures are described for single and multi-objective model calibration, In section 5.4 automated calibration based on Maximum Likelihood Estimation is described. In section 5.5 automated calibration by use of Artificial Neural Networks is presented. A summary on applicability, innovation and implementation of these procedures with respect to the research objectives in section 2.1 is provided in section 5.6.

In Chapter 6 a case study is presented where the modelling of rainfall-runoff processes in a distributed manner by Flowsim is combined with the selected Maximum Likelihood Estimation procedure for automated model calibration. The case study is performed at the Troy catchment located in the state of Idaho in the United States of America.

Conclusions are drawn with respect to usefulness of the modelling approach and the selected calibration procedure to improve PBRR modelling.

In Chapter 7 the research as presented in this thesis is discussed and conclusions are presented. Finally, recommendations for future research in the field of distributed PBRR modelling are presented.

Rainfall-runoff modelling



2.1 Introduction

Rainfall-runoff modellers deal with the question, as Penman formulated it in 1961;

“What happens to the rain”.

Ever since progress has been made in modelling the relation between rainfall and runoff. Rainfall-runoff modelling involves many aspects of hydrology since runoff as gauged in the channel network can be interpreted as the integrated effect of all upstream flow processes and meteorological processes like precipitation, evaporation and transpiration. Precipitation in the form of rainfall will result in the generation of runoff in the channel network due to infiltration water that moves through the unsaturated and saturated subsurface or over the land surface to the channel. Meteorological processes that act in a catchment are precipitation, evaporation and transpiration of vegetation. In section 2.2, the hydrologic cycle at the catchment scale is discussed since rainfall-runoff modelling to a large extent involves the quantification of the various components of this cycle.

The relation between rainfall and runoff can be described by computer codes that, erroneously, often are termed mathematical models. A computer code is a ‘source code’, ‘computer programme’ or ‘a listing of lines of a computer language’ that, when compiled by a software compiler, produces a computer programme that enables a modeller to create a hydrologic model. By such model the hydrologic catchment behaviour can be simulated. A mathematical model is defined as a set of mathematical equations and logical statements that, when combined, allows the simulation of a hydrologic system. The complexity of a mathematical model to a large extent is defined by the selected model concept. This since selections on for example the model discretisations, the number of flow processes to be simulated, the necessary flux exchanges between flow processes primarily are defined in the model concept. In runoff hydrology a large number of mathematical models are developed ranging from very simple models to very complex.

Mathematical models are categorised and classified in deterministic and stochastic ones. In this study it is decided that a deterministic rainfall-runoff model will be used. This class of mathematical models is subdivided in ‘Black Box’ (BB) models, ‘Conceptual Rainfall-Runoff’ (CRR) models and in ‘Physically-based Rainfall-Runoff’ (PBRR)

models. For each subclass, aspects relating to the mathematical model and the model concept are briefly described in section 2.3.

Early scientific interests to describe the rainfall-runoff relation by an a-priori defined model concept date from the fifties. The development of BB and CRR model concepts has been a general research topic ever since. From 1980 hydrologic research redirected due to the development and usage of advanced data capture and data storage facilities and the, relatively, enormous increase in computing and processing capacities. Model approaches also became more advanced and complex and distributed conceptual models were developed. In the late eighties and early nineties complex environmental issues once again redirected the research due to a growing societal interest to simulate real world processes by real world process descriptions. This resulted in increased efforts towards the development and application of physically-based model approaches.

2.2 The catchment hydrologic cycle

The generation of runoff at a catchment due to rainfall deals with several stages of water transport in the hydrologic cycle. Figure 2.1 presents a schematic of the hydrologic cycle at the catchment scale where only the most important meteorological and hydrologic processes are added.

The key process for the generation of runoff from a catchment is precipitation that is spatially and temporally distributed. Subject to the geographical position of the catchment and the time of the year expressed by seasonal effects, precipitation can be in the form of snow, hail, dew, rain and rime. In this study precipitation is considered to be in the form of rain only.

Rainfall reaching the earth surface can be intercepted and stored at the vegetation canopy. In case of continuing rainfall, stem flow and water drip from the canopy is produced and water can be intercepted at the canopy. Interception is known as a loss function to catchment runoff depending on the vegetation type and vegetation density. Interception losses, however, only are of significance when rainfall events are short and when the rainfall depth is small. After rainfall ceases, intercepted water evaporates and the ability of the canopy to store rainfall water increases again. Rainfall reaching the land surface is known as 'throughfall' and often is termed 'effective' rainfall. Rainfall remains at

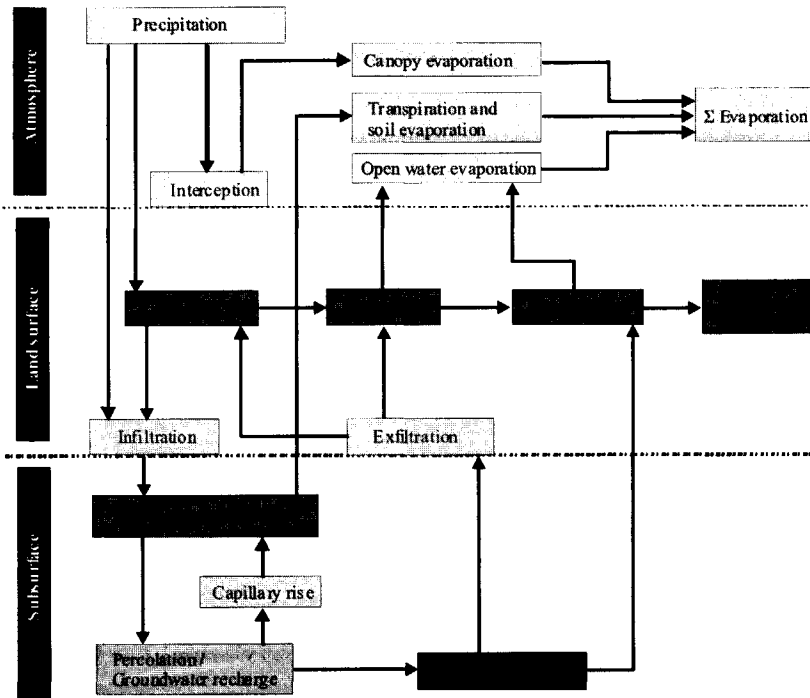


Figure 2.1: Major processes of the schematised cycle at the catchment scale (modified after Chow et al., 1988).

the land surface as depression storage and either evaporates, infiltrates or is discharged as overland flow. Soil water evaporates from the subsurface or, in case of a vegetation cover, transpires from the vegetation due to water uptake by the roots. Both processes contribute to the reduction of water volumes stored in a catchment. By infiltration of rainwater, the soil water content in the unsaturated zone increases. Infiltration water moves primarily in downward direction by unsaturated subsurface flow and recharges the saturated subsurface. This process is termed percolation or natural recharge and fills the aquifers of the groundwater system.

Evaporation and transpiration at the land surface cause the decrease of water storage in the subsurface. As a consequence unsaturated flow in upward direction is generated. This upward flow is termed capillary rise and is subject to the hydraulic pressure gradient across the unsaturated zone. This pressure gradient is highly non-linear and is bounded by the

pressure head at the water table and the pressure head at the land surface. By capillary rise, the volume of water stored in the saturated zone reduces.

Through interactions between the groundwater system and the catchment drainage system, groundwater is discharged through the channel network system. Aquifers of the groundwater system also can discharge groundwater across the catchment boundary. Unsaturated zones, especially at the bottom part of a hill slope, may become saturated during a period of rainfall. Under specific catchment flow conditions, which are described extensively in subsection 3.2, water exfiltration at the land surface could occur. At the land surface overland flow is then generated that is discharged to the channel network system as rill and stream flow. The part of rainfall that is not lost by evaporation, canopy interception and depression storage is called saturation excess rainfall.

The various flow components can be quantified in a water balance. Components may have very different magnitudes and time scales subject to climatic, physiographic and geomorphologic factors and geographic position of the catchment. Examples of climatic factors are precipitation and potential evaporation while the most important physiographic catchment factors are a) geometry factors like size, shape and b) physical factors like soil type distributions and land use (Chow, 1964).

Physiographic channel characteristics are size and shape of the channel cross-section, slope and length of channel segments and channel bed roughness. Geomorphologic factors for the subsurface are for example the granular compositions of soil layers and the number and geometry of the geologic layers. For the land surface the elevation, slopes and the drainage density are characteristic geomorphologic characteristics.

Geographically a catchment is referenced by its longitude, latitude and altitude.

Water balances can be defined for any time domain such as hour, day, week, decade, month, year and any space domain. The space domain can be the catchment scale, sub-catchment scale, a discretised spatial unit or a flow domain. Catchments and sub-catchments are bounded by water divides that are assumed to be in correspondence with topographic divides. This implies that effective rainfall falling within a topographic divide must be discharged as stream flow or as deep groundwater flow or

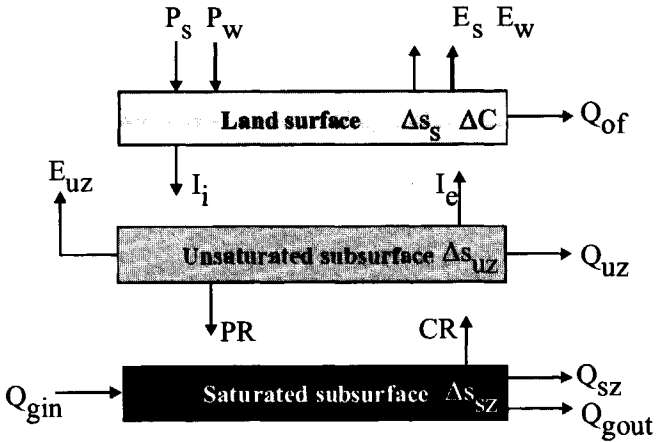


Figure 2.2: Water balance components for specific catchment domains.

it must evaporate. Characteristic domains within a catchment are the land surface, unsaturated subsurface and saturated subsurface.

The water balance components in $[L T^{-1}]$ for any balance period of interest, ΔT , for the specific catchment domains are presented in figure 2.2. For each of the catchment domains, the change of water storage is calculated over the balance period and is expressed in $[L]$.

P_s = precipitation on the land surface

P_w = precipitation on open water bodies

E_s = evaporation from the land surface

E_w = evaporation from open water bodies

E_{uz} = evaporation from the unsaturated zone

Q_{sf} = runoff from the land surface

Q_{uz} = runoff from the unsaturated zone

Q_{sz} = runoff from the saturated zone

ΔC = change of the canopy interception

ΔS_s = change of water storage at the land surface zone

ΔS_{uz} = change of water storage in the unsaturated zone

ΔS_{sz} = change of water storage in the saturated zone

I_i = infiltration at the land surface

I_e = exfiltration at the land surface

Q_{gin} = groundwater inflow

Q_{gout} = groundwater outflow

CR = capillary rise from the groundwater table

PR = percolation to the groundwater table

2.3 Deterministic rainfall-runoff model approaches

Over the past decades many efforts are made to develop techniques to simulate the rainfall-runoff relation. Rainfall-runoff model approaches are developed to describe and to calculate the hydrologic response of a pre-defined geographical area, i.e. a catchment, a hill slope or any region of interest, in terms of a channel flow discharge due to rainfall.

Model input data and model output data of such models are stochastic or deterministic by nature. A model is termed stochastic when model input and output variables are expressed by a probability density distribution. In deterministic modelling data input is uniquely defined, that in combination with pre-defined initial and boundary conditions, gives the model output with an assumed deterministic uniqueness.

Model input data and model output data are lumped or spatially distributed over the model domain. A rainfall-runoff model is termed a lumped model if the spatial distribution of model input data is averaged over the spatial model domains and expressed by single values. In distributed rainfall-runoff models the spatial variations of model input data are simulated by uniform or non-uniform grid elements. These elements are interconnected and make up a model grid layer. By use of multiple overlaying grid layers vertical distributions of input data are simulated. For each of the grid elements model input data is lumped and as such, the term lumped is applicable to spatial units of any size. Such unit can represent an entire catchment, a sub catchment or a grid element of a model grid layer.

Models require model parameter values for the parameterisation of the model equations. In this thesis a model parameter stands for model input data that remains constant in time. Such parameters serve to parameterise the model equations and to represent catchment

characteristics such as elevation, hydraulic conductivity and thickness of a soil layer. A state variable is a characteristic of a system that is measured and that assumes different values at different times such as rainfall intensity, soil moisture content or runoff discharge. In hydrologic modelling the common objective is to simulate hydrologic variables that are of interest to the modeller. Such variables generally are termed 'calculated state variables' since variables represent model-calculated counterparts of observed real world state variables.

As described in section 2.1, the group of deterministic rainfall-runoff model approaches is sub-classified in BB, CRR and PBRR. Differences between the sub-classes predominantly relate to the selected model concept and the mathematical model. The usefulness of the various approaches is subject of ongoing discussion and debate. With regard to the mathematical models, the author identifies the following principle differences. At the core of the mathematical model of a BB model approach a set of equations resides that allows the modelling of input-output patterns based on empiricism only. At the core of mathematical models of a CCR model approach a set of equations resides that is based on a conservation equation of mass combined with equations that describe the hydrologic model behaviour by an empirical expression. At the core of the mathematical model of a PBRR model approach a set of equations resides that describe the real world physics that governs nature. Such set is based on conservation equations of mass, momentum, energy and, in particular cases, also entropy. Since literature about each sub-class of model concepts is widely available, characteristics of the sub-classes are discussed here only briefly.

In **black box** modelling mostly empirical relations are simulated by use of (multiple) regression type equations. By such equations the discharge or the water level for a selected location and time is described as a function of a number of rainfall and runoff observations and/or water levels. Time series of observations may be from one station or from multiple gauging stations.

The general form of such a function is:

$$Q_{x,t} = f(Q_x^{t-1}, Q_x^{t-2}, \dots, Q_y^{t-1}, Q_y^{t-2}, \dots, P_m^{t-1}, P_m^{t-2}, \dots, P_n^{t-1}, P_n^{t-2}, \dots) + \varepsilon_t \quad [1.1]$$

Where:

$$\begin{aligned}
 Q_x^t &= \text{discharge observation at location } x \text{ at time instant } t & [L^3 T^{-1}] \\
 Q_x^{t-1} &= \text{discharge observation at location } x \text{ at time instant } t-1 & [L^3 T^{-1}] \\
 Q_y^{t-1} &= \text{discharge observation at location } y \text{ at time instant } t-1 & [L^3 T^{-1}] \\
 P_m^{t-1} &= \text{precipitation observation at location } m \text{ at time instant } t-1 & [L T^{-1}] \\
 P_n^{t-1} &= \text{precipitation observation at location } n \text{ at time instant } t-1 & [L T^{-1}] \\
 \varepsilon_t &= \text{error term} & [L^3 T^{-1}].
 \end{aligned}$$

In black box modelling, the number of observations and the weight every observation must have in the mathematical model has to be defined.

Weights are defined by regression analysis and are expressed by a regression coefficient (see Rientjes and Boekelman, 2001). Model output in general consist of a summation of the weighted observations:

$$Q_{x,t} = \alpha_1 Q_x^{t-1} + \alpha_2 Q_x^{t-2} + \alpha_3 Q_x^{t-3} + \alpha_4 Q_y^{t-1} + \beta_1 P_m^{t-1} + \beta_2 P_n^{t-1} + \beta_3 P_n^{t-2} + \varepsilon_t \quad [1.2]$$

Black box modelling is based on empiricism and causes that the selected model approach always is catchment dependent and not exchangeable to other catchments. The long term validity of regression models is restricted since values of the time-invariant regression coefficients are based on historical observations. When model performance becomes inconsistent with measured hydrograph data due to for example land use or climate change, models must be re-calibrated and re-validated.

A second group of BB model concepts are Artificial Neural Networks (ANN). Applications of ANNs in general are in the field of recognising certain system input-output patterns such as a rainfall-runoff relation. ANNs often are characterised a function approximator that simulates some uncertain function. The model concept and applications of ANNs in the field of rainfall-runoff modelling are further described in section 5.5.

In **conceptual rainfall-runoff** modelling a pre-defined and designed concept to model processes is adopted where the mathematical model is based on the conservation of mass equation combined with equations that describe the hydrologic model behaviour by means of empirical expressions. Model concepts may be classified as lumped or distributed and describe topographic, physiography and climatic factors in a very

simplified manner. In the approaches, a large number of catchment characteristics is not modelled explicitly but, model wise, are aggregated into model parameters that in general have a weak physical meaning. The use of aggregated model input data make CRR model approaches relatively simple and cause that approaches still are very popular.

Although mass balance equations make part of the mathematical model, model concepts and model input requirements differ and are subject to the chosen empirical expressions. A very well known and one of the oldest examples in CRR modelling is the Unit Hydrograph (UH)-model concept as introduced by Sherman [1932]. Simplifying model assumptions in the UH theory are:

- effective rainfall is spatially and temporally uniformly distributed over the model domain for specified rainfall duration,
- the base time of a runoff Hydrograph is constant for any effective rainfall of unit duration,
- ordinates of the direct-runoff hydrographs have a common base time and are directly proportional to the total volume of direct runoff as defined by the total rainfall excess; this is known as the principle of linearity or proportionality,
- the runoff hydrograph caused by the rainfall depth for a given period, reflects all the aggregated physiographic characteristics of the catchment; the latter is known as the principle of time invariance.

By these model assumptions, the UH-theory only is applicable to event based rainfall-runoff simulation in areas smaller than the sub fluvial scale ($< 10^4 \text{ km}^2$). The applicability of CRR model approaches in general relies on the simplifying assumptions such as described for the UH-theory. Subject to the selected assumptions and model equations, CRR model approaches differ significantly and cause this group to be the largest group. In lumped CRR modelling, very well known examples are Sacramento (Burnash et al., 1973) and Stanford (Crawford and Linsley, 1966) model approaches. In distributed CRR modelling well known examples are the Hydrologiska Byråns Vattenbalansavdelning (HBV) (Bergström and Forsman, 1973) and the Topmodel (Beven and Kirkby, 1979) model approaches. CRR modelling is not described further since this is outside the scope of this thesis.

Physically-based rainfall-runoff modelling approaches apply a distributed model domain and apply a set of equations that are based on conservation equations of mass, momentum, energy and, in specific cases, also entropy. Mathematical models always include physical characteristics and properties of the 'real world' and models require input of initial and boundary conditions since flow processes are described by differential equations. In the computer codes, numerical procedures are applied to solve model algorithms. This causes mathematical models to be more complex compared to mathematical models of BB and CRR approaches. Also computational demands become much higher.

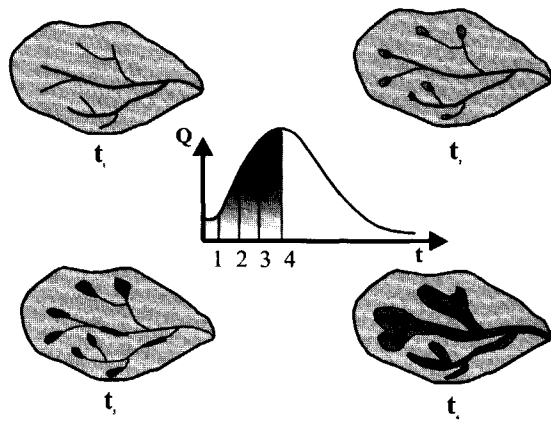
Due to the real world character of physically-based modelling we are able to calculate the hydrologic runoff behaviour in a (sub)catchment, to quantify single flow processes and to calculate state variables for any time instant over the model domain. Models often are termed process models and/or multi-output models since models are able to describe the processes in detail and since multiple state variables can be simulated simultaneously. The detailed simulation of all flow process and components of the hydrologic cycle, however, becomes very demanding for input data. Large amounts of time variant and time in-variant data are required to simulate the flow processes. Despite the mathematical complexity and high data demand this type of modelling came within reach mainly due to the availability of new methods and facilities to collect, store and process data. Although considerable progress has been made in PBRR modelling over the past two decades, developments still are at an experimental stage. In Chapter 3 an extensive review of distributed rainfall runoff modelling is presented.

In describing the relation between rainfall and runoff, the runoff response of a catchment often is expressed by a channel flow hydrograph that is observed at the catchment outlet. By an understanding of the catchment runoff behaviour it is obvious that the shape of the hydrograph is a function of all upstream processes and thus a hydrograph must be interpreted as an integrated response function of all upstream flow processes. Runoff in this respect refers to a (runoff) discharge such as the channel flow discharge, the overland flow discharge or a groundwater flow discharge while a flow process only refers to the actual movement of water within a catchment. In this thesis this differentiation

is adapted so when referring to a flow process this does not necessarily mean that, by the movement of water, catchment runoff is generated.

3

Review of Physically-Based Rainfall-Runoff modelling



3.1 Historic perspective

Since approximately 1960 research is carried out after the development and validation of distributed PBRR models. In this section a brief review on this research is presented that is followed by more detailed reviews on runoff hydrology and PBRR modelling in sections 3.2 and 3.3 respectively.

Research by Betson [1964], Ragan [1968]; Dunne and Black [1970a], among others, had a focus on identifying hill slope and catchment scale hydrologic processes. The main research objective was to gain an understanding of the hydrologic runoff behaviour at the hill slope and catchment scale where runoff was due to rainfall. Research was supported by field evidence (see Betson, 1964; Dunne and Black, 1970a,b; Freeze, 1972a,b) and has significantly contributed to our perception of the catchment runoff behaviour. During the time, an interest was developed for PBRR modelling. Freeze and Harlan [1969] outlined a blueprint for a physically-based digitally hydrologic simulation model and stated:

“the necessary numerical solutions to mathematical boundary problems for groundwater flow, unsaturated porous media flow, overland flow, and channel flow were already available” and “that developments in digital computer technology at the time could provide the impetus for a necessary redirection of research in digital simulation”.

Onstad and Brakensiek [1968], Dunne and Black [1970b] and Freeze, [1971] also reported on design and modelling aspects of distributed model approaches and selected process schematisations. At a later stage the focus was on quantifying effects of spatial and temporal variability of model input parameters and variables on runoff generation (see Freeze, 1980 and Klemeš, 1983). Research in modelling primarily focussed on simulating single flow processes thus ignoring many aspects that are of relevance for the rainfall-runoff transformation process. In this respect Beven [1985] stated:

“the development of distributed modelling has been a slow, faltering process. The modelling of individual processes has been the subject of numerous papers, but relatively few papers have appeared on models interacting processes and on the application of catchment-scale models to real world problems.”

Research on PBRR modelling gained much attention during the late eighties and early nineties when modelling became increasingly more important. Research focussed on the development of integrated model approaches in which the most relevant runoff processes are simulated. Special attention was paid to fundamental modelling aspects such as process schematisations to be applied and model algorithms to be selected (see e.g. Beven, 1989; Grayson et al., 1992a). The design and development of few model concepts and computer codes was reported by Beven et al. [1987], Bathurst et al. [1986a,b], Moore and Grayson [1991], among others. In research it was demonstrated that model performance was low due to high parameter uncertainty and our inability to define most optimal parameter sets. In research the scale issue was identified as the main source of parameter uncertainty. Beven [1989] stated:

“particularly for distributed physically-based models a central issue to deal with is the problem of scale and spatial variability.”

This statement refers to discrepancies that exist between our detailed mathematical descriptions of the real world runoff behaviour and our inability to simulate the runoff behaviour in a consistent manner at relatively large grid scales. Freeze [1972b] already had described this aspect of distributed modelling and stated that scale issues could be a potential cause of poor model performance. Bronstert [1999] addressed the scale issue after reporting poor simulation results by the ‘Hillslope’ model. The scale issue was identified as the main cause of poor model performance. In section 3.2 various aspects of scale issues are discussed in more detail.

For the past decade research had a focus on issues of model calibration and parameterisation (see Beven and Binley, 1992; Refsgaard, 1997, among others). By an understanding of the complexity of PBRR modelling, it also was understood that model calibration results were poor due to, among other aspects, model over-parameterisation, the high demand for model input data and scale issues (see Rientjes and Reggiani, 2001). Nowadays in runoff modelling it is common knowledge that the practical implementation of PBRR models is seriously hampered and the awareness is still growing that building reliable and trustworthy models by far is a trivial task. Distributed PBRR modelling in terms of model concept development and model calibration is still an important subject of academic research

3.2 Catchment runoff behaviour

3.2.1 Flow processes

Chow [1964] distinguishes surface runoff, subsurface runoff and groundwater runoff as three dominant runoff contributing components. Chow defines these runoff components as follows.

- Surface runoff is *“that part of the runoff which travels over the ground surface and through channels to reach the basin outlet”*.
- Subsurface runoff is *“that part of precipitation which infiltrates the surface soil and moves laterally through the upper soil horizons towards streams as ephemeral, shallow, perched groundwater above the main groundwater level”*.
- Groundwater runoff is *“that part of the runoff due to deep percolation of the infiltrated water which has passed into the ground, has become groundwater, and has been discharged into the stream”*.

Flow processes that are of importance in these runoff components are described as follows.

- Surface runoff: Flow processes are **overland flow**, **stream flow** and **channel flow**. **Overland flow** is defined as the water flow over the land surface following the contours of the highest downslope gradient and is subject to the hydraulic characteristics of the land surface. Flow is as a thin water layer over the land surface (i.e. ‘sheet flow’) or as converged flow into small rills (i.e. ‘rill flow’). Overland flow is known as **Horton overland flow** or **saturation overland flow**. In sub-section 3.2.2 mechanism by which these processes are generated are discussed in detail. Overland flow is observed as sheet flow, rill flow or stream flow. At hill slopes rill flow is initiated by sheet flow that generally only is observed at very small spatial scales. Travel distances of sheet flow are very small and hardly observable since small rills are easily shaped by the presence of small topographic irregularities at the land surface. After convergence of multiple rill flow pathways small streams develop. **Stream flow** is defined as water flow in small streams due to the convergence of rill flow discharges. At a hill slope the lengths of travel paths of rill flow discharges are short as compared to the length of the flow path of stream flow discharges.

Stream flow gradually converges into **channel flow** and is defined as the flow of water in the catchment channel system.

- Subsurface runoff: Flow processes are **unsaturated subsurface flow**, **perched subsurface flow** and **macro pore flow**. Based on research by Pilgrim et al, [1979], the definition of Chow of subsurface runoff is modified in such manner that macro pore flow also contributes to subsurface runoff. Subsurface runoff is generated by infiltrated water moving through the upper soil layers towards the streams and channels where subsurface runoff is in Darcian and Non-Darcian flow conditions. In Darcian flow conditions the subsurface forms a continuum of the anisotropic and heterogeneous soil matrix while in Non-Darcian flow conditions the soil matrix is discontinuous due to the presence of voids, natural pipes and cracks in the soil.

Unsaturated subsurface flow is observed in Darcian flow conditions where flow is governed by hydraulic pressure gradients. The dominant flow direction of unsaturated subsurface flow is the vertical direction since variations of the soil moisture contents in vertical direction are much larger than in horizontal direction and since water moves in the direction of decreasing energy status. Runoff contributions due to unsaturated flow are very small and generally of no significance for the total catchment runoff. **Perched subsurface flow** is observed in perched (saturated) subsurface conditions where water moves in lateral flow direction and where the movement of water is subject to lateral hydraulic head gradients. For the generation of perched subsurface flow, the hydraulic conductivity of a given soil layer must significantly be lower than the hydraulic conductivity of the overlying soil layer. By the lower hydraulic conductivity, infiltration of water in the less permeable layer is obstructed and infiltrated water is drained laterally. Perched subsurface flow can have significantly contributions to runoff generation and is often observed in catchments where the upper soil layers are characterised by relatively high hydraulic permeabilities. In many catchments upper layers are less compacted and also are more permeable by the presence of roots. When upper layers are densely rooted, the soil matrix of upper soil layers often is discontinuous by the presence of macro pores. Macro pores such as voids, natural pipes, cracks and fractures are caused by drought, by animal life, by rooting of vegetation or by physical and chemical geological processes. **Macro pore flow** is characterised as a Non-

Darcian subsurface flow process in voids, natural pipes and cracks in the soil structure. Water flow is not governed by hydraulic pressure gradients but occurs at atmospheric pressure. Runoff contributions by macro pore flow may be significant in mountainous, densely vegetated and fractured rock areas. Macro pore flow that is not directly discharged as subsurface runoff recharges the unsaturated or saturated zone of the groundwater system.

- Groundwater runoff: Such runoff is generated by percolation of infiltrated water that causes the filling of the groundwater system and consequently a rise of the water table. Groundwater is discharged as **rapid groundwater flow** in the upper part of the initially unsaturated subsurface domain or as **delayed groundwater flow** in the lower part of the saturated subsurface that, prior to the rainfall, already is saturated. Some hydrologists consider rapid groundwater flow as 'groundwater flow on top of the groundwater system' while delayed groundwater flow is considered as 'the flow through the deeper aquifers'.

In figure 3.1 a cross section of a hill slope is presented and a simplified representation of the flow processes is added. Each of the processes has a characteristic time and space scale and, when observed in a catchment, make up the catchment runoff behaviour.

3.2.2 Mechanisms of runoff generation

Since the 1960's theories on runoff generation are developed as based on field research. Catchment runoff behaviour at the real world scale is a function of physiographic, geologic and meteorological catchment conditions and is (very) complex and highly dynamic. In the following the mechanisms that cause the generation of runoff and the most important runoff processes that cause the (rapid) development of a peak runoff discharge are described. Flow processes described are Horton overland flow, saturation overland flow and the aggregated subsurface storm flow processes of perched subsurface flow, macro pore flow and rapid groundwater flow. Runoff generating mechanisms are the infiltration excess, saturation excess and subsurface storm flow mechanisms.

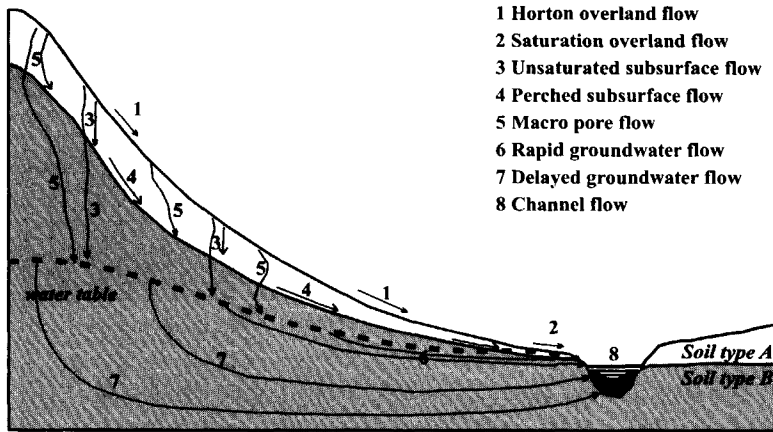


Figure 3.1: Cross-sectional presentation of hill slope flow processes.

Infiltration excess mechanism

The mechanism that controls the amount of water available for overland flow is infiltration. Horton in 1933 identified the role of infiltration in the hydrologic cycle and in runoff generation in particular. Horton described the relation between rainfall intensity and the capacity of the soil to absorb water. Rubin and Steinhardt [1963] described the Horton infiltration theory in a more scientific framework. Conceptual infiltration models are developed by Philip [1957]; Holtan [1961]; Morel-Seytoux, [1976], Smith and Parlange [1978], among others.

Amerman and McGuinness [1967] stated:

“in the simplest form, the infiltration theory of runoff predicts that prolonged rain falling on the slopes of a drainage basin having a uniform initial infiltration capacity will, if its intensity is greater than the lower limiting infiltration capacity, ultimately produce overland flow (Hortonian) more or less simultaneously over all the basin after an initial abstraction due to surface storage.”

Freeze [1980] described the conditions for the generation of overland flow by the Horton infiltration theory:

“the rainfall rate must exceed the saturated hydraulic conductivity of the top soil and the rainfall duration must be longer than the required ponding time of the land surface.”

This so called '*Horton overland flow*' (Dunne, 1978; Freeze, 1980; Kirkby, 1988), is common in areas where rainfall intensities are high and where soil hydraulic conductivities are low while the hydraulic resistance to overland flow is small. In literature the terms '*concentrated overland flow*' and '*infiltration excess overland flow*' are also applied. In this thesis the term '*Horton overland flow*' is used. According to Dunne [1978], [1983] and Bras [1990], Horton overland flow is common in arid climatic zones when rainfall events are heavy and when mountainous hill slopes are bare or covered by thin vegetation.

For a long period of time, Horton overland flow was identified as the only overland flow process that caused the rapid rise of a channel flow discharge although extensive field evidence was not present that large Horton overland flow runoff volumes had caused high channel flow discharges. The mechanism by which Horton overland flow is generated is termed '*infiltration excess mechanism*' and is simulated in most PBRR model approaches (see Freeze, 1971; 1980; Correia and Matias, 1991; Abbott et al., 1986a,b; Cabral et al., 1990; Grayson and Moore, 1988).

Saturation excess mechanism

A different overland flow process identified by Ragan [1968] and Dunne and Black [1970a] and described by Dunne [1978] and [1983] is termed '*saturation overland flow*' or, as some researchers prefer '*saturation excess overland flow*'. In this thesis the first term is used. Saturation overland flow is generated as the soil becomes saturated due to the rise of the water table to the land surface or due to the lateral and vertical percolation of infiltration water above an impeding horizon (Dunne and Black, 1970a,b; Bonell and Gilmour, 1978; Dunne, 1983). Under the latter conditions perched subsurface flow conditions prevail. Also for the latter case the rise of the water table controls the soil saturation and thus runoff generation by saturation overland flow. This phenomenon is commonly referred to as the '*saturation excess mechanism*' or '*saturation overland flow mechanism*'. Some researchers (e.g. Bras, 1990 and O'Connell, 1991) characterise the saturation process by stating that '*saturation from below rather than from above*' causes the runoff generation. Saturation overland flow is due to water that exfiltrates the subsurface and due to rainfall falling on these fully saturated, exfiltration zones. Saturation overland flow often is identified as an important runoff process in densely vegetated land surfaces in mountainous areas where

hillsides are concave in combination with shallow water tables and thin top soil layers (Dunne, 1978).

A major difference between both mechanisms is that by infiltration excess the subsoil becomes saturated by infiltrated water from the land surface while by saturation excess the subsoil becomes saturated due to a (rapid) rise of the perennial or perched water table. Soil moisture distributions in the subsurface for both runoff mechanisms are different as they evolve over time during a rainfall event. Although shortly after the onset of a rainfall event similar infiltration fronts develop over time, this front will change after a certain period. In case of infiltration excess the soil becomes saturated by infiltration water and cause the wetting front to move in downward direction while in case of saturation excess a saturation front develops due to a water table rise. Such saturation front is caused by lateral subsurface flow contributions of perched subsurface or groundwater flow. The phenomenon of soil saturation mostly is encountered at the bottom of a hill slope and cause that saturation overland flow is generated near the channels.

The saturation of the subsurface for both infiltration and saturation excess mechanisms is illustrated in figure 3.2 where soil moisture distributions during a rainfall event are presented. Figure 3.3 is after Dunne [1978] and shows schematics of overland flow generation for both mechanisms. Horton overland flow is generated at the ponding time at instant t_3 (fig. 3.3a), while saturation overland flow is generated when the water table rises to the land surface at time instant t_5 (fig. 3.3b).

For the infiltration excess mechanism, runoff is generated due to (very) high rainfall intensities that often only are of short duration. Based on the saturation excess mechanism, runoff is generated by long duration rainfall events that often are of low intensity. Particularly when the subsurface is shallow saturation overland flow is easily generated by the small subsurface storage capacity.

Field evidence learns that variations in runoff contributions are due to the changing size of the areas from which the runoff is generated. These areas are termed the '*runoff contributing areas*' or '*runoff source areas*' (Betson, 1964; Dunne and Black, 1970a; Dunne, 1978). The expansion and contraction of the overland flow source areas is a highly dynamic and non-linear phenomenon (Kirkby, 1988; O'Connell, 1991) that is a

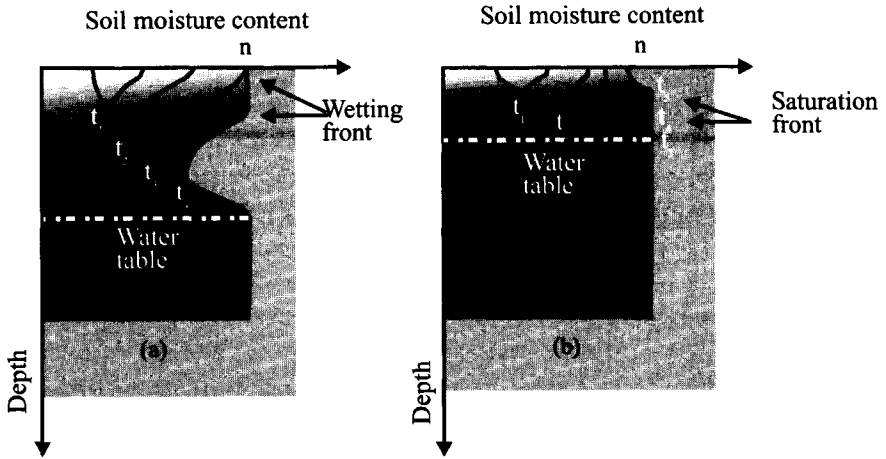


Figure 3.2: Soil moisture contents versus depth profiles for a) Infiltration excess mechanism b) Saturation excess mechanism (Dunne, 1978).

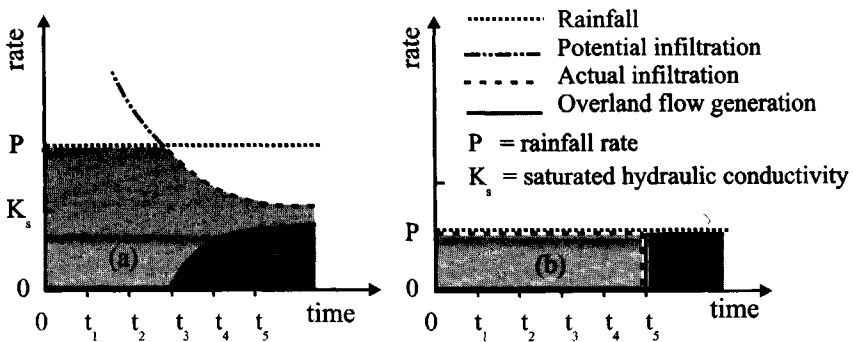


Figure 3.3: Overland flow generation for a) Infiltration excess mechanism b) Saturation excess mechanism (Dunne, 1978).

function of the spatial distribution of rainfall, rainfall intensity and (sub) surface flow conditions. In sub-section 3.2.3 this is further described.

Subsurface storm flow mechanism

Subsurface storm flow processes are perched subsurface flow, macro pore flow and rapid and delayed groundwater flow. The complexity of the runoff mechanism that governs the runoff generation by these processes was not fully understood by the early researchers who developed the theories of the overland flow runoff mechanisms. Nowadays subsurface storm flow is regarded as an aggregated flow process with flow

contributions from various processes that, in general, cannot be observed separately due to strong process interactions.

An example herewith is the differentiation between rapid and delayed groundwater flow. Such differentiation in fact is rather artificial and arbitrary since both processes are continuous processes in space and time. Both processes often are governed by the same hydraulic gradients in the soil matrix and groundwater runoff by 'rapid' and 'delayed' groundwater flow is generated simultaneously by the displacement of water in the shallow and more deeper groundwater system. Groundwater discharges also change along a hillslope since hydraulic heads change along a hill slope and since hillslope depths generally are smaller at lower parts. Also at lower parts the water table generally is much closer to the land surface compared to the upper part. Hence, at the lower part the time delay of infiltrated water to percolate to the groundwater system will be short and cause the quick generation of groundwater runoff. Based on this reasoning, at the upper part of the hill slope runoff response times are much larger. The terms 'rapid' and 'delayed' actually much more reflect a time and space integrated response function of infiltrated water to become catchment runoff.

Subsurface storm flow also is generated by perched subsurface flow that is generated when the infiltration of water in a soil layer is obstructed by its low infiltration capacity. Burt [1986] states,

“as the ratio between the hydraulic conductivity of the upper and lower layers increases, more perched subsurface storm flow is generated and the flow direction becomes more nearly parallel to the slope”.

In the same article it also is describes that the rainfall intensity greatly must exceed the hydraulic conductivity of the obstructing layer. Perched subsurface flow basically is a groundwater flow process with similar flow characteristics and also is governed by Darcian flow conditions. In case the ratio of the hydraulic conductivity of two layers becomes smaller or when obstructing layers are discontinuous in space, perched subsurface flow does not contribute significantly to catchment runoff. Under such conditions some infiltration water maybe discharge as perched subsurface flow while also the water table may be recharged. Runoff contributions from perched subsurface flow and groundwater flow then cumulate in the channel where runoff volumes are uncertain. The groundwater water table as well as a perched water table also can be recharged by macro pore

flow. Macro pore flow easily bypasses the entire unsaturated soil profile by the presence of cracks, voids and pipes and so can cause that the groundwater system becomes recharged shortly after the onset of a rainfall event. By the same mechanism macro pore flow also contributes significantly to the generation of perched subsurface flow. Up till the work of Mosley [1979], Pilgrim et al. [1979] and Beven and Germann [1981, 1982], the significance of macro pore flow on catchment runoff generation was often underestimated, ignored or even not understood. Germann [1990] describes the field conditions for generation of macro pore flow:

“macro pore flow will be generated when the infiltration rate into a top soil matrix is less than the water input to the entire soil surface”.

Macro pore flow is generated in any predefined area with discontinuous macro porous top soils in case the rainfall rate exceeds the infiltration rate of the soil matrix that intersects the land surface. The infiltration excess water moves as overland flow over the land surface to the macro pores where macro pore infiltration takes place at atmospheric pressure. In macro porous top-soils overland flow distances are neglectable small.

By the description of the mechanisms that control the generation of subsurface storm flow it is clear that the soil physiography of the catchment plays a dominant role. The flow conditions for subsurface storm flow generation are closely related to hydraulic characteristics of the subsurface and to subsurface storage capacities. Although the mechanisms to generate subsurface storm flow are well understood, the quantification of the relevant flow processes during a rainfall event is still very difficult due to many aspects involved.

3.2.3 Runoff source areas

Rainfall-runoff modelling deals with the simulation of the hydrologic response of a system due to rainfall where the objective mostly is to simulate the channel flow hydrograph at the catchment outlet. Rainfall-runoff modelling in a distributed manner is closely related to the simulation of the runoff generation mechanisms as described in subsection 3.2.2 and to the simulation of the source areas where runoff is generated by the various flow processes. A number of researchers (e.g. Betson, 1964; Troendle, 1985; O’Loughlin, 1987; Freeze, 1970, 1981; Dunne, 1978, 1983; Kirkby, 1978, 1988) report about the theory of the

runoff contributing areas. Reviews about the subject are presented by Dunne [1978, 1983]. Based on the Horton overland flow mechanism the so called '*partial area concept*' is developed by Betson [1964]. In this concept it is assumed that only a part of the catchment area is contributing to generate runoff by Horton overland flow. The theory of the partial area concept evolved from observations that runoff estimates, that were calculated based on the summation of rainfall minus evaporation and infiltration produced 'linear errors' to observed runoff (see Kirkby and Chorley, 1967; TVA, 1968). For 14 catchments with different physiographic conditions Betson [1964] identified that only a portion (5 to 36%) of a catchment area produced quick catchment runoff due to rainfall. Observed runoff volumes could not realistically be reproduced when infiltration rates as measured in the field were applied to the entire catchment. The cause of the mismatch was not explained by the input of wrong infiltration rates but by the too large size of the area these infiltration rates were applied to. At the time it was understood that only the rainfall on a small and fairly constant part of a catchment area was able to contribute to the runoff during the hydrograph peak. Although the highly dynamic and non-linear character of catchment response was not fully understood, a better insight in the appearance of runoff processes was achieved.

In sub-sections 3.2.1 and 3.2.2 it is described that various surface and subsurface storm flow processes contribute to catchment runoff. Hewlett and Hibbert [1967] and Ragan [1968] presented an early theoretical assessment about catchment runoff production due to runoff contributions from multiple flow processes. These researchers introduce the term '*variable source concept*' since it was understood that areas where saturation overland flow, Horton overland flow and subsurface storm flow is generated vary temporally and spatially in size. In Figure 3.4 an example of the dynamic behaviour of runoff source areas by the saturation excess mechanism is presented

Hewlett and Hibbert [1967] stress the importance of:

"a belt of saturation, lying along stream channels, and varying in width in response to rainfall, as the critical zone from which subsurface water and groundwater emerge to form a flood peak".

Based on field evidence, Hewlett and Hibbert [1967] concluded that the size of the saturation overland flow source areas changes during rain

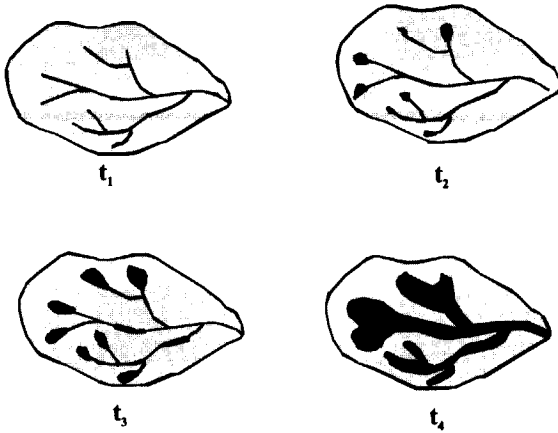


Figure 3.4: *Dynamic behaviour of the saturation overland flow source area during a storm event (Hewlett and Hibbert, 1967).*

events and inter-storm periods. In the theory about the variable source concept it was understood that the size of the runoff contributing area must be related to the size of the area where runoff is generated.

Saturation of the subsurface is caused by percolation of rainwater and by lateral subsurface flow from upslope areas. In lower sections of a hill slope the transmissivity of the upper soil layers in general decreases since, by the lowering of the surface elevation, the thickness of the upper soil layers decreases. In case of saturation of the downslope soils the capacity of a soil to transmit water laterally is easily exceeded. When the downslope soils are saturated, subsurface water will exfiltrate and so becomes overland flow. Saturation overland flow is due to the combined effect of exfiltration and rainfall on the saturated soil (see sub-section 3.2.2). In case of deep permeable soils, the runoff contributions due to saturation overland flow become less pronounced since catchment runoff is mainly due to subsurface storm flow. The theory of runoff generation by the variable source concept is generally applicable to areas of local scale ($1 \text{ km}^2 - 10 \text{ km}^2$). For areas of spatial scales larger than 10000 km^2 effects of runoff generation as described in the variable source concept have less effects on the peak runoff rate at the catchment outlet. This since the routing of water in the channel network system cause dampening and attenuation and effects of runoff generation processes become mitigated.

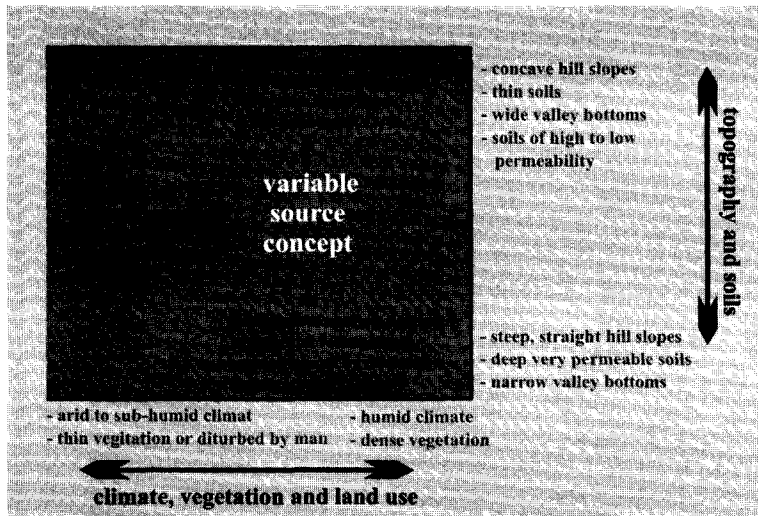


Figure 3.5: *Diagram of the occurrence of various overland flow and subsurface storm flow processes in relation to their major controls (Dunne, 1978).*

A diagram (fig. 3.5) of the various runoff processes of Horton overland flow, saturation overland flow and aggregated subsurface storm flow processes in relation to their major controls is presented by Dunne [1978; 1983]. The term 'return flow' as applied in the diagram refers to the generation of saturation overland flow by a perched groundwater table. The diagram illustrates that the occurrence of various runoff processes can be related to common catchment characteristics in terms of topography and soils and to climate, vegetation and land use.

In the diagram only processes are considered that can be characterised by relatively short response times. The arrows between the runoff groups imply a range of storm frequencies as well as catchment characteristics.

Although the scheme relates the occurrence of specific runoff processes to common climatic and catchment characteristics, in the real world most processes can occur at any hilly catchment although the extent and significance of each process for runoff generation differs. The catchment response due to rainfall is caused by contributions of multiple and aggregated flow processes while the relevance and magnitude of each process contributing to catchment runoff is subject to the physiographic, geologic and meteorological catchment properties.

In modern research, the accurate mapping of the runoff source areas is still identified as one of the key problems in PBRR-modelling for flow simulation and forecasting.

3.2.4 Characteristics of flow processes and scales issues

Runoff processes can be characterised by lag time that express the time period after which rainfall is transformed into runoff as observed at the catchment outlet. Lag times can be interpreted as an average residence or travel time and is subject to the spatial scale of a catchment. Generally, lag times of surface flow processes are smallest since travel path at the surface are short and since storage volumes to temporally store water are small. Lag times of groundwater flow processes are longest since flow velocities generally are small and since subsurface storage volumes are large. For aggregated subsurface storm flow processes lag times are in between. The lag time for macro pore flow is smallest while for perched subsurface flow the lag time is relatively long.

In figure 3.6 diagrams (after Anderson and Burt, 1990) are presented for the lag times of Horton and saturation overland flow and the aggregated subsurface storm flow processes and for the magnitude of the peak runoff rates both as function of the catchment scale. The diagram is based on extensive analyses of the runoff behaviour from various catchments (see Dunne, 1978) and supports the description of catchment runoff behaviour as presented in the variable source concept. From both overland flow processes Horton overland flow has smallest lag times while a slightly longer lag time is ascribed to saturation overland flow. Horton overland flow mostly is observed in arid climatic zones and is generated by high intensity rainfall events of relatively short duration. In the diagram lag times for Horton overland flow generation at catchment with sizes $< 10000 \text{ m}^2$ are not indicated since lag times (< 0.1 hour) are too small to be presented. Saturation overland flow mostly is observed in humid climatic zones particularly when catchments are characterised by shallow and highly permeable subsurface.

In the diagram the lag time for aggregated subsurface flow is largest since subsurface storm flow by macro pore flow, perched subsurface flow and rapid groundwater runoff is characterised by relatively long residence times. In the diagram it is assumed that the magnitude of specific peak runoff rates is highest for Horton overland flow and lowest for the

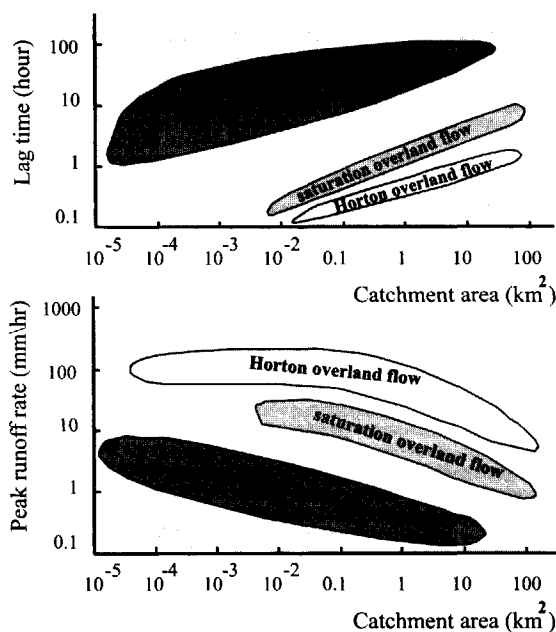


Figure 3.6: Catchment responses by of Horton and saturation overland flow and aggregated subsurface storm flow processes in terms of a) lag times b) specific peak runoff rates (modified after Kirkby, 1985).

aggregated subsurface storm flow processes. Slightly lower peak runoff rates are generated by saturation overland flow.

The diagram suggests that catchment runoff behaviour is dominated by only one of the runoff processes and that noticeable differences exist in the behaviour of the runoff processes. Such differences relate to the lag time to generate runoff and the magnitude of the peak runoff rates. Although such differences exist in the real world, it is questionable whether such differences are as clearly observable as presented in the figure. As described in section 2.3, any runoff hydrograph must be interpreted as an integrated response function of all upstream flow processes and channel flow runoff at the catchment outlet. Quantifying runoff contributions separately is very difficult and cannot be based on the simple classification as presented in figure 3.6. The diagram primarily serves as a illustration to compare the different lag times and runoff intensities of various processes in relation to the catchment size.

By an understanding of the dynamic character of the catchment runoff behaviour and rainfall-runoff processes it has become clear that each flow process can be characterised by a spatial and a temporal process scale. In table 3.1 (Rientjes, 1999a) the rainfall process and flow processes are characterised by spatial and temporal process scales. The process scale is defined as the scale at which natural phenomenon are observable through measurements.

In the table it is shown that ranges of spatial and temporal process scales overlap and that ranges of temporal process scales for the surface and subsurface flow processes are much larger than spatial scales. By this it is concluded that spatial process scales have a more dominant effect on the runoff behaviour. This is explained by the fact that any catchments can be interpreted as a large storage or filter volume that dampens effects of temporal process scales and, to a smaller extent, the effects of spatial scales.

Table 3.1: *Spatial and temporal process scales of the rainfall-runoff processes*

Process	100 m – 100.000 m	1 min. –days
	10 m - 100 m	1 min - 15 min.
	10 m - 1.000 m	5 min - hours
	10 m - 100 m	1 min - hours
	1 m - 100 m	10 min. - days
	10 m - 1.000 m	10 min. - 1 day
	1 m - 100 m	1 min. - 1 hour
Channel flow	100 m - 100.000 m	1 day - years
Ground flow	100 m - 10.000 m	10 min - days

As pointed out in section 3.1, Beven [1989] emphasises the role of scale and variability in PBRR modelling:

“particularly for distributed physically-based models a central issue to deal with is the problem of scale and spatial variability”.

When simulating rainfall-runoff processes using distributed deterministic models, in theory the modeller has to know all spatially and temporally distributed catchment properties that govern rainfall-runoff processes. In practise generally much too little real world data is available to fully describe such properties at appropriate scales. For that reason

many simplifying assumptions are introduced in distributed PBRR modelling. A major model simplification is the discretisation of a catchment into uniform or non-uniform grid elements that make up a model grid layer. At grid elements time invariant catchment properties and characteristics are represented by model parameters for which some value must be defined. Parameter values are required by the model algorithms and serve to parameterise the model. Since observations of processes, parameters or variables mostly is achieved by sampling at a limited number of locations, the representativeness of such observations may be questioned particularly when they are applied to much larger spatial and temporal scales. For any process the observation scale should ideally be equal to the process scale and should also match the scales to which model equations are applied. In PBRR models always a large gap exists between scales of observation and model scales in terms of grid element size and calculation time step. Scale issues seriously hinder successful PBRR modelling and to large extent cause that model performance is low.

3.3 Research efforts in physically-based rainfall-runoff modelling

During the past decades a relatively large number of distributed rainfall-runoff model approaches are developed that are termed 'physically-based' by the fact that real world physiographic and meteorological catchment data are used as model input data. Most of these approaches apply grid layers with rectangular elements and mostly only are able to simulate (flow) processes that are observed at the land surface. The main objective for model design and development was to improve our ability to simulate environmental impacts that are due to rainfall. Examples are soil erosion, sediment and solute transport and runoff production. Some model approaches apply conservation equations of mass and momentum to simulate overland and channel flow processes but combine these sub-models with conceptual and/or empirically based sub-models that simulate subsurface flow processes. Other approaches simulate subsurface flow behaviour by use of simple mass balance equation but apply simple travel time procedures to simulate overland and channel flow. By a detailed description of the catchment topography in terms of elevation, slope gradient, slope aspect, local drain direction, land use,

etc., it is believed that the relation between rainfall and runoff can be modelled. The use of such model approaches in runoff hydrology is questionable since real world runoff generation mechanisms and flow processes are not simulated. In literature these approaches often are termed and classified as physically based since real world physiographic catchment characteristics such as elevation and land slope served as model input. By the classification of deterministic models approaches in section 2.1, such classification is incorrect and approaches must be classified as distributed conceptual. Examples herewith are TOPMODEL from Topography based hydrologic MODEL (Beven and Kirkby, 1979); KINEROS from KINematic runoff and EROsion, (Woolhiser et al., 1990); ANSWERS from Areal Non-Point Source Watershed Environment Response Simulation, (Beasley et al., 1980, 1982); WEPP from Water Erosion Prediction Project, (Lane et al., 1988); AGNPS from AGricultural Non-Point Source pollution, (Young et al., 1987, 89) and CREAMS from Chemicals, Runoff, and Erosion from Agricultural Management Systems, (United States Department of Agriculture, 1980; Knisel, 1982).

The number of model approaches that only have physically-based flow equations at the core of at their mathematical models is very small. Such approaches primarily are developed in the late eighties and a small group of researchers present in a range of articles their research objectives, developments and achievements. The main objective of research was to see whether the runoff production mechanisms could be simulated by distributed PBRR model approaches. Hydrologic catchment response had to be simulated by an integrated model approach in which the most dominant runoff processes are simulated. In literature the design and development a small number of PBRR computer codes is reported. The designed model concepts underlying the codes however differ significantly and establishing the most appropriate concept became a general research topic.

Model concepts differed by the:

- simulated flow processes,
- schematisations of the flow processes,
- applied catchment partitioning theory and,
- applied flow equations (Rientjes et al., 1999a).

In this thesis four model approaches are reviewed, analysed and evaluated. Within each approach, runoff processes at the land surface, the unsaturated zone and the saturated zone are distinguished. Computer codes are developed based on the approaches and are applied to specific study sites.

Distributed PBRR approaches reviewed are *Système Hydrologique Européen* (SHE) (sub-section 3.3.1), *THALES* (sub-section 3.3.2), *Institute of Hydrology Distributed Model* (IHDM) (sub-section 3.3.3) and *Distributed Basin Simulator* (DBSIM) (sub-section 3.3.4).

For each model approach, model assumptions, applied process schematisations and flow equations are described. Process schematisations and model equations are described for flow processes at the land surface, unsaturated zone and saturated zone. Also simple descriptions on modelling rainfall, evapotranspiration and interception are given. For each of the approaches simulation results are shown and evaluated.

3.3.1 *Système Hydrologique Européen* (SHE)

In a number of articles Abbott et al., [1986a,b] introduce SHE that from 1976 onwards is developed by combined efforts of the Danish Hydraulic Institute (DHI), Institute of Hydrology in the United Kingdom and the French consulting company SOGREAH.

Introduction

SHE is a hydrologic model approach in which precipitation, snow melt, canopy interception, evapotranspiration, infiltration, exfiltration, overland flow, channel flow, unsaturated subsurface flow and groundwater flow are simulated. The approach is very advanced since all flow processes as well as mass exchanges and model interactions are simulated by conservation equations of mass and momentum. Runoff may be due to rainfall and/or snow melt. Overland flow, channel flow, unsaturated subsurface flow and groundwater flow are simulated by finite difference approximations of the partial differential equations.

For representing a catchment in a distributed manner, a partitioning theory is applied where a three-dimensional matrix of rectangular grid elements is constructed. In horizontal perspective all grid elements of all model layers are of equal size while in vertical perspective all layers are

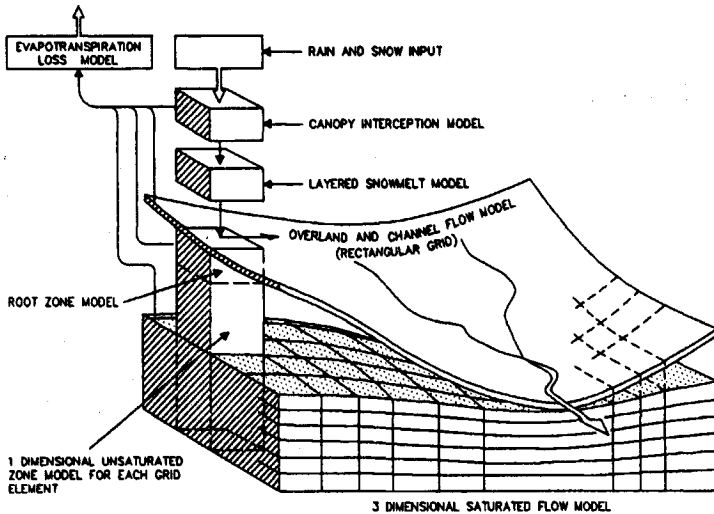


Figure 3.7: Schematic of the SHE (Abbott et al, 1986a,b).

of equal thickness. On the applied model domain Abbott et al., [1986a] state:

“the spatial distribution of the catchment parameters, the precipitation input and the catchment response is achieved in the horizontal through representation of the catchment by a rectangular raster network and in the vertical by a column of horizontal layers at each grid square”.

All model input variables like precipitation intensities and soil hydraulic conductivities may vary over the model domain but are lumped at the scale of a grid element and are assumed to represent an averaged value for the grid element area.

Flow schematisation

Land surface

Surface runoff is described by Horton and saturation overland flow and channel flow. Overland and channel flow are simulated by separate flow equations but mass exchanges are simulated when a grid elements of the overland flow and channel flow models coincide. For each calculation time step overland flow discharges are entered into the channel flow model. Model algorithms for overland and channel flow apply different

time steps to match the temporal process scales. For the simulation of overland flow a Digital Elevation Model (DEM) is used for defining slope gradients and slope aspects of the grid elements. In SHE overland flow is simulated as sheet flow. For the simulation of channel flow a DEM is used for defining bottom slope gradients. The applied governing equation for overland flow simulation reads:

$$\frac{\partial A_{of}}{\partial t} + \frac{\partial Q_{of}}{\partial x} + \frac{\partial Q_{of}}{\partial y} = S_{sf} \tag{3.1}$$

where

- A_{of} = cross-sectional flow area overland flow [L²]
- Q_{of} = overland flow discharge [L³ T⁻¹]
- t = time [T]
- x, y = horizontal space co-ordinates [L]
- S_{sf} = sink/source term surface layer [L² T⁻¹].

When v_x and v_y are flow velocities in x and y-direction respectively and h_s a local water depth at the land surface then Eq.[3.1] for a unit width of flow yields:

$$\frac{\partial h_s}{\partial t} + \frac{\partial (v_x h_s)}{\partial x} + \frac{\partial (v_y h_s)}{\partial y} = S_{sf} \tag{3.2}$$

with the sink/source term, S_{sf} , expressed per unit area, [L¹ T⁻¹]. The relation between the change of the water depth, h_s , over the land surface in x and y direction, $\partial h_s / \partial x$ and $\partial h_s / \partial y$ respectively, is simulated by the diffusion wave theory.

$$\frac{\partial h_s}{\partial x} = S_{ox} - S_{fx} \quad \text{and for} \quad \frac{\partial h_s}{\partial y} = S_{oy} - S_{fy} \tag{3.3}$$

where

- S_{ox}, S_{oy} = ground slopes in the x and y direction [-]
- S_{fx}, S_{fy} = friction slopes in the x and y direction [-].

In this theory the friction force is proportional to the friction slopes. When applying the Strickler-Manning law to simulate the relations of Eq.[3.3] and when the flow is expressed per unit width in x and y direction, the relation between the flow velocities and the overland flow depth becomes:

$$v_x h_s = k_{m,x} i_x^{1/2} h_s^{3/5} \quad \text{and for} \quad v_y h_s = k_{m,y} i_y^{1/2} h_s^{3/5} \tag{3.4}$$

where

$$k_{m,x}, k_{m,y} = \text{Strickler roughness coefficients in } x - y \text{ direction} \quad [L^{1/3} T^{-1}]$$

$$i_x, i_y = \text{water surface gradient in } x - y \text{ direction} \quad [-].$$

Equation [3.4] is at the core of the model algorithms applied for simulation of the overland flow discharges in Eq.[3.1]. The conservation equations of mass Eq.[3.2] and momentum Eq.[3.4] make up the diffusion wave equations that are simplified expressions of the hydrodynamic Saint Venant equations (Saint Venant, 1871) for simulation of water flow in open channels.

For the simulation of overland flow a two-dimensional finite difference scheme is applied. Abbott et al, [1986b] report that this scheme is solved by an explicit numerical calculation method as described by Preismann and Zaoui [1979]. In 1993 the DHI reports that the explicit scheme is replaced by an implicit calculation scheme as described by Thomas [1973].

Channel flow is simulated by basically the same diffusion wave equations where flow equations are now solved in one direction only. Model input now are channel characteristics. The set of equations is solved by an implicit finite difference scheme.

Unsaturated zone

In the unsaturated zone water flow is simulated in upward or downward direction only. The zone is bounded by the land surface and the phreatic water table and varies in thickness over the model domain by fluctuations of the water table. Water flow in the unsaturated zone is simulated by 'Richards equation' (Richards, 1931) that is solved in one dimension. Processes that are simulated in SHE by Richards equation [Eq.3.5] are unsaturated flow, infiltration, capillary rise and percolation.

$$C \frac{\partial \Psi}{\partial t} = \frac{\partial}{\partial z} \left(k_{(\theta)} \frac{\partial \Psi}{\partial z} \right) + \frac{\partial k_{(\theta)}}{\partial z} - S_{uz} \quad [3.5]$$

where

$$C = \partial \theta / \partial \Psi = \text{specific water capacity} \quad [L^{-1}]$$

$$\theta = \text{soil water content} \quad [-]$$

$$\Psi = \text{soil pressure head} \quad [L]$$

$$z = \text{vertical space co-ordinate} \quad [L]$$

$$k_{(\theta)} = \text{hydraulic conductivity subject to } \theta \quad [L T^{-1}]$$

$$S_{uz} = \text{sink/source term for unsaturated subsurface} \quad [T^{-1}].$$

Eq.[3.5] Is solved by making use of the soil characteristic relations between the soil water content, θ , and the unsaturated hydraulic conductivity, $k(\theta)$, and the soil water content, θ , and the soil water tension as expressed by the soil pressure head, Ψ (after Abbott et al.,1986b). The relation between the soil water content and the pressure head is known as the soil water retention curve and often called the 'pF-curve'. For solving the finite difference equations a one-dimensional implicit calculation scheme is applied.

The accurate modelling of the unsaturated zone is very important since overland flow generation is closely related to the infiltration characteristics and water storage capacity of this zone.

Saturated zone

Abbott et al. [1986a,b] describe that groundwater flow is simulated in a single model layer by a two dimensional non-linear Boussinesq-type flow equation:

$$S_y \frac{\partial h_p}{\partial t} = \frac{\partial}{\partial x} \left(k_x H \frac{\partial h_p}{\partial x} \right) + \frac{\partial}{\partial y} \left(k_y H \frac{\partial h_p}{\partial y} \right) + R_{sz} \quad [3.6]$$

where

S_y	= specific yield	[-]
h_p	= hydraulic head of phreatic water table	[L]
k_x	= saturated hydraulic conductivity in x direction	[L T ⁻¹]
k_y	= saturated hydraulic conductivity in y direction	[L T ⁻¹]
H	= saturated thickness	[L]
R_{sz}	= recharge of saturated zone	[L T ⁻¹].

In the approach changes of the phreatic water table are simulated that are due to percolation from and capillary rise to the unsaturated zone model layers. Exfiltration is simulated in case the column of grid cells of the initially unsaturated zone becomes over-saturated. Detailed descriptions of calculation procedures to simulate exfiltration are not presented in literature.

DHI [1993] has reported the development of a three-dimensional multi layer model approach that allows the simulation of equifers and aquitards in deeper groundwater systems. This approach is not further discussed since it is of little relevance in rainfall-runoff modelling.

Atmospheric water and interception

In SHE rainfall, evapotranspiration and interception are simulated. Model algorithms to simulate these processes are not discussed since this is out of scope. Here it is only mentioned that spatial distributions of rainfall are simulated by Thiessen polygons, that evapotranspiration is calculated Penman-Monteith equation (Monteith, 1965) and that the 'Rutter accounting procedure' (Rutter et al., 1971) is applied to simulate interception losses.

Results

Bathurst et al. [1986a,b] report after the very first simulations with SHE on calibration and validation tests for a case study of the upland Wye catchment (10.55 km²) in mid-Wales. In the numeric simulations, grid elements of model layers had size 250 m. × 250 m. In total 169 grid elements are defined and each element covers an area of 0.59% of the total catchment area. Grid elements outside the topographic catchment divide are ignored in model simulations. For the Wye catchment, all processes of rainfall, interception, evapotranspiration, overland flow, channel flow, unsaturated subsurface flow and groundwater flow are simulated. For the calibration and validation of the catchment model, five rainfall events are selected to represent a variety of climatic and hydrologic conditions. The first event is used for model calibration while the four other events are used for model validation. Model input data is derived from field measurements or from published data.

Model calibration is achieved by changing a small number of model input data for which the model is expected to be sensitive. For the unsaturated zone model, the saturated hydraulic conductivity in vertical direction, initial soil water content and shape of soil water tension curve are changed. For the saturated zone the saturated hydraulic conductivity and the initial phreatic surface water level are changed while for the land surface flow roughness coefficients for overland flow and channel flow are changed. Calibration by modifying parameter values focused on 'physical reasoning' (Bathurst, 1986a). During calibration it turned out that the initial phreatic water level and the saturated hydraulic conductivity of the saturated model zone had major effect on simulated catchment runoff. In the catchment model the saturated hydraulic conductivity was spatially distributed as function of the soil type distribution. In the validation tests calibrated parameter sets were

applied. The initial groundwater level was set to an expected depth based on physical reasoning (measured depths were not available). The main conclusion for the validation tests was that for nearly all four events the observed and simulated hydrographs matched reasonably well.

Model sensitivity analyses towards runoff generation are presented by Bathurst [1986b]. Sensitivity analyses of the Wye catchment model focused on;

1. applied spatial rainfall distributions,
2. applied grid resolution and calculation time steps,
3. defining the most sensitive model parameters and,
4. uniqueness of parameter sets; it was researched if equally satisfactory calibration results can be obtained by different parameter sets.

ad 1) effects of simulating spatially distributed rainfall by Thiessen polygons as compared to uniform rainfall were only minor. Conclusions why effects are only minor were not presented. A possible, but most likely, cause of the minor sensitivity is that rainfall for the simulation period input is rather homogeneously distributed.

ad 2) A change of the model resolution by changing the element spacing from 250 m² to 500 m² only had significant effects on runoff generation when catchment conditions were dry. In case of relatively wet initial conditions effects were only minor. An explanation for this model behaviour is that is the spatial resolution of the model does not effect the exfiltration process that is simulated by the saturated flow model, An increase of the model simulation time step from 0.1 hour to 0.5 hour for the unsaturated flow, overland flow and channel flow models caused delayed catchment response. The overall runoff volumes did not change significantly.

ad 3) Parameter sensitivity tests are executed for a number of sub-models. For the overland flow model a change of the Manning roughness coefficient showed significant effects. Vegetation related parameters that effect interception and evapotranspiration only showed minor effects but this could be due to the short time base of the events. In the unsaturated zone model, the initial soil water content and the vertical saturated hydraulic conductivity show significant effects on runoff generation. Sensitivity analyses of saturated hydraulic conductivities indicated significant effects on the base flow.

ad 4) Bathurst [1986a,b] states that extensive parameter sets can produce equally satisfactory model calibrations. It is argued that changes in parameter values of multiple parameters may counter balance single effects and as such a similar model output could be generated. For model calibration Bathurst [1986b] proposes that several rainfall events must be used for model calibration to obtain an optimum parameter set. Such set represents averaged catchment properties (see also Klemeš, 1986) and produces the best calibration results.

Although calibration, validation and sensitivity results only were briefly discussed in Bathurst, [1986a,b] they stated that the model simulations were encouraging. Differences between measured and predicted runoff discharges range from 5 to 25% of the observed discharges. Additional validation tests have been carried out on gauged and ungauged watersheds with catchment sizes ranging from 0.3 to 600 km² in a variety of climatic settings.

Remarks

Some remarks on the model approach are:

- The procedure to create the DEM is not discussed although it is known that DEM's can be very inaccurate in representing catchment elevations. It is surprising that this aspect of modelling is not addressed in the early reports on SHE.
- Bathurst et al., [1986b] state that changes of grid spacing and changes of model parameter values may have a comparable effect on simulation results. Research after such effects has not been reported although it was understood that these effects could have implications towards model calibration.
- By the complexity of the model approach a large amount of catchment data is required for model parameterisation. The fact that the large amount of input data could potentially cause problems in defining most optimum parameter set was not regarded a real setback in PBRR modelling although it was understood that multiple parameter sets could be defined that all could give satisfactory simulation results.
- In the reports on SHE, little attention is paid to scale issues that relate to the spatial resolution of the model. Dimensions of the model grid elements and cells are just fixed and implications of such procedure are not addressed.

3.3.2 THALES

Moore and Foster [1990], Moore and Grayson [1991] and Grayson et al., [1992a] present the THALES model approach that is named after 'Thales of Miletos', a Greek philosopher who revealed the role of topography in runoff generation.

Introduction

In the approach a DEM is created by a catchment partitioning theory that is called 'contour based terrain analysis method' (Moore et al., 1988; Moore and Grayson, 1991). This method is based on the 'stream path analogy' as introduced by Onstad and Brakensiek [1968]. In the 'stream path analogy', contour lines of the catchment elevation are assumed to be equipotential lines while stream lines are simulated orthogonal to these contour lines. Two adjacent stream lines make up a 'stream tube' or 'stream path' while interconnected stream path make up a flow net of non-uniform elements. Onstad and Brakensiek [1968] state;

"a flow net consists of a collection of flow lines intersecting a collection of equipotential lines. The slope between equipotential lines is maximum when flow lines intersect orthogonally, and it is along this gradient that surface water is assumed to flow".

In figure 3.8 an example of a DEM is presented that is partitioned by the stream tube analogy. This DEM is constructed by interconnected stream tubes that are discretised in non-uniform grid elements that are bounded by elevation contour lines. A relatively large number of papers have appeared on catchment partitioning by stream tubes (see Onstad and Brakensiek, 1968; Kozak, 1968; Onstad, 1973; Tisdale et al., 1986; Moore and Grayson., 1992a, among others). The topic of catchment partitioning to create discretised model domains is still a subject of ongoing scientific research and is of major importance in distributed runoff modelling.

Moore and Grayson [1991] motivate the usage of the stream tube approach by stating;

"For hydrologic modelling, the physics of the process in question should make up the model concept and so define the model demands" and "Analysis in complex terrain needs a partitioning theory different from the theory of the commonly used rectangular grid systems applied in raster DEM's".

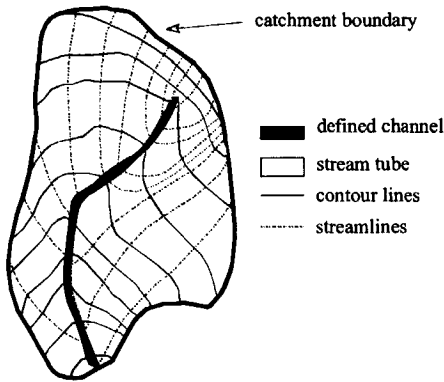


Figure 3.8: Hypothetical catchment showing elements shaped by intersections of adjacent streamlines and elevation lines (Brakensiek, 1968).

Another statement is;

“For overland flow the hydraulics of fluid flow in the landscape make up the data structure” and “The non-uniform elements constitute a vector based DEM. Such a DEM is capable of providing a topographic structure which is based on the physics of water movement on the land surface where a priori knowledge of the terrain is not required”.

In the algorithm for catchment partitioning, for each grid element the following attributes are defined; element area, total upslope contributing area, element numbering of upslope and downslope connected elements, x, y, z , co-ordinates of element centroids, x, y, z , co-ordinates of midpoints at downslope boundary of an element, average element slope, width of upslope and downslope element boundaries, length of the element, aspect or azimuth of the element and plan curvature. The algorithm for catchment partitioning is described in Moore and Grayson [1991]. The DEM discretisation is used to simulate distributions of model input parameters, model variables and flow discharges.

For simulation of runoff, a combined kinematic surface-subsurface flow model approach (after Moore and Grayson, 1991) is applied. Surface runoff is simulated by channel flow and overland flow that is simulated as sheet flow, and runoff from the subsurface is simulated in shallow saturated flow conditions only. By the description of flow processes in sub-section 3.2.1, shallow subsurface runoff basically can be interpreted

as rapid groundwater flow. In the THALES approach it is assumed that rapid groundwater flow is generated by a groundwater table rise as caused by lateral groundwater flow and percolation. The kinematic surface-subsurface flow model is developed by Takasao and Shiibi [1988] and is based on the one dimensional mass balance equation:

$$\frac{\partial A_f}{\partial t} + \frac{\partial Q_e}{\partial s} = \frac{i_n A_e}{\Delta s_e} \tag{3.7}$$

where

- A_f = cross-sectional flow area [L²]
- Q_e = discharge from grid element [L³ T⁻¹]
- i_n = net rainfall intensity [L T⁻¹]
- A_e = plan area of grid element [L²]
- s_e = flow distance along a streamline in a grid element [L]
- t = time instant [T]
- s = location along a stream line [L].

During model simulations the cross-sectional flow area, A_f , is defined for the runoff processes of Horton overland flow, saturation overland flow and rapid groundwater flow.

Nodal points in the network correspond to the midpoints on the upslope and downslope contour lines bounding each element. Momentum equations are solved in one-dimensional perspective at each nodal point in the network. For the momentum equations, the resistance equations of Darcy and Manning are applied for respectively the rapid groundwater flow and overland flow model approaches. Water flow in a catchment model is represented by a series of one-dimensional momentum equations. Coupling of equations is realised through a finite difference form of the continuity of mass equation that is applied to the catchment grid elements. The flow equation to simulate surface and subsurface runoff across a stream tube was originally developed by Brakensiek [1967]. By simulated infiltration and exfiltration processes, water exchanges between the overland flow and the groundwater flow models is possible.

The THALES model concept was designed and developed to prove the usefulness of the described catchment partitioning theory in distributed PBRR modelling. In this respect Moore and Grayson [1991] refer to a statement of Beven [1989] who, in an article about scale considerations

in hydrologic modelling, criticised distributed rainfall-runoff modelling efforts:

“Computer models must take account of the need for a theory of the lumping of sub-grid scale processes; for a closer correspondence in scale between model predictions and measurements; and for closer correspondence between equations and field processes”.

By the applied spatial discretisation and selected model algorithms, the THALES model approach was expected to meet these demands.

Flow schematisation

Land surface

At the land surface channel flow and overland flow are simulated by a combined conservation equations of mass and momentum. In the mathematical model, the momentum equation is described by the Manning equation that is expressed by:

$$Q_f = \alpha A_f^m \quad [3.8]$$

where

Q_f = flow discharge	$[L^3 T^{-1}]$
A_f = cross-sectional flow area	$[L^2]$
m = coefficient	$[-]$
α = coefficient	$[-]$.

The dimension of α is subject to the process modelled. The overland flow discharge is calculated by:

$$Q_{of} = n^{-1} \cdot \omega^{-\frac{2}{3}} \cdot \tan^{\frac{1}{2}} \beta \cdot A_{of}^m \quad [3.9]$$

where

Q_{of} = overland flow discharge	$[L^3 T^{-1}]$
N = Manning resistance coefficient	$[T L^{-1/3}]$
ω = width of grid element orthogonal to the streamline	$[L]$
β = local slope of land surface	$[-]$
A_{of} = cross-sectional flow area overland flow	$[L^2]$
m = coefficient with value 5/3	$[-]$.

Channel flow is simulated by basically the same equation. Only model input data is slightly modified: 1) the value coefficient m is set to 4/3, 2) the cross sectional flow area is defined for the channel, A_{ch} , 3) the

element width, ω , is replaced by a coefficient, υ , that describes the relation between hydraulic radius, R_h , and cross-sectional flow area: $R_h = \upsilon \cdot A_{ch}^{1/2}$ (Moore and Burch, 1986; Moore and Foster, 1990).

For routing of overland flow and channel flow a numerical solution of the conservation equation of mass as developed by Brakensiek [1967] is applied. For simulation of overland flow this one-dimensional equation has the form:

$$A_{of4} + 2Q_{of4} \frac{\Delta t}{\Delta s_e} = A_{of1} - A_{of2} + A_{of3} + 2Q_{of2} \frac{\Delta t}{\Delta s_e} + 2i_n A_e \frac{\Delta t}{\Delta s_e} \quad [3.10]$$

where

- A_{of} = cross-sectional overland flow area [L²]
- Q_{of} = overland flow discharge of a grid element [L³ T⁻¹]
- Δs_e = increase of flow distance along a streamline [L]
- i_n = net rainfall intensity [L T⁻¹]
- A_e = plan area of the element [L²]
- Δt = time increment [T].

The subscripts 1-4 refer to the time-space domain of the applied equations; the subscripts 1 and 3 refer to time t at positions s and $s+\Delta s_e$, respectively, and subscripts 2 and 4 refer to time $t+\Delta t$ at the same positions. The terms on the left hand side of Eq.[3.10] are solved during model calculations where A_{of4} is related to Q_{of4} by a non-linear relation. Applying a method of Newton and Raphson (Moore and Foster, 1990; Moore and Grayson, 1991) Eq.[3.10] is solved for Q_{of4} or A_{of4} following the description of Eq.[3.8]. Although not described in Grayson [1992], it is assumed that for simulation of channel flow by Eq.[3.10], the overland flow discharge, Q_{of} , is replaced by a channel flow discharge, Q_{ch} . Also the cross sectional overland flow area, A_{of} , is replaced by the cross sectional channel flow area, A_{ch} .

In the THALES model approach it is assumed that Horton overland flow is generated when the land surface becomes ponded by rainfall while the subsurface remains unsaturated. The time to ponding, t_p , is defined by:

$$t_p = \frac{K_{s,r}(\theta_s - \theta_i)H_c}{i_n(i_n - K_{s,r})} \quad [3.11]$$

where

$K_{s,r}$ = re-saturated hydraulic conductivity of the Green and Ampt infiltration formula (Green and Ampt, 1913)	[L T ⁻¹]
θ_s = saturated soil water content	[-]
θ_i = initial soil water content	[-]
H_c = effective capillary drive	[L]
i_n = net rainfall intensity	[L T ⁻¹]

(Mein and Larson, 1973; Morel-Seytoux, 1988a, after Moore and Grayson, 1991).

The infiltration rate and the infiltration volume are calculated for each element to define the rainfall excess rate.

Unsaturated zone / saturated zone

Infiltration is calculated either by a Horton type infiltration equation Eq.[3.11] or by an infiltration equation as described by Smith and Parlange [1978] Eq.[3.12] (see Grayson et al., 1992a):

$$f = K_{s,r} + \frac{1}{\kappa \Delta t} (i_p - K_{s,r}) \left(e^{\kappa \Delta t} - 1 \right) e^{-\kappa(t-t_p)} \quad [3.12]$$

where

f = infiltration rate	[L T ⁻¹]
κ = constant	[T ⁻¹]
Δt = time increment	[T]
i_p = rainfall intensity that induced ponding	[L T ⁻¹]
t = time instant	[T].

Morel-Seytoux [1988a,b] demonstrate that a constant κ can be defined as function of $K_{s,r}$, θ_s , θ_i , and H_c as applied in the Green and Ampt infiltration model (Green and Ampt, 1913):

$$\kappa = \frac{8K_{s,r}}{[(\theta_s - \theta_i)H_c]} \quad [3.13]$$

The re-saturated hydraulic conductivity, $K_{s,r}$, usually is smaller than the saturated hydraulic conductivity, K_s . In practice κ generally is a fitted parameter (Moore and Grayson, 1991).

The infiltration equation of Smith and Parlange [1978] has the form (Grayson et al., 1992a):

$$f = K_s \frac{e^{F/B}}{e^{F/B} - 1} \quad [3.14]$$

where

f = the infiltration rate [L T⁻¹]

K_s = saturated hydraulic conductivity [L T⁻¹]

F = the volume of water infiltrated per area unit [L]

$B = H_c (\theta_s - \theta_i)$ [L].

A clear description on the implementation and effectiveness of both infiltration theories is not presented in the articles by Moore and Foster [1990], Moore and Grayson [1991] or Grayson et al., [1992a].

For rain periods t_d where the rainfall intensity i_n falls below the infiltration capacity, the unsaturated hydraulic conductivity, K_θ , is calculated. Morel-Seytoux (1988a) presents equations for calculating the unsaturated hydraulic conductivity when $t > t_d$ in case $i_n = 0$ and in case $0 < i_n < K_s$.

For $t > t_d$ and when $i_n = 0$:

$$K_\theta = \frac{F_d K_{\theta,d}}{F_d + \mu K_{\theta,d} (t - t_d)} \quad [3.15]$$

for $t > t_d$ and when $0 < i_n < K_s$:

$$K_\theta = \frac{i_n \left(\frac{K_{\theta,d}}{K_{\theta,d} - i_n} \right) e^{\mu i_n (t - t_d) / F_m}}{\left(\frac{K_{\theta,d}}{K_{\theta,d} - i_n} \right) e^{\mu i_n (t - t_d) / F_m} - 1} \quad [3.16]$$

where

F_d = infiltration volume for an unit area at time t_d [L]

F_m = the mean infiltration volume for an unit area between any time instant t and t_d [L]

K_θ = hydraulic conductivity as function of θ [L T⁻¹]

$K_{\theta,d}$ = hydraulic conductivity as function of θ at time t_d [L T⁻¹]

$\mu = 3 + 2/\lambda$ [-]

λ = pore size index [-]

(Morel-Seytoux, 1988a; Moore and Foster, 1990 and Grayson et al., 1992a).

The initial soil water content, θ_i , is calculated by the Brooks Corey equation (Brooks and Corey, 1964) Eq.[3.17]. In this equation the unsaturated hydraulic conductivity, K_θ , is calculated by:

$$K_\theta = K_s \left(\frac{\theta - \theta_r}{\theta_s - \theta_r} \right)^\mu \quad [3.17]$$

where

K_s = saturated hydraulic conductivity [L T⁻¹]

θ_s = saturated soil water content [-]

θ_r = residual soil water content [-]

$\mu = 3 + 2/\lambda$ [-]

λ = pore size index [-]

When replacing soil water content, θ , by initial soil water content, θ_i , and when replacing unsaturated hydraulic conductivity, K_θ , by unsaturated hydraulic conductivity $K_{\theta,d}$ at time t_d (Eq's. [3.15]; [3.16]) then, when solving Eq.[3.17] for θ_i , the initial soil water content at a grid element is calculated by:

$$\theta_i = \left(\left(\frac{K_{\theta,d}}{K_s} \right)^\frac{1}{\mu} \right) \theta_s - \left(\left(\frac{K_{\theta,d}}{K_s} \right)^\frac{1}{\mu} - 1 \right) \theta_r \quad [3.18]$$

Moore and Grayson [1991] describe that at inter-storm periods the distribution of the soil water content over the catchment is calculated by Eq.[3.18].

The recharge rate to the saturated zone is given by the hydraulic conductivity as calculated by the Brooks-Corey relation (Brooks-Corey, 1964) Eq.[3.17]. The soil water content of the unsaturated grid elements is calculated by a soil water accounting procedure where infiltration water is added to the grid element and percolation water is subtracted from the grid element. During a model simulation for all time steps the soil water content and the thickness of the saturated zone are updated for all grid elements. Saturation overland flow generation is calculated in combination with groundwater flow (see fig. 3.9).

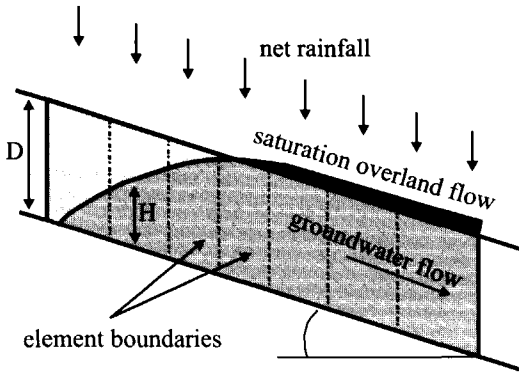


Figure 3.9: Schematic representation of the flow system being simulated by the saturation overland flow - groundwater flow model (Moore and Grayson, 1991).

In the THALES approach it is assumed that saturation overland flow is generated in case the capacity of the subsoil to transmit water in lateral direction is exceeded. Groundwater flow is calculated by Darcy's equation and is assumed to flow laterally above an impervious layer. The applied equation has the form:

$$Q_g = K_s \frac{A_{gf}}{\gamma} \sin \beta = \omega H K_s \quad \text{for } 0 \leq A_{gf} \leq \omega \gamma D \quad [3.19]$$

where

Q_g	= rapid groundwater flow discharge of a grid element	$[L^3 T^{-1}]$
K_s	= saturated hydraulic conductivity	$[L T^{-1}]$
A_{gf}	= cross-sectional flow area groundwater flow	$[L^2]$
γ	= effective porosity	$[-]$
β	= the local slope of the land surface	$[-]$
ω	= width of the element orthogonal to the streamline	$[L]$
H	= depth of flow above the impermeable layer	$[L]$
D	= thickness of hydrologic active soil profile	$[L]$

The combined saturation overland flow - groundwater flow equation (Eq's. 3.9 and 3.19) is expressed by:

$$Q = \omega D K_s \sin \beta + \alpha A_r^m \quad \text{for } A_r \geq \omega \gamma D \quad [3.20]$$

Moore and Grayson [1991] refer to this equation as the kinematic surface-subsurface flow equation.

Atmospheric water

Rainfall is simulated by spatially uniform distributions. In model simulations, rainfall intensities may vary over the simulation period. In the approach, processes of evapotranspiration and interception are ignored.

Results

In the first application of the THALES model approach, the performance is tested at laboratory scale and few real world catchments. An extensive article about the performance of hydrologic models of the Wagga Wagga and the Lucky Hills catchments is presented by Grayson et al., [1992a]. In the Wagga Wagga catchment in south-eastern Australia runoff mainly is due to saturation overland flow and groundwater flow while runoff generation in the Lucky Hills catchment is dominated by Horton overland flow.

The Wagga Wagga catchment has a size of 7.03 ha. and, in the simulations, is partitioned into 1854 elements with an average size of approximately 37,9 m² (1 element covers about 0.055% of the catchment area). The land surface slope gradients vary from 5% to 20% and the predominantly loamy soils are categorised into 4 zones with different ranges of surface soil saturated hydraulic conductivities. Soil parameter values of hydraulic conductivity, water content at field capacity and soil porosity are obtained from field measurements. In table 3.2 the number of measurements, the mean and the standard deviation of the saturated hydraulic conductivities for the 4 zones are presented.

Soil depth measurements were obtained from irregularly spaced locations and have been interpolated over the catchment model domain. Grayson et al [1992a] describe that for the Wagga Wagga catchment the antecedent subsurface water contents over the grid elements are simulated by a topographic index, $\ln(A/b \tan \beta)$, that is applied to all grid elements. The specific catchment area, A/b , is calculated by dividing the upslope area of a grid element in a stream tube, A , by the width of the grid element, b , while the local slope gradient β is obtained from a DEM. The use of this index for the simulation of antecedent soil water contents is described by Beven and Kirkby [1979] who introduced the index into the TOPMODEL model concept. For simulating the hydraulic resistance at the land surface the Manning resistance coefficient is applied as a constant over the model domain. Rainfall data is obtained from a gauging

station 500 m. outside the catchment. Data is observed at a temporal gauging resolution of minimum 100 minutes while the spatial variability in model simulation is ignored since information on this variability was not available.

Table 3.2: Soil hydraulic conductivity at the Wagga Wagga Catchment

Zone	Number of measurements	Mean saturated hydraulic conductivity	Standard deviation
I	31	37	59
II	20	46	42
III	25	133	78
IV	7	286	155

Figure 3.10 presents the simulation results of a storm event comprising three rainfall periods.

In their comments on the modelling results Grayson et al., [1992a] state;

“the maximum runoff rates for the first two peaks are in close agreement with the measured data but the third peak is substantially underestimated and of a different shape”.

Grayson et al., [1992a] state that the mismatch is due to the low temporal rainfall resolution. In an additional simulation the third rainfall peak is simulated by a high intense rainfall event with an equal rainfall volume but simulated with duration of only 5 minutes. The simulation produced a significant better result for the peak discharge and shape of the hydrograph indicating high model sensitivity to rainfall input. The simulation of the base flow discharges however remained very poor. Simulation with increased saturated hydraulic conductivities to 1000 mm per hour caused a good fit between measured and simulated runoff (fig. 3.11). The mismatch of the peak discharge of the third event remains however.

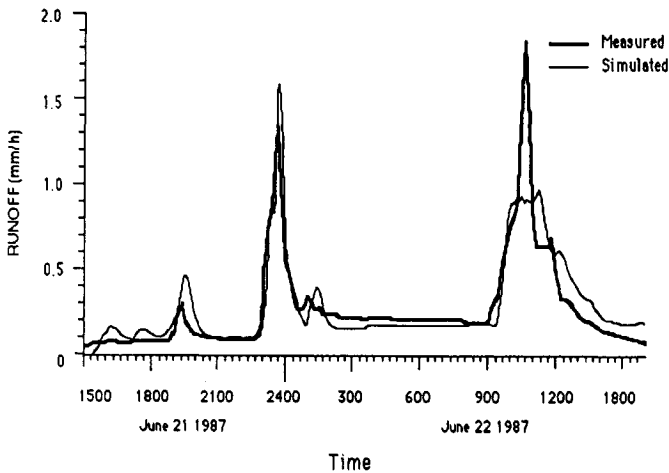


Figure 3.10: Comparison of simulated and observed discharge for measured rainfall (Grayson et al., 1992a).

In their article Grayson et al., [1992a] are not conclusive about a possible cause of this mismatch;

“a wrong model concept, erroneous measurements at the measuring flume or ‘ineffective’ soil surface hydraulic conductivities are possible causes”.

Ineffective means that, although the conductivity values are obtained by measurement, in model calculations such values do not produce satisfactory simulation results. Sensitivity tests towards the simulation of spatially distributed saturated hydraulic conductivities versus spatially uniformly applied saturated hydraulic conductivities indicate only little improvement.

On the Lucky Hills catchment in the state of Arizona, USA, a second test is performed. In this catchment Horton overland flow is known as the dominant runoff flow process. This catchment, subdivided into 3 subcatchments, has a size of 4.4 ha. and is partitioned into 2928 elements with an average size of approximately 15 m². (1 element \approx 0.034 % of the catchment area). Hill slopes vary from 1% to 100% but generally are less than 30%. The dominant soil type is sandy loam that, at shallow depth, is underlain by bedrock. The catchment is located in an arid climatic zone where the average annual rainfall depth is 303 mm over the period 1965-1981.

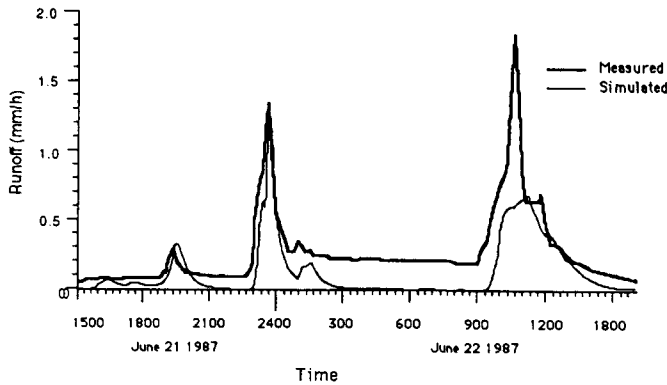


Figure 3.11: Comparison of simulated and observed discharge using $K_s = 1000 \text{ mm h}^{-1}$ (Grayson et al., 1992a).

In model simulations, saturated hydraulic conductivities and soil physical parameters as total porosity, residual soil water content, soil water content at saturation, soil water content at field capacity and wilting point of the soils, as required by the infiltration formulas, are estimated from soil textural information. The saturated hydraulic conductivity is corrected for rock content, vegetation cover, erosion pavement and crusting and is optimised by calculations with the 'KINEROS' computer programme (Goodrich, 1990) to obtain 'effective' conductivity values. The Manning's resistance coefficient is set to $0.066 [\text{sec}/\text{mm}^{1/3}]$ for overland flow processes and $0.044 [\text{sec}/\text{mm}^{1/3}]$ for channel flow processes. The antecedent soil water content is uniformly distributed over the catchment. This content is calculated by the computer programme 'CREAMS' (Knisel, 1982) by calculating the soil water deficit as a fraction of the saturated water content. Whether the calculated value of the soil hydraulic parameters as function of water content is effective is questionable since, in real world field situations, these values are closely related to the soil texture. Sharma et al., [1980] and Loague and Gander [1990], however, indicate that soil texture properties and hydraulic parameters can be unrelated and Grayson et al., [1992a] justify the use of the procedure. The spatial distributions of the soil parameters over the grid elements are simulated by use of Thiessen polygons based on the soil type distribution. The DEM grid discretisation is overlain by the Thiessen polygons and soil hydraulic values are assigned to the grid elements. Rainfall is gauged at a minimum resolution of 2 minutes

although the exact temporal gauging and simulation distributions are not presented by Grayson et al., [1992a]. Spatially variable rainfall distributions are not simulated since data from only one rainfall station is available. For all 3 sub-catchments observed runoff data is available. Simulation runs are executed for all three sub-catchments. The overall conclusion on simulation results in the Lucky Hill catchment is that results are very poor. In describing the results, Grayson et al., [1992a] identify the inaccurate simulation of the temporal rainfall resolution as a possible cause of poor model performance. Other identified sources of error are the inaccurate simulation of interception and depression storage at the land surface, the inaccurate simulation of the recovery of the infiltration rate between events, a wrong model concept and uncertainty associated with soil parameter values (Grayson et al., 1992a). Tests with applying spatially distributed soil parameter values compared to uniformly distributed (i.e. catchment averaged) values over the model domain produced only a slight increase in peak discharges.

Sensitivity tests towards the use of an enlarged channel network indicate significant changes in peak runoff and runoff volume. Model simulations with decreased Manning resistance coefficients for overland flow and channel flow cause an increase in runoff peak and runoff volume.

Remarks

Some remarks on the modelling can be made:

- The theory of catchment partitioning by 'stream tubes' and the applied model concept is very sound. Applications of this theory in THALES model simulations are disappointing since observed channel flow hydrographs are reproduced satisfactorily. It is not clear, however, whether the low model performance is due to the applied catchment partitioning, the selected model algorithms or wrong DEM model input data.
- Hydrologic models by the THALES model approach have been developed and tested on relatively small sized (< 7 ha) catchments. The applicability at larger sized catchments with, possibly, combined Horton overland flow, saturation overland flow and subsurface storm flow processes is not studied.
- Model simulations appear to be (very) sensitive to the applied temporal and spatial rainfall distribution and to the saturated soil

hydraulic conductivity. By the simulation results it is concluded that rainfall and infiltration must be simulated more accurately.

- An important source of error for the mismatch between observed and simulated hydrographs is the poor simulation of base flow related runoff processes. Model results prove that effective soil hydraulic parameter data should be used. A physical basis for transforming observed field data into model 'effective' parameter value is not presented.
- It appears that the size of the channel network has a significantly effect on the simulation results. When defining a channel network system in a catchment model by use of a DEM, objective criteria must be defined that help to define the most appropriate channel network system in terms of shape and size.

3.3.3 Institute of Hydrology Distributed Model (IHDM)

IHDM is developed during the period 1977 - 1992 by the Institute of Hydrology (UK) by:

"the desire to make flood forecasts on ungauged catchments and by the desire to predict the hydrologic effects of land use changes" (Beven et al., 1987).

Reports on the earliest applications of IHDM are known for few experimental catchments in Wales. In the selected catchments the runoff mechanisms of saturation overland flow and subsurface flow dominated the catchment runoff behaviour. These catchments are characterised by a relatively high altitude, their undulating hill slope topography and shallow subsurface. It was expected that both overland flow runoff mechanisms could be simulated by the IHDM model concept. After the first applications of IHDM only a (very) small number of model studies are reported in literature.

Introduction

In IHDM model approach runoff is generated by Horton overland flow, saturation overland flow, perched subsurface flow and groundwater flow while runoff is due to rainfall or snow melt. For simulation of these processes in a distributed manner, catchment topography is partitioned in so called 'hill slope planes' (Beven et al., 1987). Such planes are a series of grid elements that make up flow paths with varying grid elements

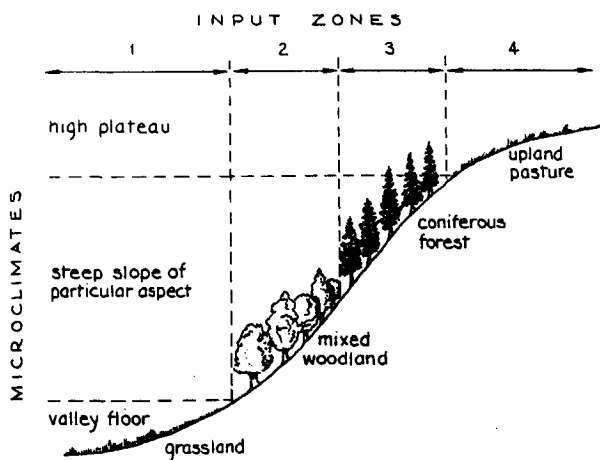


Figure 3.12: Schematic of the model input zones (Beven et al., 1987).

width. Flow paths are bounded by hill slope plane lines that are projected orthogonal to elevation contour lines and that follow the greatest hill slope gradients. By this methodology a grid layer is created that forms a DEM consisting of non-uniform grid elements of various size. Beven et al., [1987] motivate the methodology of hill slope plane partitioning by stating:

“hill slope planes can simulate the essential effects of topographic convergence and slope variations without the number of solution nodes required in a fully three-dimensional representation”.

For modelling the spatially distributed model input data, a number of model input zones are applied. These zones must represent variations of the hill slope characteristics such as land use, topography, vegetation etc. In figure 3.12 an example is presented where a zonation is applied as based on land use and topographic characteristics.

For any hill slope plane a zonation of input data is applied. Zones of model input data are bounded by the hill slope plane lines that are arbitrarily chosen elevation contour lines. The elevation contour lines are chosen by the modeller and reflect the significant changes of catchment characteristics. By this procedure the size and the shape of a model input

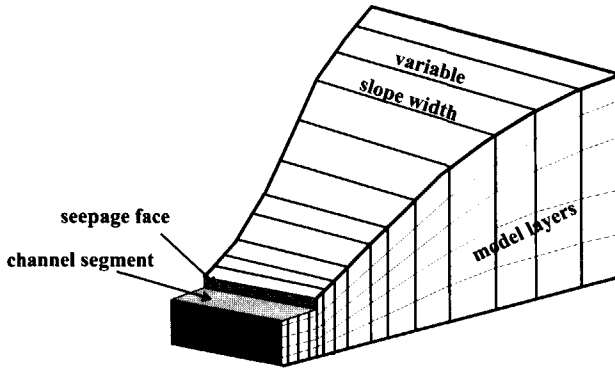


Figure 3.13: Hill slope partitioning as applied in IHDM (Beven et al., 1987).

zone varies to simulate specific catchment characteristics. Beven et al., [1987] state:

“each input zone can differ in meteorological inputs, elevation range, slope angle, slope aspect and vegetation type”.

The hill slope planes as overlain by the hill slope zones of model input data are partitioned into a finite element scheme for flow calculations. Figure 3.13 presents an example of the hill slope plane partitioning as applied in IHDM.

About the methodology of catchment partitioning Calver [1988] states:

“A model is set up in a cascading modular structure of hill slope sections and channel sections comprising the whole catchment”.

It is apparent that some resemblance exists with the ‘stream tube’ partitioning theory as applied in the THALES model concept (Moore and Grayson, 1991). Partitioning in vertical direction is achieved by applying a number of model layers. The land surface is represented by a DEM while the subsurface is represented by a number of subsurface model layers. Subsurface model layers are characterised by soil hydraulic properties.

Flow processes in IHDM are simulated by flow equations that are based on conservation equations of mass and momentum. In IHDM single flow processes are simulated with a simulation time step that should represent the dynamics of the real world processes and so four simulation time step levels are defined. Time step levels are defined for the time dependant

input data, for simulating overland flow discharges, for simulating subsurface flow and channel flow processes, and for the conversion of overland flow discharges in channel flow discharges. In IHDM evaporation is also simulated by conservation equations of mass and momentum. Interception is simulated by a water accounting procedure.

Flow schematisation

Land surface

The flow of water at the land surface is represented by overland flow and channel flow. By the design of the IHDM model concept, surface runoff is generated by the mechanisms of Horton overland flow and saturation overland flow and by snow melt. Overland flow is generated when the topsoil becomes saturated. Such saturation takes place when the rainfall intensity exceeds the infiltration capacity of the surface soil (i.e. Horton overland flow) or when the water table rises to the land surface (i.e. saturation overland flow).

Overland flow is simulated by the governing equation Eq.[3.21] that describes the flow of water in one dimension (after Beven et al.,1987).

$$\varpi \frac{\partial Q_{of}}{\partial t} + c_k \frac{\partial \varpi Q_{of}}{\partial l_d} - \varpi q_{lr} c_k = 0 \quad [3.21]$$

where

Q_{of} = overland flow discharge	$[L^3 T^{-1}]$
ϖ = variable slope width	$[L]$
q_{lr} = lateral inflow rate per unit down slope length	$[L^2 T^{-1}]$
l_d = downslope distance	$[L]$
c_k = kinematic wave velocity	$[L T^{-1}]$.

The applied momentum equation for simulation of overland flow reads:

$$Q_{of} = C_h s^{1/2} A_{of}^b \quad [3.22]$$

where

Q_{of} = Overland flow discharge	$[L^3 T^{-1}]$
C_h = Chézy overland flow roughness coefficient	$[L^{1/2} T^{-1}]$
s = local slope	$[-]$
A_{of} = cross sectional flow area overland flow	$[L^2]$
b = a constant with value 5/4	$[-]$.

When substituting the momentum equation Eq.[3.22] for Q_{of} in Eq.[3.21], the governing equation for simulating overland flow is obtained.

The overland flow depth is defined by dividing the cross sectional flow area, A_{of} , by the locally varying slope width, ω . Flow routing is achieved by solving the set of equations of Eq.[3.21] over the computational nodes of the surface grid layer by a numerical solution scheme. This scheme is a four-point implicit finite difference scheme and is adapted from Li et al., [1975]. In the scheme, overland flow at the hill slope sections is simulated in the sequence of hill slope planes following the downslope flow path. In IHDM an option is available to densify the surface grid layer by additional computational nodes as compared to the subsurface nodal density. The surface grid layer applies a higher nodal density than the subsurface grid layers.

Channel flow is calculated by an adapted form of the conservation of mass equation Eq.[3.21]. In the adapted equation, overland flow discharge, Q_{of} , is replaced by a channel flow discharge, Q_{ch} . The channel flow discharge is calculated by a momentum equation similar to Eq.[3.22] where the cross sectional overland flow area, A_{of} , is replaced by the cross sectional channel flow area, A_{ch} . The channel network system is simulated by a sequential calculation of flows following the channel segments in downstream direction.

Unsaturated zone/saturated zone

Subsurface flow in IHDM is only simulated in Darcian flow conditions where water flow in two dimensions (x, z) is simulated. By such an approach, flow processes of unsaturated subsurface flow, perched subsurface flow and rapid groundwater flow are simulated. Although for all three flow processes the same model algorithm is applied each process is simulated in the approach. The simulation of the processes has close relation to the applied parameterisation of the subsurface model layers and the prevailing flow conditions. The flow of water in saturated and unsaturated flow conditions is simulated by a two-dimensional form of Richards equation, (Richards, 1931). Richards equation is applied in vertical (z_d) and downslope (x_d) direction and is adapted to the flow conditions in the subsurface model domain. The applied two-dimensional governing equation in IHDM has the form (Beven et al., 1987):

$$\varpi \frac{\partial \theta}{\partial t} - \frac{\partial}{\partial x_d} \left(\varpi K_{x(\theta)} \frac{\partial \phi}{\partial x_d} \right) - \frac{\partial}{\partial z_d} \left(\varpi K_{z(\theta)} \frac{\partial \phi}{\partial z_d} \right) = S_{ss} \quad [3.23]$$

where

ϖ	= variable slope width	[L]
θ	= soil water content	[-]
t	= time	[T]
x_d	= horizontal downslope distance	[L]
z_d	= vertical distance from arbitrary stratum	[L]
$K_{x(\theta)}$	= hydraulic conductivity in x direction subject to θ	[L T ⁻¹]
$K_{z(\theta)}$	= hydraulic conductivity in z direction subject to θ	[L T ⁻¹]
ϕ	= hydraulic head potential	[L]
S_{ss}	= sink/source term subsurface	[L T ⁻¹].

Richards [1931] solved Eq.[3.23] for unsaturated subsurface flow conditions by introducing the specific water capacity, $C_{(\psi)} = d\theta / d\psi$ that describes the unique relation between the soil water content, θ , and the capillary soil potential, ψ . In model studies with IHDM, the relation of $C_{(\psi)}$ must be defined for all soil types. For modelling the relation between the soil water content, θ , and the unsaturated hydraulic conductivity $K_{(\psi)}$, as function of the capillary soil potential, some modified relationships as originally developed by Campbell [1974] are applied. When p is defined as a relative potential, ψ / ψ_0 , where ψ_0 is the air entry potential, then $\theta / \theta_s = p^\alpha$ where θ_s is the porosity of the soil under saturated conditions and α a constant. For any relative potential, p , the specific water capacity, $C_{(\psi)}$, is defined by (Beven et al.,1987):

$$C_{(\psi)} = \frac{\theta_s \alpha p^{\alpha-1}}{\psi_0} \quad [3.24]$$

This equation is applicable to saturated soil conditions when the hydraulic head potentials, ϕ , become greater than zero and applicable to unsaturated subsurface flow conditions when the specific water capacity $C_{(\psi)}$ is defined for relative potentials that range between the value of p and 0 (Beven et al., 1987).

The unsaturated hydraulic conductivity K_{us} is defined by:

$$K_{us} = K_s \cdot p^{(-2+3\alpha)} \quad [3.25]$$

Introducing $C_{(\psi)}$ in Eq. [3.23] gives the flow equation for modelling water flow Eq. [3.26] in the unsaturated and the saturated zone. In unsaturated flow conditions, the unsaturated hydraulic conductivity can be expressed for any ψ by $K_{x(\psi)}$ or $K_{z(\psi)}$:

$$\omega C_{(\psi)} \frac{\partial \theta}{\partial t} - \frac{\partial}{\partial x_d} \left(\omega K_{x(\psi)} \frac{\partial \phi}{\partial x_d} \right) - \frac{\partial}{\partial z_d} \left(\omega K_{z(\psi)} \frac{\partial \phi}{\partial z_d} \right) = S_{wz} \quad [3.26]$$

For simulating subsurface flow, the partitioning of the catchment hill slope is adapted in a finite element calculation scheme. For all grid elements of the subsurface domain Eq. [3.26] is solved for the dependent variable ϕ . In the mathematical model of the finite element scheme, basis functions $N_i(x_i, z_i)$ are used at the n nodal points:

$$\phi = \sum_{i=1}^n N_i(x_i, z_i) \phi_{(t)} \quad [3.27]$$

for $i = j$ $N_i(x_j, z_j)$ is 1, for $i \neq j$ $N_i(x_j, z_j)$ is 0. The solution is known as the 'Galerkin method' and is widely used in the field of subsurface hydrology. The time domain of Eq. [3.23] is solved by a backward finite difference scheme. For an extensive description on the mathematical model, reference is made to Beven et al., [1987].

No-flow boundary conditions in the numerical approach are defined at the topographic water divide, the bottom of the model, and at calculation nodes beneath the mid-point of a channel segment. Flux boundaries are defined for unsaturated flow conditions at the top layer representing the land surface (see fig 3.14). Fluxes at the land surface are simulated by the evapotranspiration module or are due to infiltration that is simulated by the unsaturated flow equation of Richards.

At the saturation overland flow source area, the flux boundary is changed in a head boundary. In case of Horton overland flow or when a saturated infiltration front develops, the soil water potential of the computational nodes at the surface layer is set to atmospheric pressure. By this approach a constant infiltration flux is created. The change of the boundary conditions might occur locally on the grid slope and is subject to the soil surface saturation. Exfiltration at the land surface is simulated under the condition that the total soil profile becomes over-saturated. Infiltration fluxes at the land surface are simulated for all calculation time steps of subsurface flow model.

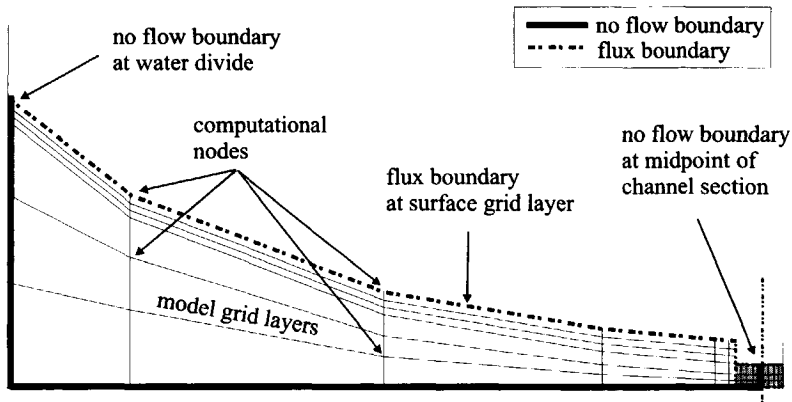


Figure 3.14: Cross-sectional presentation of hill slope finite element mesh with applied boundary conditions.

Atmospheric water and interception

Interception is simulated by a modified form of 'the Rutter' interception model approach (Rutter et al., 1975) and takes account of the size of the area covered by vegetation and a leaf area index. The output of the interception module is an effective precipitation depth that is used as a surface layer input flux. For periods of overland flow, evaporation is simulated at a potential rate and is subtracted from the overland flow water depth. For simulation periods without overland flow, the actual evaporation rate is modelled by a linear function of the ratio of actual and potential evaporation and the soil water potential (fig.3.15). In this figure ψ_w is the capillary soil potential at wilting point, ψ_i is the capillary soil potential at which evaporation is maximum, ψ_s is the an-aerobiosis point at which evaporation falls to zero. Potential evaporation is calculated by the Penman-Monteith equation (1975). The method is described by Feddes et al., [1976]. The evaporation fluxes from a grid element are calculated by regarding the size of the vegetative cover and a root density function.

Results

The performance of IHDM is tested on few, small sized, upland catchments in mid-Wales. The most comprehensive study is reported by Calver [1988] and deals with the calibration, sensitivity and validation of the Tanllwyth catchment model. This catchment has a size of 0.92 km²

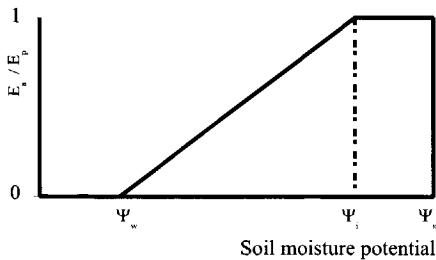


Figure 3.15: *Dependency of actual evaporation, E_a , on potential evaporation, E_p , and capillary soil potential, ψ , (Feddes et al., 1976).*

and has a predominantly coniferous forest land cover. Performance tests on models created by IHDM are realised for four individual rainstorm events. One event was used for model calibration, the other events were used for model validation. The catchment was partitioned in two hill slope sections and one channel section. Required model input data are, a topographic description of the catchment, effective precipitation depth, roughness coefficients for overland and channel flow, channel width and slope, and for the hill slope sections soil hydraulic properties of porosity, saturated hydraulic conductivity in vertical and horizontal directions, the relation of the saturated hydraulic conductivity, K_s , and the soil water content, θ , and the relation of the soil capillary potential, ψ , and θ (Calver, 1988). The procedure of catchment initialisation for ψ is not described although sensitivity tests towards a change of initial soil water content indicated only minor effects on runoff generation when modelling comparable antecedent winter conditions.

The sizes of the grid elements as applied in the finite difference scheme for the surface layer and also the finite element scheme for the subsurface layer is not described by Calver [1988]. An accurate description on the applied spatial and temporal distributions of the model input parameters and variables also is not presented by Calver [1988]. From the sensitivity analysis and considering the small size of the catchment it is assumed that most catchment parameters and variables are spatially uniformly distributed except for the topographic parameters.

For any soil layer, the soil physical properties also are assumed to be uniformly distributed. Model parameters and variables are obtained by observation or by physical reasoning based on comparable modelling

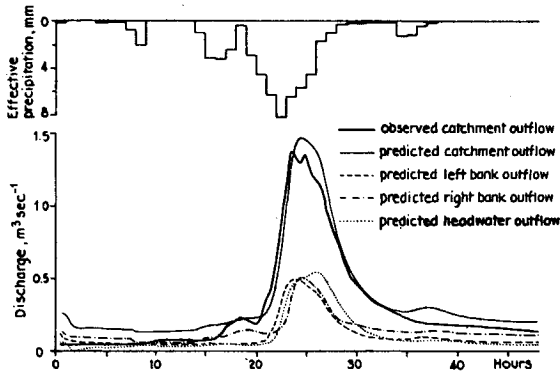


Figure 3.16: Best fit simulations for the storm event of 19 Nov. 1977 on Tanllwyth catchment (Calver, 1988).

efforts. This resulted in a data set where a best-fit simulation run could be produced. In figure 3.16 the simulated and measured hydrographs and lateral flow and headwater contributions to catchment outflow are presented. Calver [1988] stated that runoff is primarily due to saturation overland flow as caused by exfiltration. About 15% of the runoff volume is due to base flow contributions as caused by groundwater flow while the remaining 85% of the runoff volume is due to overland flow.

Sensitivity tests focus on describing the effect

“key physical variables of hydraulic conductivity, porosity, initial water content and surface roughness” (Calver, 1988) have on runoff generation”.

In the tests it appeared that IHDM is very sensitive towards a change of the saturated hydraulic conductivity. Higher conductivities result in lower peak discharges while lower conductivities produce higher peak discharges. By an understanding of the saturation excess mechanism, this model behaviour is surprising and is in contradiction with real world physics. A change of the porosity yielded only observable effects in the initial stages of simulation due to a change of the storage capacity. When the porosity decreases the runoff peaks appear to be higher and at an earlier stage in the simulation while the inverse holds for an increase of the porosity.

The sensitivity towards a change of the surface roughness coefficients indicated a major effect. The peak discharge as well as the time to peak

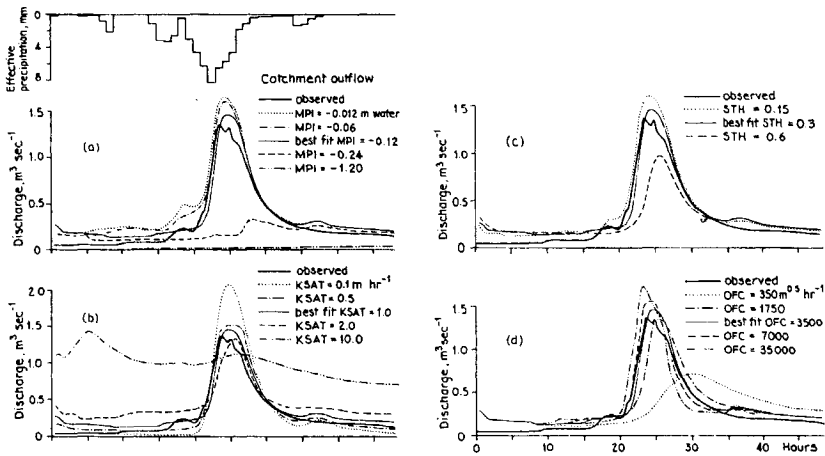


Figure 3.17: Sensitivity of model output to a) initial water potential (ψ_i), b) saturated hydraulic conductivity (K_s), c) porosity (P_o), and d) overland flow roughness coefficients (C_h) (Calver, 1988).

appeared to be sensitive to the roughness coefficients. The high sensitivity is explained by the high overland flow contributions to catchment runoff. Figure 3.17 presents an overview of the sensitivity tests. In an article about the application of IHDM to the Wye catchment in mid-Wales, Beven et al., [1985] also report a high sensitivity towards the saturated hydraulic conductivity and the Chézy roughness coefficient. Calver [1988] validated the Tanllwyth catchment model for 3 additional rain storm events with similar meteorological and physiographic catchment conditions. In the simulations calibrated parameter values were used in the validation runs. For all three rain storm events it was concluded that measured and simulated hydrographs fitted fairly well.

Remarks

Some remarks about IHDM can be made:

- The performance of IHDM to small-scale experimental catchments in general is satisfying. The overall simulation results are promising although the sensitivity test toward the saturated hydraulic conductivity showed some unexplainable model behaviour. It is concluded that the model concept of IHDM is very suitable for

simulating the runoff generation mechanisms of saturation and Horton overland flow and rapid groundwater flow.

- IHDM performance on larger scale catchments with spatially variable physiographic and climatic characteristics and (multi layer) geological conditions is not studied and is uncertain.
- Although the simulation results are satisfying the usefulness of the selected spatial discretisation of the DEM in terms of 'hill slope planes' compared to rectangular grid elements is not proven. It is also questionable whether the topographic discretisation should make up the applied spatial discretisation of the subsurface in plane perspective.
- The kinematic wave approximation for surface water flow as combined with Richards equation for simulation of subsurface flow appears to be well suited for simulation of rainfall-runoff processes in sloping areas. In the articles about IHDM it is clear that, when applying these equations, effective values for model parameters must be applied.
- Model sensitivities to applied temporal and spatial rainfall distributions are not described by Rogers et al., [1985], Beven et al., [1987] or Calver [1988].
- Changes of land use can be simulated based on physical reasoning and must be quantified in terms of changed porosity, saturated hydraulic conductivity and possibly overland flow roughness coefficients.

3.3.4 Distributed Basin Simulator (DBSIM)

Cabral et al., [1990] and Garrote and Bras [1995a] report about the development of the DBSIM at the Massachusetts Institute of Technology (MIT). They characterise DBSIM as;

"a distributed physically-based, rainfall-runoff model incorporating topography for real-time flood forecasting at catchment scale".

Introduction

In the model concept of DBSIM, runoff is generated by saturation overland flow, perched subsurface flow and groundwater flow. Garrote and Bras [1995a], state that the model concept consists of two major components that are the runoff generation module and the flow routing module. Spatial distributions of topography, rainfall and soil hydraulic parameters in a catchment model are represented by a grid system

applying rectangular grid elements of equal size. A DEM is used to simulate terrain slopes and the channel network system. Terrain slopes of the surface layer grid elements are characterised by a slope gradient and slope aspect, the channel network segments are indexed through a Strahler order scheme. The channel network is automatically generated by an upstream element calculation procedure. Based on a user defined threshold value of upstream grid elements that drain to a channel grid element, grid elements are characterised as a channel element. Overland flow and channel flow routing are simulated by a travel time procedure. Such procedure basically is a conceptual routing procedure and is not based on conservation equations of mass and momentum. For this reason the DBSIM concept cannot be classified as a PBRR code as been done by Cabral et al., [1990] and Garrote and Bras [1995a]. In this thesis the code is selected for evaluation since the subsurface flow processes are simulated based on partial differential equations of mass en momentum conservation and since the model concept differs significantly from the other concepts.

For simulation of spatial rainfall distributions over a catchment Thiessen polygons are applied where rainfall depths are simulated at each model grid element. Subsurface flow in saturated and unsaturated conditions is simulated by kinematic approximations of conservation equations of mass and momentum. The kinematic approximation implies that the hydraulic gradients are due to gravitational forces only.

Soil hydraulic parameters are distributed over the model grid layer based on a soil type classification. Parameter values of the catchment models are obtained through field observation or from literature. Infiltration and unsaturated subsurface flow are simulated within a grid element by soil water accounting procedures. For the simulation of infiltration and unsaturated subsurface flow, analytical solutions of combined continuity equations of momentum and mass are applied in one-dimensional, vertical perspective. Infiltration at the land surface is simulated for saturated (i.e. ponded surface) and for unsaturated conditions. For simulation of perched subsurface flow, groundwater flow equations are applied to computational nodes of the subsurface grid elements that make up the saturated model domain.

Flow schematisation

Land surface

In DBSIM overland flow runoff is assumed to be a stream flow process rather than a sheet flow process. Cabral et al., [1990] report that overland flow and channel flow routing are simulated by travel time procedures. Model parameters required to define the travel time are the length of the flow path and the flow velocity value. The routing of overland flow across the DEM grid elements is simulated from upslope elements to elements that represent the channel network system through the flow path with highest gradients. In Cabral et al., [1990] the velocity value for overland flow and channel flow are assumed to be time-invariant and are spatially uniformly distributed over the catchment grid elements and the channel network elements respectively. 'Effective' velocity values are obtained through calibration by fitting the simulated hydrographs to the observed (Garrote and Bras, 1995a). A modification towards the routing module is reported by Garrote and Bras [1995a] and dealt about introducing the power law relation of Eq.[3.28] By this approach the relation between catchment discharge and the hill slope flow velocities are described. The hill slope flow velocity becomes a time variant property that is subject to catchment runoff as simulated at the grid elements. The average hill slope velocity value, $v_{h(\tau)}$, is calculated by:

$$v_{h(\tau)} = c_v [Q_{\tau,o}(\tau)]^r \quad [3.28]$$

Calibration parameter r controls the degree of catchment non-linearity while by coefficient c_v , the unique relation between catchment discharge at the catchment outlet, $Q_{\tau,o}(\tau)$, and the average hill slope flow velocity is simulated. In DBSIM channel flow velocities also become time variant since these are calculated by a factor, ξ , expressing the ratio of average hill slope flow velocity, $v_{h(\tau)}$, and the average channel flow velocity, $v_{c(\tau)}$.

In the travel time procedure the loss of channel water due to infiltration is ignored. Garrote and Bras [1995a] present the convolution equation [3.29] for simulating surface runoff at the catchment outlet by all runoff contributions at the saturation overland flow source area:

$$Q_{Ac(t)} = \int_0^t \int_0^{A_c t} R_{v(x,y,\tau)} h_{(x,y,t-\tau)} d\tau dA_c \quad [3.29]$$

where

- $Q_{Ac(t)}$ = calculated surface runoff of the catchment [L³ T⁻¹]
- $R_{v(x,y,\tau)}$ = function describing the rate of runoff generation [L T⁻¹]
- $h_{(x,y,t-\tau)}$ = instantaneous response function of a grid element [T⁻¹]
- t, τ = time instants [T]
- A_c = size of catchment area [L²].

For every time instant τ , the instantaneous response function of a grid element, $h_{\tau(x,y,t)}$, is simulated by a Dirac delta function of travel times:

$$h_{\tau(x,y,t)} = \delta \left[\frac{l_h}{v_{h(\tau)}} + \frac{l_c}{v_{c\tau}} \right] \tag{3.30}$$

where l_h and l_c are the length of the hill slope flow path and channel flow path respectively. By the travel time procedure no distinction is possible if overland flow is in the form of sheet flow and/or stream flow.

Unsaturated zone

Infiltration is simulated through a wetting zone that at top and the bottom is bounded by a saturated front. The depths of both fronts are dynamic properties and are subject to the simulated unsaturated and/or saturated flow conditions (see fig.3.18). Soil hydraulic parameters required are the saturated and unsaturated hydraulic conductivity, the saturated and residual soil water content and a pore size distribution index. Infiltration rates are simulated by a kinematic flow equation as based on conservation equations of mass and momentum.

The governing equation is applied in a one-dimensional, vertical perspective and is solved for unsaturated and saturated flow conditions. In unsaturated flow conditions the soil water distribution at the infiltration front forms a sharp interface. The one-dimensional discretised form of the continuity equation reads:

$$\frac{d\theta}{dt} + \frac{dq_{z(\theta)}}{dz} = 0 \tag{3.31}$$

where

- $q_{z(\theta)}$ = specific discharge at depth z and subject to θ [L T⁻¹]
- θ = volumetric soil water content [-]
- t = time [T]
- z = depth below surface [L].

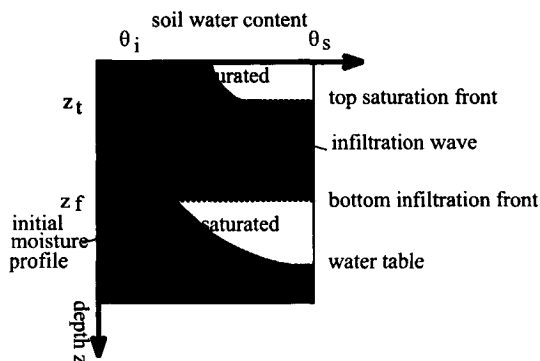


Figure 3.18: Soil water profile in a grid cell (Garrote and Bras, 1995a).

The infiltration model is based on the kinematic assumption that imposes that hydraulic pressure gradients are due to gravitational forces only. The general Darcy equation for simulating subsurface flow in unsaturated flow conditions has the form:

$$q_{z(\theta)} = -K_{(\theta)} \left(\frac{\partial \Psi_{(\theta)}}{\partial z} + 1 \right) \quad [3.32]$$

where

$K_{(\theta)}$ = hydraulic conductivity at water content θ [L T⁻¹]

$\Psi_{(\theta)}$ = soil pressure head [L].

By the kinematic flow assumption $q_{z(\theta)}$ becomes equal to the hydraulic conductivity as subject to the volumetric soil water content, θ . When z is defined positive in downward direction $q_{z(\theta)} = K_{(\theta)}$.

In the infiltration model the unsaturated hydraulic conductivity, $K_{(\theta,z)}$, for any depth z , is defined by the Brooks Corey equation (Brooks Corey, 1964):

$$K_{(\theta,z)} = k_{s(z)} \left(\frac{\theta - \theta_r}{\theta_s - \theta_r} \right)^\lambda \quad [3.33]$$

where

$K_{s(z)}$ = saturated hydraulic conductivity at depth z [L T⁻¹]

θ = volumetric soil water content [-]

θ_s = saturated water content [-]

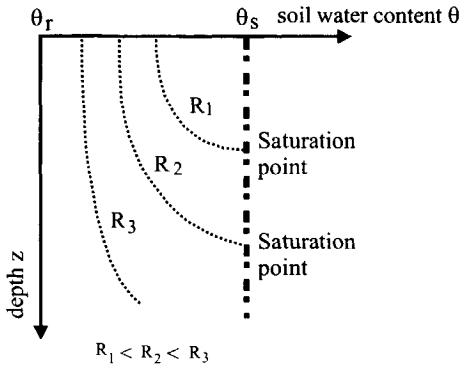


Figure 3.19: Soil water profiles, $\theta_{(R,z)}$, for rainfall rates $R_{1..3} < K_s$ (Cabral, 1990).

- θ_r = residual water content [-]
- λ = pore size distribution index [-].

For the saturated hydraulic conductivity the assumption is made that the conductivity decreases exponentially with depth. Field evidence to support this assumption is presented by Beven [1982, 1984].

$$K_{s(z)} = K_0 \times e^{-fz} \tag{3.34}$$

where

- $K_{s(z)}$ = the saturated hydraulic conductivity at depth z [L T⁻¹]
- K_0 = the saturated hydraulic conductivity at the land surface [L T⁻¹]
- f = a parameter [L⁻¹].

The general description of the distribution of the hydraulic conductivity over depth, $K_{(\theta,z)}$, is obtained by substituting the expression of $K_{s(z)}$ Eq.[3.34] in Eq.[3.33]:

$$K_{(\theta,z)} = k_o e^{-fz} \left(\frac{\theta - \theta_r}{\theta_s - \theta_r} \right)^\lambda \tag{3.35}$$

Cabral et al., [1990] introduce in the DBSIM approach a ‘critical’ depth, $z^*_{(R)}$, that is defined as the depth the actual rainfall rate, R , is assumed to be equal to the saturated hydraulic conductivity, $K_{s(z)}$. By substitution of $z^*_{(R)}$ for z in Eq.[3.34] and when solving this equation for $z^*_{(R)}$, an expression is obtained for calculating the depth of the infiltration front as subject to the rainfall rate:

$$Z^*_{(R)} = \frac{1}{f} \cdot \ln \frac{K_0}{R} \quad [3.36]$$

Flow conditions at the infiltration front are unsaturated for $z < z^*_{(R)}$ and saturated for $z > z^*_{(R)}$.

For simulating the soil water content in the subsurface, the actual rainfall rate, R , is substituted for $K_{(\theta,z)}$ in Eq.[3.35] and solved for the water content. By this procedure, the water content at certain depth becomes a function of the rainfall rate and is expressed by $\theta_{(R,z)}$. The water content, $\theta_{(R,z)}$, is calculated by the Brooks Corey equation Eq.[3.33] when this equation is rewritten for $\theta_{(R,z)}$:

$$\theta_{(R,z)} = \left(\frac{R}{K_0} \right)^{\frac{1}{\lambda}} \cdot e^{\frac{f \cdot z}{\lambda}} \cdot (\theta_s - \theta_r) + \theta_r \quad [3.37]$$

By Eq.[3.37] the exponential decrease of the subsurface water content above the infiltration front is simulated. Figure 3.19 presents soil water profiles that are functions of the rainfall rate and are simulated by Eq.[3.37].

The change of the hydrologic state of a grid element is defined by the continuity equation Eq.[3.31] where both equation terms are integrated over depth:

$$\frac{d}{dt} \int_{z_1}^{z_2} \theta \cdot dz + \frac{d}{dz} \int_{z_1}^{z_2} q_{z(\theta)} \cdot dz = 0 \quad [3.38]$$

The second term of Eq.[3.38] is defined by substitution of the actual rainfall rate, R , for the flow discharge $q_{z(\theta)}$ at the land surface (i.e. depth z_1) and by substitution of the catchment recharge rate, R_i , for $q_{z(\theta)}$ at the water table depth (i.e. depth z_2):

$$\frac{d}{dt} \int_{z_1}^{z_2} \theta \cdot dz + R - R_i = 0 \quad [3.39]$$

The catchment recharge rate, R_i , is calculated by Q_{base} / A_c where Q_{base} is the observed base flow in [$L^3 T^{-1}$] and A_c the catchment area [L^2].

The first term of Eq.[3.39] expresses the change of the total soil water content between the land surface and the water table over time. By Eq.[3.37] the soil water distribution over depth, $\theta_{(R,z)}$, is defined as

function of the rainfall rate, R , and the initial soil water distribution, $\theta_{(R_i, z)}$, as subject to the catchment recharge rate, R_i .

The total water content of a grid element is simulated through integration of the soil water distribution between the land surface at depth z_1 and the infiltration front at depth, z_f , and through integration of the distribution between the infiltration front and the water table at depth z_2 :

$$\int_{z_1}^{z_2} \theta .dz = \int_{z_1}^{z_f} \theta_{(R, z)} .dz + \int_{z_f}^{z_2} \theta_{(R_i, z)} .dz \tag{3.40}$$

When replacing $\theta_{(R, z)}$ and $\theta_{(R_i, z)}$ with simulated water distributions as expressed by Eq.[3.37] this yields:

$$\begin{aligned} \int_{z_1}^{z_2} \theta .dz = & \left(\frac{R}{K_0} \right)^{\frac{1}{\lambda}} (\theta_s - \theta_r) \left(\frac{\lambda}{f} \right) \left(e^{\frac{f \cdot z_f}{\lambda}} - e^{\frac{f \cdot z_1}{\lambda}} \right) + \theta_r (z_f - z_1) + \\ & \left(\frac{R_i}{K_0} \right)^{\frac{1}{\lambda}} (\theta_s - \theta_r) \left(\frac{\lambda}{f} \right) \left(e^{\frac{f \cdot z_2}{\lambda}} - e^{\frac{f \cdot z_f}{\lambda}} \right) + \theta_r (z_2 - z_f) \end{aligned} \tag{3.41}$$

The first term of Eq.[3.39] is obtained by differentiating Eq.[3.40] with respect to time:

$$\frac{d}{dt} \int_{z_1}^{z_2} \theta .dz = \frac{dz_f}{dt} \left[\theta_{(R, z_f)} - \theta_{(R_i, z_f)} \right] \tag{3.42}$$

or, when regarding Eq.[3.41]:

$$\begin{aligned} \frac{d}{dt} \int_{z_1}^{z_2} \theta .dz = & \frac{dz_f}{dt} \left[\left(\frac{R}{K_0} \right)^{\frac{1}{\lambda}} (\theta_s - \theta_r) e^{\frac{f \cdot z_f}{\lambda}} + \theta_r \right] - \\ & \frac{dz_f}{dt} \left[\left(\frac{R_i}{K_0} \right)^{\frac{1}{\lambda}} (\theta_s - \theta_r) e^{\frac{f \cdot z_f}{\lambda}} + \theta_r \right] \end{aligned} \tag{3.43}$$

By substitution of Eq.[3.42] in Eq.[3.39] the expression for simulating the change of the depth of the wetting front in time, dz_f / dt , for unsaturated flow conditions is given:

$$\frac{dz_f}{dt} = \frac{R - R_i}{\theta_{(R,z_f)} - \theta_{(R_i,z_f)}} \quad [3.44]$$

Infiltration under saturated flow conditions is simulated by basically the same flow equations were they are adapted to the saturated flow conditions. The saturation of the subsurface occurs when the infiltration front has passed the critical depth $z_{(R)}^*$.

When $z_f > z_{(R)}^*$, a perched zone develops where the depth of the saturated infiltration front, z_f , and the depth of the top, z_t , of the perched zone must be calculated.

The change of the depth of the saturated infiltrated front over time is simulated by:

$$\frac{dz_f}{dt} = \frac{K_0 \cdot e^{-f \cdot z_f} - R_i}{\theta_s - \theta_{(R_i,z_f)}} \quad [3.45]$$

When comparing Eq.[3.45] to Eq.[3.44], the differences between both equations are due to the substitution of K_s for R and θ_s for $\theta_{(R,z_f)}$. K_s is expressed in the form of Eq.[3.34]. The bottom of the perched zone moves downward when $K_{z(\theta,z_f)} > R$.

The change of the top of the perched zone, z_t , over time is simulated by:

$$\frac{dz_t}{dt} = \frac{K_0 \cdot e^{-f \cdot z_t} - R}{\theta_s - \theta_{(R,z_t)}} \quad [3.46]$$

When comparing Eq.[3.44] to Eq.[3.43] the differences between both equations are due to the replacements of R for R_i and $\theta_{(R,z_t)}$ for $\theta_{(R_i,z_f)}$. The top of the perched zone moves upward in case $K_s < R$.

The infiltration equations Eq's.[3.42], [3.43] and [3.44] is solved for heterogeneous soils and for spatially variable rainfall rates. An extensive description of the infiltration model and the vertical subsurface flow model is presented in the work of Cabral et al., [1990].

For simulating mass conservation within a model grid element, the total water depth above the wetting front, M_t , is introduced as a third state variable. The total water depth, M_t , of a model grid element can change due to infiltration that is expressed by infiltration rate $M_{in(R,K_0)}$, due to a change of the wetting front depth, or due to subsurface inflow, $Q_{ss,in}$, and/or subsurface outflow, $Q_{ss,out}$:

$$\frac{dM_t}{dt} = \frac{dz_f}{dt} \theta_{(R_t, z_f)} + M_{in(R, K_0)} + \frac{Q_{ss, in} - Q_{ss, out}}{A_e} \tag{3.47}$$

where A_e is the size of an grid element. Exfiltration is simulated when M_t exceeds the water storage capacity of the column of subsoil above the wetting front.

Perched subsurface runoff, Q_{ss} from a grid element is simulated for saturated flow conditions only. The applied flow equation has the form:

$$Q_{ss} = W \int_{z_1}^{z_f} q_{sh(z)} dz \tag{3.48}$$

where W is the width of flow and $q_{sh}(z)$ is the specific horizontal subsurface flow at depth z that is calculated by (Bras et al., 1990):

$$q_{h(z)} = \frac{\tan(\alpha) \tan(\alpha)_d}{\tan(\alpha) + \tan(\alpha)_d} K_0 e^{-fz} \tag{3.49}$$

(α) And $(\alpha)_d$ are the hill slope gradient and lateral deflection angle respectively of the infiltration front with respect to the vertical direction. The lateral deflection angle expresses the angle of deflection of infiltrated water due to the exponential decrease of the saturated hydraulic conductivity over depth, $K_{z1} \neq K_{z2}$, this as expressed by factor f . The saturated conductivity above the wetting front is higher than at the wetting front thus flow is constraint by continuity. This causes a lateral deflection of flow above the wetting front at an angle α_d with respect to the vertical direction.

The governing equation for perched subsurface flow reads:

$$Q_{ss} = W.K_0 \cdot \cos(\alpha) \cdot \sin(\alpha) e^{-\frac{f \cdot z_f}{\lambda}} \left[\frac{1}{f} \cdot (e^{-fz_f} - e^{-fz_1}) - (z_f - z_1) \right] \tag{3.50}$$

Cabral et al., [1990] prove that this equation is equal to Eq.[3.48].

The routing of perched subsurface flow across the catchment grid is simulated by an 'element coupling' procedure (Cabral et al., 1990). The coupling procedure basically is a water accounting procedure where outflow from a grid element is the inflow to the neighbouring grid element that is characterised by the highest down slope gradient. The total flow into an element will be equal to the summation of the outflows of the surrounding upslope elements. The hydrologic state of an element is updated by the inflow and outflow after which, by the new hydrologic

state, the lateral subsurface discharge is calculated. Interactions between groundwater flow and channel flow is simulated in the channel network grid elements.

Saturated zone

In DBSIM, groundwater flow equations are applied to simulate groundwater flow and to initialise the catchment model in terms of the depth of the water table across the grid elements. This depth is simulated by Eq.[3.51] that combines Eq.[3.46] and Eq.[3.48] where the subsurface inflow and outflow equations are substituted. The depth of the water table, z_{wt} , is simulated by:

$$\frac{dz_{wt}}{dt} = \frac{\frac{Q_{in} - Q_{out}}{A_e} - R_i}{\theta_s - \theta_{(R_i, z_{wt})}} \quad [3.51]$$

The subsurface outflow equation Eq.[3.48], as applied to the groundwater flow domain reads:

$$Q_{out} = W \int_{z_{wt}}^{z_{imp}} K_0 \cdot e^{-fz} \cdot \frac{\Delta\phi}{\Delta x} dz \quad [3.52]$$

where

Q_{out} = groundwater discharge out of grid element	$[L^3 T^{-1}]$
W = width of flow perpendicular to the direction of flow	$[L]$
ϕ = hydraulic head	$[L]$
z_{imp} = depth of impervious base	$[L]$.

In case of a relatively deep single aquifer this equation changes to:

$$Q_{out} = W \tan(\alpha) - \frac{Z_{wt(i)} - Z_{wt(j)}}{L} \frac{K_0}{f} e^{-fz_{wt}} \quad [3.53]$$

where (α) is the hill slope gradient and where $Z_{wt(i; j)}$ are the depths of the water table for the elements i and j with j situated downstream from element i . For simulation of the groundwater flow across the grid elements an approach similar to the element coupling scheme for simulating subsurface runoff is applied. The order of computation starts at the catchment boundary where Q_{out} of grid element i is substituted for Q_{in} of the downstream grid element j .

The groundwater flow system is assumed to have one aquifer only that is recharged at the constant recharge rate, R_i , throughout the catchment.

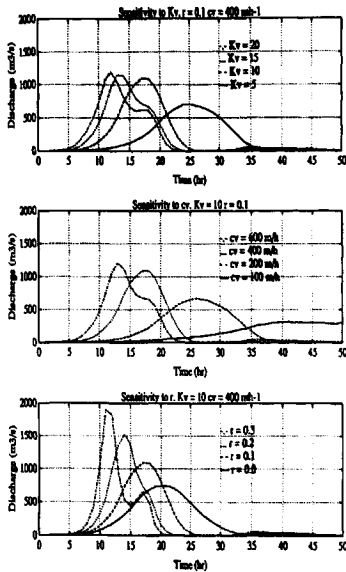


Figure 3.20: Sensitivity of basin response to surface flow routing parameters (Garrote and Bras, 1995a).

Results

Cabral et al., [1990] and Garrote and Bras [1995a] report on model validation tests on the ungauged Sieve catchment in the Tuscany region in Italy. The Sieve catchment has a size of 840 km² and has moderate to steep hill slopes. The average elevation is 470 m. above mean sea level with a highest point at 1657 m. The catchment is partitioned in a grid layer with squared grid element of 400 m. (one element equals approximately 0.019% of the total catchment area). Cabral et al., [1990] state;

“the resolution of 400 m. seems to be lower than the desirable element scale for the appropriate representation of the catchment relief. The DEM resolution disables the detailed modelling of the catchment drainage system”.

In the catchment model of the river Sieve, a channel flow grid element is generated in case a grid element of the DEM has more than 8 cumulative upslope grid elements.

In the Sieve catchment model 17 different soil types are distinguished. For the different soil types the soil hydraulic parameters K_0 , θ_s , θ_r , and λ are determined either by observation at similar soils in other catchments or from data in literature. Subsurface model parameter values are obtained by averaging the available data. Parameter values are simulated as function of the soil type and are lumped at the spatial scale of the grid elements. Cabral et al., [1990] report that the spatial rainfall distribution over the catchment grid is simulated by Thiessen polygons where data from four measuring stations is used. Due to the distribution of the stations only one station is situated in the catchment causing this station to cover 75 % of the catchment area. Since orographic effects have a significant effect on the spatial rainfall distribution (Cabral et al., 1990), it is questionable whether the applied rainfall distributions are appropriate for accurate rainfall-runoff modelling. The temporal resolution is simulated by time intervals of 20 minutes. For some rainfall events, rainfall data of 6 stations are available with a gauging resolution of one hour. Garrote and Bras [1995b] report in an article about DBSIM the option of applying radar recorded rainfall distributions in DBSIM. Simulation results however are not reported.

Cabral et al., [1990] report the use of 12 rain storm events for model testing and model calibration. Spatially uniform flow velocity values for overland flow and channel flow have been obtained by calibration. Calibrated flow velocities are 0.11 m/s for overland flow and 1.66 m/s for channel flow. Garrote and Bras [1995a] apply the travel time procedure according to Eq.[3.26] and Eq.[3.27]. It appears that the model is very sensitive to travel time parameters K_v , c_v , and r as shown in figure 3.20.

The magnitude of the peak runoff rate, the shape of the hydrograph and the lag time of the peak runoff are very sensitive to the model parameters.

For model simulation, the Sieve catchment is initialised for 'typical wet', 'averaged' and 'dry' antecedent catchment conditions. Such initialisation is based on the monthly base flow discharges that have probabilities of exceedance of 10%, 50% and 90% respectively. Such percentages are defined by long term base flow observations and represent statistical probabilities of exceedance of averaged monthly minimum flow discharges

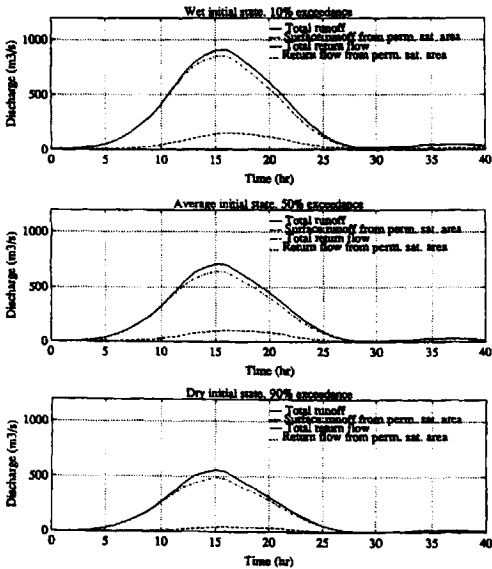


Figure 3.21: Catchment response decomposed for different runoff contributions, antecedent catchment conditions with 0, 50 and 90% probability of exceedance (Garrote and Bras, 1995a).

The base flow discharge relates to the catchment recharge rate and so to the depth of the water table as simulated by Eq.[3.47] and to the initial soil water distribution through $\theta_{(Ri,z)}$ analogues to Eq.[3.35].

The selected catchment conditions are simulated by Cabral et al., [1990] for all 12 rainstorms to study the effect of the initial state of the catchment on the accuracy of a simulation. Garrote and Bras [1995a] reported that the effect of the catchment initial condition was significant (see fig. 3.21) and can increase even more in case different combination of parameter values is used. Recharge rates in BDSIM also are defined by use of observed base flow observations.

During model testing it appeared that the catchment model was sensitive to parameter f expressing the exponential decrease of the saturated hydraulic conductivity with depth. By an understanding of the runoff generation mechanisms of perched subsurface flow and saturation overland flow, the sensitivity of the catchment model to parameter f can be explained. During model calibration f is defined at $5 \cdot 10^{-4} \text{ mm}^{-1}$ for the Sieve catchment model and is simulated as a constant for the entire

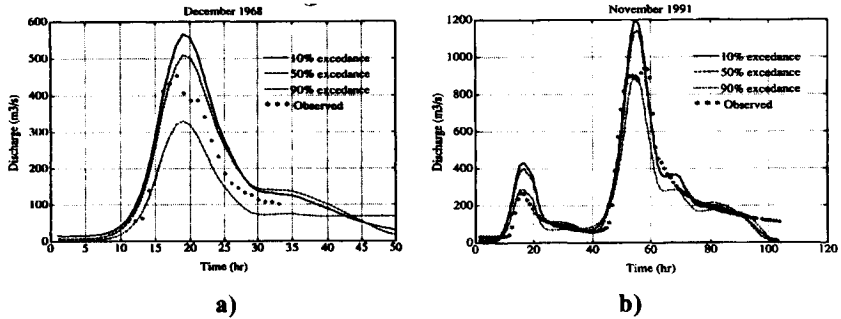


Figure 3.22: Observed and predicted hydrographs for two storm events by considering effects of the initial state of the catchment (Garrote and Bras, 1995a).

catchment area. Cabral et al., [1990] conclude that the saturated hydraulic conductivity is the most sensitive parameter in DBSIM for runoff generation.

Out of a wide range of model simulations a best fit simulation for a storm event of December 1968 is presented by Garrote and Bras [1995a]. Figure 3.22a presents these results as obtained by applying calibrated values for travel time parameters and subsurface flow parameters. For the simulation, the catchment is initialised for wet, average and dry conditions. Figure 3.22b presents simulation results for a rain storm in November 1991. These results are obtained by applying validated model parameters to a rainfall-runoff event that is gauged by 30 rainfall stations and a continuous channel flow gauge. The results appear to be accurate in terms of timing of the peak discharge volume and the shape of the hydrograph. The effect of the temporal rainfall gauging distribution is not described although Garrote and Bras [1995b] suggest that radar generated rainfall data could produce better simulation results.

Remarks

Some general remarks can be made about the modelling efforts.

- Model simulations rely on a conceptual travel time procedure for simulating surface runoff across the DEM. By such a procedure, runoff only is predicted at the location of the stream gauge and effects of wave propagation through the channel network are ignored. Also the effects the (distributed) inflow of overland along a channel reach

as well as groundwater inflow is ignored. A major advantage of this procedure is the parsimonious model parameterisation.

- The applicability of the model concept has to be tested on smaller size catchments too since it is expected that scale effects of model input parameters and variables become more pronounced in catchment models of smaller size.
- The simulation of the overland flow source areas through the presented infiltration procedure and the catchment initialisation procedure appears to be suitable in rainfall-runoff modelling. Both procedures depend only on the catchment recharge rate and the exponential decrease of saturated hydraulic conductivity with depth. Such an approach is very beneficial with regard to the limited number of subsurface model parameters that are required.
- Simulation runs are expected to improve significantly when the saturated hydraulic conductivity at the land surface and the factor f are simulated more accurate.
- For simulating catchment runoff a limited number of model parameters is required. This is the most advantageous aspect of the DBSIM model concept since catchment parameterisation becomes less uncertain.

3.4 Conclusions

In the literature review of section 3.2 it is concluded that the hydrologic catchment behaviour that causes the generation of catchment runoff is well understood. The behaviour of single flow processes as well as aggregated flow processes and the runoff production mechanisms are well described in literature and descriptions are based on and supported by field evidence.

For simulating the runoff generation mechanisms and flow processes, a small number of PBRR computer codes are developed. Such codes primarily are developed during the late eighties and early nineties by the desire to describe the rainfall-runoff relation in a physically consistent and distributed manner. At the time it was believed that by such modelling approach the effects of land use changes in particular could be simulated and that simulation results could be analysed based on physical

reasoning. Designed model concepts of PBRR modelling approaches were fundamentally different from common conceptual model approaches like the lumped Sacramento or distributed Topmodel approaches.

Research in the field of PBRR modelling focused on designing valid model concepts and developing mathematical models for the simulation of the runoff generation mechanisms. Models must be able to describe and to simulate the highly dynamic, non-linear real world runoff behaviour at the catchment scale. By reviewing the research developments and by evaluating PBRR model concepts presented in literature it is concluded that, although simulation results in general are satisfying, PBRR modelling is still in a phase of research. Objective conclusions to the 'best suitable' or 'most optimal' model concept cannot be drawn since comparative studies are not executed. For each of the models described in the sections 3.3.1 - 3.3.4 a number of remarks are made in this thesis and conclusions only can be drawn by comparison of the designed model concepts, data requirements and by analysis of the simulation results.

3.4.1 Model concepts

By an analysis and comparison of the model concepts of SHE, IHDM, THALES and DBSIM, as described in the sub-sections 3.3.1 - 3.3.4 respectively, it is concluded that significant differences exist. Differences primarily are due to a small number, but fundamental and elementary, modelling considerations and assumptions. In the IHDM and THALES model concepts for example, much emphasis is laid upon the accurate representation of topography by use of raster DEM with non-rectangular and a-symmetrically spaced grid elements while in the SHE and DBSIM model concepts rectangular and symmetrically spaced elements of equal size are applied. The simulation of geometric catchment parameters such as elevation, channel network layout and also subsurface geometry depend on the chosen partitioning theory the land surface is simulated with. Differences in model concepts also are due to the number of flow processes simulated and selected process schematisations. As a consequence, model equations, model algorithms and data requirements differ. The last factor that causes differences is the number and approach the meteorological processes are simulated.

Evaluation of each of these differences with respect to the simulation results is difficult since comparative modelling studies on selected catchments are not reported in literature. Model concepts have different degrees of complexity and are applied to catchments of local and regional scale in different climatic zones while catchments are characterised by different physiographic subsurface properties. For this reason it is concluded that each of the four model concepts has some deficiency in representing the real world runoff behaviour. A common catchment characteristic that is dealt with in any of the catchment models is the simulation of the undulating hill slope topography.

Conclusions on suitability (of parts) of model concepts must be based on an inventory of the simulated flow processes, the applied model algorithms and specific aspect of the model concept like applied spatial discretisations in three-dimensional model space.

In table 3.3 meteorological and hydrologic processes are shown that are simulated in the approaches. Numbers in the table correspond to the flow processes considered in the lower table. In table 3.4 some characteristics of the model concepts are presented that relate to for example the applied catchment partitioning theory in terms of the applied DEM, the number of subsurface model layers and the size of grid elements. Characteristics of applications relate to the catchment scale size and the time domain.

By these tables and the descriptions in sub-sections 3.3.1 - 3.3.4, a number of conclusions are drawn.

1. In the design of the four model concepts the generation of saturation overland flow and rapid subsurface storm flow is allowed for. All concepts are valid to simulate the rainfall-runoff relation although simulation results of THALES are very poor.
2. The effectiveness of the use of non-rectangular grid elements of variable size for simulating overland flow and channel flow compared to the use of rectangular grid elements has not been proven to be favourable. Although in real world systems the shape of the land surface has a (major) effect on the rainfall-runoff relation, it is concluded that the shape of the land surface also is reasonable well described by DEM's with rectangular grid elements. The size of the rectangular elements should be relatively small while, as applied in

SHE, the overland flow algorithm must be solved in two flow directions over the grid.

3. The effect of the adaptation of the land surface discretisation to the subsurface is uncertain with regard to the performance of catchment models. By the fact that runoff generation by saturation overland flow is a result of the groundwater behaviour it is surprising that such procedure is not questioned and hardly discussed in literature. In research much emphasis is laid on representing the topography in a model as accurate as possible but this emphasis is lacking when representing the subsurface geometry and heterogeneity.
4. The simulation of evaporation and interception is a necessary model requirement when runoff has to be simulated on a continuous time base. For event based modelling this simulation is less restrictive since both processes only have a minor effect on runoff volumes especially when runoff is due to rainfall events of relatively long duration.
5. Spatially uniform or non-uniform distributions are applied for the simulation of the rainfall input. Spatially uniform distributions are applied to small catchments (Grayson et al, 1992 and Beven et al. 1987) while semi-distributions (i.e. Thiessen polygons) are applied to larger scale catchments (e.g. Bathurst et al., 1986a,b and Cabral et al., 1990). The accurate simulation of temporal rainfall distributions is hardly addressed in literature in the field of PBRR modelling. This is surprising since each model concept particularly is developed to show how well the runoff production mechanisms are simulated in the model approaches. The accurate simulation of temporal and spatial rainfall distributions is a pre-requisite in PBRR modelling.
6. The simulation results showed that results are (very) sensitive to the combined effects of the simulated rainfall intensity and the saturated hydraulic conductivity. It is expected that much better simulation results can be obtained if the temporal and spatial rainfall distributions are simulated more accurately and when saturated and unsaturated hydraulic conductivity values are estimated more accurately.
7. For the simulation of overland and channel flow a DEM is required. The flow path at the land surface and the drainage network layout are derived from the DEM that can be based on rectangular grid elements of equal size or non-rectangular grid elements of variable size.

8. Water flow at the land surface is simulated by a diffusive wave or kinematic wave model or by a travel time procedure. Although travel time procedures in general are computationally and parametrically very efficient, its application should be rejected in PBRR modelling since such procedures generally are based on convolution integral procedures. In such procedures the effects of channel flow routing are ignored and cannot be quantified. In the research it is not described what criteria are applied to select either the diffusive wave or kinematic wave equations for simulating channel flow and overland flow.
9. Macro pore flow is not considered explicitly in any of the designed model concepts. Macro pore is simulated as an aggregated flow process in the selected unsaturated zone flow algorithms. Water movement in the unsaturated zone is best simulated by Richards equation. By such approach, the processes of infiltration, unsaturated subsurface flow and exfiltration can be simulated when appropriate boundary conditions at the land surface are implemented. The most important advantage of the use of Richards equation is that the soil saturation in the vicinity of the channel network system is simulated in a distributed manner. In case a soil column becomes over-saturated, exfiltration will occur and saturation overland flow will be generated. Such simulation requires that a) the unsaturated zone model is interactively linked to the groundwater flow model and b) that the subsurface is discretised in a column of grid elements.
10. For simulating groundwater flow the Darcy flow equation is applied. Groundwater flow is simulated in shallow and perched flow conditions where phreatic conditions prevail. Groundwater flow models must be interpreted as rapid groundwater flow models. The thickness of the saturated zone is variable and is simulated in one model layer only. For simulating perched subsurface flow it is a pre-requisite that the unsaturated zone flow algorithm automatically adapts to saturated flow conditions and that lateral flow is simulated as well. The vertical, unsaturated flow algorithm must be able to discharge subsurface water laterally when the vertical drainage capacity is exceeded by the infiltration fluxes.

Table 3.3: Review of hydrologic processes simulated. (Rientjes, 1999a)

Model concept Processes	→				
		1+2+4	1+3	1+2+4	1+4
		1+3	2+4	1+3	2+4
		1	2	1	3
		1	2	2	3
		1	2+3	1	3
		1	2	1	3
		2	2	1	1
		2	1	1	3

Aspects of processes considered

¹ 1 = rainfall	2 = snow melt	3 = uniform	4 = Thiessen
² 1 = canopy interception	2 = no interception	3 = evaporation	4 = no evaporation
³ 1 = diffusive wave	2 = kinematic wave	3 = travel time	
⁴ 1 = diffusive wave	2 = kinematic wave	3 = travel time	
⁵ 1 = Richards	2 = Horton	3 = Smith	4 = other
⁶ 1 = Richards	2 = Darcy	3 = other	
⁷ 1 = Darcy	2 = no perched flow		
⁸ 1 = Darcy	2 = no groundwater flow		

Table 3.4: Model concept characteristics (Rientjes, 1999a)

Model concepts Characteristic	→				
catchment scale applications		2	1	1	4
usage DEM		1	2	2	1
shape grid elements		1	2	2	1
⁴ surface layer element size		2	2	3	1
number of model layers		3	2	3	1
⁵ model type		1+2	2	1+2	2
⁷ computing requirement		1+2+3	3	4	3

Aspects of characteristics

¹ 1 = size < 1 km ²	2 = size < 10 km ²	3 = size < 100 km ²	4 = size > 100 km ²
² 1 = raster	2 = vector		
³ 1 = rectangular	2 = non-rectangular		
⁴ 1 = < 0.15%	2 = < 1%	3 = unknown	
⁵ 1 = 1 layer	2 = ≤ 5 layers	3 = ≥ 10	
⁶ 1 = event based	2 = continuous		
⁷ 1 = mainframe	2 = work station	3 = PC.	4 = unknown

By these conclusions some recommendations are made for defining a most effective and appropriate model concept.

- Rainfall must be simulated accurately in terms of spatial and temporal distributions by use of multiple, spatially distributed rainfall maps and by appropriate temporal distributions. Spatial rainfall distributions can easily be simulated by use of interpolation schemes that, over a raster grid, interpolate rainfall observations at gauging stations. Proposed local and global interpolation schemes are the inverse distance weighing scheme and the Kriging estimation scheme respectively. Temporal distributions must be simulated by use of distribution functions that are based on analysis of time series. Time scales in general, however, can become larger with increasing catchment size since the effects of small-scale temporal rainfall variability will be dampened by storage effects in the subsurface.
- For the simulation of evaporation a simple approach as proposed by Feddes et al. [1976] can be applied. In their approach evaporation is simulated by a loss function since evaporation is interpreted as a loss term in a catchment water balance. Such loss functions have proven to be appropriate descriptors of the evaporation process in runoff modelling and are computationally simple. For event based runoff models the simulation of evaporation is not a necessity since evaporation losses during rainfall events are small. A disadvantage of ignoring the evaporation process is that, prior to the modelling, the initial hydrologic model state (e.g. soil moisture distribution) has to be defined by a procedure that simulates the effect of evaporation. Evaporation acts as an atmospheric loss function and depletes the subsurface. Simulating evaporation is a way of keeping track of the soil moisture storage and distribution in the unsaturated zone for defining the (initial) model state prior to a rainfall event.
- In runoff hydrology it is common knowledge that interception can be relatively large for short duration rainfall events and relatively small for long duration rainfall events. For PBRR modelling interception can be simulated by simple loss functions that are a function of land use.
- For simulating overland flow and channel flow a raster DEM with symmetrically spaced and rectangular grid elements of equal size is appropriate. The size of the grid elements, however, should be

relatively small compared to the size of the catchment model and the DEM should reflect the main topographic catchment features. The use of such a DEM requires that the overland flow algorithm is solved in at least two flow directions (i.e. x, y).

- For simulating overland and channel flow in undulating and hilly catchments the use of the diffusion wave equation is appropriate. This since topographic gradients are relatively high and any change in momentum by changes in the flow velocity over time and along a hill slope plane and channel can be neglected.
- Overland flow must be simulated by the Strickler-Manning equation as a sheet flow process rather than a stream flow process to limit the complexity of the model approach. Compared to the sheet flow approximation, stream flow can be simulated by introducing a dimensionless scale factor to the Strickler-Manning equation. The factor is equal to the ratio of the grid element width to the average width of the real world stream flow paths within the grid element. Such scale factor can be defined through observation or through model calibration.
- The use and integration of a (Hydro-)GIS in the modelling efforts is not described in any of the studies. Topographic attributes like elevation, hill slope gradient, hill slope aspect and catchment topographic divides can easily be simulated by a GIS. A GIS also is very useful for simulating rainfall maps, spatial distributions of soil data and initial model conditions. Spatial model output such as groundwater table positions and overland flow depth can also easily be visualised. In PBRR modelling a GIS must be used for pre- and post processing.
- The most important conclusion of the literature review is that it is uncertain what the effects of differences in the applied catchment partitioning theory, the model equations, the applied process schematisations etc. are on runoff generation. For gaining a better insight in the performance of PBRR models and designed model concepts, it is recommended to carry out comparative studies at selected catchments for selected periods of time.

3.4.2 Data requirements and model performance

For the modelling of the real world hydrologic runoff behaviour large quantities of data are required. Meteorological data are required to simulate rainfall, evaporation and interception while topographic and subsurface data are required to simulate surface flow and subsurface flow processes respectively. Model input data are meteorological input data, initial model conditions and model parameters that represent catchment attributes such as elevation and porosity. For each of the four model concepts a set of parameters is defined to represent the 'real world' characteristics. By the review in section 3.3 it appeared that sets are dissimilar and subject to the applied catchment partitioning theory and the applied model equations. Model equations also require input from non-observable (numerical) parameters such as the grid size dimensions and number of model layers. For each of the four concepts an overview for the required model parameters is presented in table 3.5. Although large numbers of parameters are added to the table, most likely it is incomplete since model algorithms and required model input data of some codes are not well described in literature. By this table it is clear that enormous amounts of parameter values are required for each grid element and parameter demand ranges from 16 to 30. When disregarding the evaporation and interception the number of parameters still range from 15 till 20. The parameter demand is highest for multi layer models such as SHE and IHDM since the subsurface is described in a three-dimensional perspective. The high parameter demand is a consequence of the complexity of the mathematical model where multiple flow processes are simulated from which some interact through calculated state variables.

Model complexity increases even more when the effect of time varying input data must be simulated. Such complexity causes that the performance is far from optimal. Relations between model complexity, data requirements and model performance are represented in figure 3.23. Prior to describing these relations it is stated that each of the relations is not based on extensive quantitative analyses but much more on logical 'reasoning' and on 'insight' of the various simulation aspects. It is stated that additional analyses of the four model concepts with further applications to real world systems will support the relations.

Table 3.5: Required model parameters (Rientjes, 1999a).

Computer code	SHE	TIALES	HDM	DBSIM
<i>Model input data</i>				
Interception				
- canopy drainage parameters	*	-	*	*
- canopy storage capacity	*	-	*	*
- interception capacity coefficient	*	-	*	*
- leaf area index	*	-	*	*
- ground cover indices	*	-	*	*
- throughfall coefficients	*	-	*	*
Evaporation				
- canopy resistance to water transport	*	-	*	-
- vegetation aerodynamic resistance	*	-	*	-
- ground cover indices	*	-	*	-
- ratio actual / potential evaporation	*	-	*	-
- maximum root zone storage	*	-	*	-
- root distribution with depth	*	-	*	-
Land surface				
- surface roughness coefficient	*	*	*	-
- detention storage capacity land surface	*	*	*	-
- coefficient relating to stage-discharge	*	*	*	*
- overland flow velocity parameter	*	*	*	*
Number of parameters	30	16	27	26

A causal relation encountered in most rainfall-runoff models is that an increase of applied temporal resolution of model input data as well as the model time step results in an increase of required spatial model resolution. The reasoning is that the simulation of high temporal resolutions only is functional when runoff dynamics can be simulated at appropriate spatial scales as well. The relation between the temporal resolution and the spatial resolution is expressed as a, fairly arbitrary, linear relation. With an increase of the temporal resolution also the required spatial resolution will increase that must be associated with an uncertainty band in which a specific temporal resolution is associated with a small, suitable range of spatial model resolutions. This range increases with increasing temporal resolutions and thus can be interpreted as a 'band of model uncertainty'.

For distributed runoff modelling the inverse of the relation also holds: an increase of spatial model resolution mostly requires an increase of the temporal resolution as well. An important consequence of such causality is that data requirements increase significantly with increasing model resolutions. As described, for each grid element a number of parameter values have to be defined subject to the applied mathematical model. For complex detailed models with high spatial and temporal resolutions, it is most likely that data requirements increase exponentially. This causality also must be associated with uncertainty since a small range of model complexities can be defined that all require data sets of similar size.

The third relation in figure 3.23 is the relation between model complexity and model performance. In this relation it is assumed that an optimum model performance can be defined as subject to the model complexity. Very simple and very complex models suffer from poor performance while a trade off can be identified between model complexity and model performance. By analysis of the four codes, it is concluded that PBRR models are very complex models that do not show an optimal performance although the performances of the SHE, IHDM and DBSIM in general were satisfactory. It is concluded that the model complexity and subsequently the high parameter demand hamper the performance of the models. It is also concluded that model concepts must be kept simple resulting in a significant decrease of the parameter demand.

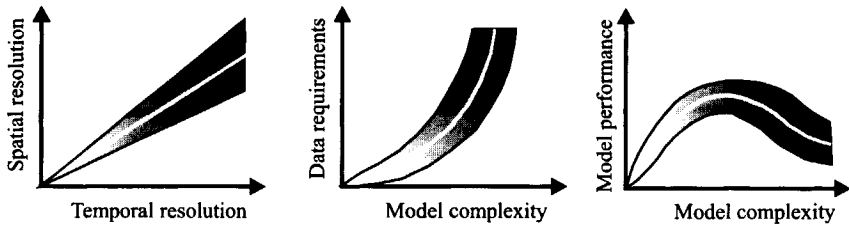


Figure 3.23: *Data requirements, model performance and model complexity relations (Rientjes and Hassanizadeh, 1999).*

Options to gain parameter reduction, however, are limited by the a-priori designed and defined model concepts. The common philosophy here is to keep model equations simple, to apply parameter zones and to use model parameters by which aggregated flow processes are simulated. Simple examples of parameter zoning are the simulation of spatial distributions of soils and land use by similar parameter values. Model parameters like porosity, hydraulic conductivity and Strickler-Manning coefficients are simulated over large numbers of grid elements covering the same soil type and land use. This approach is common to PBRR models and must not be rejected in future model applications. The use of 'aggregated' parameters also is common practice. Macro pore flow, rapid and delayed groundwater flow and perched subsurface flow are not simulated explicitly but only a single 'aggregated' flow equation is applied. Such aggregated flow equation is parameterised through aggregated model parameters for which grid effective values must be defined. In addition sheet flow, rill flow and stream flow are not simulated explicitly but processes are aggregated and simulated by a single overland flow equation. In the model descriptions in sub-section 3.3.1 through 3.3.4, for any grid element continuum assumptions are made with respects to system characteristics and variables. Catchment characteristics, initial model conditions and meteorological model input are averaged and lumped at the spatial scale of the grid elements although field observations of these variables mostly are taken at the much smaller point scale. The spatial variability at very small scales is ignored and aggregated and averaged values are assigned to the grid element. This procedure also is common practice in PBRR modelling and must be maintained in future model applications.

For improving the performance of PBRR models, the overall conclusion is that research must focus on improving the procedure to estimate and optimise model parameter values. Model performance must not only be judged by visual interpretation of the modelling results but also by quantitative data that help to define and to identify the best parameter values.

3.5 Model parameterisation and model calibration

Procedures of aggregation and lumping limit detailed simulations of runoff behaviour since real world process scales (see table 3.1) and small-scale variability are ignored. In this respect Beven [1989] declared that future developments in PBRR modelling

“must take account of the need for a theory of the lumping of sub grid scale processes; for closer correspondence in scale between model predictions and measurements; (and) for closer correspondence between model equations and field processes”.

The development of such theory as based on field observations, however, is questionable due to the many scale issues involved. Such lumping theory would require that the micro scale variability is simulated as based on field observations and that multiple processes can be aggregated into a single flow process. As a last step also effective model parameter values must be defined. The development of such lumping procedure is very complex and probably not feasible due to the large demand towards real world data. The procedure also would lack universal applicability since each catchment is characterised by different property distributions.

A different procedure to define lumped model parameters is to improve model calibration procedures. In parameter estimation through model calibration, scale issues relating to the process scale, observation scale and equation scale come together when parameter values have to be defined for grid elements (i.e. the model parameterisation). After making prior estimations of the parameter values, fine-tuning and optimisation of parameter values is achieved by modifying parameter values based on a model performance criterion. In such a procedure the objective is to define grid effective values that are interpreted as lumped and averaged parameter values. Such procedure is very suitable for estimating aggregated model parameters and implementing such procedures is

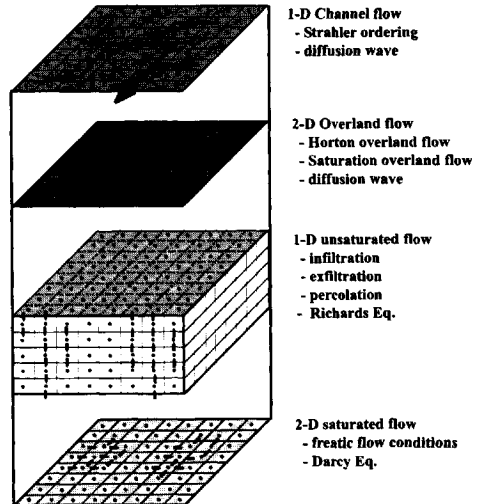
common practice in hydrologic modelling. A number of researchers (e.g. Refsgaard et al., 1996) reject the implementation of calibration procedures in PBRR modelling since they believed that parameter estimations based on field observations do not require optimisation. The procedure of parameter estimation by model calibration, however, becomes complicated when large amounts of parameter values have to be defined such as in PBRR modelling. In model calibration model parameters are modified in such a manner that the state variable of interest is simulated as close as possible to its observed counterpart. In catchment scale runoff modelling the channel discharge is the state variable of interest where the runoff hydrograph must be interpreted as integral response functions of all upstream processes. Multiple flow and runoff processes of different behaviour, extent and magnitude contribute to runoff production at a hill slope and cause that parameterisation becomes a difficult task. As shown in table 3.5, large numbers of parameters and parameter values have to be quantified and, by the estimation procedure, a large number of parameter sets can be generated that all will yield satisfactory simulation results. In research this phenomenon often is mentioned as a major cause of poor model performance and various expressions such as '*non-uniqueness*', '*equivalency*' and '*over-parameterisation*' exist to refer to this phenomenon. Although each expression follows a slightly different definition, all three expressions basically imply that multiple parameter sets can be defined that all produce a model output that is 'satisfactory' to the modeller. *Over-parameterisation* actually means that the effects single parameters have on the calculated model output cannot be defined exclusively as caused by unknown dependency relations between parameters. Such dependencies often are present when large numbers of model parameters are required. Dependencies often are expressed by (spatial) correlations where parameters may be positively or negatively correlated. As a result, effects certain parameters have on the model output become less pronounced and models may appear to be insensitive to certain parameters even though the model in fact is sensitive to the parameters. *Non-uniqueness* means that within a parameter set many different combinations of parameter values can be defined that all give satisfactory simulation results. Although parameter values are optimised and uniquely defined, many different but yet optimised parameter values can be defined. Parameter values as such have a non-unique character and

correctness of optimised values is uncertain. *Equivalency* refers to single parameter sets that are equivalent to each other in such a manner that each parameter set gives a satisfactory model output. Equivalency may occur as a result of model over-parameterisation and/or non-uniqueness.

In order to overcome the effects of parameter set equivalence, non-uniqueness and over-parameterisation, the procedures to estimate and optimise parameter values must be improved. In modelling such optimisation mostly is achieved by model calibration that is referred to as the fine-tuning of a model. In this respect, the use of automated calibration procedures in the field of PBRR modelling is advocated since parameter optimisation by manual procedures do not overcome the problems relating to non-uniqueness, equivalency and over-parameterisation. Such procedures are very appealing with regard to a number of modelling aspects. Two main advantages are a) multiple parameters can be optimised simultaneously and b) parameter estimation is achieved for the model domain as a whole. In order to reduce the complexity of the parameter estimation process a selection of model sensitive parameter must be made prior to the model calibration. In this methodology, parameters used for calibration purposes are termed optimisation parameters while the other parameters are termed fixed parameters. For model calibration only a relatively small number of parameters must be selected for optimisation while the values of the secondary parameters remain fixed at a certain value.

Recently developed automated model calibration procedures are described in Chapter 5 and conclusions on applicability and implementation are drawn. Procedures are known as inverse calibration procedures and are reviewed and analysed on suitability in PBRR modelling. For each of the procedures, estimated and optimised model parameter values must be interpreted as grid effective parameter values. By the review a selection is made for a procedure that yield specific information on parameter dependencies and parameter identifiability. The selected procedure is applied to the Troy case study as described in Chapter 6.

Model concept Flowsim



4.1 Introduction

Flowsim stands for FLOW SIMulation and denotes the name of a model concept as well as computer code that is designed and developed for the simulation of real world runoff behaviour in natural, hilly catchments. In the approach, runoff mechanisms of Horton and saturation overland flow are simulated in a distributed manner and model algorithms of relevant flow processes are based on conservation equations of mass and momentum. Guidelines for the design of the model concept as well as selected model algorithms are based on conclusions in section 3.4. The computer code is newly developed for this thesis and has required (very) extensive coding efforts.

Flowsim is classified as a distributed PBRR model approach by the applied model algorithms. In Flowsim, sub-models are developed for simulating rainfall, evaporation, overland flow, channel flow, unsaturated subsurface flow and saturated subsurface flow. Other processes of the hydrological cycle that are simulated are infiltration, percolation, capillary rise, exfiltration and channel seepage. Diagrams of the designed runoff and rainfall model concepts are presented in figure 4.1 and figure 4.2 respectively.

In Flowsim, overland flow runoff is generated when the rainfall intensity exceeds the infiltration capacity (i.e. Horton overland) or when a column of grid cells of the subsurface flow model becomes over-saturated (i.e. saturation overland flow). Catchment runoff is also generated by mass exchanges between the channel and groundwater flow models.

Subsurface storm flow processes of macro pore flow, perched subsurface flow and rapid groundwater flow are not simulated explicitly. In the subsurface flow models it is assumed that Darcian flow conditions prevail.

In the model concept multiple grid layers are required to simulate the various catchment characteristics. To all grid layers the discretisation of the DEM is applied and thus all grid elements of all sub-models in horizontal plane are squared and equally sized. For the subsurface elements a third space dimension is added that represents the thickness of the cell. This thickness may change from element to element and so any soil layer of varying thickness is simulated. By this approach is soil

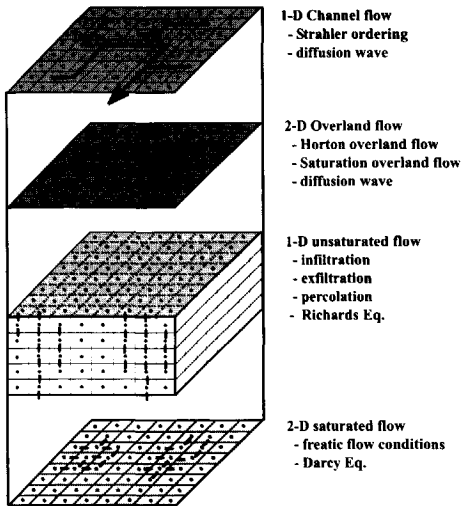


Figure 4.1: Schematic of runoff model concept.

layer geometry simulated by a fully distributed three-dimensional model domain. Grid layers also serve to simulate spatial distributions of soil characteristics as porosity, hydraulic conductivity and soil thickness. By use of multiple model layers, soil parameter distributions are simulated in three-dimensional model space.

In the remaining of this thesis three-dimensional grid elements are termed grid cells. Cell volumes of grid cells are defined by multiplying the area of DEM grid elements by the thickness of the grid cells. For simulating rainfall, evaporation, overland flow and channel flow, model layers with grid elements are applied. For simulating unsaturated and saturated flow grid cells are applied. In the approach any local densification of grid elements or grid cells is not allowed.

In the Flowsim model approach, elevation heights of grid cells are defined by subtracting the cumulated cell depths from the elevation height of the DEM grid elements. In this procedure the subsurface model is coupled to the DEM that serves as an elevation reference for model calculations. The DEM is also required in the overland and channel flow models and hence is of great importance.

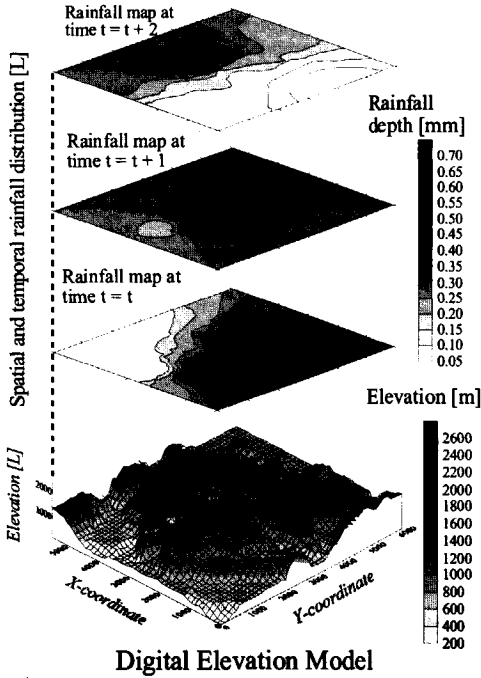


Figure 4.2: Schematic of rainfall model concept.

In table 4.1 hydrological and meteorological processes that are simulated are presented where also the number of required model layers is added. Model input of the sub-models is processed by use of the GIS “ARCVIEW” that serves as a pre-processor.

Table 4.1: Sub-models in Flowsim and number of model layers required.

Processes	Sub-model	Number of layers
Evaporation	Yes	> 1
Evaporation	Yes	> 1
Channel flow	Yes	1
Overland flow	Yes	1
Overland and subsurface flow	Yes	> 1
Rapid groundwater flow	Yes	1

Precipitation and evaporation also are simulated as a spatially variable input variable by use of multiple grid layers. Each of the sub-models is discussed briefly in the following sections. More detailed descriptions of the mathematics involved in each of the sub-models are presented in Appendix A.

4.2 Rainfall

By the literature review, it is concluded that the inaccurate simulation of rainfall is an important cause of error in model simulations. It is also concluded that rainfall must be simulated by a methodology in which the dynamics of the real world rainfall processes in terms of temporally and spatially variability is represented. For this reason, in the rainfall model multiple grid layers are used to represent the temporal variability while the spatial variability is represented within a grid layer. In figure 4.2 a diagram of the rainfall model concept is presented in which the temporal and spatial variable rainfall distributions are simulated.

For rainfall simulation, rainfall maps in terms of grid layers are generated for sequential time instants. Spatial rainfall distributions are obtained through interpolation of rainfall depths that are observed at a small number of observation points. For modelling rainfall a GIS is necessary as pre-processor that is used for storing the locations of the rain gauges, for storing the observed rainfall data and for interpolation and generation of rainfall maps.

4.2.1. Spatial rainfall distribution

The spatial distribution of rainfall is simulated within a grid layer by calculating a rainfall depth at any grid element. Rainfall often is observed by only a small number of gauging stations and observations must be processed to create spatially distributed rainfall maps. Rainfall maps mostly are generated by interpolation techniques where point observations are processed to create spatial continuous rainfall maps. The information on spatial and temporal rainfall variability often is incomplete since only information from a finite set of point observations is available. Conclusions on rainfall variability and distributions are subject to the applied spatial and temporal gauging resolutions and as such model input distributions only are simple approximations of the real world rainfall variability.

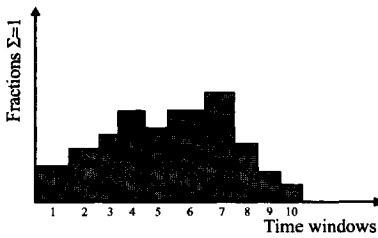


Figure 4.3: *Simulation of temporal rainfall distribution.*

To describe the spatial variability at larger spatial scales (e.g. regional scale), the rainfall process is described by a semi-variogram in which the spatial variability of the rainfall is expressed by a semi-variance as function of distance. Spatial interpolation is realised by use of local estimation techniques such as Inverse Distance Weighing schemes or by global estimation schemes such as Simple and/or Ordinary Kriging. For the latter approach the theory of random functions is adopted. By this theory, the rainfall process is treated as a random process in real space. The mathematics of the interpolation techniques is described in detail in Appendix A; section 'I Rainfall'. For the Troy case study that is described in Chapter 6, spatial interpolation is not implemented due to the very small size of the basin. Rainfall is simulated by homogeneous spatial distributions.

4.2.2 Temporal rainfall distribution

A common problem in the field of rainfall modelling is the simulation of temporal rainfall distributions. Rainfall depths mostly are gauged by collectors that gauge rainfall at regular time intervals such as every hour, day or decade. Ideally this observation interval is in correspondence with the spatial interval in terms of the network density. For the simulation of the rainfall-runoff relation at catchments of local scale as compared to regional scale, a higher temporal gauging resolution is preferred for the smaller scale catchment. This by the fact that runoff dynamics and runoff generation at smaller spatial scales is more pronounced than runoff generation at larger scales. If spatial and temporal gauging resolutions are not in accordance, rainfall observations must be re-scaled in such a manner that a physically realistic and consistent model approach is developed.

In the Flowsim model approach multiple grid layers are used to simulate the temporal rainfall distribution. Each grid layer represents a rainfall map with accumulated rain depths that are representative for a specific rainfall period. In the model approach, for each rainfall map a temporal rainfall distribution (see fig. 4.3) is defined and applied to all grid elements of the rainfall map. Common scaling and/or aggregation procedures to re-scale rainfall distributions in time are not addressed in this thesis. In this study only observed time series of rainfall measurement are used and temporal distributions that are applied to the simulation are defined by simple calculus. An observed rainfall depth, h_{observed} , is multiplied by a distribution function that describes the % fraction of h_{observed} that is fallen within a specified time window. Each window is bounded by a begin time, t_b , and end time, t_e , and is used to calculate a rainfall input, h_{rain} , for any model time step Δt :

$$h_{\text{rain}}^{\Delta t} = h_{\text{observed}} \cdot \frac{\Delta t}{t_e - t_b} \cdot \frac{\text{fraction}}{100} \quad [4.1]$$

Fractions sum up to 1 and the number of fractions is equal to the number of time windows. In this approach it is clear that an identical temporal distribution function is applied to all elements and that any rainfall depth over the spatial model domain is transformed in a similar manner. Temporal rainfall distributions hence are simulated by multiple rainfall maps and a temporal distribution function that is defined and applied to each map.

4.3 Evaporation

Evaporation is simulated by exactly the same procedure as applied in the rainfall model approach. Model input consists of a number of evaporation maps where evaporation depths are added to the grid elements. Such evaporation depth are re-distributed in time by use of a temporal distribution function and evaporation depths are, as subject to the flow conditions, subtracted from either the overland flow water depth or subtracted from the soil moisture storage in the subsurface grid cells. In case the overland flow depth drops to zero also some water is subtracted from the top cell of a column of grid cells of the subsurface model. In case top cells are unsaturated, water is subtracted from the top cell or, in case a top cell has fallen dry, the highest not entirely dry cell is selected.

Actual evaporation fluxes from the unsaturated cells are calculated by:

$$Ev_{act} = \frac{Ev_{pot}}{1000} \left(\frac{\theta - \theta_r}{\eta - \theta_r} \right) \quad [4.2]$$

where

Ev_{act}	= actual evaporation flux in meter	[L T ⁻¹]
Ev_{pot}	= potential evaporation flux in meter	[L T ⁻¹]
θ	= soil water content grid cell	[-]
θ_r	= residual soil water content	[-]
η	= porosity	[-].

Numerically, evaporation is simulated by a sink term in the overland flow and unsaturated subsurface flow models where the magnitude of the sink term reflects the actual evaporation.

4.4 Overland flow

In Flowsim, overland flow is generated by the infiltration and saturation excess mechanism as described in subsection 3.2.2. Flow processes and mass exchange terms simulated by the model approach are a) water transport at the land surface b) mass exchange between the overland flow and channel flow model c) mass exchange between overland flow model and the (un)saturated zone model to allow for infiltration and exfiltration and d) atmospheric stresses by rainfall and evaporation.

For the simulation of overland flow a raster DEM with rectangular elements of equal size is used. The use of such a DEM is advantageous since the DEM easily can be adapted in the numerical scheme that requires the use of a spatially discretised model domain. Also the catchment boundaries and slope gradients of the surface layer are easily defined by such DEM. A limitation of the applied partitioning is that much information on topographic variability at the element scale is lost. Aspects relating to spatial partitioning and the use of DEM's in overland flow simulation are described in Chapter 3 and are not repeated. The appropriateness of using rectangular grid elements of equal size in the model approach hence is not discussed further.

In Chapter 3 it is concluded that overland flow can be simulation by the diffusion wave approximation that combines the momentum equation of Strickler-Manning and conservation equation of mass. The diffusion wave equation is a simplified form of the momentum equation of Saint

Venant [Barre de Saint Venant, 1874]. When neglecting the wind shear stress and the eddy losses, the momentum equation of Saint Venant in conservation form in one-dimension gives:

$$\frac{1}{A} \frac{\partial Q}{\partial t} + \frac{1}{A} \frac{\partial}{\partial x} \left(\frac{Q^2}{A} \right) + g \frac{\partial h}{\partial x} - g(S_o - S_f) = 0 \quad [4.3]$$

where

A = cross sectional flow area	[L ²]
Q = discharge	[L ³]
t = time	[T]
x = horizontal Cartesian co-ordinate	[L]
g = acceleration of gravity	[L T ⁻²]
h = water depth	[L]
S _o = bed slope	[-]
S _f = friction force slope	[-].

By neglecting the local and convective acceleration terms, that are the first two terms of Eq.[4.3] respectively, water transport is due to pressure and gravitational forces only:

$$g \frac{\partial h}{\partial x} - g(S_o - S_f) = 0 \quad [4.4]$$

By such approach, the hydrodynamic effects of upstream water transport on downstream water levels and discharges are ignored. In a real world system such effects only are observable when slope gradients are small (i.e. < 0.001 m/m).

In Eq.[4.4], the gravity as driving force is set to be equal to the soil friction force. The gravity force so is proportional to the bed slope, S_o, and the change of the river stage, h, over distance x while the friction force is proportional to the friction slope, S_f. (Chow et al., 1988). This approximation is commonly known as the diffusion wave approximation that also is applied to the Flowsim code. Discharges by this approximation are simulated by the Strickler-Manning hydraulic resistance equation Eq. [4.5].

In the overland flow model discharges are calculated by:

$$Q_{of} = k_m \cdot b \cdot \sqrt{i_{sl,x}} \cdot h_{of}^{5/3} \quad [4.5]$$

where

Q_{of}	= specific discharge overland flow	$[L^3 T^{-1}]$
k_m	= reciproke of the Manning coefficient	$[L^{1/3} T^{-1}]$
b	= width of grid element	$[L]$
$i_{sl,x}$	= hydraulic gradient x-direction	$[-]$
h_{of}	= overland flow water depth	$[L]$.

In the overland flow model, the water layer at an element is assumed to be of uniform depth and so sheet flow is simulated.

In the mathematical model of Flowsim the bed slope is set to be equal to the hydraulic gradient that is defined by summing the grid elevations of the DEM and the calculated river stages. By use of a DEM with rectangular grid elements, a two-dimensional model algorithm is developed that allows the simulation and redistribution of overland flow in two flow directions. Such approach, as compared to a one-dimensional flow approximation, is in more correspondence with real world runoff behaviour since real world topographic variability at the spatial scale of an element also causes the redistribution of overland flow in multiple flow directions. A disadvantage of the approach is that discharges are calculated over too long travel distances (see fig. 4.4) as compared to one-dimensional flow approaches as well as the length of the one-dimensional real world flow paths. This since water transport is calculated in between the calculation nodes of the DEM and results in significantly longer travel distances and travel times. Travel distances now always are equal to two times the length of the grid element.

The applied conservation equation of mass has the form:

$$b \frac{\partial h_{of}}{\partial t} + \frac{\partial Q_{of,x}}{\partial x} + \frac{\partial Q_{of,y}}{\partial y} = S_{of} \quad [4.6]$$

where

h_{of}	= overland flow depth	$[L]$
t	= time	$[T]$
b	= width of flow	$[L]$
$Q_{of,x}$	= discharge overland flow in x direction	$[L^3 T^{-1}]$
$Q_{of,y}$	= discharge overland flow in y direction	$[L^3 T^{-1}]$
x,y	= horizontal Cartesian co-ordinates	$[L]$
S_{of}	= sink/source term overland flow model	$[L^2 T^{-1}]$.

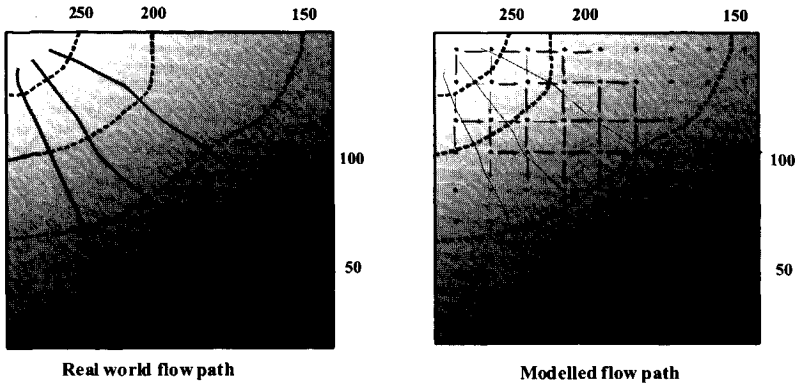


Figure 4.4: Comparison of flow paths as simulated in the 2D overland flow model and real world flow paths.

The sink/source term is an exchange term of water volumes between the various sub-models. By this term rainfall input, evaporation loss and infiltration to the unsaturated subsurface are simulated as well as the exchange of mass between the overland flow and channel flow model. The value of S_{of} is positive when water is added to the overland flow model and negative when water is subtracted.

By the applied conservation equation of mass, a two-dimensional numerical scheme is developed. This scheme is according to the diagram of figure 4.5. By Eq. [4.6], the water depth at a grid element is to be defined by the runoff discharges of the four orthogonal connected grid elements. When discretising Eq. [4.6] and when rewriting this equation for the overland flow water depth at time instant $t+1$ this gives:

$$h_{of,j,i}^{t+1} = h_{of,j,i}^t + (Q_{of,j-1/2,i} - Q_{of,j+1/2,i} + Q_{of,j,i-1/2} - Q_{of,j,i+1/2}) \frac{\Delta t}{A} + S_{of} \frac{\Delta t}{A} \quad [4.7]$$

where

- $Q_{of,j-1/2,i}$ = overland flow discharge at $j-1/2,i$ [L³ T⁻¹]
- $Q_{of,j+1/2,i}$ = overland flow discharge at $j+1/2,i$ [L³ T⁻¹]
- $Q_{of,j,i-1/2}$ = overland flow discharge at $j,i-1/2$ [L³ T⁻¹]
- $Q_{of,j,i+1/2}$ = overland flow discharge at $j,i+1/2$ [L³ T⁻¹]
- Δt = time increment [T]
- A = surface area of grid element [L²]
- S_{of} = sink/source term overland flow model [L³ T⁻¹].

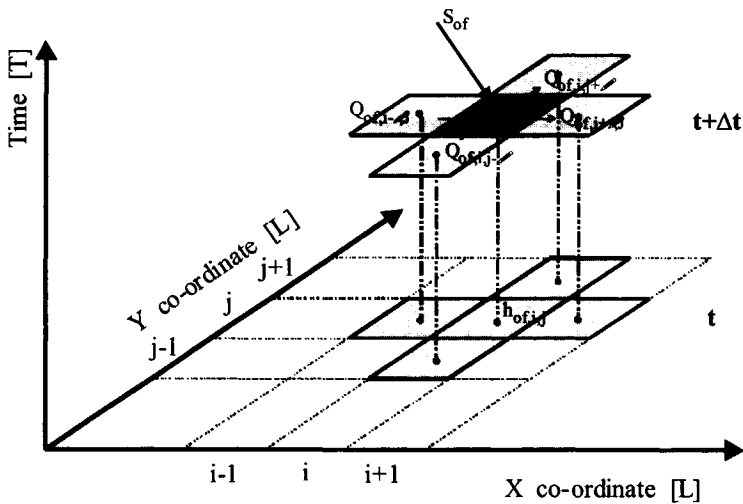


Figure 4.5: Schematic of the finite difference scheme of the overland flow algorithm.

For the simulation of the overland flow discharges $Q_{j-1/2,i}$, $Q_{j+1/2,i}$, $Q_{j,i-1/2}$, and $Q_{j,i+1/2}$, the Strickler-Manning equation Eq.[4.5] is substituted. Eq.[4.7] makes up the governing equation of the overland flow model in which overland flow discharges are simulated by a mixed numerical scheme. In such scheme the overland flow water depths at time instants t and $t+1$ of the orthogonal connected grid element are used for defining $h_{of,j,i}$ at time instant $t+1$. Numerical aspects of the model algorithm are described in detail in Appendix A; section 'II Overland flow model'.

The use of the Strickler-Manning equation Eq.[4.5] requires a value of the Manning coefficient. In literature a number of tables are presented in which values of this coefficient are defined. In most tables, the values relate to the type of land use and to topographic characteristics. Tables, however, present different values for similar land use and/or topography and cause that values are non-unique. The most commonly applied table is the table of Engman [1986] that also is selected for this thesis.

Model parameters for each grid element are the elevation height, the dimensions (i.e. length and width) of an element, the Manning coefficient while time dependent inputs are the rainfall and evaporation depth and the infiltration and exfiltration depth as simulated by the coupled sub-models.

4.5 Unsaturated subsurface flow

In sections 3.2.1, *Flow processes of the hydrologic cycle at the scale of a catchment*, and 3.2.2, *Mechanisms of runoff generation*, it is described that the generation of saturation overland flow is closely related to the water storage and groundwater table dynamics in the near vicinity of the channel network system. In case a soil column in the subsurface becomes fully saturated, exfiltration and subsequently saturation overland flow is developed. Changes in water storage in the (un)saturated subsurface are due to evaporation, infiltration, percolation, capillary rise and saturated flow that cause the groundwater table depth to change. By the objectives of this thesis a mathematical subsurface flow model is developed that allows the simulation of this behaviour.

Specific flow processes and mass exchanges simulated by the unsaturated zone model are the flow of water across a column of grid cells of the unsaturated model domain, infiltration at the top cells and recharge to the saturated flow model. For the saturated flow model simulated processes are the rise of the water table due to saturated flow, recharge and exfiltration at the land surface in case a column of grid cells becomes over-saturated. By the model approach only Darcian flow systems are simulated and so macro-pore flow is not simulated explicitly. In the approach the simulation of perched subsurface flow is ignored.

The flow of water within a column of subsurface cells is simulated by a one-dimensional conservation equation of mass as combined with Richards momentum equation (Richards, 1931). The applied conservation equation of mass reads:

$$\frac{\partial \theta}{\partial t} + \frac{\partial q_{sf,z}}{\partial z} + S_{sf} = 0 \quad [4.8]$$

where

θ	= soil water content	[-]
t	= time instant	[T]
$q_{sf,z}$	= specific discharge unsaturated flow in z direction	[L T ⁻¹]
z	= elevation height	[L]
S_{sf}	= sink/source term subsurface flow model	[T ⁻¹]

while the momentum equation reads:

$$q_{sf,z} = -k(\theta) \left(\frac{\partial(h(\theta))}{\partial z} + 1 \right) \quad [4.9]$$

where

$q_{sf,z}$	= specific discharge unsaturated flow in z direction	[L T ⁻¹]
$h(\theta)$	= pressure head subject to θ	[L]
$k(\theta)$	= hydraulic conductivity subject to θ	[L T ⁻¹]
z	= elevation head	[L].

The (negative) pressure head, that arises from micro scale interactions between the soil moisture and soil particles, as well as the unsaturated hydraulic conductivity both are functions of the soil water content. Both relations are described by the soil characteristic curves $k(\theta) - \theta$ and $h(\theta) - \theta$ that are functions of the soil texture and structure. For the simulation of the soil characteristic curves, the Van Genuchten relations (Van Genuchten, 1980) are implemented. The relation between the pressure head, $h(\theta)$, and the effective soil water content is expressed by:

$$\theta_e = \left[\frac{1}{1 + (h(\theta)\alpha)^n} \right]^m \quad [4.10]$$

where

α	= constant	[L ⁻¹]
m	= constant	[-]
n	= constant	[-].

A second and common expression for the effective water content is given by Eq.[4.11] and implies that only a part of the water content contributes to the flow processes:

$$\theta_e = \frac{\theta - \theta_r}{\eta - \theta_r} \quad [4.11]$$

where

η	= porosity	[-]
θ_r	= residual water content	[-].

When rewriting Eq.[4.10] for $h(\theta)$ and after substitution of Eq.[4.11] for θ_e the following expression for defining the pressure head is obtained:

$$h(\theta) = \frac{1}{\alpha} \left[-1 + \left(\frac{\theta - \theta_r}{\eta - \theta_r} \right)^{\frac{1}{m}} \right]^n \quad [4.12]$$

The hydraulic conductivity also is a function of the soil water content and is described by:

$$k(\theta) = k_s \cdot \left(\frac{\theta - \theta_r}{\eta - \theta_r} \right)^{\frac{1}{2}} \cdot \left[1 - \left(1 - \left(\frac{\theta - \theta_r}{\eta - \theta_r} \right)^{\frac{1}{m}} \right)^m \right]^2 \quad [4.13]$$

where

$$\begin{aligned} k(\theta) &= \text{hydraulic conductivity subject to } \theta & [L T^{-1}] \\ k_s &= \text{hydraulic conductivity in saturated conditions} & [L T^{-1}]. \end{aligned}$$

The governing equation is obtained by substitution of the momentum equation for $q_{s,f,z}$ in the conservation equation of mass equation Eq.[4.8]. After discretisation of the resulting equation, for all simulation time steps his equation is updated for the soil water content, the soil pressure head and the hydraulic conductivity. The resulting equation is solved for the soil water content that is the dependent state variable Eq.[4.14]. The pressure head and the hydraulic conductivity, that both are functions of the soil water content, are updated at the beginning of a simulation time step.

The discretised conservation equation of mass for simulation of the soil water content at time instant $t+1$ reads:

$$\theta_n^{t+1} = \theta_n^t + \left(q_{n-1/2}^t - q_{n+1/2}^t \right) \frac{\Delta t}{z_{n+1/2} - z_{n-1/2}} \quad [4.14]$$

where

$$\begin{aligned} \theta_n^{t+1} &= \text{soil water content at point } n \text{ at time instant } t+1 & [-] \\ \theta_n^t &= \text{soil water content at point } n \text{ at time instant } t & [-] \\ q_{n+1/2}^t &= \text{specific discharge at point } n+1/2 \text{ and time instant } t & [L T^{-1}] \\ q_{n-1/2}^t &= \text{specific discharge at point } n-1/2 \text{ and time instant } t & [L T^{-1}] \\ z_{n+1/2} &= \text{layer elevation at point } n+1/2 & [L] \\ z_{n-1/2} &= \text{layer elevation at point } n-1/2 & [L] \\ \Delta t &= \text{time increment} & [T]. \end{aligned}$$

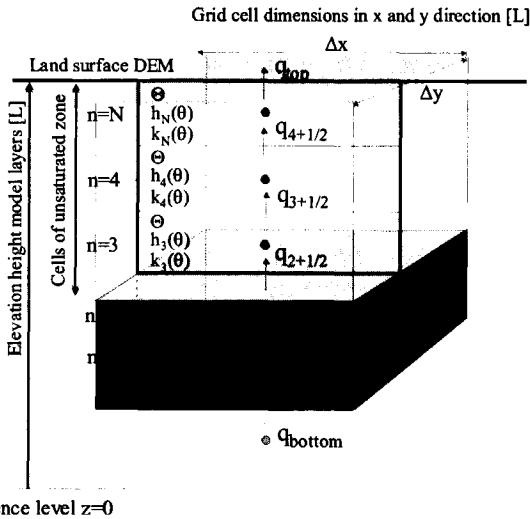


Figure 4.6: Schematic of the model concept for the unsaturated zone.

After substitution of discretised expressions for the momentum equations $q_{n+1/2}^i$ and $q_{n-1/2}^i$, the governing flow equation of the unsaturated zone model is obtained by which the soil moisture contents of each cell are defined.

A point n represents a space index at the centre of a grid cell at which the soil moisture content is defined while $n+1/2$ represents a space index at the interface between two cells at which the flux is defined. The layer elevations in the model approach are referenced to the datum of the DEM. Elevations of grid cells are defined by subtracting the cumulated depths from the elevation height of the DEM. The momentum equation Eq. [4.9] is solved in upward direction and fluxes are simulated subject to the hydraulic gradient of the interfacing grid elements. In figure 4.6 a diagram of the unsaturated zone model is presented.

For simulation of the rainfall-runoff relation, the accurate simulation of the infiltration process is most important. The infiltration process on the land surface acts as a separation mechanism for rainwater to infiltrate at the land surface or to be discharged across the land surface. In Flowsim, infiltration and exfiltration processes at the land surface are simulated by q_{top} that, mathematically, is interpreted as a flow-boundary condition commonly known as Neuman boundary condition. For each simulation

time step q_{top} is updated with respect to the water depth at the land surface and the hydraulic head of the top grid cell. Flow through the bottom of a model is allowed for by use of a head-dependant boundary flow condition, q_{bottom} , that is known as the Cauchy boundary condition. The model bottom is simulated as either impervious or pervious that as such must be defined by the modeller.

The rise or lowering of the water table due to percolation and capillary rise respectively is simulated over all simulation time steps in the unsaturated flow model. At the end of each time step the effect of saturated flow on the water table is simulated. Saturated flow may cause a rise of the water table during a rainfall event or a lowering of the water table depth during inter-storm periods. Subsurface depletion also is caused by evaporation. The rise or lowering of the water table requires that the soil water contents in an unsaturated soil column is updated and redistributed over the unsaturated cells. For simulation of unsaturated flow and for the redistribution of soil water due to saturated flow a 'predictor-corrector' methodology is implemented that is solved by an explicit calculation scheme.

Numerical aspects of the unsaturated flow model are further described in Appendix A; section '**III Unsaturated subsurface flow model**'.

4.6 Saturated subsurface flow

For simulation of saturated subsurface flow, a concept similar as to the overland flow model is applied. Saturated subsurface flow is simulated in a two-dimensional perspective by a model algorithm that is based on conservation equation of mass as combined with Darcy's equation. Saturated flow is simulated within a single grid layer where the applied discretisation of the DEM is adapted to the saturated flow domain. In vertical perspective saturated cells of a soil column are aggregated into one cell. The depth of such cells is equal to the depth of the saturated zone that is bounded by the simulated hydraulic head and the bottom of the model. This depth hence varies over the grid layer by the spatially distributed hydraulic head and the distributed model bottom. In the model approach only saturated flow under phreatic flow conditions is possible and thus (rapid) groundwater runoff in shallow systems is simulated.

The conservation equation of mass that is applied reads:

$$S \frac{\partial h_{h,wt}}{\partial t} + \frac{\partial q_{gf,x}}{\partial x} + \frac{\partial q_{gf,y}}{\partial y} = S_{sf} \quad [4.15]$$

where:

S	= storage coefficient	[-]
$h_{h,wt}$	= hydraulic head of groundwater table	[L]
$q_{gf,x,y}$	= specific discharge groundwater flow in x-y direction	[L ² T ⁻¹]
S_{gf}	= sink/source term groundwater flow	[L T ⁻¹].

Darcy's momentum equation reads:

$$q_{gf} = -k_s h_{sat} \frac{dh_{h,wt}}{dl} \quad [4.16]$$

where

q_{sf}	= specific discharge groundwater flow	[L ² T ⁻¹]
k_s	= saturated hydraulic conductivity	[L T ⁻¹]
h_{sat}	= thickness of saturated layer	[L]
l	= distance in direction of flow	[L].

The thickness of the saturated layer is spatially variable and is updated for each simulation time step by the simulated hydraulic head. In the saturated flow model this head is the dependent state variable and is defined according to Eq. [4.17]. In the numerical approach the hydraulic head at each grid cell now is obtained after substitution of all four groundwater flow discharges into the conservation of mass equation Eq. [4.15]. After discretisation of the resulting expression the following Boussinesq-type equation is obtained that resides at the core of the model algorithm for saturated flow:

$$h_{h(j,i)}^{t+1} = h_{h(j,i)}^t + \left(\frac{q_{gf(j-1/2,i)}^t - q_{gf(j+1/2,i)}^t}{\Delta x} + \frac{q_{gf(j,i-1/2)}^t - q_{gf(j,i+1/2)}^t}{\Delta y} + S_{sf} \right) \frac{\Delta t}{S} \quad [4.17]$$

where

$h_{h(j,i)}^{t+1}$	= hydraulic head at grid cell j,i and at time t+1	[L]
$h_{h(j,i)}^t$	= hydraulic head at grid cell j,i and at time t	[L]
$q_{gf(j+1/2,i)}^t$	= specific discharge groundwater flow at j+1/2,i	[L ² T ⁻¹]
$q_{gf(j-1/2,i)}^t$	= specific discharge groundwater flow at j-1/2	[L ² T ⁻¹]

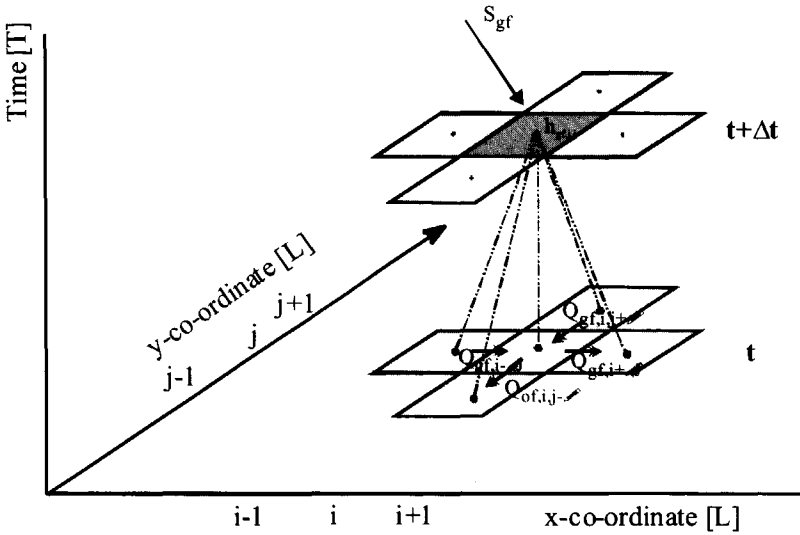


Figure 4.7: Schematic of the finite difference scheme for the saturated subsurface.

- $q_{gf(j,i+1/2)}^t$ = specific discharge groundwater flow at $j,i+1/2$ [L² T⁻¹]
- $q_{gf(j,i-1/2)}^t$ = specific discharge groundwater flow at $j,i-1/2$ [L² T⁻¹]
- S_{gf} = sink/source term groundwater flow [L T⁻¹]
- S = storage coefficient [-]
- Δx = space increment in x direction [L]
- Δy = space increment in y direction [L].

The discretised Darcy equation of Eq. [4.16] follows the general expression:

$$q_{gf(j+1/2,i)}^t = - \left(\frac{k_{s(j,i)} \cdot h_{h(j,i)}^t + k_{s(j+1,i)} \cdot h_{h(j+1,i)}^t}{2} \right) \cdot \frac{h_{h(j+1,i)}^t - h_{h(j,i)}^t}{x_{(j+1,i)} - x_{(j,i)}} \quad [4.18]$$

In the numerical model also the expressions of $q_{gf(j-1/2,i)}^t$, $q_{gf(j,i+1/2)}^t$ and $q_{gf(j,i-1/2)}^t$ are discretised and substituted in Eq.[4.17]. By this expression the resulting equation is solved for the dependent variable $h_{h(j,i)}^{t+1}$. The hydraulic head at time instant $t+1$ is a function of the hydraulic head at time instant t and all four inflow and outflow discharges that also are

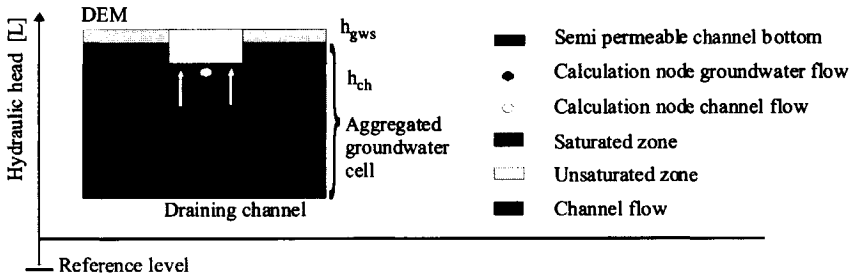


Figure 4.8: Schematic of the model concept to simulate mass exchange between the channel-subsurface flow models.

simulated by means of hydraulics heads at time instant t . Hence the mathematical model so is solved by an explicit calculation scheme. A diagram of the numerical scheme is presented in figure 4.7.

The use of aggregated cells for the simulation of groundwater flow requires that averaged parameter values are defined for parameterisation of Eq.[4.17]. Model parameters are the saturated hydraulic conductivity and the storage coefficient while the saturated depth of the flow profile acts as a cell geometry parameter. In the model the first and last parameters are combined to yield transmissivity values and these values are defined for each aggregated cell. Since groundwater fluxes are simulated at the boundaries of two connected cells, the transmissivity values are averaged over the cells and applied to Eq [4.18]. In the model approach the storage coefficient of Eq.[4.18] is simulated per grid cell in the soil column and is not averaged. Such averaging is inappropriate since changes of the groundwater table have an effect on the water storage of the partially saturated cell at which the groundwater table is simulated.

The sink/source term S_{gr} in Eq.[4.16] is used to simulate any interaction between the subsurface models and channel flow model. Mass exchange is simulated by means of the Cauchy boundary condition that follows the expression:

$$q_{ch,gws} = \frac{h_{ch(j,i)} - h_{h(j,i)}}{C} \quad [4.19]$$

where

$q_{ch,gws}$	= Channel seepage discharge	[L T ⁻¹]
$h_{ch(j,i)}$	= hydraulic head of channel flow model at element j,i	[L]
$h_{h(j,i)}$	= hydraulic head at aggregated cell j,i	[L]
C	= hydraulic resistance at channel bottom	[T].

Processes simulated by Eq. [4.19] are groundwater drainage to the channel and infiltration from the channel. Such infiltration is simulated in either saturated and unsaturated flow conditions and exchange fluxes are added or subtracted from the grid cell in which the channel bottom is simulated. Fluxes are simulated per grid cell by the multiplication of $q_{ch,gws}$ by the cross sectional flow area of the channel bottom. In figure 4.8 a diagram is presented of the channel - groundwater exchange model.

Mathematics involved in the groundwater flow and channel - groundwater exchange models are described in more detail in Appendix A; section '**IV Saturated subsurface flow model**'.

4.7 Channel flow

For simulating water transport in the channel network a one-dimensional flow model is developed. The mathematical model is applied to the channel grid elements that make up the channel network. This network is partitioned in a number of channel segments of variable length where each segment has an inflow element and an outflow element. Segments are connected through these elements and channel flow is simulated from upstream segments to the connected downstream segments to end up at the outlet element of the catchment model. Segments are made up by a number of connected grid elements that are geo-referenced by the DEM. Each segment follows either a column or a row of the DEM grid layer and results in a network system of orthogonal connected segments. In figure 4.9 a diagram is presented on the projection of a channel network system. In the same figure a Strahler order scheme is adapted that will be discussed later.

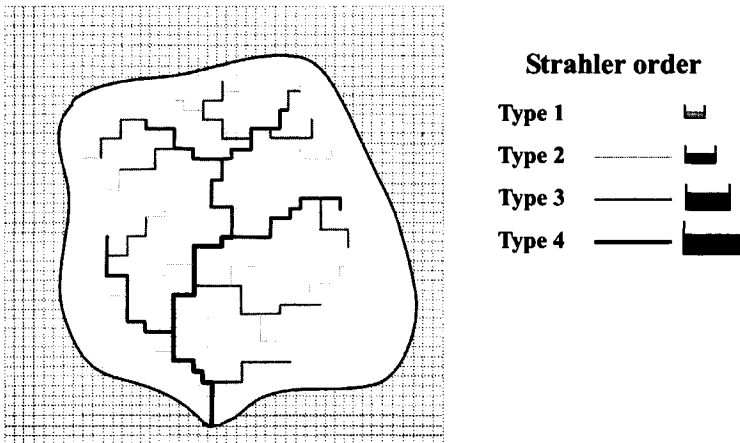


Figure 4.9: Schematic of Strahler ordering scheme.

For the simulation of water flow a one-dimensional flow model is developed that is based on conservation equation of mass combined with the Strickler-Manning hydraulic resistance equation. The conservation of mass equation reads:

$$\frac{\partial h_{ch}}{\partial t} + \frac{\partial q_{ch}}{\partial l} - S_{ch} = 0 \quad [4.20]$$

where

h_{ch}	= thickness of water layer in channel segment	[L]
q_{ch}	= specific channel flow discharge	[L ² T ⁻¹]
S_{ch}	= sink/source term channel flow model	[L T ⁻¹]
l	= spatial co-ordinate in flow direction	[L].

while the Strickler-Manning equation reads:

$$Q_{ch} = k_m \cdot A_{ch} \cdot R^{\frac{2}{3}} i^{\frac{1}{2}} \quad [4.21]$$

where

Q_{ch}	= discharge	[L ³ T ⁻¹]
k_m	= reciprocal of Manning coefficient	[L ^{1/3} T ²]
A_{ch}	= wetted cross sectional area	[L ²]
R	= hydraulic radius	[L]
i	= energy gradient line	[-].

After discretisation of Eq.[4.20] in time and space and after rewriting for the water depth at grid element j and time instant $t+1$ this gives:

A similar expression for the channel flow discharge is developed at the inflow boundary of cell j . When both expressions for $Q_{j+1/2}$ and $Q_{j-1/2}$ are divided by the cross sectional flow area and when multiplied by the grid size then the resulting expressions can be substituted for $q_{j+1/2}$ and $q_{j-1/2}$ respectively. In the expression of Eq.[4.21] the cross-sectional flow area, A_{ch} , is simulated by a rectangular flow profile and is calculated by multiplication of the width of the channel section, b_{ch} , by the thickness of the water layer h_{ch} . The hydraulic radius, R , in Eq. [4.21] so becomes equal to $b_{ch} / (2 + b_{ch}/h)$ and, in discretised form, is applied to Eq. [4.21].

A diagram of the numerical scheme is presented in figure 4.10. The water depths are defined at the calculation nodes of the channel elements while discharges are defined at the element boundaries. The channel flow discharge in Eq.[4.23] is simulated by water depths at time instants t and $t+1$. The procedure hence is characterised as a mixed scheme with an explicit component and an implicit component. The calculation scheme is solved by an iteration procedure that is based on a double sweep procedure that also is applied to the overland flow model. The scheme is solved by a three-point approach where the water depths of two connected elements are weighted by a factor. This factor is uniformly applied to all elements and weights the effects each water depth must have on the simulated discharge.

By the sink/source term, S_{ch} , runoff contributions from overland flow and from channel drainage are simulated. The volume of these runoff contributions are defined over a simulation time step, Δt , and are divided by the surface area of the channel elements. The resulting water depth is added to the water depth at the element prior to simulation of water transport.

In the channel flow model a Strahler ordering scheme is adapted that is used to classify each channel segments for its geometrical aspects. For each Strahler order a rectangular cross sectional channel flow area and a Manning coefficient are defined (see figure 4.9). Segments of equal Strahler order are all supplied with uniform parameter values for size and shape of the cross-sectional flow area and channel bottom roughness. In this manner a significant parameter reduction is achieved and makes the model less complex and reduces parameter demand. By such ordering approach the simulation of the channel network and the parameterisation of the flow equations are based on a channel

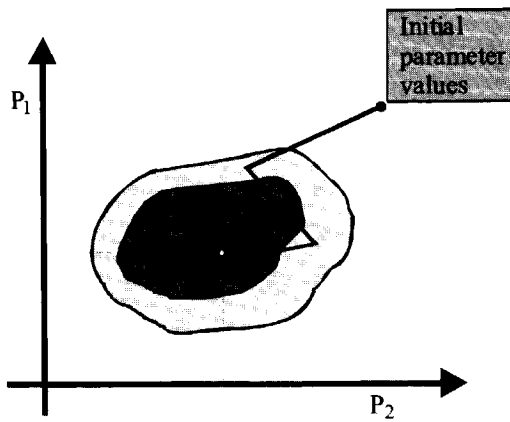
segmentation procedure. By this procedure a gross simplification towards representing the real world channel network is introduced.

The ordering of the channel segments, the design of the network layout and the extent of the network are defined by the modeller. With respect to each of these aspects, objective guidelines that help to design a channel network system are not available in literature. Channel network designs always must be based on observation of the real world channel system.

Mathematics involved in the numerical scheme are further described in Appendix 1; '**V Channel flow model**'.

5

Model calibration



5.1 Introduction

Society only benefits from modelling studies when models have a sufficiently high level of performance and when models are reliable and trustworthy as well. Model performance in hydrology in general is evaluated by a comparison of observed and model simulated state variables such as channel flow discharges, soil water contents and/or groundwater table depths. In rainfall-runoff modelling, usually the channel flow discharge is the state variable of interest and observed discharges are compared to model simulated discharges. Conclusions on model performance are based on such comparisons and performance is assumed high when models simulate the observed discharges accurately.

To evaluate the performance of a model, the channel flow discharge appears to be an attractive variable since discharges easily are observed in a catchment and since, with respect to runoff simulation, it usually is the only state variable of interest. Channel flow discharges, however, have important characteristics that are not attractive for model evaluation. Discharges for example continuously change over time and different hydrographs are observed at different locations within the channel network. Discharges also may change from peak flow to base flow over relatively short time periods where any discharge observation is a function of the upstream, highly dynamic and non-linear runoff catchment behaviour. As described in section 3.2, any discharge observation must be interpreted as an integral response function of all upstream flow processes.

Comparisons between observed and simulated channel discharges in general are made over a range of meteorological and hydrologic conditions. By these conditions, discharges range from base flow to peak flow and are reflected by the shape of the hydrograph. In runoff modelling time series of observations and model simulated counterparts are compared where the objective is to simulate the observed hydrograph as good as possible. Differences between observed and simulated discharges change over time as subject to the meteorological influences and the catchment runoff behaviour. Differences may be small for some time instants and large for other instants and as such differences are not homogeneously distributed over the simulation period. In modelling, differences between observations and model calculated counterparts are

termed residual errors that are generated due to various causes. Residual errors are interpreted as cumulative errors that arise from:

- insufficiencies in the model concept,
- incorrectness of parameter values,
- erroneous simulation of meteorological and hydrologic influences such as rainfall, evaporation and (possibly) boundary conditions and
- observation errors with respect to applied state information.

Errors generated by each of these causes are of a different magnitude, they change over time and are subject to the effectiveness of the model approach. For example, specific runoff models may be effective in estimating base flow discharges but may be less effective in estimating peak flow discharges. The residual error due to insufficiencies in the model concept for simulation of base flow then most likely is small while the opposite is true for peak flow simulations. Also correctness of parameter values may change over time as the range of simulated model response modes also changes over time. Uncertainties involved in quantifying the magnitude and the behaviour of each of these errors makes runoff modelling a science that is associated with great uncertainty, difficulty and complexity. In modelling practice it is common to interpret the residual error as a cumulative error that must be minimised. The residual error also often is termed the model error.

By evaluating the performance of a model over a time series of observations, models are tuned to improve model simulations. Such tuning is termed 'model calibration' or just 'calibration' and may be accomplished by improving the model concept, optimising parameter values or by improving the manner meteorological model inputs and hydrologic influences are simulated. In literature, such approach generally is referred to as inverse modelling and means that observations of state variables are used for calibration of a model (see e.g. Valstar, 2001; te Stroet, 1995; among others).

The development and application of new calibration procedures in PBRR modelling has gained very little attention¹ in research over the past decades while the opposite is true in CRR modelling. Since early applications of CRR models (see Burnash et al., 1973; Ibbitt, 1972; and

¹ An exception forms the development of the GLUE procedure,

Crawford and Linsley, 1966) it was understood that models needed to be calibrated to improve model simulations. By pioneering work of e.g. Johnson and Pilgrim [1976] and Pickup [1977], it has become clear that the success of any model application very much depends on how well a model is calibrated. Research on model calibration was directed by this understanding and generic aspects of model calibration were investigated. For many researchers, model calibration has become a subject of great interest that involved many aspects. As such, model calibration (still) is an important research topic and a number of researchers (Beven, 1989a, 1993b; Klemeš, 1986b; Gupta et al., 1994; Refsgaard, 1997; among others) present their thoughts and contribute to ongoing philosophical and fundamental discussions on model simulation, model calibration, trustworthiness and reliability of calibrated models.

Although most researchers and modellers agree to the paradigm that

“models should work for the right reasons”,

a number of model calibration approaches and strategies are developed and discussed. Discussions by Sorooshian and Gupta [1985], Klemeš, [1986b], Beven [1989a], Beven and Binley [1992], Jakeman and Hornberger [1993], Ambroise et al., [1995], Spear [1995], Kuczera and Mroczkowski [1998], Gupta et al., [1998], among others, focus on procedures that help to analyse the performance and trustworthiness of a model. Such analyses are not limited to visual and/or numerical comparison of observed and model simulated time series, scatter plots and/or double mass curve analysis but also focus on the issue of model uncertainty.

During the time, discussions focused on and contributed to an improved understanding of our modelling approaches and have led to an increased insight in the complexity of model simulations and (still) are of great significance to the modelling society. Modelling advanced to the use of automated calibration procedures and, for the past two decades, research on model calibration basically focussed on the following aspects (modified after Sorooshian et al., 1998):

- Development of techniques accounting for data errors; calibration was placed in a maximum likelihood estimation framework and effects of data errors on model performance were tested. Also, simulated

channel flow hydrographs must be associated with a heteroscedastic error variance.

- Determination of the information content and appropriate quantity of observation data; the information content of specific data is far more important than the quantity in terms of the length of a time series.
- Development of global parameter estimation techniques led to the use of population evolution based search strategies.
- Quantification the effect of parameter uncertainty in model responses.

For each of these aspects numerous publications (see e.g. Sorooshian and Dracup, 1980; Sorooshian, 1981; Kuczera, 1983a,b; Kuczera, 1982; Spear and Hornberger, 1980; Kuczera, 1988; Gupta and Sorooshian 1985) are written and a fundamental understanding of the calibration procedure has been gained. Research helped to define difficulties and limitations of model calibration procedures and helped to gain insight in generic aspects of model calibration. Such aspects among others relate to, a) quantifying the effect the length of the calibration period has on the identifiability of parameter values, b) defining the information content of selected time series, c) defining the appropriateness of selected objective functions and d) assessing the usefulness of model performance criteria for various model response modes.

In section 5.2 the 'Trial and Error' calibration procedure is discussed while in sections 5.3 through 5.5 automated procedures and approaches are reviewed and discussed. In this review the focus is not on describing all mathematical aspects and constrains in great detail, but much more on principal assumptions underlying the approaches and on usefulness of the approaches. Such usefulness particularly focuses on reliable and trustworthiness of models. In theory each automated procedure has universal applicability that can be applied to PBRR models as well although procedures mostly are applied to distributed and lumped CRR models only. Applications of automated procedures in PBRR modelling are very sparse and only gained little attention. Model calibration in PBRR modelling primarily focused on Trial and Error procedures by optimising parameter values thus ignoring other sources of mismatch. (see e.g. Grayson, 1992a, Refsgaard, 1996, Bronstert, 1999).

A relatively new trend in the calibration of runoff models is the application of generic algorithms such as Artificial Neural Networks

(ANNs). In section 5.6 the characteristics and applicability of this procedure will be discussed. In section 5.7 conclusions are drawn on suitability and applicability of automated calibration procedures to PBRR modelling. Also a procedure is selected that is used for the case study described in Chapter 6.

Model Calibration

As stated, the performance of a runoff model is evaluated by a comparison of observed and model simulated state variables. Comparisons of variables are made over a time series of observations and comparisons mostly are made for runoff hydrographs. In runoff modelling occasionally also piezometer heads are used as state variables for model calibration. The use of soil moisture contents as a second state variable of interest in runoff modelling is very uncommon.

Model calibration in the field of runoff simulation commonly is achieved through parameter optimisation only. In such manner model calibration ignores a number of causes that potentially cause an unsatisfactory model performance and thus the complexity of model calibration is reduced significantly. In most rainfall-runoff simulation studies this approach is adopted and an *a-priori* defined model concept is selected and maintained throughout the simulation and model calibration so becomes synonymous to parameter optimisation. It often is assumed that models are reliable in their simulation when the residual error is minimised. With respect to the reliability issue of calibrated models, Gupta et al., [1998] state:

“Hydrologic models can only be as reliable as model assumptions, inputs, and parameter estimates”.

According to this statement, model calibration must focus on validating model assumptions, on improving parameter estimations and the manner meteorological and hydrologic model inputs are simulated. Especially with regard to model assumptions it is obvious that these are of great significance for the performance of a model. Such assumptions relate to applied process schematisations, selected model equations, applied model discretisations and the manner the model inputs are simulated. It is clear that model assumptions to some extent are reflected in the design of the model concept but also, by changing the assumptions the model concept will change. Also it is clear that model calibration by parameter

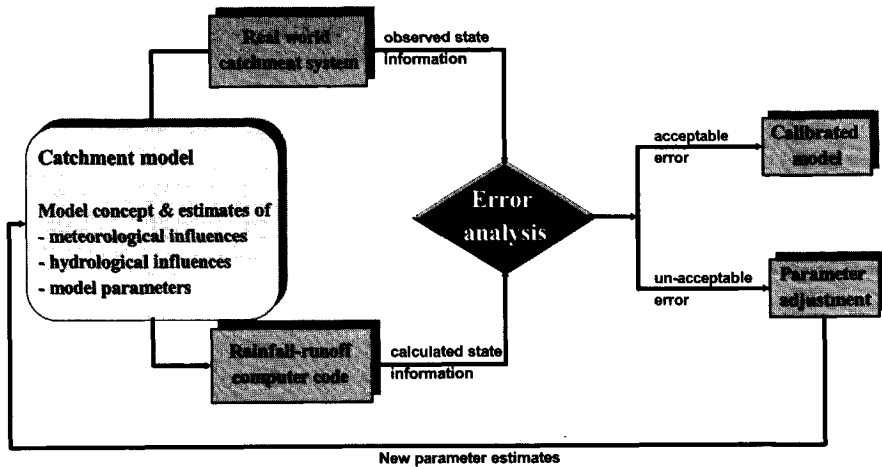


Figure 5.1: Model calibration based on parameter estimation

optimisation only is partial and that parameter values that are optimised also are a function of the applied model concept.

Parameter optimisation is achieved through various approaches and procedures. Fundamental assumptions underlying each calibration procedure differ significantly and each procedure follows a different parameter optimisation strategy. Figure 5.1 presents a flow chart on model calibration by parameter optimisation. By use of a model performance criterion that is based on residual error analysis, parameter values are estimated 'as good as possible'. In the chart a model is 'calibrated' when the residual error has reached an acceptable (low) level. Initial parameter values are obtained from information sources like maps, data-bases and, possibly, field measurements and serve as start values for the optimisation procedure.

In runoff simulation comparisons between observed and calculated state variables are made qualitatively and quantitatively. Qualitative comparisons are made by the modeller and are based on visual interpretation of the simulation results. An example is the use of scatter plots in which the simulated channel flow discharge is plotted against the measured discharge. Scatter plots may, among other runoff hydrograph characteristics, presented for runoff discharges and water levels. This practice in model performance evaluation is still common but relies on

the judgement of the modeller. Such judgement is arbitrary, subjective and basically is a reflection of the modellers understanding of the behaviour of a system and effectiveness of the model approach. In general these judgements serve as a 'soft' calibration tool and are used to redirect the calibration efforts (Anderson and Woessner, 1992).

Quantitative model comparisons are based on residual error calculations that reside at the core of model performance criteria. Two commonly applied calibration criteria in runoff hydrology are Root Mean Square Error (RMSE) and Nash-Sutcliffe efficiency (Nash and Sutcliffe, 1970). The RMSE is the standard deviation of the residual error over a selected calibration period and is the average of squared differences between observed and calculated variables:

$$\text{RMSE} = \left[\frac{\sum_{t=1}^T (Q_o - Q_c)_t^2}{T} \right]^{0.5} \quad [5.1]$$

- Q_o = observed channel flow
- Q_c = calculated channel flow
- t = index for time interval
- T = number of time intervals.

In model calibration the objective is to minimise the RMSE that traditionally is calculated as a single value over selected time series. The RMSE must be interpreted as a time integrated performance criterion over various model response modes. The use of RMSE over a range of response modes weakens the general interpretation of model performance. This since the RMSE does not provide distinct information on model performance with regard to actual response modes of the model and the system under study. Residual errors are aggregated over the selected calibration period and information on model performance over various response modes is lost. This aspect is investigated by Boyle et al., [2000] and Wagener et al., [2001] who applied the RMSE criterion over a moving time window. In their approaches specific information on model performance is obtained for selected time windows that continuously move forward with the progression of the model calculations. Applications of such approaches, however, still are in a development stage and require more testing before procedures can be applied to PBRR models.

A second performance criterion often used in runoff modelling is the Nash-Sutcliffe efficiency, R^2 , is maximised. For this criterion also the runoff discharge mostly is selected as the (only) state variable of interest. The Nash-Sutcliffe efficiency is applied to a time series of observations and is expressed by:

$$R^2 = \frac{F_o - F}{F_o} = 1 - \frac{F}{F_o} \quad [5.2]$$

where

$$F_o = \sum_{t=1}^T [Q_o - \bar{Q}_o]^2$$

$$F = \sum_{t=1}^T [Q_o - Q_c]^2$$

where

Q_o = observed channel flow discharge

\bar{Q}_o = average of observed channel flow discharge

Q_c = calculated channel flow discharge

t = index for time interval

T = number of time intervals.

F_o is the sum of the squared difference of observed discharge and average discharge over the calibration period and is indicative for the statistical variance of the discharge with respect to, average, long-term runoff discharge. High values of F_o indicate relatively high fluctuations of observed discharges and thus relate to rapidly changing response modes of the catchment. F is the sum of the squared difference of observed and calculated discharge, both over the selected calibration period.

The Nash-Sutcliffe efficiency coefficient quantifies performance of a model by the ratio of mean squared error of average runoff and mean squared residual error. A negative value of the coefficient represents a lack of agreement that is worse than if simulated flows were replaced by observed channel flow discharges. The value of the efficiency coefficient depends upon the variance of the observed flow record with respect to average long-term runoff discharge and makes that comparisons of model performances between basins by R^2 become subjective. In rainfall-runoff modelling it is often stated that a value of 0.9 for R^2 indicates a very good model performance, that a value in the range of 0.8-0.9 indicates a good model performance while R^2 in the range of 0.6-0.8

indicates a satisfactory model performance (Kachroo, 1986, among others).

Both RMSE and R^2 criteria are frequently applied in runoff modelling and sometimes both criteria are used to judge the performance of a model. On the applicability of both criteria, in runoff modelling different statements are made in literature. Research by Duan et al., [1992] on the applicability of both performance criteria to various model response modes in CRR models indicate that for base flow response modes RMSE is better suitable while R^2 is a better performance criterion for peak flow response modes. Sajikumar and Thandaveswara [1999] state that R^2 is a better model performance indicator as compared to RMSE when model performance is tested over calibration periods of different length. This is because, in the calculation of F_o , averaged values of observed discharges are used over the calibration period. R^2 is interpreted as a transformed and normalised measure with respect to variance of observed hydrograph of the overall RMSE. It is obvious that in case RMSE reduces to zero R^2 becomes 1. It is often observed that a high correlation between RMSE and R^2 exist. Conclusions on suitability, however, cannot be generalised.

Parameter optimisation is achieved by the so-called Trial and Error procedure or by automated parameter optimisation algorithms. In the first approach parameter values are optimised by manual adjustment. In automated approaches such optimisation is achieved by automated routines that require the use of objective function that is either minimised or maximised. An objective function is interpreted as a model calibration criterion and often is referred to as a 'cost function'.

5.2 Trial and Error procedure

In PBRR-modelling the most commonly applied calibration procedure is the 'Trial and Error' procedure. In the procedure, parameter values are modified manually to minimise the residual error between observed and simulated channel flow discharges. A selection of parameters for optimisation is made based on model sensitivity analyses. Model sensitive parameters are selected for optimisation while insensitive parameters are fixed as based on available information. For all four models presented in Chapter 3 the Trial and Error procedure is applied. Also in more recent research (see e.g. Refsgaard, 1996; Bronstert, 1999)

the procedure is applied despite the fact that the procedure has major weaknesses.

In the Trial and Error procedure it is assumed that a single best set of parameter values is defined when model performance criteria such as RMSE and R^2 are minimised or maximised respectively. It is assumed that a best possible fit between observed and calculated hydrograph can be achieved over entire time series of observations and that optimised parameter values may be fixed to certain values that, as such, have a unique character. It is clear that optimised parameter values reflect a high degree of arbitrariness since values are modified based on judgements of the modeller. As stated before, such judgements are subjective and different modellers will define different 'optimal' parameter sets. In such approach parameter values are not well identified although the model is sensitive to changes of selected parameter values. It is evident that this procedure of parameter estimation is very questionable and that uniqueness of single parameter values cannot be guaranteed.

A second and major shortcoming relates to problems of over-parameterisation and equivalence of parameter sets as described and discussed in section 3.5. At the core of these problems the issue resides of how well parameter values can be identified. A low parameter identifiability causes that models might not be reliable and trustworthy although model performance criteria such as RMSE or R^2 may indicate a satisfactory performance (see Bronstert, 1999). It is clear that the Trial and Error procedure for model calibration does not fulfil adequate requirements for model calibration. Examples of some simple restrictions of the procedure are (Cooley and Naff, 1990):

- No methodology exists to guarantee that simulations will proceed in a direction that could lead to a best parameter set.
- Determination when that best set has been reached is difficult.
- No way exists to quantitatively assess predictive reliability of the model.
- Deciding whether or not additional parameters or a more refined model concept would significantly improve the model is difficult.

Other restrictions of the procedure are that an insight is not gained in, for example, any temporal and spatial parameter dependency, in

uniqueness of single parameter values, in uniqueness of an entire parameter set and how well single parameter values are identified. It also is uncertain how well optimised model parameters represent the real world catchment characteristic of interest. Many researchers as for example Sorooshian and Gupta [1983] claim that by Trial and Error calibration a single best and unique parameter set cannot be defined. By these important weaknesses, a calibrated model cannot be termed reliable or trustworthy and it is concluded that Trial and Error procedures must be rejected in PBRR modelling.

5.3 Automated model calibration by the Generalised Likelyhood Uncertainty Estimation (GLUE) procedure

The GLUE procedure for model calibration is presented by Beven [1989] and is further described by Binley and Beven [1991] and Beven and Binley [1992]. The procedure is an extension to the 'Generalised Sensitivity Analysis' as presented by Spear and Hornberger [1980] and, at that time, was regarded a breakthrough in model calibration. The procedure is developed to describe uncertainty of the model response due to uncertainties that need to be associated with non-uniqueness of parameter sets and model concepts. In the procedure the first objective is to identify ranges of model parameter values that all yield satisfactory simulation results. The second objective is to simulate predictive uncertainty of model response by simulation of model output for all parameter value combinations that fall within identified parameter value ranges. For each simulation time step, model calculated values of state variable of interest are aggregated into a distribution function and statistical properties as mean value and 5% and 95% percentiles are defined that are interpreted as 'uncertainty bands' with respect to model output.

An underlying assumption in the procedure is that equally satisfactory simulation results can be obtained by use of multiple parameter sets and possibly even model concepts. Beven and Binley [1993b] refers to this phenomenon by the term 'equifinality' and states:

"an acceptable model prediction might be achieved in different ways, i.e. different model concepts or parameter sets".

In most simulation studies with the GLUE procedure an *a-priori* defined model concept is selected. The model concept hence is interpreted as a correct descriptor of the catchment that does not require optimisation.

Beven and Binley [1992] describe that the GLUE procedure is developed on the premise that for any *a-priori* defined model concept a single best and optimal parameter set cannot be defined. The objective therefore is to identify suitable parameter ranges (see Beven and Binley, [1992]; Aronica et al. [1998], Uhlenbrook et al. [1999]; among others) and thus large numbers of parameter sets must be evaluated within the entire parameter space. For all selected parameters, parameter value ranges must be identified that, when combined in a parameter set, may yield equally satisfactory model performances. A principle assumption is that, prior to model simulation, each set of parameter values is interpreted as an equally likely simulator of a catchment system.

In the GLUE procedure parameter sets are generated by a Monte Carlo parameter sampling procedure. For selected model parameters, a prior distribution function is defined within a relatively wide range of parameter values. Distribution functions may be Gaussian or uniform and are termed 'prior likelihood distribution functions' (Beven and Binley, 1992). For defining parameter sets for model simulation, for each model parameter a value is randomly drawn from the likelihood distribution functions by Monte Carlo sampling. A critical note on such procedure is that objective criteria for selecting parameter value ranges with an upper and lower bound are not presented in research. Sources that help to define appropriate ranges in general are field measurements and available maps. Large numbers of parameter sets are generated in this manner and by simulations model performance is evaluated for each parameter set by means of a performance criterion. In the GLUE procedure this performance criterion is termed the 'likelihood measure' or 'likelihood weight' and is interpreted as a measure of goodness of fit between observed and calculated state variables. It is obvious that 'likelihood' modelling in this manner is dissimilar from statistical likelihood modelling and also has a different interpretation. Likelihood measures may follow different expressions but mostly are based on common performance criteria such as for example R^2 . Objective criteria to select an appropriate likelihood measure are not presented in research. Examples of likelihood measures applied in GLUE simulation studies are the following:

- 1) $\ell = \left(1 - \frac{\sigma_e^2}{\sigma_o^2}\right)^N$ (Franks et al., 1996)
- 2) $\ell = (\sigma_e^2)^{-N}$ (Binley and Beven, 1991) [5.3]
- 3) $\ell = \left(-w \frac{\sigma_e^2}{\sigma_o^2}\right)^N$ (Lamb et al., 1998)

where

- ℓ = likelihood weight
- σ_e = variance of residuals
- σ_o = variance of observations
- N = likelihood shape factor (mostly set to 1)
- w = weight.

The calculated likelihood measure serves as an indicator whether the selected parameter set is an appropriate simulator of the catchment. Subject to the likelihood measure, an inappropriate parameter set yields a low likelihood weight and thus must be interpreted as a bad simulator of the catchment. Such parameter sets are rejected for further analysis and are termed 'non-behavioural' while the remaining parameter sets are termed 'behavioural' that serve for further analysis. A rejection threshold value of the likelihood weights is required to distinguish between behavioural and non-behavioural parameter sets. This threshold value is of great significance since further analyses are based on this selection. Objective guidelines to define threshold value and likelihood measure are not presented in research. Such selections mostly are based on subjective grounds and depend on assessment and judgement of simulation results by the modeller. In Lamb et al., [1996], Binley and Beven [1991] and Franks et al., [1996] only the best 10% of all likelihood weights, ℓ , are retained for further analyses. In literature also examples are presented where the best 50 % of the likelihood weights are retained.

A complicating factor in defining an appropriate threshold value is that different likelihood measures require a different rejection threshold value for the GLUE procedure to be successful. Especially when multiple model outputs are used in the analysis this problem becomes evident (see e.g. Lamb et al., 1998). Model evaluation based on single or multiple output variables such as channel flow discharge and

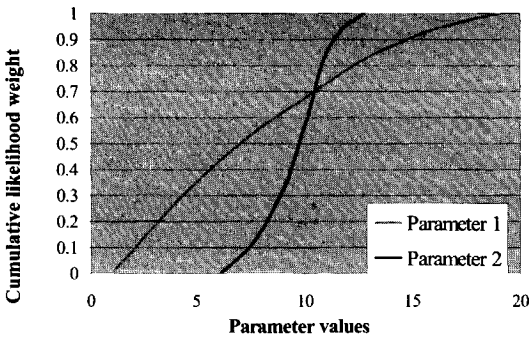


Figure 5.2: Marginal likelihood distribution functions

groundwater table data will yield different marginal likelihood distribution functions for selected model parameters. The arbitrarily chosen best 10% of all likelihood weights Eq.[5.3] may constrain further analysis especially when a model is insensitive to certain parameters. Lamb et al.[1996] and Franks et al.[1996] document this problem and state that threshold values might differ subject to the likelihood measure in case multiple state variables such as channel flow discharge, piezometric heads and observations of saturated areas are used in the likelihood function.

GLUE Analysis

After rejection of non-behavioural parameter sets, likelihood weights of remaining sets are re-scaled in such a manner that a cumulative likelihood distribution is prepared in which likelihood weights are summed to 1. Marginal likelihood distribution functions for each parameter are defined with re-scaled cumulative likelihood weight on the ordinate and parameter values on the abscissa. By re-scaled marginal likelihood distribution functions, model sensitivity to changes of selected parameter values is expressed. A steep distribution function indicates a high sensitivity and a parameter is assumed to be well identified (see fig. 5.2).

Inter-relations between parameters are expressed by mapping likelihood values for each combination of two parameters. Contour lines of equal likelihood values indicate the likelihood that parameters are interrelated (see fig. 5.3) although inter-relations are not quantified explicitly based on statistics such as a parameter correlation matrix.

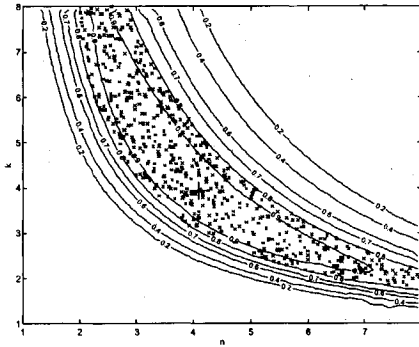


Figure 5.3: Contour lines of equal likelihood values for two parameters n and k (Werner, 2001)

By use of likelihood distributions of behavioural parameter sets a range of values of state variable of interest is calculated. For each parameter set a model run is executed and calculated state variables are aggregated and make up a new distribution function. By this procedure likelihood weights of behavioural parameter sets are transformed into a distribution function of simulated state variables and statistical quantities such as mean value, median, standard deviation or percentiles can be defined. Since distributions of state variables such as a channel flow hydrograph are skewed and heteroscedastic, the 5% and 95% percentiles of the distribution are calculated and interpreted as a lower and upper uncertainty bound (see e.g. Franks et al., 1996).

In this manner model calibration is placed in a framework of calculating prediction uncertainty due to uncertainty that needs to be associated with non-uniqueness of parameter sets. A unique and optimal parameter set is not defined but effects of parameter values as described by the likelihood distribution functions are simulated. With the GLUE procedure, the structure of a parameter set in terms of a parameter inter-dependencies such as parameter correlation are not simulated, but parameter inter-dependencies are implicitly expressed in the marginal likelihood distributions of the parameters.

An appealing aspect of the GLUE procedure is that the likelihood weight of behaviour parameter sets easily are updated when additional time series of observations becomes available. A model is tested by a split sample test where a part of the time series is used for model calibration

and the second part is used for model validation. By such a procedure it is likely that the gradient of the marginal cumulative distribution function increases and that identifiability of parameters increases since additional observation data is used by which parameter values are updated. Also parameter uncertainty then reduces and the 5 and 95% percentile uncertainty bound for calculated model output becomes smaller (see e.g. Lamb et al., 1998). For updating likelihood weights using additional time series, the probability theory of Bayes is applied. The conditional posterior likelihood distribution is calculated by use of the product rule of probabilities:

$$\ell(\Theta_i | Y, M) = \frac{\ell(Y | \Theta_i, M)\ell(\Theta_i, M)}{\sum_{\text{all } i} \ell(Y | \Theta_i, M)\ell(\Theta_i, M)} \quad [5.4]$$

where

M = expression for the applied model concept

$\ell(\Theta_i|M)$ = prior likelihood of parameter set i

$\ell(\Theta_i|Y, M)$ = posterior likelihood of parameter set i

$\ell(Y|\Theta_i, M)$ = likelihood calculated by use of additional time series Y.

The summation term in the numerator serves as a normalisation or scaling factor.

Additional observation data may also be available in the form of a time series of a second state variable of interest. The likelihood measure then is calculated by the sum rule of probabilities and likelihood measures of each state variable are combined, weighted and summed. Lamb et al., [1998] apply the following likelihood measure when groundwater table data of two piezometers and channel flow data are used:

$$\ell(\Theta_i | Y_1, Y_2, Y_n, M) = \frac{1}{C} \left[- \left(w_1 \frac{\sigma_{e,1}^2}{\sigma_{o,1}^2} + w_2 \frac{\sigma_{e,2}^2}{\sigma_{o,2}^2} + \dots + w_n \frac{\sigma_{e,n}^2}{\sigma_{o,n}^2} \right) \right]^N \quad [5.5]$$

C is a normalisation factor and Y_1, \dots, Y_n are observations of multiple state variables that condition the likelihood measure. Lamb et al., [1998], applied the Topmodel approach and used channel flow and groundwater table data for model calibration. After analysis of the simulation results it was concluded that the use of multiple state variables in the likelihood measure of Eq. [5.5] does not improve model performance significantly although parameter uncertainty decreased. Franks et al., [1996] also applied the Topmodel approach and used runoff data and observations of

saturated areas but also came to similar conclusions. Simulation results from both studies indicate that the selected model concept of Topmodel is insufficient and that the model concept must be interpreted as an incorrect descriptor of the catchment.

Some concluding remarks on the GLUE procedure are made. Although the procedure generally is accepted as a useful calibration tool some critical notes are made. The procedure shows important weaknesses with regard to the selection of a) the rejection threshold value, b) an appropriate likelihood measure and c) prior distribution functions. Objective guidelines to make these selections are not presented in literature although each of these aspects has an impact on the overall calibration results. In this respect the author shares the opinion of Clarke [1994] and Gupta et al., [1998] who regard the procedure as

“.....bold attempt to introduce some much-needed new thinking into a field that is in grave danger of becoming intellectually sterile”

Moreover, the procedure ignores effects parameter inter-dependencies have on simulation results. The overall parameter structure in terms of a parameter correlation or parameter co-variance matrices does not come available nor does the procedure present quantitative statistical information on how well parameter values are identified. The procedure also does not show significant improvements in simulation results when multiple state variables are used. The latter probably is due to insufficiencies of the applied model concept, this possibly as caused by aggregation of a number of flow processes into a single flow process. A different reason might be that the gauging resolutions of time series are inappropriate or that observation resolutions are unbalanced. Also the weights applied to each likelihood measure may be defined on subjective grounds and so are incorrect. In the work of Lamb et al., [1998] for example, equal values are selected for all weights.

5.4 Automated model calibration by evolutionary methods

The use of automated model calibration by evolutionary methods is researched and advocated by Gupta and Sorooshian [1994], Duan [1991] and Yapo [1996] Gupta, et al., [1998], among others. A principle assumption underlying the procedure is that a single best and unique parameter set can be defined through the minimisation of the residual

error. Such minimisation is achieved through optimisation of parameters only and calibration criteria such as RMSE and R^2 are selected and termed objective functions. Parameter sets are optimised by repeated evolutions of model performance that results in defining most optimal parameter set. Such optimisation requires that a model is sensitive to selected parameters and that the evolutionary search algorithm is able to find the most optimal parameter set out of a pre-defined parameter space. Prior to evolutions, a large number of prior parameter sets are generated by a Monte Carlo parameter sampling procedure. Parameter values of prior sets are sampled from uniform probability distribution functions where ranges of parameter values are bounded by upper and lower values. Hence this approach to define prior parameter sets is similar to the procedure as applied in the GLUE procedure. The objective of evolutionary methods, however, is different from the objective of the GLUE procedure. In the search procedure the large number of prior parameter sets is reduced to yield only one optimised and unique parameter set. Parameter set reduction is achieved by monitoring those parameter sets that produce a decrease of the objective function value. Such 'good' sets are maintained and used for further evolutions. The philosophy behind the evolutions is that good sets have good parameter values and that such values must be combined into new, improved, parameter sets. In these new sets, the initially defined parameter value ranges are reduced to a much smaller range and after repeated evolutions optimum values are defined. Mathematical aspects of evolutionary search procedures are explained in more detail in the following paragraphs.

Duan et al., [1992] and Yapo et al., [1996]; among others, conclude that parameter estimation by evolutionary methods must be placed in a global optimisation calculation framework. Duan et al., [1992] conclude that an objective function response surface of many local search algorithms contain numerous local optima. In this context the 'Simplex method' (Nelder and Mead, 1965), 'Rosenbrocks method' (1960), 'Pattern search method' (Hooke and Jeeves, 1961) and the 'Newton-Raphsons method' are mentioned. A local optimum could be obtained due to artefacts relating to non-convergence of the search algorithm or due to initialisation effects of the search algorithm where different initial parameter values yield different estimation optima. Evolutionary procedures therefore only are successful if, after convergence, always the

same optimised parameter set is generated. The Monte Carlo sampling procedure to define prior parameter sets thus has no effect on the optimised parameter set. In this manner a unique and most optimal parameter set is defined based on the available calibration data. Duan [1992] researched the applicability of local search methods in detail and developed a global search algorithm called the 'Shuffled Complex Evolution-University of Arizona' (SCE-UA) algorithm. The development of this algorithm is regarded a breakthrough in the field of automated model calibration since the algorithm is able to find the global optimum of the objective function response surface. Prior to this development, a large number of attempts have been reported to develop such global search algorithms but attempts were not successful.

The SCE-UA algorithm is a population evolution method and requires multiple steps to define the global optimum of the objective function response surface. In the following paragraphs, single-objective and multi-objective model calibration by evolution algorithms is presented and discussed.

Single-Objective Complex Evolution

As a first step of the SCE-UA algorithm, a relatively small population of parameter sets is generated within the feasible parameter space. By a random sampling procedure, parameter values are drawn from uniform prior parameter distributions and are combined to generate a large number of parameter sets that all contain different parameter values. In the evolutionary procedure each parameter set is interpreted as a 'point' for which a model calculation is executed. For each point, model performance is judged by a model performance criterion that serves as an objective function. For each point a different objective function value is calculated and so allows ranking of values in order of increasing magnitude. The first point in rank has the smallest objective function value and can be interpreted as the parameter set that yields best model result while the last point has the highest objective function value and thus can be interpreted as the worst parameter set.

In the following a short description after Duan et al., [1994] is given on the SCE-UA-algorithm. In the algorithm a parameter sample population, \mathbf{s} , is partitioned into \mathbf{p} complexes that all contain \mathbf{m} points. For \mathbf{m} the number of points are $\geq \mathbf{n}+1$ where \mathbf{n} is the dimension of the estimation problem and is equal to the number of parameters to be estimated.

Complex partitioning is achieved in such manner that the first complex contains every $p(k-1)+1$ ranked point, the second complex contains every $p(k-1)+2$ ranked points and so on with $k = 1, 2, 3, \dots, m$. Each complex now is evolved in parameter space according to the "Competitive Complex Evolution" (CCE) algorithm that is based on the Simplex downhill search scheme of Nelder and Mead [1965]. In this multi-step evolution procedure, sub-complexes of q randomly selected points are constructed from each complex according to a trapezoidal probability distribution. This distribution is specified such that the best point has the highest change of being chosen to form the sub-complex while the worst point has the lowest change. In the procedure the objective now is to reduce the parameter space by generating new points that have lower objective function values than selected points in the sub-complex. In the evolution procedure the selected points are called 'parents' and are disregarded from further analysis in case new points, that is called 'offspring', can be generated. For every evolution step, in each sub-complex the centroid of a sub-complex with q points is defined after rejecting the worst point in the sub-complex. Based on the location of this centroid in parameter space, an offspring point is defined by a reflection step or a contraction step. Offspring generated by a reflection step implies that the offspring point coincides with the centroid point that lies in the feasible parameter space while by the contraction step the offspring point is located half way between the centroid and the worst point in the sub-complex. In this manner each offspring point represents a parameter set with values that yield a lower objective function value than for the worst point in the sub-complex. In figure 5.4a-f an illustration of the evolution process by the CCE algorithm is presented where each \bullet represents a parent point within the sub-complex and where a $*$ represents an offspring point. Contour lines in the figure are lines of equal objective function value and serve to guide the parameter optimisation procedure. For each sub-complex the centroid is defined after rejecting the worst point of the distribution. A reflection step for the worst point through this centroid now is performed and such new point is analysed whether it falls within the feasible parameter space. If this new point is better than the worst point than this point is replaced by the offspring point (see fig. 5.4a,b,d) that, after repeated evolutions, narrows down the parameter space. If the new point is worse, than a contraction step is attempted by computing a point halfway between the

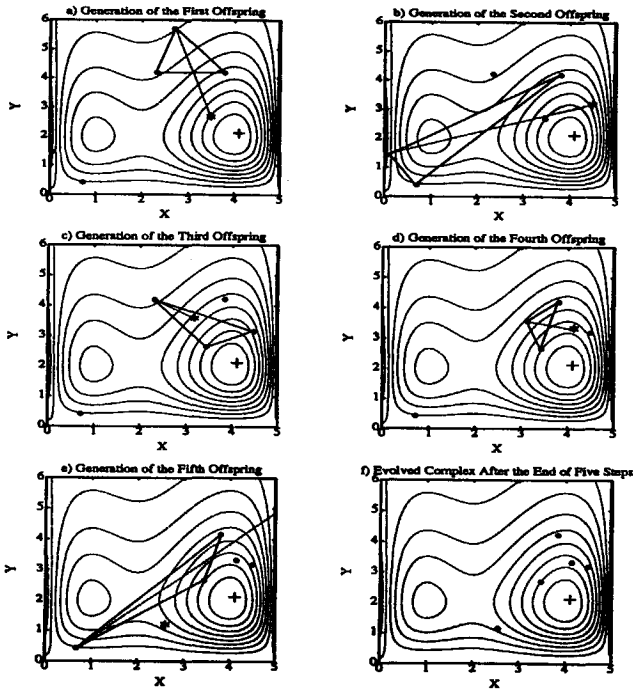


Figure 5.4: *Illustration of the evolution steps in each complex (Duan et al., 1994)*

centroid and the worst point (fig. 5.4c). If this offspring point is better than the worst point in the sub-complex then a replacement takes place while otherwise the worst point is replaced by a randomly generated point (fig. 5.4e). In this approach, each point of a complex is a potential parent with the ability to participate in the process of producing offspring. It is clear that the objective of the CCE evolution procedure is to generate offspring that is better than a parent point and that parameter space is narrowed down in each evolution step.

The following step in the SCE-UA algorithm is to combine or 'shuffle' the points of the evolved complexes and to create a new sample. From this sample new complexes are generated by the previously described random search procedure. The number of complexes however decreases by the repeated rejection of the worst points in the CCE algorithm since only points are maintained in the evolution with lowest objective function values. By re-shuffling of the sample population at periodic

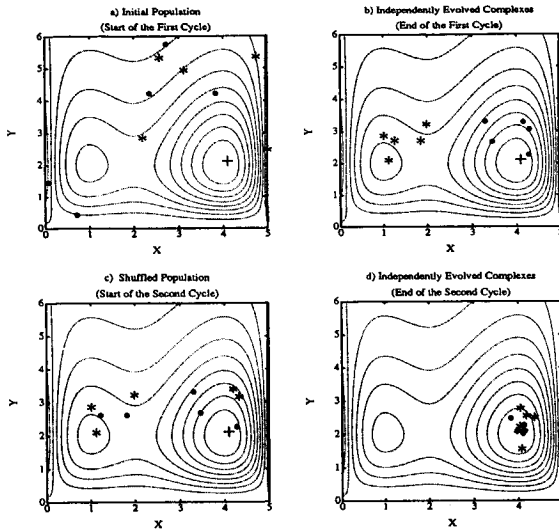


Figure 5.5: Illustration of the SCE-UA algorithm (Duan et al. 1994)

stages, parameter sets (i.e. point) are re-assigned to complexes and share information of the, so far, optimised parameter sets. By the repetitive evolution-shuffling procedure the entire population tends to converge towards the neighbourhood of the global optimum provided that the initial population size is sufficient large. The procedure stops if pre-defined convergence criteria of the algorithm are satisfied and the global optimum for all evolutions is reached. At the global minimum the single best and unique parameter set is generated.

In figure 5.5a-d an illustration of the SCE-UA algorithm is presented. In this figure two complexes are generated from the initial sample population s and points within a complex are represented by \bullet and $*$. Similar to figure 5.4, contour lines in the figure are lines of equal objective function value and serve to guide the parameter optimisation procedure. For each complex 5 parent points are selected for evolution by the CCE algorithm that, after repeated evolution, are replaced by offspring points with a lower objective function value (fig. 5.5b). In figure 5.5b offspring points in the two complexes converge towards a local and global objective function minimum. In order to converge towards the global minimum, new complexes are created by re-shuffling offspring points (fig. 5.5c) and a second optimisation cycle is started. For

these new complexes the CCE algorithm will generate offspring points and by repeated evaluations, offspring points converge toward the global minimum (fig. 5.5d).

Duan et al., [1992] state that the SCE-UA algorithm combines the strength of the simplex procedure of Nelder and Mead [1965] with the concepts of controlled random search (Price, 1987), competitive evolution (Holland, 1975) and the, at that time, newly developed concept of complex shuffling. The search procedure is very successful in finding global optima of the objective function response surface (see Duan et al., 1993; 1994; Yapo et al., 1996). By the procedure the initial parameter space is narrowed down to yield only most optimal values for the parameter set as a whole as for each single parameter. For detailed descriptions on the mathematical aspects of the evolution algorithm reference is made to Duan et al., [1992], [1994] and Yapo et al., [1996].

The algorithm is regarded 'effective and efficient' in the sense that for large number of prior parameter sets single best parameter set are estimated successfully and that limited function evaluations are required to define the optimum parameter values (Duan et al., 1992). Duan et al., [1994] applied the algorithm in CRR modelling to the Sacramento Soil Moisture Accounting (SAC-SMA) model (Burnash, 1973). They calculated single best parameter values by the Single Least Squares (SLS) and Heteroscedastic Maximum Likelihood Estimation (HMLE) objective functions (see table 5.1) for a two and six parameter estimation problem. Yapo et al., [1996] also used the SAC-SMA model and selected HMLE and Daily Root Mean Squared Error (DRMS) objective functions and applied the SCE-UA algorithm to a 13 parameter estimation problem. The model performance was evaluated by use of Percent Bias (PBIAS) and Nash-Sutcliffe model performance criteria (see table 5.1). During simulations it emerged that dissimilar optimal parameter values were obtained for HMLS and DRMS objective functions. It also emerged that model performance expressed by NS or BIAS criterion is subject to the a) selected objective function and b) response mode of the catchment that is expressed by the various runoff stages in the runoff hydrograph. In further analysis, time series of observations were divided in two samples with observations that are 'below mean' and 'above mean'. Thus each sample characterised a specific catchment response mode and by simulations it appeared that for both samples model performance also is subject to the selected objective function. By Duan et al., [1992] it is

established that for different model response modes different objective functions must be selected and that each objective function will yield different parameter sets when estimated by the SCE-UA algorithm. The overall conclusion on the evolutionary procedure by the SCE-UA algorithm is that model calibration basically is a multi-objective parameter estimation problem that requires parameter optimisation routines that are able to optimise a parameter set when multiple objective functions are minimised simultaneously. Such an algorithm was proposed and described by Gupta et al., [1998], Yapo et al., [1998] and Sorooshian et al., [1998] and is termed the 'Multi-Objective COMplex Evolution-University of Arizona' (MOCOM-UA) algorithm. This algorithm is an extension of the SCE-UA algorithm and follows a similar evolution search strategy.

Multi-Objective Complex Evolution

In runoff hydrology a large number of objective functions are developed for model calibration. A selection of commonly applied functions is presented in table 5.1. Each of the functions also can be used in automated model calibration while a number of functions are developed to describe specific characteristics of the runoff hydrograph. In the multi-objective complex evolution procedure a number of objective functions are selected and combined to make up an aggregated objective function. The objective now becomes to minimise such function by minimising all selected objective functions simultaneously. In such approach the complexity of minimisation of the aggregated function reduces to an, in essence, single-objective optimisation problem.

Mathematically, the aggregated objective function, $F(\Theta)$, is minimised as function of parameter set Θ that is applied to each of the selected objective functions:

$$F(\Theta) = \min\{f_1(\Theta), \dots, f_m(\Theta)\} \quad [5.6]$$

Each objective function f_1, \dots, f_m , is minimised with respect to the residual error for a time series of observations $1, \dots, n$. For each parameter set a residual error, $e(\Theta)_n$, is defined over the calibration period for the aggregated function:

$$E(\Theta) = \sum_1^m f[S_c(\Theta) - (S_o)] = \{e(\Theta)_1, \dots, e(\Theta)_n\} \quad [5.7]$$

where

$E(\Theta)$ = residual vector of calculated and observed state variables

$e(\Theta)_{1..n}$ = residual error over time step 1...n

f = function for linear or non-linear transformation (e.g. min, max)

$S_c(\Theta)$ = vector of calculated state information subject to set Θ

S_o = vector of observed state information.

Table 5.1: Selection of objective functions used by the National Weather Service for calibrating the SAC-SMA model (modified after Basil et al., 1981).

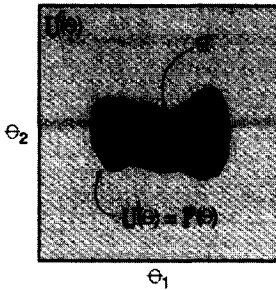
	Daily Root Mean Squared Error	Mimimise w.r.t. Θ	$\sqrt{\frac{1}{n} \sum_{t=1}^n (d_t - o_t(\Theta))^2}$
	Total Mean Montly Volume Squared Error	Mimimise w.r.t. Θ	$\sum_{i=1}^{n\text{month}} \frac{1}{n\text{day}(i)} \sum_{t=1}^{n\text{day}(i)} (d_t - o_t(\Theta))^2$
	Mean Absolute error	Mimimise w.r.t. Θ	$\frac{1}{n} \sum_{t=1}^n d_t - o_t(\Theta) $
	Maximum Absolute Error	Mimimise w.r.t. Θ	$\max d_t - o_t(\Theta) $
	Nash-Sutcliffe Measure	Mimimise w.r.t. Θ	$1 - \frac{\frac{1}{n} \sum_{t=1}^n (d_t - o_t(\Theta))^2}{\frac{1}{n} \sum_{t=1}^n (d_t - \bar{d})^2}$
HMLE	Heteroscedastic Maximum Likelihood Estimation	Mimimise w.r.t. Θ, λ	$\text{HMLE} = \frac{1}{n} \sum_{t=1}^n w_t (q_{t,\text{obs}} - q_{t,\text{calc}})^2$ $\left[\prod_{t=1}^n w_t \right]^{\frac{1}{n}}$
BIAS	Bias (mean daily error)	Mimimise w.r.t. Θ	$\frac{1}{n} \sum_{t=1}^n (d_t - o_t(\Theta))$

Similar to single-objective model calibration, also for the aggregated objective function, $F(\Theta)$, a parameter set is selected and optimised by a global optimisation algorithm.

As stated above, all selected objective functions are minimised simultaneously while this minimisation is achieved through various combinations of functions f_1, \dots, f_m . Optimised parameter set are defined

for each combination of objective functions. By such approach, a number of optimised parameter sets are generated that are dissimilar from any other set. It is obvious that by moving from one such combination to another combination, a large range of parameter sets are tested and trade-off functions of single parameters can be defined with respect to $F(\Theta)$. Such trade-off functions are defined for any combination of objective functions and express the effect each parameter has on the aggregated objective function value. While selected parameter values applied to some functions may cause a significant optimisation improvement, the same parameter value applied to other functions may cause deterioration.

In multi-objective model calibration the philosophy now is that a large number of parameter sets can be simulated that all will yield an equally low objective function value for $F(\Theta)$. By an understanding of the complexity of such calibration procedure, it is obvious that parameter values are dissimilar and that multiple combinations of parameter values can be found that all will yield an equally low objective function value. In the procedure the initial parameter space is narrowed down to a much smaller parameter space in which any combination of selected parameter values perform equally well. When these parameter sets are combined they make up a new parameter space. In multi-objective model calibration this optimised parameter space is termed the 'Pareto space' or 'Pareto set' $P(\Theta)$. Through the optimisation procedure the initial or prior parameter space is subdivided in two parameter spaces; a small space with optimised parameter values and a remaining much larger parameter space that is rejected for further application. Gupta et al., [1998] state that every parameter set or member Θ_p of the Pareto set will match some characteristic of the hydrograph better than every other member of the Pareto set, but the trade-off will be that some other characteristics of the hydrograph will not be as well-matched. In the theory on multi-objective model calibration, the parameter sets defined within the Pareto space are termed 'good' solutions or 'Pareto' solutions while all other parameter sets are termed 'bad' solutions or 'non-Pareto' solutions. The definition of the Pareto set is such that any member Θ_p has the following properties (after Sorooshian et al., 1998):



- Θ^* = Member of Pareto set
 $P(\Theta)$ = Pareto set
 $U^f(\Theta)$ = uncertainty of the parameter space
 (i.e. Pareto space)
 $U^o(\Theta)$ = prior uncertainty of parameter space
 $\theta_{1,2}$ = parameters

Figure 5.6: Reduction of the prior parameter space to Pareto space (Sorooshian et al., 1998).

1. for all non-members Θ_d of the Pareto set there exist at least one member Θ_p such that $F(\Theta_p)$ is strictly less than $F(\Theta_d)$. This implements that the parameter space can be partitioned in good and bad solutions.
2. it is not possible to find Θ_d within the Pareto set such that $F(\Theta_d)$ is strictly less than $F(\Theta_p)$. This implements that, in the absence of additional information, it is not possible to distinguish between any of the good Pareto solutions to be objectively better than any of the other good solutions.

'Strictly less than' means that $f_k(\Theta_d) < f_k(\Theta_p)$ for all $k = 1, \dots, m$

In the procedure it is important to select objective functions f_1, \dots, f_m that are 'relatively unrelated' (Gupta et al., 1998) and 'non-commensurable' (Yapo et al., 1998) to preserve the data content of the observation time series. Selected objective functions must measure different aspects of the difference between observed and model calculated state information and this information must be transformed into parameter estimates. The size and shape of the Pareto set is defined by this transformation and the Pareto set forms an aggregated parameter set with members that all are subject of the aggregated objective function $F(\Theta)$. An inefficient aggregated objective function $F(\Theta)$ so will yield an inefficient Pareto set while an efficient function will yield an efficient Pareto set. Objective criteria for the selection of $F(\Theta)$ are not presented although it is obvious that selected objective functions must be relatively unrelated and non-commensurable.

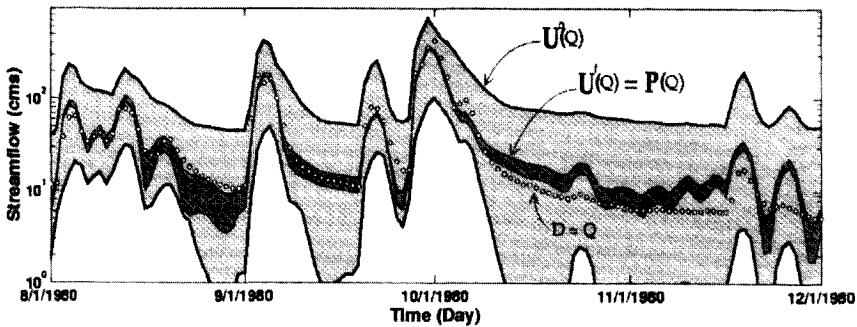


Figure 5.7: Illustration of parameter and hydrograph estimates obtained using the multi objective calibration approach. Q = observed channel flow, $U^i(Q)$ = model output uncertainty for Pareto set, $U^o(Q)$ = model output uncertainty for prior parameter space (Sorooshian et al., 1998).

The identification of a Pareto set has some appealing features. Each member of the Pareto set can be interpreted as a single best parameter set. Each set, however, is associated with uncertainty that is bounded by the size and shape of the Pareto space. In this manner the inherent multi-equivalence character of parameter sets is accommodated for and model performance can be tested over a range of equally satisfactory parameter sets. Sorooshian et al., [1998] describe model simulations for each member of the Pareto set and hydrograph model output is aggregated into one distribution function that is bounded by an uncertainty band. In this manner, parameter uncertainty as expressed by the size and shape of the Pareto set is transformed into a hydrograph uncertainty band (see fig. 5.7). By an understanding of the meaning of such uncertainty band it is clear that a large band indicates that the model is (very) sensitive to the selected parameter sets while a small band indicates low model insensitivity. Although the range of parameter values is calculated within the Pareto set, the effect each parameter has on the simulated hydrograph over a range of model response modes is uncertain. Some parameters could be very sensitive when simulating base flow discharges while they could be insensitive when peak flow discharges are simulated. Based on this reasoning, parameter values change over time with the change of the model response modes. This aspect of model calibration is not researched in multi-objective model calibration.

A second feature of the Pareto set is that insufficiencies in the design of the model concept may become apparent in the simulation results. In figure 5.7 a hydrograph uncertainty band is simulated by use of all possible parameter sets that are drawn from the Pareto space.

Theoretically, the Pareto parameter space represents the feasible parameter space for which the model performance is optimal. The Pareto space as generated by the multi-objective modelling approach is applicable to the entire range of catchment response modes. With respect to the information content of available time-series that are selected for model calibration, this information content is utilised in the most optimal manner. When, by use of the entire Pareto set, the hydrograph uncertainty band does not cover the observed hydrograph, it is concluded that the designed model concept is insufficient. In figure 5.7, it is observed that the base flow discharge for large time windows is under or over-estimated and indicates that runoff production from the groundwater domain of the selected SAC-SMA model approach is insufficiently simulated during inter-storm periods.

An efficient tool to calculate the Pareto set is the MOCOM-UA algorithm that is an extension of the SCE-UA algorithm. Similar to the SCE-UA algorithm, a population of points (i.e. parameter sets) is drawn randomly by a uniform sampling distribution from the initial or prior parameter space. For each point the aggregated objective function value $F(\Theta)$ is computed and the population is ranked and sorted by applying a Pareto-ranking procedure that is suggested by Goldberg [1989]. In this procedure simplexes of $s+1$ points are selected from the population according to a robust rank-based selection method (Whitley, 1989). In the MOCOM-UA algorithm, a newly developed multi-objective extension of the downhill simplex method is used to evolve each simplex in a multi-objective improvement direction. In this method the entire population of points will converge toward the Pareto optimum by iterative application of ranking and evolution procedures where iterations terminate when all points of the continuously reduced population fall within the Pareto space. While in the SCE-UA algorithm only one optimised parameter set is defined, in the MOCOM-UA algorithm the Pareto parameter space is defined. In the MOCOM-UA algorithm, the concepts of controlled random search (Price, 1987) and the competitive evolution (Holland, 1975) also are implemented. Differences are due to the implementation of the multi-objective

extension of the downhill simplex method and the exclusion of the complex shuffling strategy. The mathematical aspects of this tool are described in detail by Sorooshian et al., [1998] and are not repeated.

Some concluding remarks on automated model calibration by evolutionary methods can be made. Evolutionary methods are applicable to single objective model calibration as well as to multi-objective model calibration. In the first case the objective is to find a most optimal parameter set that is interpreted as 'single best' and 'unique' in a manner that further improvement cannot be gained by further parameter optimisation. Parameters are identified based on the selected objective function and are subject to the information content of the time series of observations of the calibration period. Single-objective model calibration by evolutionary methods is a traditional model calibration procedure in a sense that a single best and unique parameter set is defined. Compared to the manual Trial and Error calibration procedure, the use automated evolutionary method is very advantageous since the most optimal parameter values as well as parameter set is defined. Further efforts in improving the optimised parameter set will not result in improved model performance and many of the limitations of Trial and Error procedures is circumvented for. Limitations of the automated procedure are that parameter optimisation is achieved for one objective function only and that information on parameter inter-relations and dependencies is not provided.

In multi-objective model calibration, a number of objective functions are aggregated into one objective function and model calibration is achieved by simultaneous optimisation of the selected single-objective functions. Such procedure is very advantageous since multiple optimal parameter sets are defined that are subject to the selection of objective functions. By the procedure, for each parameter a range of values is defined for which the model performance is optimal. The entire parameter space is termed the Pareto parameter space and any selected parameter set within this space performs equally well. The Pareto space represents the optimised parameter space for which model performance is optimal and, for each parameter, this space is interpreted as a parameter uncertainty space. This uncertainty is transformed into a hydrograph uncertainty band when for each parameter set a model calculation is executed. In such manner insufficiencies of the model concept become apparent when the observed runoff hydrograph for the various model response

modes falls outside the uncertainty band. A weakness of the procedure is that any dependency between single parameters is not described. A parameter correlation matrix is not generated and information on how well parameters are identified relies on the model sensitivity. Statistical information on such parameter identifiability is not provided.

Conclusions on parameter identifiability for the various model response modes are vague due to the inherent multi-objective character of the parameter optimisation procedure. The procedure, however, has a (very) high potential for runoff modelling and the procedure is very suitable to be applied to PBRR modelling.

5.5 Automated model calibration by Maximum Likelihood Estimation (MLE)

Introduction

Automated model calibration by MLE mostly is achieved by optimising parameters only. In the procedure of model calibration an *a-priori* defined model concept is selected that does not require improvement or optimisation and, similar to the calibration approaches described in sections 5.2-5.4, model calibration is reduced to a procedure of parameter optimisation. In MLE such optimisation is accomplished by minimising a single objective function by least squares estimation. State variables of interest can be any of the state variables applied in the objective functions of table 5.1. Also in automated model calibration by MLE, a model is calibrated in case the objective function value is minimised as a result of parameter optimisation.

In MLE statistical properties of the calibration process guide the parameter optimisation and therefore is fundamentally different from other approaches described in this thesis. Carrera and Neumann [1986] advocated inverse modelling by means MLE on the premise that

“for any given measured head and flow field only one set of the optimal parameters exists” (i.e. ‘uniqueness’) and “a unique set of parameter values yields a unique head and flow field” (i.e. ‘identifiability’).

‘Uniqueness’ and ‘identifiability’ are inversely related and this principle resides at the core of the calibration methodology. Since the early applications of MLE by Carrera and Neumann [1986], inverse modelling by MLE is widely applied in groundwater modelling while applications

in PBRR modelling have not gained (much) attention. Reviews of MLE calibration procedures as well as new developments and applications of such procedures in numerical groundwater modelling are presented by Te Stroet, [1995]; Hill, [1998], Olsthoorn, [1998]; Valstar, [2001], among others. Such review is not repeated here but only a brief description on basic aspects of parameter estimation by MLE is presented instead.

In numerical hydrologic modelling, calculated state variables commonly are expressed by a linear system of equations:

$$\begin{aligned}
 h_{sc1} &= x_{11}p_1 + x_{12}p_2 + \dots + x_{1n}p_n \\
 h_{sc2} &= x_{21}p_1 + x_{22}p_2 + \dots + x_{2n}p_n \\
 h_{sc3} &= x_{31}p_1 + x_{32}p_2 + \dots + x_{3n}p_n \\
 &\dots\dots\dots \\
 h_{scm} &= x_{m1}p_1 + x_{m2}p_2 + \dots + x_{mn}p_n
 \end{aligned}
 \tag{5.8}$$

The entire set of calculated state variables, $h_{sc1..m}$, over a spatially discretised model domain are calculated by a set of parameters $p_{1..n}$, and a set of operators $x_{11..mn}$. Rewriting Eq.[5.8] in matrix notation yield Eq.[5.9] and encompass a one-dimensional matrix vector of calculated state variables of size m , a 1-dimensional vector of model parameters of size n and a two-dimensional matrix vector of size $m \times n$ of system operators. In modelling terms, such operators stand for the model approach that is expressed in terms of the model concept, simulated meteorological influences and applied boundary and initial conditions.

$$\begin{bmatrix} h_{sc1} \\ \cdot \\ h_{scm} \end{bmatrix} = \begin{bmatrix} p_1 \\ \cdot \\ p_n \end{bmatrix} \cdot \begin{bmatrix} x_{11} & \dots & x_{1n} \\ \cdot & \dots & \cdot \\ x_{m1} & \dots & x_{mn} \end{bmatrix}
 \tag{5.9}$$

or, when expressed in vector notation this yields:

$$\mathbf{h}_{sc} = \mathbf{Xp}
 \tag{5.10}$$

When rewriting Eq.[5.10] for parameter vector \mathbf{P} , the inverse expression for state vector \mathbf{h}_{sc} is obtained that is at the core of automated model calibration by MLE.

Maximum likelihood estimation

MLE is based on weighted least squares estimation in which the goal is to minimise the weighted squared residual error between observed and model calculated state variables. The weighted least squares estimation expression reads:

$$\mathcal{Q} = \sum_{i=1}^m w_i (h_{so} - h_{sc})^2 \quad [5.11]$$

where

- \mathcal{Q} = objective function value
- w_i = weight for measurement number i
- h_{so} = observed state variable
- h_{sc} = calculated state variable
- m = number of observations.

In weighted least squares estimation the residual error is interpreted as a cumulated error that arises from various error sources such as incompleteness of the model concept, uncertainties associated with estimates of parameter values and observation of state variables. Each of these error sources contributes to the cumulated residual error and any observed state variable can be expressed as follows:

$$h_{so} = h_{sc} + e_m + e_p + e_o \quad [5.12]$$

where

- e_m = residual error due to incompleteness of the model concept
- e_p = residual error due to parameter uncertainty
- e_o = residual error due to inaccurate observations.

Prior to the model calibration, in theory error functions must be defined for each of these error sources. Following the expression of Eq.[5.12], error functions are defined for e_m , e_p and e_o and effects of each function on the parameter estimation can be simulated. In the practice of hydrological modelling, however, it is common to apply simplifying assumptions to each of these error functions. From a statistical point of view for example, residual errors of e_m , e_p and e_o often are assumed to have a random character and errors are interpreted as random variables that follow a specific probability distribution function. Such functions generally are considered to follow a Gaussian distribution with zero mean and a known variance and thus errors are evenly distributed throughout a model simulation. Since model calibration is achieved

through parameter optimisation only, residual errors associated with e_m , and e_o are ignored. Mostly an *a-priori* defined model concept and time series of observations are selected that are not associated with uncertainty and randomness. Although this assumption must be questioned its implementation is very advantageous since the residual error e_m then reduces to zero. Ignoring residual errors that are due to observation inaccuracies also is questionable since, in general, the temporal and spatial observation scales hardly coincide with model scales in terms of the simulation time step and the grid element scale. Also with regard to the parameters that need to be optimised a number of simplifying assumptions can be made. It could for example be assumed that a probability distribution function of the parameters is known prior to the parameter estimation or, contrary, it may be assumed that such function itself is unknown although parameter values follow a probability distribution function. It also could for example be assumed that parameter values are uniformly distributed instead of the commonly assumed Gaussian distribution.

Many different calibration approaches are known by these assumptions and the use of prior knowledge on e_m , e_p and e_o . Reviewing these approaches is out of scope of this thesis and one is referred to Te Stroet [1995]; Olsthoorn, [1998] and Valstar, [2001] where various aspects are discussed. Here only common simplifications that are at the core of the parameter optimisation algorithm that is applied to the Troy case study of Chapter 6 are addressed.

The first assumption is the use of an *a-priori* defined model concept that causes that the residual error e_m is ignored. A second assumption is that parameter values are completely unknown and that a probability distribution function also is unknown. The only assumption is that the probability density function is Gaussian distributed and that its covariance is known. For the state observations, the assumption is made that a probability distribution function of observation errors, e_o , can be ignored although each state observation is associated with an observation variance. By these assumptions, the procedure of parameter estimation is placed in a framework of MLE. Kendall and Stuart, [1997] describe that in MLE parameter values are estimated for which the conditional probability density function, $p(h_o|p)$, is maximum and thus, estimates of parameter values are interpreted as statistical true values.

Expressing the weighted least squares estimation equation [5.12] in a MLE framework yields:

$$\vartheta = ((\mathbf{h}_{so} - \mathbf{h}_{sc})^T \mathbf{W} (\mathbf{h}_{so} - \mathbf{h}_{sc})) = \mathbf{e}^T \mathbf{W} \mathbf{e} \quad [5.13]$$

where \mathbf{W} is a block matrix with dimension $m \times m$ of observation weights and where \cdot^T indicates a transpose operation. In the equation \mathbf{h}_{so} and \mathbf{h}_{sc} represent vector matrices of selected observed and model calculated state variables respectively while \mathbf{e} represents the state vector of residual errors. In the objective function Eq.[5.13] the variances of the residuals are weighted by the elements of the matrix \mathbf{W} that are either uniformly or non-uniformly distributed over the observations. In the former the minimisation of Eq.[5.13] is reduced to become a simple least squares estimation problem while in the latter the relative importance of each observation is weighted. Weighing is particularly useful when state observations of a different kind and possibly different magnitude are applied in the calibration. In multi-output models such as PBRR models where channel outflow data and groundwater table data can be used simultaneous as state variables of interest, this aspect of model calibration by MLE is very attractive. By weighing also the effect of clustered observations can be accommodated for.

The weight matrix is defined by various techniques. Weights most commonly are defined in such a manner that the weight reflects the accuracy of the measurements (see Carrera and Neuman, 1986; Hill, 1998). Other techniques that are known but not commonly applied are Kalman filtering (te Stroet 1995), Kriging (Isaaks & Srivastava, 1989) and stratification based on the sizes of homogeneous units (Zaadnoordijk and Stein, 1997). The weight matrix \mathbf{W} with dimension $m \times m$ can be reduced to become a block diagonal matrix when it is assumed that observations are mutually independent. This implies that the mean of measurement errors is zero and that observations have no underlying spatial or temporal structure. By this principle assumption, the covariance of each observation may serve as the weight in matrix \mathbf{W} and such matrix becomes a covariance matrix of observation weights. By MLE, the calculated state vector is obtained when the inverse of the covariance observation vector, \mathbf{C} , is substituted for \mathbf{W} in Eq.[5.13]:

$$\mathbf{W} = \mathbf{C}^{-1} = \begin{bmatrix} \frac{1}{C_1} & 0 & 0 & 0 \\ 0 & \frac{1}{C_2} & 0 & 0 \\ 0 & 0 & \frac{1}{C_3} & 0 \\ 0 & 0 & 0 & \frac{1}{C_4} \end{bmatrix} \quad [5.14]$$

In such approach the squared head residuals are weighted by the inverse of the observation covariance matrix. For non-correlated measurements the covariance matrix has diagonal elements only and weighting factors are equal to the reciprocals of the measurement errors. As a result, the objective function value of Eq. [5.13] becomes dimensionless and makes that different state variables can be processed simultaneously. This aspect of MLE by weighted least squares estimation make applications in PBRR modelling very appealing.

Maximum likelihood estimates are obtained by minimising Eq. [5.15] in which the inverse of the covariance matrix of the observation errors \mathbf{C} is substituted for the weight matrix \mathbf{W} and where the calculated state vector \mathbf{h}_{sc} is replaced by the expression of Eq. [5.10]:

$$\vartheta = ((\mathbf{h}_{so} - \mathbf{Xp})^T \mathbf{C}^{-1} (\mathbf{h}_{so} - \mathbf{Xp})) \quad [5.15]$$

Minimising the objective function of Eq. [5.15] with respect to the parameter estimations, a column matrix of parameter set \mathbf{p} is calculated by the calculated vector matrix of state variables:

$$\begin{aligned} \vartheta &= ((\mathbf{h}_{so} - \mathbf{Xp})^T \mathbf{C}^{-1} (\mathbf{h}_{so} - \mathbf{Xp})) \\ &= \mathbf{h}_{so}^T \mathbf{C}^{-1} \mathbf{h}_{so} - \mathbf{h}_{so}^T \mathbf{C}^{-1} \mathbf{Xp} - \mathbf{X}^T \mathbf{p}^T \mathbf{C}^{-1} \mathbf{h}_{so} + \mathbf{X}^T \mathbf{p}^T \mathbf{C}^{-1} \mathbf{Xp} \end{aligned} \quad [5.16]$$

Minimisation is achieved by taking the derivative

$$\frac{\partial \vartheta}{\partial \mathbf{p}} = 2(\mathbf{X}^T \mathbf{C}^{-1} \mathbf{X}) \mathbf{p} - 2\mathbf{X}^T \mathbf{C}^{-1} \mathbf{h}_{so}$$

where parameter vector \mathbf{p} is expressed by:

$$\mathbf{p} = (\mathbf{X}^T \mathbf{C}^{-1} \mathbf{X})^{-1} \cdot \mathbf{X}^T \mathbf{C}^{-1} \mathbf{h}_{so} \quad [5.17]$$

Eq. [5.17] often is referred to as the 'normal equation' and provides a unique solution in case the number of observations is larger than or

equal to the number of parameters. Under such conditions the column matrix \mathbf{p} is singular that easily is calculated. The estimator of Eq. [5.17] is interpreted as the 'Best Linear Unbiased Estimator' (BLUE) of the set of true system parameters \mathbf{p}_{true} . Isaaks and Srivastava [1989] state that this estimator is linear because estimates are weighted linear combinations of the available data; it is unbiased since it tries to have the mean residual error equal to zero and it is best because it aims at minimising the variance of the residual error. In BLUE it is assumed that the expected values of the calculated parameters are equal to the statistically 'true' value of the parameter it is trying to estimate. The expression of \mathbf{p} in Eq.[5.17] now is interpreted as a minimum variance estimator. When \mathbf{h}_{sc} in Eq.[5.10] is rewritten for $\mathbf{X}\mathbf{p}_{\text{true}}$, when \mathbf{e} is a head residual error and when the observed state vector \mathbf{h}_{so} is expressed by

$$\mathbf{h}_{\text{so}} = \mathbf{X}\mathbf{p}_{\text{true}} + \mathbf{e} \quad [5.18]$$

then the estimated parameter set is equal to

$$\begin{aligned} \mathbf{p} &= (\mathbf{X}^T \mathbf{C}^{-1} \mathbf{X})^{-1} \cdot \mathbf{X}^T \mathbf{C}^{-1} (\mathbf{X}\mathbf{p}_{\text{true}} + \mathbf{e}) \\ &= (\mathbf{X}^T \mathbf{C}^{-1} \mathbf{X})^{-1} \cdot \mathbf{X}^T \mathbf{C}^{-1} \mathbf{p}_{\text{true}} + (\mathbf{X}^T \mathbf{C}^{-1} \mathbf{X})^{-1} \mathbf{X}^T \mathbf{C}^{-1} \cdot \mathbf{e} \\ &= \mathbf{p}_{\text{true}} + (\mathbf{X}^T \mathbf{C}^{-1} \mathbf{X})^{-1} \mathbf{X}^T \mathbf{C}^{-1} \cdot \mathbf{e} \end{aligned} \quad [5.19]$$

The estimated parameter set \mathbf{p} equals \mathbf{p}_{true} when the expectation of the residual error $E[\mathbf{e}]$ equals zero. By Eq. [5.19] the spatial dependency of parameters is calculated in terms of a covariance matrix \mathbf{C}_{ep} :

$$\begin{aligned} \mathbf{C}_{\text{ep}} &= E[(\mathbf{p} - \mathbf{p}_{\text{true}})(\mathbf{p} - \mathbf{p}_{\text{true}})^T] \\ &= E\left[\left((\mathbf{X}^T \mathbf{C}^{-1} \mathbf{X})^{-1} \mathbf{X}^T \mathbf{C}^{-1}\right) \cdot \mathbf{e}\mathbf{e}^T \cdot \left((\mathbf{X}^T \mathbf{C}^{-1} \mathbf{X})^{-1} \mathbf{X}^T \mathbf{C}^{-1}\right)^T\right] \\ &= E\left[\left((\mathbf{X}^T \mathbf{C}^{-1} \mathbf{X})^{-1} \mathbf{X}^T \mathbf{C}^{-1}\right) \cdot E[\mathbf{e}\mathbf{e}^T] \cdot \left((\mathbf{X}^T \mathbf{C}^{-1} \mathbf{X})^{-1} \mathbf{X}^T \mathbf{C}^{-1}\right)^T\right] \end{aligned}$$

or

$$\begin{aligned} \mathbf{C}_{\text{ep}} &= E\left[\left((\mathbf{X}^T \mathbf{C}^{-1} \mathbf{X})^{-1} \mathbf{X}^T \mathbf{C}^{-1}\right) \cdot \mathbf{C}_e \cdot \left((\mathbf{X}^T \mathbf{C}^{-1} \mathbf{X})^{-1} \mathbf{X}^T \mathbf{C}^{-1}\right)^T\right] \\ &= E\left[\left((\mathbf{X}^T \mathbf{C}^{-1} \mathbf{X})^{-1} \mathbf{X}^T \mathbf{C}^{-1}\right) \cdot \sigma^2 \mathbf{I} \cdot \left((\mathbf{X}^T \mathbf{C}^{-1} \mathbf{X})^{-1} \mathbf{X}^T \mathbf{C}^{-1}\right)^T\right] \end{aligned} \quad [5.20]$$

$$\mathbf{C}_{\text{ep}} = \sigma^2 \cdot (\mathbf{X}^T \mathbf{C}^{-1} \mathbf{X})^{-1}$$

where

\mathbf{C}_e = covariance matrix of residuals

σ^2 = reference variance of the head residuals

\mathbf{I} = unit matrix

The covariance matrix represents the statistical covariance of each parameter combination. For the off-diagonal elements the covariances are calculated while the parameter variances are calculated for the diagonal elements. The variance of the head residuals is interpreted as a 'reference variance' in case weights are not evenly distributed and is calculated by

$$\sigma^2 = \frac{\mathcal{S}}{m-n} \quad [5.21]$$

where m is the number of observations and n is the number of parameters while $m-n$ is the degree of freedom in the estimation process.

For simulation of non-linear relations such as in rainfall-runoff modelling, Eq's. [5.15], [5.17] and [5.20] are not valid since \mathbf{Xp} (Eq. 5.10) represents a linear operator. For simulating non-linear relations, linearization between parameters and calculated state variables, \mathbf{h}_{sc} , is required and are calculated by:

$$\mathbf{h}_{sc}^i = \mathbf{h}_{sc}^{i-1} + \mathbf{J}(\mathbf{p}^i - \mathbf{p}^{i-1}) \quad [5.22]$$

where

i = iteration index for non-linear optimisation

\mathbf{J} = Jacobian matrix.

For non-linear parameter estimation, Eq. [5.22] is substituted for \mathbf{h}_{sc} in the objective function of Eq. [5.15]:

$$\mathcal{S} = \left(\left(\mathbf{h}_{so} - \mathbf{h}_{sc}^{i-1} + \mathbf{J}(\mathbf{p}^i - \mathbf{p}^{i-1}) \right)^T \mathbf{C}^{-1} \left(\mathbf{h}_{sm} - \mathbf{h}_{so}^{i-1} + \mathbf{J}(\mathbf{p}^i - \mathbf{p}^{i-1}) \right) \right) \quad [5.23]$$

The jacobian matrix has dimensions $m \times n$ with m rows of state observations and n columns of parameters. The Jacobian is calculated by iteration either by an adjoint-state approach or by a perturbation method. By the perturbation method parameter optimisation is achieved by repeated optimisation runs where parameters are updated by use of a parameter upgrade vector Eq.[5.25]. Such method is computationally much more intensive than adjoint-state approaches but has the advantage that it can be applied separately and independently from any model. Hence, parameter optimisation algorithms based on perturbation methods

is seen as a numerical post-processor to any model. By the non-updated parameter set, for each combination of parameter-variable, a model run is executed. These derivative are expressed by the Jacobian matrix that serves to (slightly) update the parameter set. Elements of the Jacobian matrix are the partial derivatives of each observation with respect to each parameter and hence such matrix is interpreted as a model sensitivity matrix:

$$\mathbf{J} = \frac{\partial(\mathbf{h}_1 \dots \mathbf{h}_m)}{\partial(\mathbf{p}_1 \dots \mathbf{p}_n)} = \begin{vmatrix} \frac{\partial \mathbf{h}_1}{\partial \mathbf{p}_1} & \cdot & \cdot & \frac{\partial \mathbf{h}_m}{\partial \mathbf{p}_1} \\ \cdot & \cdot & \cdot & \cdot \\ \frac{\partial \mathbf{h}_1}{\partial \mathbf{p}_n} & \cdot & \cdot & \frac{\partial \mathbf{h}_m}{\partial \mathbf{p}_n} \end{vmatrix} \quad [5.24]$$

For non-linear optimisation, the parameter values \mathbf{p} are defined by iterative procedures where the parameter values are upgraded by use of a parameter upgrade vector:

$$\begin{aligned} \mathbf{U}_p &= (\mathbf{J}^T \mathbf{C}^{-1} \mathbf{J})^{-1} \mathbf{J}^T \mathbf{C}^{-1} (\mathbf{h}_{sm} - \mathbf{h}_{sc}) \\ \mathbf{P}^i - \mathbf{P}^{i-1} &= (\mathbf{J}^T \mathbf{C}^{-1} \mathbf{J})^{-1} \mathbf{J}^T \mathbf{C}^{-1} (\mathbf{h}_{sm} - \mathbf{h}_{sc}) \end{aligned} \quad [5.25]$$

By the upgrade vector, parameter estimations are improved subject to the minimisation of the objective function value \mathcal{J} Eq.[5.22]. The iteration procedure to optimise the parameter set stops when the objective function value is minimised. A principal assumption in this procedure is that for the selected time series of state variables the global minimum of the objective function can be defined. At such global minimum the estimation of the parameter set as a whole cannot be improved any further. In case local minima in the response surface are present, parameter estimation might be trapped in such minimum. Since the best parameter set only is defined at the global minimum, parameter optimisation is still improved. At any local minimum, additional parameter sets within the remaining parameter space are defined that perform equally well. In figure 5.8 the iterative improvement of initial parameter values towards the global minimum of the objective function response surface for a two parameter (p_1, p_2) estimation problem is presented. At the global minimum the set of single best and unique parameters is calculated. Contour lines in the figure are lines of equal

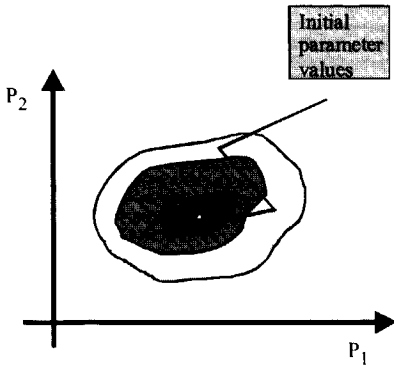


Figure 5.8: Iterative improvement of initial parameter values towards the global objective function minimum for a two parameter (p_1, p_2) estimation problem (Watermark, 1994).

objective function value and thus at any line equally weighted-variances of the head residuals are expressed.

For non-linear parameter estimation the operator \mathbf{X} in Eq's. [5.15], [5.19] and [5.20] is replaced by the Jacobian matrix. For non-linear parameter estimation the parameter vector is calculated by Eq.[5.26]

$$\mathbf{P}^i = \mathbf{P}^{i-1} + (\mathbf{J}^T \mathbf{C}^{-1} \mathbf{J})^{-1} \mathbf{J}^T \mathbf{C}^{-1} (\mathbf{h}_{sm} - \mathbf{h}_{sc}) \quad [5.26]$$

and the covariance matrix is calculated by:

$$\mathbf{C}_{cp} = \sigma^2 (\mathbf{J}^T \mathbf{C}^{-1} \mathbf{J})^{-1} \quad [5.27]$$

By use of the parameter covariance matrix of Eq. [5.20], a parameter correlation matrix \mathbf{C}_{rp} is calculated that is interpreted as the parameter structure. In such structure the spatial dependencies between parameters is expressed and is calculated by:

$$\mathbf{C}_{rp} = \frac{\mathbf{C}_{cp}}{\sigma_i \sigma_j} \quad [5.28]$$

where σ_i, σ_j are the standard deviations of parameters i and j that are obtained from the covariance matrix Eq. [5.27].

The parameter correlation structure is very useful to help analyse the reliability and trustworthiness of the model. When analysing simulation results, the effect each single parameter has on the calculated output must be quantified. Simulation, however, become unreliable and not

trustworthy when parameters are (highly) correlated. Such correlation expresses how parameters in model space are dependent and causes that model sensitivity to single parameters is uncertain and undefined. While some parameters, may be positively correlated, others may be negatively related. Hence it is difficult to identify the effect single parameters have on the model output and parameter are not well identified. Although the mutual effect such parameters have on the simulation result is defined, single parameter values are not defined in a unique manner and optimised values must be interpreted as non-unique.

A second matrix that gives quantitative information on how well parameter values are identified is the matrix of the normalised eigen-vectors of the parameter covariance matrix. This symmetric matrix has dimension $n \times n$ with eigen-vectors and eigen-values. For each parameter set an eigen-value or characteristic value of the estimation problem is calculated that represents the variance of the parameter combination specified by the eigen-vector. In an n dimensional parameter estimation problem n eigen-values and n eigen-vectors are calculated where each eigen-vector comprises n elements. Mathematically, eigen-values λ and eigen-vectors \mathbf{Z} are defined by

$$\mathbf{C}_b \mathbf{Z} = \lambda \mathbf{Z} \quad [5.29]$$

or, when rewritten by use of unit matrix \mathbf{I} :

$$(\mathbf{C}_b - \lambda \mathbf{I}) \mathbf{Z} = 0 \quad [5.30]$$

The eigen-values and eigen-vectors are calculated by the characteristic determinant $\mathbf{D}(\lambda)$ and the characteristic equation:

$$\mathbf{D}(\lambda) = \det(\mathbf{C}_b - \lambda \mathbf{I}) = \begin{vmatrix} p_{11} - \lambda & p_{12} & \cdot & \cdot & p_{1n} \\ p_{21} & p_{12} - \lambda & \cdot & \cdot & p_{2n} \\ \cdot & \cdot & \cdot & \cdot & \cdot \\ \cdot & \cdot & \cdot & \cdot & \cdot \\ p_{n1} & p_{n2} & \cdot & \cdot & p_{nn} - \lambda \end{vmatrix} = 0 \quad [5.31]$$

The following description on the eigen-values and eigen-vectors analysis is given by Olsthoorn [1998]:

“Eigen-values and vectors are a result of rotating the covariance matrix in parameter space such that only diagonal values remain (the eigen-values). The axes of this new parameter space point in the direction of the eigen-vectors. Each eigen vector, all of which have a length 1, represents a parameter combination that is independent of the parameter combinations specified by all other eigen-vectors. In this new parameter space all mutual correlations are eliminated”.

Eigen-values and eigen-vectors give specific statistical information on identifiability of parameters. The parameter set with the lowest eigen-value is interpreted as the best parameter set while a relatively high eigen-value indicates a bad parameter set. By analysis of the eigen-vector, quantitative statistical information on parameter identifiability becomes available. Analysis must focus whether each eigen-vector is dominated by one parameter. In such case the identifiability of each of these single parameters is termed high since the optimised parameter value is associated with a low variance. In case multiple parameters dominate an eigen-vector it is concluded that parameter identifiability is low.

A well-known algorithm to perform MLE by weighted least squares estimation is the Gauss Marquardt Levenberg algorithm. The optimisation algorithm searches by automated procedures for the global optima of the objective function response surface. The Gauss Marquardt Levenberg algorithm also is at the core of parameter estimation software such as PEST2000 (Watermark Computing, 2000) and UCODE (Hill, 1998). For this study the PEST2000 software is selected.

Some concluding remarks on MLE by weighted least squares estimation can be made. The procedure is developed to define single best and unique parameter sets by minimising a single-objective function. In this function multiple state variables can be selected and weighted in the estimation process by use of an observation covariance matrix. This makes the procedure very suitable for application to multi-output models such as PBRR models. Parameter values are inversely defined and optimised by MLE. Parameter estimates are optimised when the global optimum of the objective function response surface is found. A global search algorithm for MLE is provided by the Gauss Marquardt Levenberg algorithm. In the procedure it is not (yet) possible to quantify the effects of parameter uncertainty on model output. This is considered a major restriction of the procedure.

A major advantage of the procedure is that quantitative statistical information on spatial dependencies of parameters becomes available through a parameter correlation matrix. Information on parameter identifiability becomes available through eigen vector- eigen value matrixes.

Approaches of MLE in the field of PBRR modelling must focus on analysing its potential in such modelling. An interesting question for example is whether different parameter sets are defined when a model is calibrated for various catchment response modes. By physical reasoning, different parts of the catchment contribute to the runoff production and thus different optimal parameter values can be defined as well.

Parameter sets must for example be defined separately for base flow and peak flow discharges to see whether a new parameter space can be defined. A second question deals about the use of multiple state variables for model calibration where it is uncertain whether model performance improves or deteriorates by such use. Research, for example, by the GLUE-procedure on the use of multiple output variables has not been successful while calibration approaches on evolutionary methods mostly are applied to lumped CRR models in which the channel flow discharges is the only state variable of interest.

5.6 Automated calibration by Artificial Neural Networks (ANN)

A relatively new approach towards the simulation of rainfall-runoff relation deals with the application of ANNs or shortly NN. In runoff hydrology NN applications have been pioneered by Hornik et al., [1989], Karunanithi et al., [1994] and French et al., [1992], among others. Hornik et al., [1989] applied NNs to simulate catchment scale runoff relations, Karunanithi et al., [1994] explored applications for runoff forecasting and French et al., [1992] forecasted rainfall distributions in time and space. During the time, applications were regarded promising while nowadays many applications in rainfall-runoff hydrology are known. During the nineties a general knowledge on ANNs applications towards rainfall-runoff modelling has been developed. More recent applications in the field of rainfall-runoff modelling primarily are in the field of rainfall forecasting (see e.g. Toth et al., 2000) and runoff forecasting (see e.g. Hsu et al., 1993, 1997,

Shamseldin, 1997; Minns and Hall, 1996). Recent applications also are known in the field of surface water management, operational water management, groundwater modelling and water quality modelling (e.g. Maier and Dandy, 1996). Such applications are not elaborated on here and are out of scope.

5.6.1 ANN model concept

Model concepts of ANNs are based on the premise that any complex linear or non-linear relation can be described by a weighted sum of model inputs and interacting model components. Hornik et al., [1989] consider an ANN as a 'general non-linear approximator' while Fausett [1994] characterises an ANN as

"a computational or mathematical technique that is powerful for modelling systems where the explicit form of the relationship between the variables is unknown".

Some types of ANNs often are termed and interpreted as function approximators that are suitable to recognise a certain pattern that exists between input and output signals of a system. Generally such ANNs are categorised as black box models (section 2.3) although ANNs apply a model concept different from any of the model concepts as described in section 2.3. A diagram of a widely applied type of NN is presented in figure 5.9 and is termed a Feed Forward Neural Network (FFNN).

The model concept of a FFNN encompasses a model input layer, hidden layers, a model output layer and an optimisation algorithm. The input layer is build up by input elements² that pass input signals into the NN while hidden layers and the output layer are build up by computational elements that are termed neurons. At each neuron specific 'activities' take place such as receiving the input data, weighting and transforming the input data or just the passing of data to other neurons. Input signals may be of a different type and magnitude such as snow depth, precipitation depth, temperature or runoff discharge (see e.g. Tokar and Johnson, 1999). From a computational point of view input signals generally are sealed in the model. In a classical FFNN, at the neurons of a hidden layer the input signals are combined, weighted and transformed to calculate an output signal at that particular neuron. In general, output

² Although the input layer solely consists of units that just pass inputs into the network, in literature these units often are termed neurons as well.

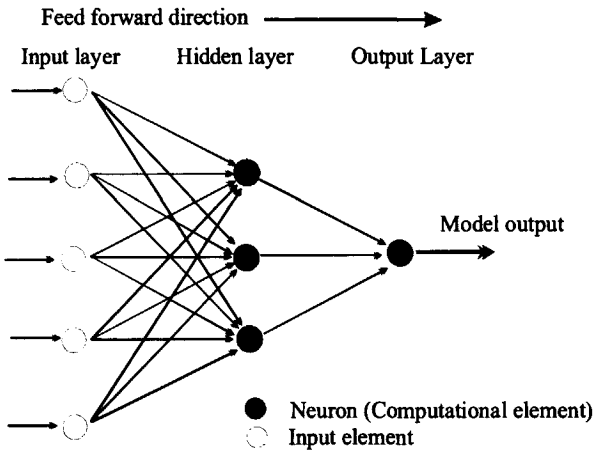


Figure 5.9: *Diagram of a FFNN*

signals have no physical meaning but only serve as an input signal to further connected neurons. Subject to the NN model architecture signals can be forwarded or backwarded to other neurons, even to neurons within the same layer.

In hydrology, however, mostly so called FFNNs are applied (see e.g. Imrie et al., 2000, Zealand et al., 1999; Toth et al., 2000) that briefly are described in the following. In FFNN e.g. information is only passed from neurons in one layer to neurons of a succeeding layer as shown in the diagram in figure 5.9 where the arrows indicate the forward directions. Information is passed from input elements to neurons of the hidden layer and from neurons of the hidden layer to neurons of the output layer. The connectivity structure as well as the number of input elements, neurons and hidden layers, are defined by the modeller and have an important effect on the performance of the network. The output layer generally only consists of one neuron at which the state variable of interest is calculated. Subject to the system to be modelled and the availability of field data, observation time series for example may be entered into the ANN with a time-lag factor. Also simulated model errors may be entered back into the network.

During the early stages of ANN developments, Lippmann [1987] formulated a general guideline to quantify on the necessary number of neurons in the hidden layer. He stated that the number of hidden

neurons should be large enough to form a model structure that is as complex as is required by a given problem. Hence for any problem, simple as well as complex ones, an optimum model structure can be defined. Generally speaking, the more complex a problem is the more complex the structure of an ANN becomes and thus the larger the decision region in terms of the required number of neurons becomes. In ANN modelling, as such the number of hidden neurons generally is not fixed *a-priori* but is optimised based on the performance of the ANN. The number of hidden layers also has to be defined by the modeller although in most hydrologic applications the use of one hidden layer gives an optimal model performance. This since any continuous non-linear function can be approximated by a ANN with one hidden layer with specific transfer functions applied to neurons of the hidden layer and output layer.

Inappropriate ANN model concepts are developed when too few neurons are applied resulting in a too parsimonious network or, on the other hand, when too many neurons are applied which may lead to overfitting (Masters, 1993). In the latter case it means that noise in the calibration data set is fitted that will not yield any improvement in the performance. Hammerstom [1993] states that an appropriate number of neurons can be found by calibrating the network and evaluating its performance over a range of increasing neurons of the hidden layer. By experiment, the goal is to find near optimum performance with as few neurons as necessary. One could say that the optimal structure of a NN must be 'sensibly parsimonious' in the number of neurons required.

Input signals to a NN generally are observations of meteorological and hydrologic state variables and often are of different type and magnitude. In multi-layer NN e.g. input elements receive e.g. observations of rainfall while at other elements snowfall, hydraulic heads, runoff discharges, temperatures or any time-independent characteristic of a catchment can be entered. Such characteristics e.g. can be the surface area, the drainage density and land use. At the neurons of the hidden layers and output layer a net input signal is defined in which inputs from connected neurons and input elements are weighted, combined and transformed.

This procedure to calculate the net input is often referred to as the propagation rule and follows the mathematical description of Eq. [5.31].

$$Y_j = \sum_{i=0}^n w_{ji} x_i \quad [5.31]$$

where

Y_j = net input to neuron j

w_{ji} = weight of each input i to neuron j

x_i = input from neuron i

n = number of inputs

In addition to the inputs, each neuron receives an input term that is commonly called 'bias' and is expressed as x_0 . The bias signal is equal to 1 while the weight w_{ji} has to be defined by the model algorithm. The expression of Eq. [5.31] is applied to all neurons except for the elements from the input layer.

The output signal of a neuron now is defined after implementing the activation rule in which the net input is transformed into an output signal by means of a transformation function. Such functions often are called 'transfer functions' or 'activation functions' and follow a non-linear mathematical description. Hsu et al., [1995] state that the most commonly applied function is the steadily increasing S-shaped curve called a 'sigmoidal' function. A large number of sigmoidal functions can be defined but Blum [1992] and Hsu et al., [1995] state that the most often applied function is the logistic function (see e.g. Imrie et al., 2000; Shamseldin, 1997; Toth et al., 2000). Commonly applied sigmoidal functions in ANNs are presented in figure 5.10. Mathematically these functions follow the general description:

$$Y_{out,j} = f(Y_j) = \frac{1}{1 + e^{-Y_j}} \quad [5.32]$$

where $Y_{out,j}$ is the output or the transformed net input of neuron j . The logistic function acts as a re-scaling function to the input signal and as such re-scales the net input Y_j to lie in between 0 and 1. This function basically serves as a non-linear transformation function and is applied to net input signals of neurons of the hidden and output layer.

The output signal at a neuron represents the newly calculated state of that neuron and must be interpreted as an optimised and transformed output variable from all input signals according to the connectivity structure.

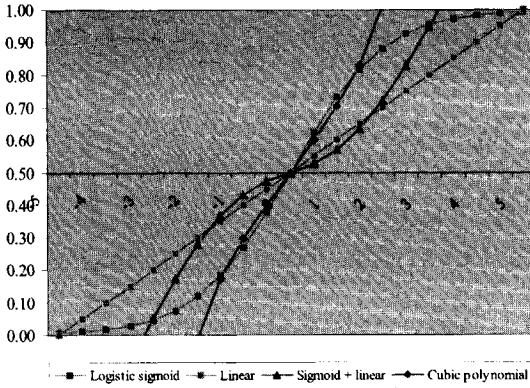


Figure 5.10: Sigmoidal function for re-scaling the net input

During the so called ‘training’ of the ANN, weights, w_{ji} , are optimised for each input signal of the input elements and connected neurons. Training in this respect is the tuning of the ANN through the mapping of model input on output signals by means of weight optimisation. Weights are defined by use of an automated global optimisation algorithm that minimises the residual error between observed and calculated state values. For quantifying the residual error the Mean Squared Error (MSE) objective function is frequently used that, by use of the training data set, is calculated for any time instant by:

$$MSE_t = \frac{1}{n} \sum_{i=1}^n (Y_c^t - Y_o^t)^2 \tag{5.33}$$

where

n = number of time instants

Y_o^t = observed state variable at time t

Y_c^t = calculated state variable at the neuron of the output layer at time t .

Other performance criteria such as RMSE or R^2 , also are applied.

For defining weights in FFNN applications, Rummelhart et al., [1986] state that a back propagation algorithm is most appropriately used. The optimisation equation reads:

$$w_{ij}^{t+1} = w_{ij}^t + \Delta w_{ij}^{t+1} + \mu \Delta w_{ij}^t \tag{5.34}$$

where

$w_{i,j}^{t+1}$ = optimised weight for input signal i at element j at time $t + 1$

$w_{j,i}^t$ = weight at element j for input signal i at time t

$\Delta w_{j,i}^{t+1}$ = weight increment

μ = momentum parameter.

The weight increment is calculated by use of a gradient decent search algorithm that resides at the core of the optimisation algorithm:

$$\Delta w_{j,i} = \eta \frac{\partial \text{MSE}}{\partial w} \quad [5.35]$$

where η is the learning rate that governs the size of the weight adjustment. Changes to the weights are made in the direction of the steepest decent of the objective function response surface. The goal of the optimisation routine is to find the global minimum of the response surface of Eq. [5.33]. to prevent the entrapment of the algorithm at a local response surface minimum the momentum parameter is introduced. This term adds inertia to the training procedure that effectively increases the learning rate when the gradient of the steepest decent becomes smaller. At the end of the training process the weights are defined in an optimal manner that can be applied to the ANN for model simulation.

In literature, many different ANN model concepts and different optimisation algorithms are described. Muttiah et al.,[1997] for example apply a cascade correlation architecture while Toth et al.,[2000] train the network by use of the Levenberg-Marquardt algorithm that is known to be very quick and efficient optimisation algorithm. Most optimisation algorithms follow a mathematical description that minimises an objective function by use of gradient based search methods. Describing the mathematical aspects of these algorithms is out of scope of this thesis. An overview on such aspects as well as optimisation algorithms is presented in ASCE [2000] and de Vos [2003].

5.6.2 Real world physics and ANN model concepts

On the applications of ANN in PBRR modelling little research has been reported. For such applications, ANNs must be combined with physically-based hydrodynamic flow models such as described in Chapter 3 and ANNs now must serve to improve the parameter

estimation. A literature survey on this subject learned that such use in runoff modelling, generally speaking, has not gained much attention. In the field of hydraulic modelling, an example of any such coupling is reported by Schleider [2000,] who coupled an ANN to a 2-dimensional hydraulic flow model to improve model performance by improved parameter estimation. ANN approaches to solve differential equations, that also are at the core of PBRR models, are presented in Aarts and Van der Veer, [2001,a,b]. In subsection 5.5.3 these approaches are briefly discussed. First however, some ANN simulation approaches are discussed to circumvent for the lack of an explicit 'model history' that is inherent to the applied model concept of ANNs.

Model history

In PBRR modelling an initial hydrologic condition over the entire model domain is required at the start of a simulation. Initial model conditions are expressed in terms of state variables such as groundwater depth, channel flow water depth and soil moisture contents and should represent the real world hydrologic state in a model prior to actual model simulation. During model simulation meteorological influences such as precipitation and evaporation are simulated and entered into the runoff model. During model simulation the effect such influence has are defined by the applied equations of mass conservation and momentum. In this manner any calculated state variable becomes, among other factors, a function of the initial model conditions and entered meteorological influences. As the model simulation progresses over time, newly calculated hydrologic states thus become a function of all previously entered meteorological input signals and all previously calculated states. In physically-based modelling this phenomenon is referred to as the 'model history' and plays an important role in the performance of a model and the acceptance of simulation results. In ANNs such model history is not simulated explicitly but effects of time dependant model input can be circumvented for by modifying the connectivity structure of the ANN and/or through adding extra input signals as described below.

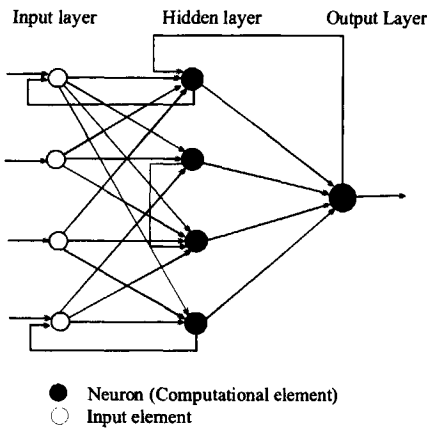


Figure 5.11: *Diagram of recurrent ANN*

As described in subsection 5.1.1, at each input element an input signal is entered to the ANN where input signals may be of a different kind and be dissimilar. In this manner it is possible to enter observations of precipitation and/or discharges into the ANN for a number of time instants. Especially in real time runoff forecasting this procedure is beneficial since only the short-term history of a model is important for practical applications. For model input, time series of spatially distributed rainfall observations or discharge measurements can be used while combinations of both data types also are possible (see e.g. Zealand et al., 1999). During the training of the network, emphasis then is laid on simulating the time dependency of input signals that are most relevant for the performance of the network. An example of such approach is given by Hsu et al., [1995]. Hence, the long-term model history is not simulated explicitly but effects of such history are expressed in the weights that are updated during the training.

An ANN approach in which effects of the internal model behaviour is accounted for in the model output is provided by recurrent ANNs. In such networks, feed-backward connections are simulated in addition to the feed-forward connections (see figure 5.11). Calculated model output and also calculated internal model states are entered back into the network by a feed backward connection.

In the model concept such feed-backward connections can be defined for any combination of neurons over the various model layers and/or neurons also may be connected within one layer. Neurons of the output

layer, however, often are connected to elements of the input layer and the effect model output has on the succeeding simulation time step is defined in such manner (see e.g. Toth et al., 2000). The net input as defined by Eq.[5.31] also receives an input signal from the neuron of the output layer. In Sajikumar and Thandaveswara [1999], model output from the output neuron is backward connected to neurons and input elements of the hidden layer and input layer respectively. In the same approach also neurons within the hidden layer are backward connected. In recurrent ANNs, neurons in any layer may receive an input signal from neurons from the preceding and succeeding layer and the layer itself. In such procedure, the weight values as defined during the training period also become a function of model output from previous time steps and, possibly, internal calculated states. Also time delays to certain input signals in feed backward connections maybe introduced that make applications more flexible. ASCE [2000] states that recurrent networks operate in a dynamic mode and that networks become inherently dynamic by nature by the feed backward procedure. Within the class of recurrent networks a number of different sophisticated approaches are known (see Islam and Kothari, 2000).

A third approach to circumvent for the lack of model history in ANNs is to define clusters of input data with similar characteristics. By the clustering of observations, a pre-selection of input data is made for the training of the network. Through the clusters, specific (hydrologic) states of the system to be simulated are sealed into the NN and overcome the problem that other input signals dominate the NN simulation. By the clustering, the information content of the selected time series of observations increases as compared to time series of non-clustered data. Clustering is very practical, simple and convenient particularly when the information content of the observations must be increased. In such approach the extra information content of the clustered data is added to the network and weights are defined for more unique cause-effect relationships. Weights defined during the training process thus, implicitly, carry information on the model history. This, however, is restricted to runoff events that lie inside the range of clustered data values that are used for training. It is obvious that for each of the data clusters a gross generalisation is made with respect to the runoff behaviour. For clustered data, implicitly it is assumed that observations are comparable in a sense that all observations are subject to

a unique cause-effect relation. Whether such assumption is true in runoff hydrology is questionable due to the large number of factors that effect runoff production by rainfall. In runoff hydrology data clusters can be defined for e.g. peak flow discharge, total runoff volume, mean runoff volume and time to peak.

Model uncertainty

An important limitation of ANN deals about quantifying the uncertainty that must be associated with the model approach. Model output as mostly defined as a time series is uniquely calculated by means of the optimised weights, the model concept and the selected model input. Calculated model output from ANN's is not associated with any uncertainty such as calculated by the GLUE procedure in section 5.3 and the multi-objective model calibration of subsection 5.4. Effects of parameter uncertainty are not quantified and also information on parameter dependencies and identifiability as described in section 5.5 does not become available. ANN model performance generally is judged by visual interpretation of the simulation results and quantitatively by use of calibration criteria such as MSE, RMSE and R^2 (see e.g. Imrie et al., 2000; Toth et al., 2000; Shamseldin, 1997; Zealand et al., 1999; Sajikumar and Thandaveswara, 1999; among others). In the review study on ANNs, it has become apparent that aspects relating to model uncertainty only have gained little attention.

5.6.3 Improved Physically-based Modelling by use of ANNs

While ANNs are very well suitable to recognise certain patterns between a systems input and output signals, it is still under research how ANNs can be applied to describe real world physics that underlie the simulated pattern. One of the limiting factors for easy combination is that neurons as well as hidden layers have no physical significance but are purely artificial model features. Also, and contradictory to ANNs, physically-based models obey to the conservation of mass and momentum principles that causes that simulated hydrologic states are a function of all previously entered hydrologic influences and calculated hydrologic states.

Recently research is started after applications of ANNs to models that apply differential equations. Examples of such research are presented by Schleider [2000] who estimated parameter values for a hydrodynamic

flow model by use of an NN and by Aarts and Van der Veer [2001,a,b] who applied ANNs to solve differential equations. Both these approaches will briefly be discussed and serve as an illustration how ANNs possibly can be used in PBRR-modelling.

First the approach of Schleider [2000] will be discussed who applied a two-dimensional hydrodynamic flow model for coastal zone wave simulation and combined this model with a procedure that updates parameter estimates during each model simulation time step. In the approach, the shallow water flow equations are solved over a model grid domain and a state vector was updated for each simulation time step. The state variable of interest was the wave height while the bottom friction coefficient was the parameter of interest.

In the model approach the goal was to improve the model performance by optimising the bottom friction coefficient for each simulation time step, this by minimising the residual error between measured and simulated wave heights. During the model simulation the bottom friction parameter could be changed over time where its value was a function of simulated turbulence and characteristics of the bottom surface. Parameter estimation was achieved by a 're-enforcement learning parameter adaptation approach' (Schleider, 2000). By this approach parameter values are modified based on learning rules that need to be defined and updated for each simulation time step. By the learning rules a value function for parameter modification is defined and this function is applied to optimise the parameter values. Appropriate learning rules are defined by a calculation procedure, that also is based on neural network applications, in which the magnitude and direction (i.e. + or - sign) of the parameter change are defined. Parameter values as such become a dynamic property and thus also depend on the calculated states of the numeric simulation model. Schleider [2000] described a calculation scheme termed 'unified adaptation system state model' that links the input and output of the flow model and the ANN models to update the parameter values and to evaluate the simulated states. In the approach a calculated water level of a reference point of the model grid layer is compared to a measured water level at the same location in the real world. This residual error is minimised during the model calibration and serves to guide the parameter estimation. An extensive description about the calculation procedure is given in Schleider [2000].

This procedure is different from the calibration procedures described in sections 5.2 through 5.5 in a sense that parameter values are updated in real time for each simulation time step. Parameter values as such become a dynamic property and serve to improve the model performance for the succeeding time step. With respect to PBRR modelling it is questionable whether similar procedures can be applied efficiently. This particularly since model concepts of PBRR models are far more complex as compared to the model approach of Schleider [2000]. A major problem deals about the number of parameters used by PBRR models. Schleider [2000] only modifies the friction bottom coefficient while PBRR models have a large number of parameter that effect model performance. The key issue now becomes to select an appropriate set of parameters that require optimisation and to select the appropriate set of learning rules to modify parameter values during consecutive simulation time steps.

A second example to combine ANN with physically-based model equations is presented by Aarts and Van der Veer [2001a,b] who solve differential equations through ANN applications. The type of differential equations to be solved may be partial (Aarts and Van der Veer, 2001a) and first order linear (Aarts and Van der Veer, 2001b). Although in all these approaches differential equations are solved through a series of connected NNs, approaches also show some differences. In the scope of this thesis these differences will not be discussed here but instead a general description is given here how differential equations are solved by means of NN approaches. The approaches are based on the fact that a multiple input, single output, single hidden layer FFNN with multiple input elements and a linear output layer with no bias are capable to arbitrarily well approximate many functions and its derivatives. While such approaches are common, the main idea now is that knowledge on the physical processes must be added to the differential equations, its boundary and initial conditions. Hence, such knowledge is incorporated into the structure and training set of the NN and therefore NN structures are specific to the processes and system to be simulated and thus also to the selected differential equations. For training of the connected networks an evolutionary method is applied to (sub-)population(s) while the connected NNs are solved simultaneously. The procedure aims at finding the solution of the differential equation and its initial and, possibly, boundary condition. Example applications of the method are the simulation of the one-

dimensional non-steady groundwater flow equation with initial and boundary condition or the simulation of forced vibration without damping.

5.7 Conclusions

In the model calibration procedures described in this Chapter the focus is on optimising parameter values using an *a-priori* defined model concept. Model calibration is achieved by optimising parameter only thus ignoring any other aspect of the model approach that could have an effect on model performance.

Parameter optimisation can be achieved by simple manual Trial and Error procedures or by automated procedures that can be based on Monte Carlo simulations (i.e. GLUE), evolutionary procedures (i.e. single and multi-objective estimation) or MLE. For each of these procedures a number of applications are reported in literature although applications in PBRR modelling only have gained little attention. In PBRR modelling it is still common practice to apply the Trial and Error procedure and conclusions on the performance and trustworthiness of such models are based on visual interpretation of calibration results and the use of a calibration criterion (see e.g. Refsgaard, 1996; Bronstert, 1999). Such applications are questionable since the procedure has major weaknesses that relate to parameter estimation issues such as parameter uniqueness and identifiability. For any Trial and Error calibration it is uncertain whether the most optimum parameter set is found and whether the calibration can be improved further. For numerous reasons as described in section 5.1 it is concluded that the procedure should be rejected in runoff modelling.

The GLUE procedure is an automated calibration procedure in which model output is simulated for a range of parameter sets. The procedure is based on a Monte Carlo simulation method where a large numbers of prior parameter sets are randomly generated by prior parameter distribution functions. The generated parameter sets are tested for their performance by a predefined model performance criterion that is termed the likelihood measure for which its value is termed the likelihood weight. By introducing a cut-off value for the likelihood weight a selection of good parameter sets is made. Mostly only the best 10% of the parameter sets are maintained for further analysis and marginal

cumulative distribution functions are constructed. The shape of these functions serves as a tool to quantify parameter identifiability. The ranges of values in the functions express parameter uncertainty and model output uncertainty is expressed for each time instant by calculating the outflow for each parameter set. The procedure is appealing by the fact that parameter uncertainty as well as model output uncertainty is simulated. The procedure can simply be applied to multi-output models although simulation results from Franks et al., [1996] and Lamb et al., [1998] did not show any significant increase in model performance when multiple state variables are applied to the procedure. Weaknesses of the procedure are that it is uncertain how large the cut-off value should be, how the performance measure should be selected and how prior distributions functions should be selected. The procedure also is not able to identify possible insufficiencies in the model concept and cannot calculate any inter-dependency of parameters in terms of, for example, a correlation matrix. By these weaknesses the application of the GLUE procedure in PBRR modelling is not advocated.

A second procedure for automated parameter optimisation is provided by single-objective and multi-objective evolutionary methods. These methods reduce the initial parameter space to a much smaller, optimised, parameter space. Minimisation of the objective function is achieved by global optimisation routines. In multi-objective model calibration, a number of unrelated objective functions are aggregated into an aggregated but single objective function that is minimised. Selected objective functions must be unrelated and are minimised simultaneously. Between selected objective functions, a trade-off can be defined with respect to model performance since for each objective function a most optimum parameter set can be defined. In multi-objective model calibration by evolutionary methods such parameter sets are combined and a new feasible parameter space called the Pareto space or Pareto set is defined. For all parameter sets within the Pareto space an equally low objective function value is obtained and thus it is assumed that model performance is equally satisfactory. By the size and shape of the Pareto set, parameter values are not unique but are uncertain and as such a range of parameter values is defined. For each parameter set a model simulation is executed and the range of model outputs is expressed and interpreted as an uncertainty band. This aspect of defining the Pareto set is very appealing since insufficiencies of the model concepts become

apparent when the model output does not match observed catchment response in terms of, for example, peak flow or base flow discharges over certain periods of time. A limitation of the procedure is that spatial dependencies of parameters are not simulated explicitly but dependencies are expressed implicitly by the size and shape of the Pareto set. Multi-objective model calibration mostly is applied to CRR models where applications are very successful (see Sorooshian, 1998, among others). In PBRR modelling such applications are (still) unknown although the procedure has a high potential.

A third automated model calibration procedure deals about MLE by weighted least squares estimation. In the procedure, parameter values are inversely optimised by statistical analysis of the residual error. An initial parameter set is updated through an iterative procedure where for each calculation time step parameter optimisation is inferred from calculated state information. In such approach, many different procedures are available although it is common to minimise single-objective functions only. Objective functions mostly follow a weighted least squares estimation expression and minimisation often is placed in the framework of MLE. Application of such estimation procedure is very appealing to multi-output models such as PBRR models since the procedure allows model calibration for multiple state variables simultaneously. Multiple state variables may be of a different kind and order and weighted in the objective function by a covariance observation matrix. By the procedure a parameter correlation matrix is defined that gives specific information on the spatial dependencies of single parameters. The procedure also yields eigen vector-eigen value matrixes that give specific information on the parameter identifiability and uniqueness.

In PBRR modelling, hydrologic state information that can be used for model calibration are piezometer observations or channel flow stages although combinations of both also can be selected. In this manner a number of single best and unique parameter sets are defined that, when combined, yield a range of parameter values suitable for the model. By the parameter value ranges a new and optimised parameter space is created. Such space however is not comparable to the Pareto space since optimised parameter sets in MLE do not perform equally well. By the procedure it is questionable whether insufficiencies of the model concept can be identified. Only in case unrealistic parameter values are estimated this is indicative that the model approach is inadequate.

Applications of MLE in PBRR modelling have not gained much attention in research although numerous applications are reported in groundwater and hydraulic modelling studies. At this stage of research the applicability of MLE must be tested and its potential for PBRR modelling must be researched. Model calibration must focus on whether the use of multiple output variables will improve model performance and whether a new parameter space can be constructed.

A fourth automated calibration procedure that is reviewed deals about the application of generic algorithms such as ANNs. ANNs are interpreted as BB-models that are particularly suitable to recognise patterns between system input and output signals. In runoff hydrology the most commonly applied ANNs are feed forward networks although for specific applications other network configurations are known. As described in section 5.6, an ANN is constructed by an input layer with input elements, an output layer and hidden layers with a certain number of neurons. Also the connectivity structure between neurons, the selected input signals and applied transfer functions at the neurons are defined during the design of an ANN. During the training process of the ANN, the model structure is optimised and further defined.

Applications of ANNs to rainfall-runoff hydrology are numerous especially in real-time runoff forecasting while applications in parameter optimisation and physically-based modelling are very sparse. Recently a study is reported in the field of parameter optimisation for hydrodynamic flow models. The objective of the application was to improve model performance by optimising model parameters through minimisation of the residual error. In the approach, parameter values of the flow model are updated for each simulation time step in such a manner that values become subject to the response mode of the model. Model calibration so becomes a dynamic procedure where for each simulation time step the most optimal parameter set is defined. Limitations with respect to more complex applications relate to the complexity of the flow model and the number of parameters that can be updated. The potential of ANNs as a calibration tool in PBRR modelling is uncertain although at the current state of research such applications are not yet feasible due to the large number of parameters that need to be estimated. For these reasons its use is not advocated here, first much more experience and knowledge on applicability and limitations of white box ANNs as model calibration tool must be gained.

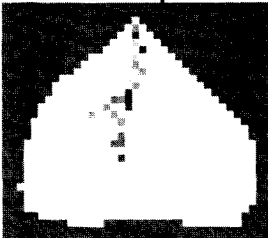
In review of this Chapter it is concluded that research after model calibration should focus on automated calibration. In this thesis it is chosen to place such simulations in a framework of MLE where parameter estimation is achieved by weighted least squares estimation. In the field of PBRR modelling such applications have not gained much attention although in theory the procedure has a high potential. A commonly applied global parameter estimation algorithm based on MLE is the Gauss Marquardt Levenberg algorithm for which many applications in groundwater hydrology are known. Attractive aspects of the procedure are that a model can be calibrated simultaneously for multiple state variables that are weighted by a covariance matrix of state observations. The procedure yields a parameter correlation matrix and eigen vector-eigen value matrixes that give specific information on parameter identifiability and uniqueness. Analyses on model performance require such information that allows much more objective judgements on model performance.

Analysis must also focus on defining effects different types of state variables have on model performance. It also must be analysed what effects the use of multiple state variables have on optimised parameter estimates. For a predefined number of simulation cases, parameter values must be optimised and parameter ranges must be defined.

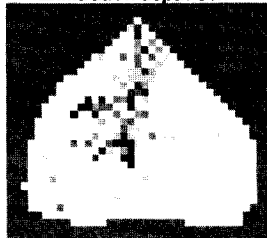
6

Case study Troy catchment

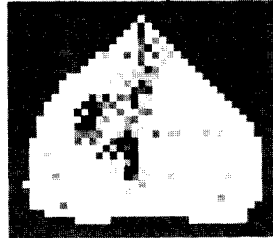
Exfiltration depth 10h



Exfiltration depth 31h



Exfiltration depth 118h



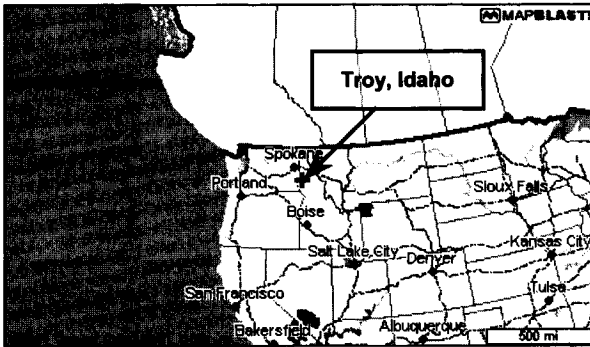


Figure 6.1: Location of the Troy-basin in Idaho, USA.

6.1 Introduction

The study site selected for this thesis is the Troy catchment that is situated near the town of Troy, Idaho, USA (see figure 6.1). For this catchment a vast amount of detailed data is collected by the University of Idaho and is made available for this thesis. Available data relate to topography, subsurface, meteorology and to hydrological state observations of groundwater piezometer heads and channel flow discharges. A brief description of the catchment is presented here that is followed by more extensive descriptions in section 6.2.

The small-scale Troy catchment has a size of about 1.6 ha and an average elevation of 838 m. above Mean Sea Level. The catchment has an undulating topography and is part of the 'Palouse ranges' that, climatically, are characterised by its dry, hot summers and wet, cold winters. In these mountain ranges the mean precipitation ranges from 500 mm/a in the west to over 830 mm/a in the east while more than 60% of the annual precipitation occurs from November to April with low intensity rainfall or snowmelt.

The Troy catchment is underlain by a fragipan at shallow depth that severely obstructs groundwater flow in vertical direction. Recharge rates to the deeper subsurface are very small and may be ignored when compared to recharge rates to the shallow subsurface. With respect to the shallow subsurface, Boll et al., [1998] report that soils are moderately well-drained and have a moderately deep profile extending to the

fragipan. The soil profile has three specific horizons (i.e. A, B, E) that vary in depth throughout the catchment.

The Troy catchment serves as a site for hydrological research at the University of Idaho (UI). Over the years, researchers of UI have performed detailed surveys on topography and spatial distributions and depths of the soil horizons and fragipan. Surveys are performed in a systematic manner by following a raster with rectangular elements of 5 meter spacing. For the soil horizons, the hydraulic conductivity, porosity and some values of the soil characteristic curves are defined through laboratory tests.

In the Troy area a piezometer network was installed in 1995 to observe water table fluctuations during the wet winter season. In 1997 this network was extended and nowadays 135 piezometers are in operation from which 102 are within the boundary of the Troy catchment.

A measuring flume (Thomson-weir) at the catchment channel outlet is installed to measure catchment outflow. Observations are made at irregular time-spacings but observation time series express the general runoff behaviour of the catchment. With regard to meteorological variables such as precipitation, evaporation and temperature, these are gauged at the Troy weather station in the catchment and also at the Helmer and Moscow weather stations that are located 15 miles east and 10 miles west of the Troy catchment respectively. Precipitation during winter and spring seasons mostly is observed as rainfall with low intensity or as snowfall where, depending on the air temperature, snow may remain on the land surface for several weeks.

From a hydrological point of view the Troy catchment is characterised as a shallow perched groundwater flow system where matrix flow conditions prevail. Macro-pores are not observed in the soil samples taken by researchers at UI although it is expected that such pores are present since the area once was covered by forest. For the past decades the land cover is undisturbed grassland. By these characteristics it is assumed that overland flow generation generally is caused by the saturation overland flow mechanism in case precipitation is in the form of rainfall. Runoff generation by snowmelt, however, also is common. Discharges from the seasonal stream vary from zero during the summer season to peak flow discharges of up to about 7 - 8 l/s during the winter and spring season.

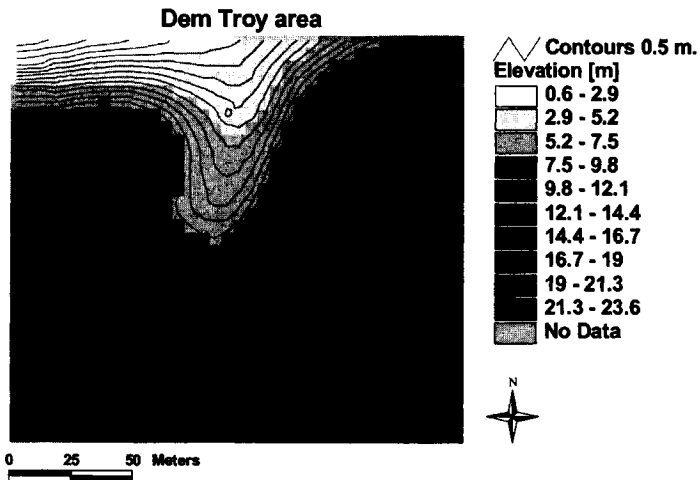


Figure 6.2: DEM of the surveyed area with elevation contour lines added.

6.2 Data collected at the Troy catchment

6.2.1 Topography.

In 1995 researchers of UI carried out a detailed survey of the elevation of an area that covers the catchment area. A rectangular area of size $85 \times 190 \text{ m}^2$ was surveyed and elevation measurements have been carried out at a $5 \times 5 \text{ m}^2$ raster grid. After finalising the survey, all measurements have been referenced to the lowest point in the area that, for digital processing, served as the datum. With these elevation measurements a DEM is created to establish a 3-dimensional representation of the catchment topography. Figure 6.2 presents a DEM of the surveyed area. Local depressions in the land surface are not removed and elevation contour lines are added.

For delineating the catchment boundary, the topographic analysis software TARDEM (Tarboton, 1997) is applied. Figure 6.3 shows the DEM of the Troy catchment where local depressions are removed and where the elevation contour lines are added. The maximum elevation difference of the catchment is 21.1 m.

Dem Troy catchment

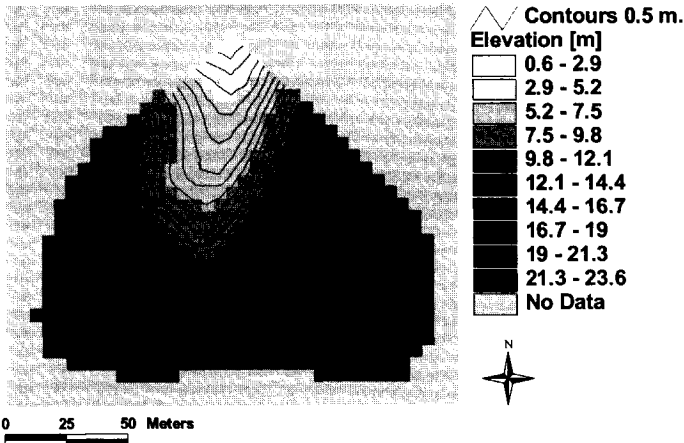


Figure 6.3: DEM of the Troy catchment, local depressions are removed and elevation contour lines are added.

By further processing with TARDEM, also a slope gradient map (see fig 6.4) and slope aspect map (Fig. 6.5) are generated.

Dem Slope Gradient

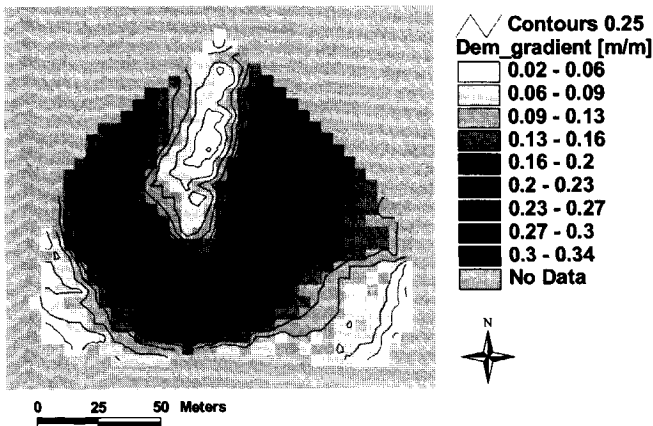


Figure 6.4: Hill slope gradient map.

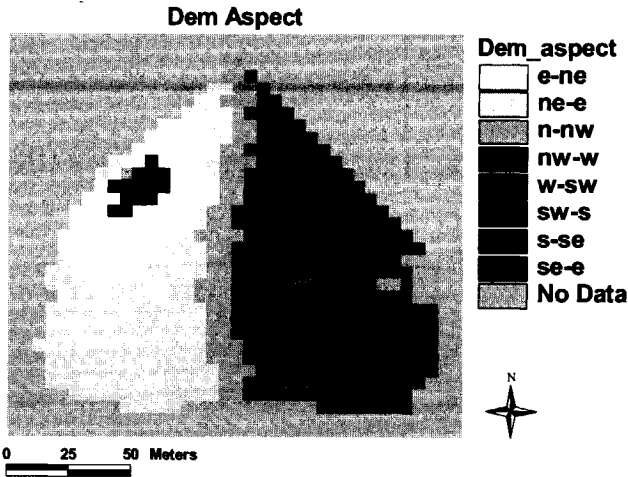


Figure 6.5: Hill slope aspect indicating the flow direction of each element.

The map shows that gradients are lowest along the catchment boundary and at the centre of the catchment. At the middle sections of the hill slopes, gradients are highest and hill slopes form a converging system towards the catchment outlet. Figure 6.6 shows a runoff contributing area

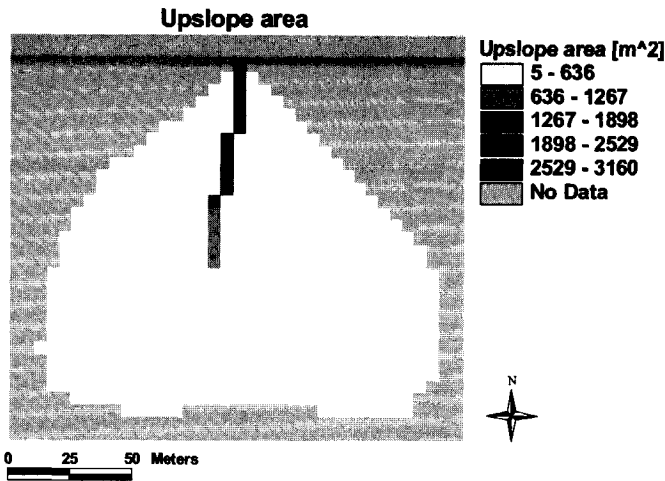


Figure 6.6: Runoff contributing area map indicating the total up-slope area that drains through an element and serves to delineate the channel drainage system.

map in which the total up-slope area is indicated that drains through a grid element. By this analysis the channel drainage system is delineated.

In runoff hydrology it generally is assumed that topographic boundaries co-inside with groundwater divides in the subsurface. It is clear that by implementing such assumption, groundwater flow across the boundary is zero and that, with respect to water balances, the only input and output terms are evaporation, precipitation and channel outflow. Whether this assumption is applicable to the Troy basin is questionable by the low topographic gradients towards the catchment outlet. Also by analysis of the elevation contour lines as added in figure 6.2 it can be stated that at lower elevations the delineation of the catchment boundary is doubtful due to the diverting contour lines. The assumption that groundwater flow across the topographic boundary is not present therefore is doubtful.

6.2.2 Shallow Subsurface

Soils

With a tractor-mounted hydraulic core sampler of 8.9 cm. diameter, soil samples up to the fragipan have been taken for each element in the DEM. The samples are used to identify the genetic horizons and to define the layer thickness. With this information, for each DEM element a soil profile is reproduced with specific thicknesses for each of the three horizons. Also a number of soil samples have been taken for analysis in the laboratory where the following soil properties were determined for each horizon: saturated hydraulic conductivity, porosity, field capacity, and wilting point. Researchers of UI have executed the survey and tests. The hydraulic conductivity of the Fragipan is derived from a Soil Survey report after Barker [1981]. Table 6.1 lists a summary of the soil properties of the horizons A, B, and E.

Table 6.1: Soil physical properties of the Troy catchment (Boll, et al., 1998).

Soil type	A	B	E
Average soil layer thickness (cm)	21.8	26.2	24.6
(K_{sat}) Saturated hydraulic conductivity K (cm/day)	160	50	20
θ_{fc} (cm ³ /cm ³)	0.51	0.43	0.38
θ_{wp} (cm ³ /cm ³) at field capacity [pF = 2.0]	0.38	0.28	0.27
θ_{wp} (cm ³ /cm ³) at wilting point [pF = 4.2]	0.11	0.08	0.08
α_{avg} (cm/cm)	0.08	0.08	0.08

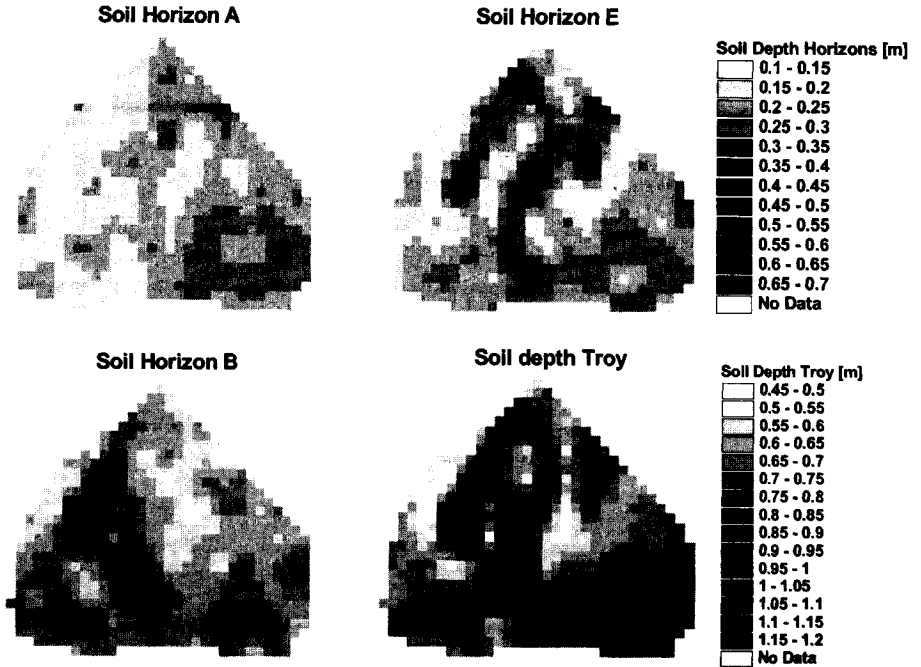


Figure 6.7: Soil depths of the Troy catchment for soil horizons A, B and E and total depth.

A description on the shallow soils is given by Boll et al., [1998] and is repeated here. The soils in the catchment are classified as the Santa Series, which consist of moderately well drained soils with a profile extending to the shallow fragipan.

Soils are formed in deep loess with small amounts of volcanic ash. The taxonomic class is coarse-silty, mixed, frigid Ochreptic Fragixeralfs. The profile contains three genetic horizons, A, Bw and E which at the bottom are restricted by a fragipan. This fragipan layer is also known as a Btxb horizon. For ease of use of abbreviations, Bw is replaced by B in the remainder of the text. The A-horizon is yellowish brown silt loam that colours dark brown when moist and has a sub-angular blocky structure that is 0 to 38 cm. deep. The B-horizon is a brown silt loam with a prismatic structure and is 38 to 68 cm deep. The E horizon is a pale brown silt loam with a massive structure that is slightly hard and is 68 to 86 cm deep.

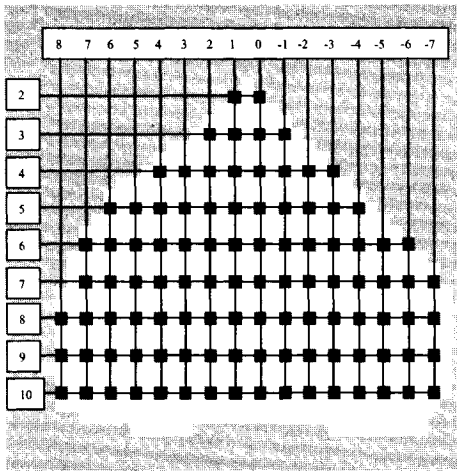


Figure 6.8: Map of piezometers in the catchment area.

Column and row numbers are added and serve as ID.

The Btxb horizon, or fragipan, is a yellowish brown silt loam and silty clay loam soil with a coarse prismatic and medium angular blocky structure that is very hard, firm, and brittle and ranges from 86 to 165 cm. deep. The fragipan with a saturated hydraulic conductivity of 0.01 cm/day forms the hydrological base of the shallow system. Figure 6.7 shows soil depths for each of the layers.

Water table observations

To observe water table fluctuations in the catchment, a piezometer network is in operation since 1995. The network comprises 135 piezometers from which 63 are installed since 1995. From these piezometers 43 are situated within the catchment and cover the western part of the catchment. In order to achieve a full coverage of the catchment, in 1997 the piezometer network was expanded with 72 piezometers in the eastern part. Piezometers were installed at the fragipan height and water table measurements represent the water table height of the perched water table above the fragipan. In figure 6.8 the locations of piezometers within the catchment area are shown. Each piezometer is indexed by a unique Identification Number (ID) that is according to the columns and row number as added in figure. 6.8. Each piezometer has a

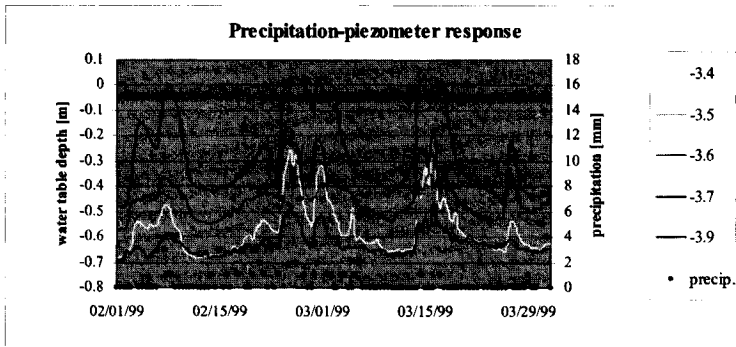


Figure 6.9: Groundwater table hydrographs of piezometers selected for model calibration.

sensor and is equipped with an automated data logger that stores the measurements of the water table depth at 12 A.M. and 12 P.M.

In the period 1998 – 1999, for all piezometers three sensor measurements were compared to three manual measurements and the absolute average error for each sensor was calculated. It was observed that five sensors did not function at all, and that 89 sensors had an error less than 5 cm of which 33 less than 2 cm. With the obtained information the UI has corrected the observation time series from which a small number are shown in figure 6.9.

The groundwater hydrographs of piezometers that are presented in this figure are a sample of the hydrographs that are used in MLE model calibration by PEST software. The selection is made after extensive analysis of (ensembles of) time series and the performance analysis of the network in general. Analyses focussed on the period January 1999 till June 1999 and are based on visual interpretation of the groundwater hydrographs. It appeared that many piezometers were unreliable in the sense that groundwater hydrographs show water depths that cannot be explained by physical reasoning. Piezometers 5.5, 4.4 and 2.4 for example show for some time periods water table heights of up to 1 meter above the land surface and piezometers 3.9, 4.5 and 6.7 show water table heights that, for some time periods, are unrealistic small. In Appendix B piezometer graphs are shown for all piezometers. A second interpretation dealt with the analysis of the rainfall-piezometer response relation.

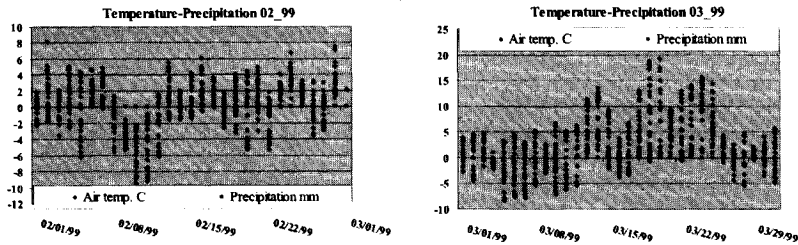


Figure 6.10: *Temperature-precipitation relation for the month February/March 1999.*

Piezometer observations series must show a clear response to rainfall events and must support the theory of the saturation overland flow mechanism that particularly is applicable to small-scale, shallow catchments with undulating topography. As such, especially when peak discharges are observed in the channel, at the lower catchment elevations with comparatively low hill slope gradients the water table must rise to the land surface. The extent of the water table rise often is not observed at higher elevations with possibly steeper hill slopes. In the up-slope areas water table rises due to recharge only and thus runoff production through groundwater exfiltration generally is not generated.

During the analyses it is revealed that the network is very unreliable with respect to representing the groundwater system dynamics that underlies the theory of the saturation overland flow mechanisms. The main cause for this uncertainty is the manner the network is installed. During installation the fragipan depth was measured at each piezometer location and this depth served as the elevation reference for the observation time series of the individual piezometers. As such, piezometer levels are gauged with respect to the bottom of the piezometer and thus the time series of observations are referenced to the fragipan depth. During the analysis, significant unexpected differences of the fragipan depth are observed at relatively short distances. Hence, this makes that also the quality of each time series to represent groundwater flow dynamics must be questioned. The performance of the network is discussed in more detail in Annex B where also selections are made for time series that are used in automated model calibration.

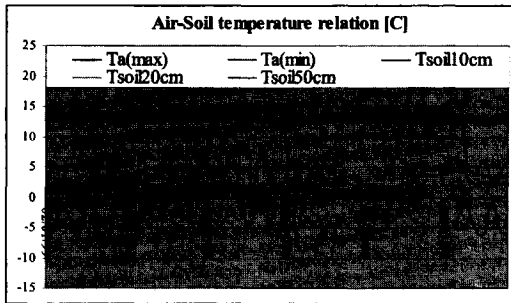


Figure 6.11: Temperature graphs for the Troy catchment. $Ta(max)$ and $Ta(min)$ are maximum and minimum day temperature respectively. $Tsoil$ is soil temperature at specified depth.

6.2.3 Rainfall-Runoff relation

Rainfall measurements

At September 26, 1996, the Troy weather station started hourly recordings for air temperature, relative humidity, wind speed, direct short wave radiation and precipitation. Also measured is the soil temperature at a depth of 10, 20 and 50 cm. Precipitation measurements are made by use of a tipping bucket gage that, at the Troy weather station, is not supplied with a windscreen. Rainfall measurements therefore are considered not to be very accurate. Also the measurements of snowfall are considered not to be accurate since snow easily blows over the gage. Also since the tipping bucket device is non-heated the snowfall measurements become uncertain. A failure of the device may for example occur when freezing conditions prevail as a result of low temperatures. In figure 6.10 the temperature-precipitation relation for the months of February and March is given. Air temperature is measured at an hourly base and in the graphs the day and night temperature range is shown. Obviously the night temperature often drops below zero while the day temperature mostly is above zero. In the Troy catchment the soil temperature is measured to analyse whether infiltration is obstructed by frozen soil conditions. In figure 6.11 the maximum and minimum air temperature distributions and soil temperature distributions at 10 cm., 20 cm. and 50 cm. depth are shown for the months of February and March 1999. Soil temperatures are measured twice daily at 12.00 A.M. and 12.00 P.M. In the figure it is shown that infiltration is not obstructed

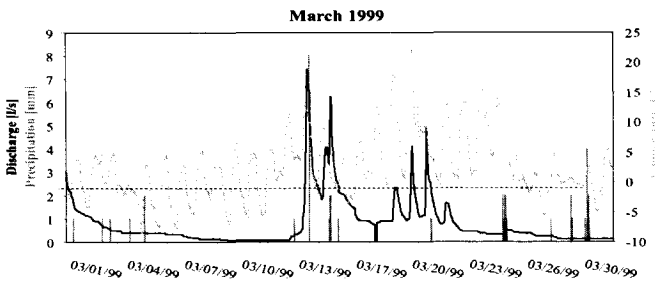


Figure 6.12: Channel flow hydrograph with precipitation depth and air temperature added.

significantly due to low soil temperatures. At a soil depth of 10 cm, the soil temperature is hardly affected by the air temperature and soil freezing at such depth does not occur. Hence it is assumed that any rainfall will infiltrate without a time delay and the stored groundwater volume will increase by infiltrated water. It is also assumed that snowmelt water most likely infiltrates without a significant delay. In case the soil crust freezes over night, the higher day air temperature cause de-freezing and snowmelt water will infiltrate.

Runoff measurements

The channel flow discharge at the catchment outlet is gauged by a circular flume (Thomson weir). The flume was installed at the end of 1998 and recordings started on January 13, 1999. The flume is supplied with an automated data logger that should make a runoff reading every 15 minutes. By analyses of the 1999 time series it appeared that large gaps existed in the time series. During the summer and autumn of 1999 data gaps of 150 and 60 days have occurred since runoff was not observed due to dry seasonal conditions. During the summer periods the perched water table drops to the fragipan and runoff generation by groundwater channel drainage does not occur. The water table then drops below the bottom of the channel and any interaction between the channel and groundwater system ceases. During the winter season observations are distorted when the air temperature drops below zero. Water in the channel and flume freezes and the sensor is unable to do reliable discharge readings. In figure 6.12 graphs of channel flow discharge, precipitation depth as well as air temperature are shown for the month of March. By the fact that

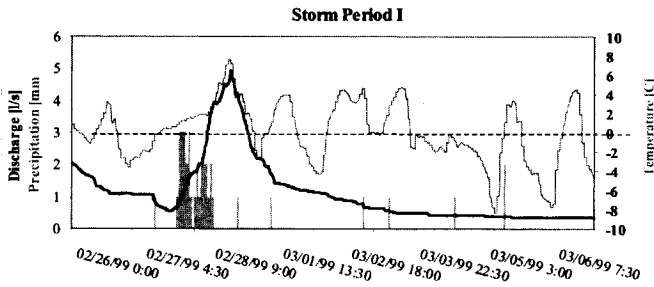


Figure 6.13: *Precipitation -runoff-temperature relation for March 1999.*

Precipitation depths are added for time intervals of 15 minutes.

data was collected at non-synchronised time moments, data series had to be completed for this thesis. Such completion is achieved through manual interpretation. The observation interval for discharges and temperature was 15 minutes while for precipitation hourly readings were available. Time series of discharge, however, were very incomplete although the general catchment runoff behaviour is expressed in the observations. During the selection of a time series of channel discharge that possibly could serve for model calibration, it became apparent that, for numerous reasons, a distinctive precipitation-runoff relation could not be defined. In figure 6.12 for example it is shown that in between March 17 till 20, three runoff peaks are observed although these peaks cannot be explained by any rain or snow fall event that occurred prior to the runoff peaks. Moreover, also for the runoff peaks at March 14 only little precipitation is observed. The fact that runoff events are shown in the time series becomes even more surprising when realising that researches of UI in 1999 concluded that, after comparing automated readings to manual readings, differences between readings were very small. After extensive analysis of the data set, for this thesis a rainfall-runoff event is selected for the period February 27 till March 3. The observed rainfall-runoff relation is presented in figure 6.13 and analyses on this event are described in Annex B.

6.3 Model calibration

Model setup

For simulation of the rainfall-runoff relation for the selected storm period I a catchment model of the Troy is constructed. With respect to the simulation of geometrical aspects of the model, the DEM of figure 6.3 is adopted and serves for discretising the model domain in two dimensions. As described in section 4.2 the raster grid is made up of rectangular elements that all are of equal size ($5 \times 5 \text{ m}^2$) and also serves for the discretizing the soil layers of the subsurface model domain. In the model set-up it is assumed that each soil horizon can be simulated by a single model layer and hence the subsurface model comprised three model layers. The depths of the soil horizons as presented in figure 6.7 are applied to simulate the depth dimension of the subsurface flow models. The applied discretisation of the subsurface model also serves to simulate soil physiographic parameters. By the small size of the Troy basin it is assumed that subsurface heterogeneity can be ignored and that parameter values are homogeneously distributed over the grid cells of the grid layers. Parameters are simulated by constant and grid cell averaged values. Prior to automated parameter optimisation, parameter values as shown in Table 6.1 are entered.

For the model layer representing soil horizon A, B and E, horizontal saturated hydraulic conductivities of 1.6 m/day, 0.5 m/day and 0.2 m/day are applied respectively. Porosity values for the three layers are fixed at 0.51, 0.43 and 0.38 respectively. Since field or laboratory values for the vertical saturated hydraulic conductivity are not available, in the model approach it is arbitrary assumed that the vertical conductivity value always is half the value for the horizontal saturated hydraulic conductivity. As such, for the three model layers, vertical hydraulic conductivities are set to 0.8 m/day, 0.25 m/day and 0.1 m/day respectively. For the parameterisation of the unsaturated flow model the soil characteristic relations are required. In section 4.4 it is described that the Van Genuchten relations are applied in Flowsim. The soil characteristic relation between the pressure head and the soil moisture content for the Troy basin is shown in figure 6.14 and is based on laboratory experiments at UI. In these experiments soil moisture

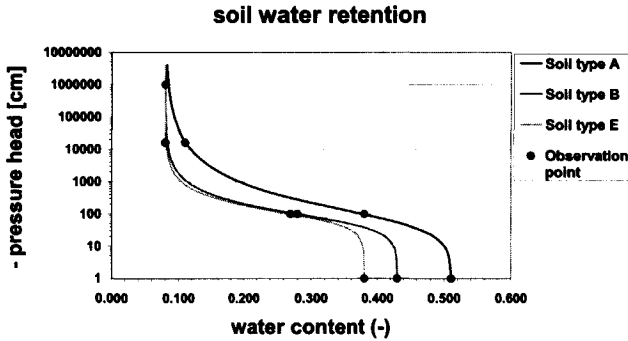


Figure 6.14 Soil water retention curves for the three soil types of the Troy catchment. Curves are based on the Van Genuchten relation (Pilot, 2002).

contents are measured at four pressure head values and are indicated by a black dot. Soil moisture contents are defined at soil saturation, field capacity, wilting point and for the residual content. For the parameterisation of these relations, Pilot [2002] selected the parameter values of table 6.2.

Table 6.2: Van Genuchten parameter sets for the three soil types of the Troy catchment.

Parameter			
	0.32	0.46	0.50
	1.47	1.86	2.00
	0.0170	0.0160	0.0125

At the lateral boundary of the model and at the bottom of the model a no-flow boundary condition is implemented. Any loss of water from the model is due to channel discharge at the catchment outlet and evaporation. Land use at the Troy is described by UI as undisturbed grassland. For the simulation of the land cover in the Troy model a Strickler-Manning coefficient of 25 [$L^{1/3} T^{-1}$] is selected and applied throughout the catchment grid layer. Rainfall input is simulated by use of temporal and spatial distributions. The applied temporal distribution is presented in figure 6.15, spatially is rainfall homogeneously distributed. By of Eq. [4.1] the rainfall depth is defined for each calculation time step.

An important input variable for event-based rainfall-runoff models is the initial model condition. By the FlowSim modelling approach, initial conditions need to be defined for the channel flow model and for the

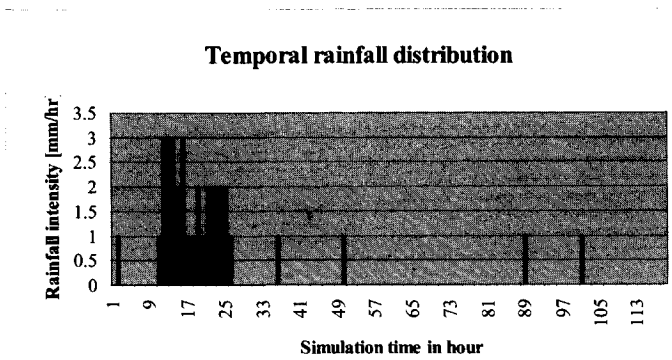


Figure 6.15 *Temporal rainfall distribution*

subsurface flow models. For the grid elements of the channel flow model an arbitrary initial water depth of 0.1 m. is defined. For simulating the initial condition of the subsurface the Initial Soil Moisture Content (ISMC) model is developed for this thesis by Pilot [2002], this in close co-operation with the author. The approach is extensively described in Pilot [2002] and in Appendix C only a brief description is presented. In this Chapter simulation results from the ISMC model are shown in figure 6.16a, b that serve as initial soil moisture content for the sub-surface model domain of FlowSim.

For any simulation, water balances are calculated for the entire model as well as for each sub-model. During model testing it proved that the model as well as each sub-models were mass conservative.

Calibration data

For this thesis one of the objectives is to apply multi-objective model calibration. Such calibration must be achieved by a calibration data set that includes channel flow and piezometer observations that express the dynamic behaviour of the groundwater table. For automated model calibration by PEST-software, 8 simulation cases are defined according to Table 6.3. In this table calibration data sets are defined for multi-objective and single objective calibration. For multi-objective calibration

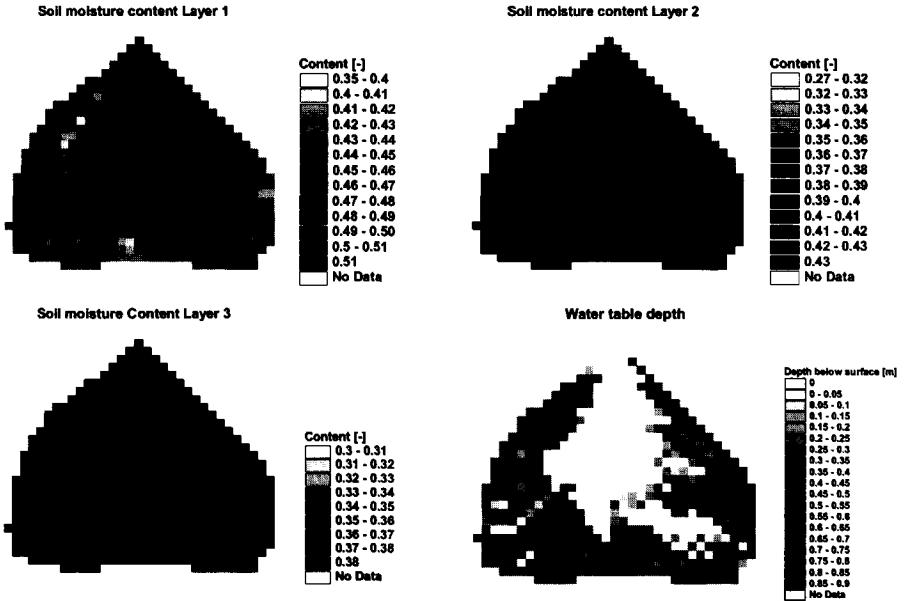


Figure 6.16a: Soil moisture distribution Case 1.

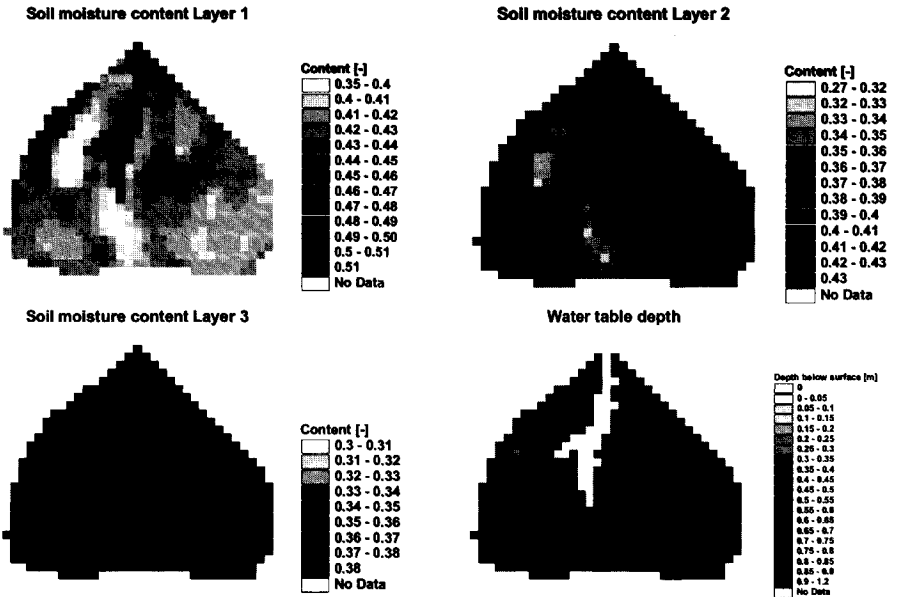


Figure 6.16b: Soil moisture distribution Case 2.

channel flow and piezometer data are selected. For single objective calibration either channel flow data or piezometer data are applied. The latter cases are defined for model comparison purposes as well as to observe whether the channel flow hydrograph can be simulated in case only piezometer data is used for model calibration. Such calibration serves to analyse the information content of piezometer data in PBRR modelling.

Table 6.3: Automated model calibration cases; number and type of state observations selected.

Case	Initial condition	Channel discharge data	Piezometer data
Ch_1	Case 1	15	0
Ch_2	Case 2	15	0
ChGws_1	Case 1	5	10
ChGws_2	Case 2	5	10
Gws_1a	Case 1	0	15
Gws_1b	Case 2	0	15
Gws_2a	Case 1	0	15
Gws_2b	Case 2	0	15

For each simulation case, parameters are optimised that are the saturated hydraulic conductivity in horizontal and vertical direction and the porosity for each of the three horizons. All other parameters are fixed and are not optimised during the model calibration. The parameter selection is based on early work from Calver [1988] and Grayson et al., [1992a,b]. State variables used for model calibration are piezometer data for selected piezometers and some channel flow observations from channel flow hydrograph shown in figure 6.17. Selected piezometer observations are shown in table 6.4a, b that are taken at 24.00 hours at February 27th and 28th and march 2nd.

These piezometer observations are selected since observations, to some extent, reflect the dynamic groundwater system behaviour that is characteristic for the saturation overland flow mechanism. Clear exfiltration periods, however, are not observed in the time series and thus the saturation overland flow mechanism is not well represented in the observations. For the three time instants, channel flow observations are

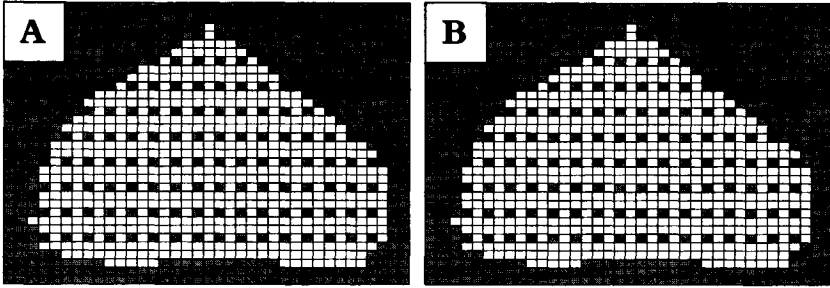


Figure 6.17: Selected piezometers for model calibration are indicated by black.

taken from figure 6.13 and represent discharges for the rising limb, the hydrograph peak and the base flow.

Automated model calibration is executed for 8 different cases as presented in table 6.3. Cases differ with respect to the applied hydrological state information and the selected initial soil moisture conditions Case 1 and Case 2 that are shown in figure 6.16a,b. For single objective calibration cases Ch_1 and Ch_2, 15 channel flow discharges are selected that are shown in table 6.5.

Table 6.4a: Case a: Observation data for piezometers 1.4; -1.4; -3.6; 0.9; 4.8

Date	Time	Piezometer number				
		1.4	-1.4	-3.6	0.9	4.8
27/2	24.00					
28/2	24.00					
2/3	24.00					

Table 6.4b: Case b: Observation data for piezometers 1.4; -1.6; -2.4; -5.10; 4.9

Date	Time	Piezometer number				
		1.4	-1.6	-2.4	-5.10	4.9
27/2	24.00	5.35	10.51	9.39	21.74	16.72
28/2	24.00	5.36	10.44	9.50	21.50	16.80
2/3	24.00	5.50	10.37	9.19	21.63	16.51

Values are obtained from the channel flow hydrograph of figure 6.13 and observations are selected for the rising limb, peak flow, falling limb and the recession curve and cover all characteristics of the hydrograph. For the single-objective cases Gws_1a, Gws_1b, Gws_2a and Gws_2b piezometer data as shown in table 6.4a,b is selected. For multi-objective calibration, the cases ChGws_1 and ChGws_2 are defined and apply piezometer observations of table 6.4b that are combined with 5 channel flow discharges of table 6.5. The black hatched cells indicate the latter observations

Table 6.5: Selected channel flow discharges

Date	Time	Q [m ³ /sec]
27/2	20.00	0.00082
27/2	24.00	0.00161
28/2	9.00	0.00360
28/2	14.00	0.00436
28/2	17.00	0.00493
28/2	21.00	0.00388
28/2	24.00	0.00303
1/3	3.00	0.00229
1/3	7.00	0.00207
1/3	11.00	0.00150
1/3	15.00	0.00136
1/3	22.00	0.00119
2/3	10.00	0.00105
2/3	22.00	0.00079
2/3	9.00	0.00061

Simulation results

Parameter optimisation is achieved for the horizontal and vertical saturated hydraulic conductivity and for the porosity values of the subsurface. For all simulations the vertical conductivity is arbitrarily set to half the value of the horizontal conductivity. Also during parameter optimisation the vertical conductivity remains fixed to the horizontal conductivity and thus any change in the horizontal conductivity is proportionally applied to the vertical conductivity. It is obvious that this assumption has an effect on the

simulation results, this aspect is not further researched since this is outside the scope. Secondly such research requires a detailed description on the spatial distribution of conductivity values that is not available at the Troy basin.

Optimised model parameter values for the defined cases are shown in table 6.6. In the table it is shown that for all cases optimisation is achieved and that parameter values generally fall within a small range. For some cases, however, significant differences exist.

Table 6.6: *Optimised model parameters*

Case	K _{rat,hor} [m/day]			K _{rat,ver} [m/day]			Porosity [-]		
	A	B	E	A	B	E	A	B	E
Field data	1.6	0.5	0.2	0.8	0.25	0.1	0.51	0.43	0.38
Ch_1	7.62	9.61	3.16	3.81	4.80	1.58	0.53	0.20	0.44
Ch_2	2.34	1.43	1.01	1.17	0.71	0.50	0.38	0.20	0.28
ChOver_1	1.19	0.21	0.58	0.6	0.10	0.29	0.54	0.45	0.30
	1.82	0.08	0.44	0.91	0.04	0.22	0.52	0.45	0.35
	1.73	1.20	0.02	0.86	0.60	0.01	0.43	0.44	0.40
	1.91	0.21	0.58	0.96	0.10	0.29	0.54	0.45	0.30
	1.64	0.54	0.03	0.82	0.27	0.015	0.44	0.49	0.35
	1.82	0.08	0.43	0.91	0.04	0.22	0.52	0.45	0.35

By these results it is concluded that selected initial model conditions that are shown in figure 6.16a,b. have a dominant effect on the optimised values. It also is shown that values depend on the data set of state variables used for calibration. In figure 6.18a, observed and simulated channel flow hydrographs are shown for the non-calibrated cases Case_1 and Case_2. For these cases the horizontal hydraulic conductivity and porosity values of table 6.1 are applied. For the non-calibrated cases quick responses to rainfall are shown where for Case_2 the magnitude of the peak flow discharge is reasonably well matched while for Case 1 this discharge is not within range. The latter, presumably, is caused by the simulated initial condition that represents a much wetter catchment as compared to Case 1. For both non-calibrated cases the recession periods are distinctive and represent clearly the depletion of the model shortly after the rainfall ceased. The time to peak is a second hydrograph characteristic and is reasonably well matched for both non-calibrated cases. The simulation

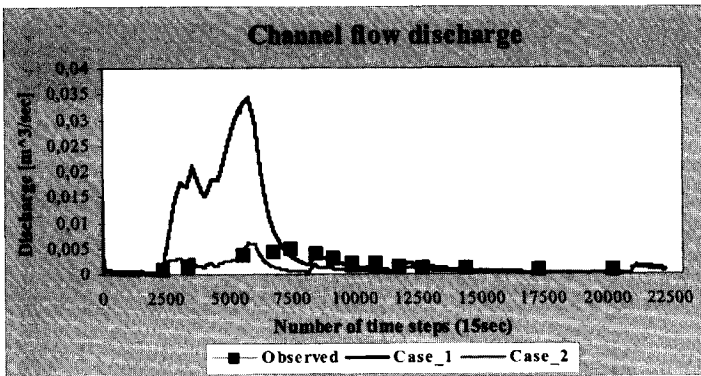


Figure 6.18a: Calculated and observed hydrographs for the non-calibrated cases Case_1 and Case_2.

results also show that the simulated hydrograph of Case_1 has a similar shape compared to Case_2 although the magnitude of the peak flow rate is much higher.

A visual comparison between the observed and simulated hydrographs of the optimisation cases is shown in figures 6.18b and 6.18c. By these figures it is shown that simulated peak flow discharges do not match well with observed ones and also that the shape of the recession curve shows a much more gradual subsurface depletion. This particularly when model calibration is achieved by groundwater table data only.

It appears that model performance is not high although this conclusion is preliminary since it is uncertain what modelling feature or aspect has dominated the results. Examples of some simple and obvious aspects that must be associated with non-quantifiable effects and that may cause unsatisfactory simulation results are:

- the observed model calibration data is in-adequate and does not represent accurately the various catchment response modes,
- the model concept of Flowsim is inappropriate to simulate the catchment runoff behaviour at the correct time and/or spatial scales,
- the model input data is incorrect or,
- the simulated initial condition is in-adequate and does not match real world initial conditions that should be applied at the onset of the simulation. Particularly in event based modelling the accurate

simulation of such condition is of great importance and to a large extent dominates the quality of the model simulations since any specific initial condition will result in a specific and associated, but possibly wrong, model output.

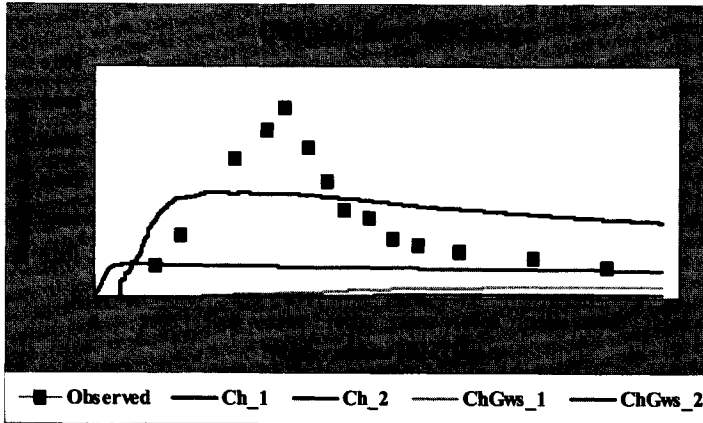


Figure 6.18b: Calculated and observed hydrographs for the cases where channel flow data and channel flow data combined with piezometer data is used for automated calibration.

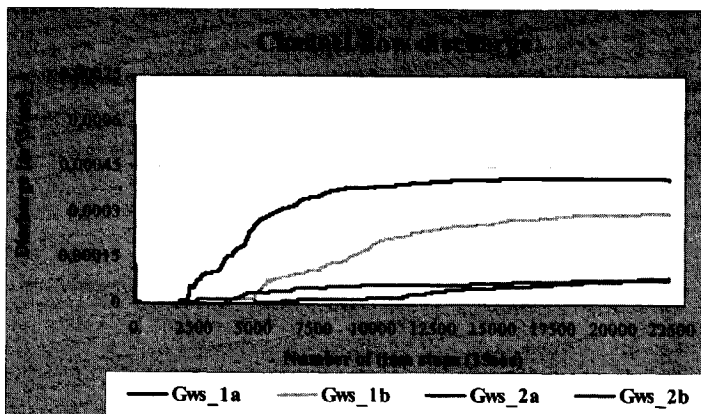


Figure 6.18c: Calculated and observed hydrographs for the cases where piezometer data is used for automated model calibration.

Consistent and clear conclusions on each of these causes are difficult to define but model performance in general is hampered by each of these causes. With respect to these causes some comments are made.

Analysis of the simulation results in which groundwater data are used for model calibration shows that such simulations do not show clear peak discharges and subsequently recession periods. In these cases, model responses towards rainfall input is not clearly observed and thus runoff production through saturation overland flow only has a small effect on the results. Given the pre-defined initial condition (figure 6.16a,b) it is obvious that to some extent overland flow occurs. By the initial condition, some subsurface model columns are fully saturated and hence exfiltration is likely to occur immediately after a model simulation is started. As described in Chapter 4, by the Flowsim model approach saturation overland flow only is simulated if all characteristics of the saturation overland flow mechanism are properly simulated. By the simulation results, it is concluded that exfiltration fluxes are small and remain fairly constant throughout the simulation period and that overland flow runoff contributions are small. It is concluded that, in the model simulation, a significant amount of rainfall is stored in the unsaturated zone model layers and only a small amount reaches the groundwater. The changes of the groundwater table depths are too small to generate additional exfiltration and saturation overland flow but primarily only cause the groundwater flow pattern to change slightly. Quantitatively, also groundwater - river interactions contribute to the river discharge but such interactions are simulated at a fairly constant and small rate. The shape of the simulated hydrograph thus is explained by small and fairly constant overland flow discharges and the small mass exchanges by groundwater - river interactions.

Also selected groundwater hydrographs (fig. 6.9) that are used for model calibration hardly show saturation overland flow zones to develop over time support the simulation results. By automated model calibration the model is tuned in such manner that the residual error is minimised and thus groundwater flow behaviour is simulated that matches the behaviour expressed in the time series. As such, in model simulation, exfiltration fluxes only are simulated as a result of the pre-defined initial soil moisture distribution. Following this reasoning, the initial soil moisture condition also becomes a model input figure that requires optimisation. Any

different initial condition yields a unique simulated groundwater flow behaviour and thus residual error.

Regarding the simulated hydrographs of the non-calibrated Case_1 and Case_2 it is concluded that the model concept of Flowsim is very well able to simulate the various catchment response modes. The various response modes are reasonably well represented in space and time based on the fact time lags to peak discharges are relatively close to observed time lags. The pre-defined initial condition, however, causes the magnitude of the peak flow discharges to be directly related to the initial condition.

The main objective of the cases GWS1a through GWS2b is to research whether groundwater piezometer observations may be of help to improve the model parameterisation and model performance in general. Regarding the previous comments, sound conclusions on suitability of MLE to improve PBRR modelling cannot be drawn since the model calibration data is too inadequate to simulate the saturation overland flow mechanism. Large exfiltration volumes and extensive runoff source areas are not simulated in the model but runoff generation through groundwater-river interaction is well simulated given the shape of the channel flow hydrographs shown in figure 6.18c.

Also when channel flow discharge data is combined with piezometer data in the calibration process hardly any improvement is observed in the simulation results. In the model calibration procedure, observations of channel flow discharges and piezometer data are equally weighted and thus channel flow discharges only have a small effect on the optimised values. This also is due to the fact that observation values of channel flow discharges are of a different order compared to piezometer observation values. Moreover, only 5 channel flow observations are used as compared to 15 observations from piezometers. Table 6.6 also shows that parameter values ranges become much larger when model calibration is based on the use of channel flow observations only.

With respect to the cases Ch_1 and Ch_2 in figure 6.18b, it is concluded that various response modes of the catchment are simulated by the Flowsim model approach. The magnitude of the peak discharge and shape of the recession curve, however, are subject for improvement. Although the rising limb of the hydrograph is well simulated, the simulated peak flow discharge has a too low value and the falling limb of the hydrograph

shows a depletion period that is too long where discharges show a too gradual decrease. A quick rise of the discharge to the peak flow discharge generally is due to a rapid increase of the saturation overland flow source area while a quick drop of discharge expressed in the falling limb is due to a rapid decrease of the size of the source area. Since for both cases such behaviour is observed in the simulated channel flow hydrographs, it is concluded that runoff process are not adequately represented. Model response is too gradual and, particularly, runoff production in space through the saturation overland flow mechanism could be improved, despite the fact that selected parameters are optimised. Specific causes to explain the observed model behaviour are, for example, wrong model input data and an in-adequate initial condition.

With respect to the first cause, DEM model input is very important since in the model approach for the generation of the exfiltration any simulated groundwater table depth is related to the DEM height. A wrongly entered representation of the catchment topography in terms of the DEM will result in an in-accurate simulation of the saturation overland flow mechanism. This since the elevation height of any simulated hydraulic head then is wrongly defined and since the observation time series are referenced to the real world catchment elevations.

The simulated initial condition also is identified as a possible cause of simulation in-adequacy. By the simulated initial condition, the depth of the water table and the soil moisture content across the model is defined and to a large extent defines the groundwater flow behaviour in the model. Also here, an incorrect initial condition results in incorrectly simulated groundwater flow behaviour and saturated model domain. Hence, simulation periods where exfiltration is generated may become too large or too small. Clearly by these two simple examples, simulation results always must be analysed critically and must be exercised with care.

Analysis of the graphical output from the PEST-software is shown in Appendix D. Such output includes 1) graphs of the parameter value evolution over the number of optimisation steps, 2) graphs of residual vs. observed Values, 3) matrices of the parameter co-variances, correlations and eigen-vectors and 4) histograms such as the Jacobian and eigen-values. For each of the eight automated calibration cases this information is generated additionally to the optimised parameter values and as such it is

concluded that MLE is very well applicable to PBRR modelling. For the eight cases however different optimised values are defined and also graphical output shows some differences. An example is that in the parameter correlation matrices for all eight cases different correlation structures are found. Also information on parameter identifiability through the eigen-vector - eigen-values matrices is not uniform. The dominance of single parameters in the eigen-vectors with lowest eigen-values changes over the various cases and causes that model results become specific to the selected cases.

Obviously, the fact that observations of a different kind and order are used and combined yields an inherent but unknown effect on the simulation results. Also the fact that two different initial conditions are applied causes model outcome to differ. Based on the physical reasoning described before, a different initial condition will yield a different groundwater flow pattern and thus different model behaviour. In the theory of the saturation overland flow mechanism, the size and shape of the saturation overland flow area are both functions of the dynamic character of the groundwater behaviour and thus such simulated behaviour has a dominant effect on the simulated channel flow hydrograph.

To become more conclusive on the reliability of the simulation results of each of the cases, an extensive mathematical analysis should be performed on the Gauss Marquardt Levenberg optimisation algorithm. Also after finalising the model simulations, it is revealed that the quality of the data set was too poor. The observed groundwater hydrograph from any piezometer must be questioned for its reliability and it is clear that selected observations most likely do not represent true observation values. Also the representation of catchment topography in terms of the DEM must be questioned. Relatively small elevation errors that are in the order of 10 cm have significant effect on the simulation results. To be more conclusive on the usefulness of MLE in PBRR-modelling, more model simulations must be executed and modelling studies must be performed at different catchments.

A critical note on the latter statement however is that it is questionable whether catchment data sets exist that have a high enough information content and that are reliable as well to allow successful multi-objective model calibration by MLE. Prior to the research in this thesis a number of

prominent rainfall-runoff researchers have personally been consulted and asked for whether they had access to a data set as required by the thesis objectives. It proved that many data sets exist but that many data sets had no detailed information on either topography, geometry of subsurface layers, physiography soil type distributions, and piezometer, channel flow and meteorological observations. Particularly time series of observation data with sufficiently high temporal and spatial resolution is not commonly available.

An alternative approach to the Troy model is to select catchments of much larger scale such as the (sub)regional scale. For such approaches, required model input and calibration data can, generally speaking, be of a lower temporal and spatial resolution. At larger scales, much more 'smoothed' or 'filtered' responses in space and time are simulated and model performance becomes much less a function of the resolution of the selected input and calibration data.

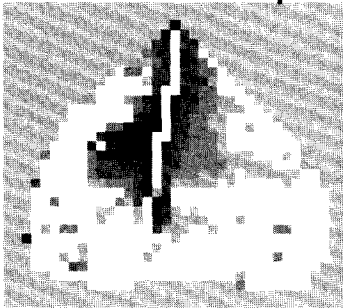
Applications of MLE in rainfall-runoff modelling also should be tested in combination with lumped CRR model approaches. Major advantages of such approaches are that much less input data is required which makes the simulation much less complex and also simulations are much less computationally demanding. In this respect, the averaged simulation time for the eight cases in this thesis were in the order of 7-8 days with a longest period of 20 days and a shortest period of 3 days on a 1.8 G.hz personal computer with 512 RAM.

In Appendix D graphical output from the PEST-software is shown in which also a more extensive description about the simulation results is presented.

7

Summary and Conclusions

Overland flow depth



Troy catchment



Based on an extensive literature study it is concluded that research in the field of PBRR modelling has gained little attention. Ever since the work of Freeze and Harlan [1969], who outlined a blueprint for a physically based digitally hydrological simulation model, relatively little progress is made in runoff simulation by such approaches. Based on theoretical descriptions of runoff production mechanisms that are developed during the late sixties, a small number of PBRR computer codes is developed to simulate runoff generation through Horton and saturation overland flow. Fundamental descriptions about both mechanisms as well as the subsurface storm flow mechanism are presented by Dunne [1978] and are repeated in section 3.2 of this thesis. By fieldwork of Hewlett and Hibbert [1967], it has become evident that runoff production through the saturation overland flow mechanism is triggered in the subsurface when soil columns become fully saturated by a rising groundwater table. Under such conditions, runoff production through exfiltration of subsurface water easily is generated at the land surface where subsequently saturation overland flow is generated.

In section 3.3 it is described that during the late eighties and early nineties the main objective for computer code development was to simulate runoff production in a distributed fashion as based on both overland flow mechanisms. Model simulations mostly were performed at catchments of local scale and focussed on the simulation of the runoff flow processes in the subsurface as well as at the land surface. Particularly the simulation of the highly dynamic and non-linear catchment runoff behaviour in the shallow subsurface gained attention in the distributed model approaches. The main objective was to simulate the changing size and dynamic character of the runoff source areas over the simulation period.

PBRR model approaches

For this thesis the model approaches of SHE, Thales, IHDM and DBSIM are extensively reviewed and short descriptions about these approaches are presented in section 3.3. Reviews particularly focussed on a comparison of the designed model concepts that underlie the approaches. In the same section also some simulation results are described and discussed. By the review it has become evident that model concepts differ significantly with respect to a number of generic aspects.

Major differences relate to three aspects that are a) the applied catchment partitioning theory in order to create a distributed and discretised model domain, b) the flow processes simulated and c) the applied flow equations. Approaches described for the creation of the DEM are based on the use of rectangular grid elements of equal size or on the use of non-rectangular elements of various sizes. In the four model approaches the applied DEM discretisation is adapted to the subsurface model layer(s). Also the approach for the discretisation of the subsurface through the use of model layers differs for each approach. Based on physical reasoning and considering that runoff production takes place in the shallow subsurface, it is questionable whether applied DEM discretisations should be adapted to the subsurface model layers. This since the geometry of the subsurface layers significantly differs from the topographic geometry. This aspect of transforming the real world into an appropriate model approach becomes even more apparent when considering the fact that, with respect to size and scale of the subsurface grid cells, model parameter values are applied to these grid cells. Any system heterogeneity within the scale of a grid cell is ignored and parameter values as well as calculated state variables are lumped to represent averaged values. Unambiguous conclusions on the effectiveness of the applied discretisations are not drawn in this thesis since effects of the applied discretisations are not clearly quantified. Also literature on model comparisons of PBRR models is very scarce since such comparisons only have gained very little attention.

With respect to the spatial discretisation approaches and considering all aspects that subsequently follows from such discretisation, it is in subsection 3.4.2 concluded that the use of rectangular elements of equal size is an appropriate approach. This since any parameter value within a grid cell must be interpreted as a grid effective value that requires optimisation through model calibration. The size and shape of an element as such becomes less relevant. The size of grid elements however must be relatively small compared to the size of the catchment and must represent the catchment characteristic of interest. Clearly, catchment heterogeneity at smaller scales causes that model parameter values cannot be extracted directly from field observations. Guidelines to make a selection on the size of a grid element are not presented here but, based on physical reasoning, it is recommended to apply DEM elements that are smaller than 1% of the catchment model size. Also for model

discretisation in vertical perspective clear guidelines are not available in literature. Such discretisation mostly is achieved through a discretisation in which all cells are of equal or varying thickness. In the latter case cells thicknesses often increase with depth where top cells are of small thickness while bottom cells are of, relatively, large thickness. Examples of both approaches are known for the model approaches that are described in section 3.3.

With respect to the applied flow equations and the mathematical models a number of conclusions are drawn. For the simulation of overland flow a two-dimensional model approach must be selected that requires the use of a raster DEM with squared elements. Such DEM serves to georeference the grid elements in the numerical model and to simulate the hill slope gradients. With respect to the complexity of the numerical model to simulate saturation overland flow adequately, it is concluded that the diffusion wave approximation is appropriate. This since topographic gradients in (small) upland catchments are relatively high. In literature it is widely acknowledged that for such conditions any change in momentum by changes in the flow velocity over time and along a channel can be ignored. For the simulation of flow discharges it is appropriate to select the Strickler-Manning equation that, in the numerical flow model, must be combined with the conservation equation. Channel flow may be simulated in a similar approach, the numerical model however must be solved in one flow direction only. In the approach the exchange of mass from the overland flow model to the channel flow model must be allowed for.

With respect to the simulation of the subsurface flow processes it is concluded that a relatively simple model approximation must be selected as compared to the real world subsurface runoff behaviour of a catchment. An extensive, theoretical, description about this behaviour is presented in section 3.2. In distributed PBRR model approaches only saturated and unsaturated subsurface flow as indicated in figure 3.1 are simulated thus ignoring flow processes of, for example, macro pore flow and perched subsurface flow. Hence, and with respect to the mathematical model, subsurface flows are simulated in matrix flow conditions only. In the model approaches saturated flow is simulated in one or two lateral flow directions across cells of a grid layer while unsaturated flow is simulated in vertical direction only. In case multiple model layers are defined such flow is across a column of grid cells. For

the simulation of saturated subsurface flow a Boussinesq-type flow equation is appropriate. By such approximation it is assumed that saturated flow takes place in phreatic flow conditions only and thus it is particularly suitable for simulation of shallow subsurface systems. For the simulation of unsaturated flow it is concluded that a one-dimensional Richards type flow model is appropriate. Such model approximation requires the use of the soil characteristic curves such as developed by van Genuchten [1980]. Additional requirements for the subsurface model approximation are that, besides water flow across the distributed model domain, the model must be able to simulate infiltration and exfiltration at the land surface and evaporation from the subsurface. Also the exchange of mass through interactions with the channel flow model must be simulated. The simulation of these processes makes that PBRR models become very complex and that simulations are seriously hampered as described in section 3.3.

Flowsim model concept

For this thesis the computer code Flowsim is developed as one of the objectives of this thesis work. The designed model concept is based on the presented conclusions in section 3.4. Aspects relating to the catchment geometry are simulated in a fully distributed three-dimensional model domain. For the flow processes a number of sub-models are developed. Meteorological influences such as rainfall and evaporation are simulated by spatially and temporally distributions. A two-dimensional overland flow model that is based on the diffusion wave theory simulates Hortonian and saturated overland flow. Unsaturated subsurface flow is simulated in vertical direction only by a multi layer flow model that is based on Richards equation. Saturated subsurface flow is simulated by a two-dimensional flow model based on a Boussinesq-type flow equation. Mass exchanges between the various sub-models such as infiltration, exfiltration, evaporation and river-groundwater system interaction are allowed for. In the approach these sub-models are combined and linked and make up the mathematical model that allows for the simulation of the highly dynamic and non-linear catchment runoff behaviour. A brief description on the approach and computer code is given in Chapter 4 while detailed descriptions on the mathematical sub-models, the mass exchange and coupling

procedures between sub-models and the model approximations are given in Appendix A.

Scale problems

Simulations by Flowsim as well as by the computer codes that are described in section 3.3 are hampered by a number of causes that primarily relate to complexity of the model approaches. In sections 3.4 and 3.5 it is concluded that particularly scale issues hamper simulations. Generally speaking, scale problems to a large extent are due to the fact that the various processes are simulated in a discretised and thus distributed model domain that, in plane perspective, is based on the adapted DEM discretisation. While specific processes require specific spatial model scales at which these processes must be simulated, this aspect of model simulation generally is ignored. Scale problems also come into play when time series of piezometer observations must be selected and applied to the model calibration procedure. Observations are taken at the point scale at specific time instants but in the model approach they are simulated at the scale of the grid cells and the simulation time step. In case observations of various state variables are used, each state variable is taken at a specific point scale while model simulated counterparts must be interpreted as averaged values for the size of the selected spatial calculation units. For the overland flow and channel flow models these calculation units are the grid elements of the DEM while for the subsurface flow models these units are the grid cells. The large amount of field data that is required for setting-up a catchment model also is a common problem. Models require extensive data input on, for example, soil type distributions, the channel network and topography. Such field data and catchment information must be obtained through extensive field surveys. Data therefore generally is not available and much information that is added to a model must be interpreted as synthetic data. In section 3.4 it is shown that large quantities of model parameters and parameter values are required to parameterise any model. By these large quantities, models easily become over-parameterised and the effect each parameter has on the model output becomes uncertain. As a consequence, PBRR model approaches must be associated with a great deal of uncertainty. Also insufficiencies in the commonly applied trial and error calibration procedure makes that any model parameterisation cannot be associated with uniqueness.

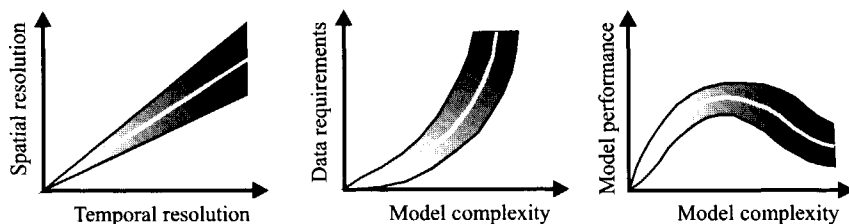


Figure 7.1: Data requirements, model performance and model complexity relations (Rientjes and Hassanizadeh, 1999).

With respect to the data requirements, the performance of PBRR model approaches and their model complexity, the relations in figure 7.1 are presented where the latter one is developed for this thesis. These relations as well as descriptions on these relations are presented in subsection 3.4.2. By philosophical and physical reasoning, the relation between the model complexity and model performance brings forward that model performance is a function of the model complexity and, more important, that an optimum model performance can be defined. Based on this relation, it is concluded that PBRR model concepts must be kept relatively simple in order to reduce the parameter demand and consequently model complexity. In this thesis it is propagated to use rectangular grid elements of equal size as compared to non-uniform grid elements of various sizes. Also the use of a one-dimensional Richards type flow equation for unsaturated zone simulation is propagated as compared to the use of multi-dimensional equations.

Model calibration

For model calibration in PBRR modelling it is common to apply the Trial and Error procedure in which parameter values are optimised manually over repeated simulation runs. In each simulation some parameter values are modified and model performance is analysed by visual interpretation of simulation results or a pre-selected calibration criterion. In section 5.2, it is described that such calibration must be rejected since the procedure has major weaknesses. Despite the fact that visual interpretations of simulation results are satisfactory, conclusions to be draw by such interpretation must be exercised with care. Examples of fundamental weaknesses of visual interpretations are that it remains uncertain whether the most optimal parameter values are defined,

whether parameters have some statistical dependency, whether parameter values are well identified and whether parameter sets may be equivalent. These aspects, among others are discussed in detail in section 5.2. In this thesis it is concluded that for model calibration automated procedures must be applied that, at least partially, overcome some of these weaknesses.

In Chapter 5 an extensive review after the development and application of automated procedures in runoff simulation showed that only few approaches are known. Approaches are developed during the nineties and are subject of ongoing philosophical discussions and debate. In this thesis the approaches reviewed are the Bayesian procedure GLUE, the single and multi-objective evolutionary procedure MOCOM-UA, the geo-statistically based MLE procedure and a novel procedure based on the use of ANNs. In each of the approaches the focus is on optimising model parameter values only and thus ignoring all other causes that possibly cause poor model performances. Hence it is assumed that for any simulation an a-priori defined model concept can be applied that does not require improvement or optimisation. Also it is ignored that meteorological stresses could be simulated in-adequately or that calibration time series of state variables are inadequate because of e.g. a too small observation resolution.

The theoretical bases of each of the approaches are described and examples of applications are analysed. By the review it has become apparent that approaches differ significantly with respect to the fundamental assumptions that underlie the applied parameter optimisation strategy. Although each procedure aims to optimise model parameter values, the outcome of the procedures in terms of supplementary calibration information differs. Specific requirements with respect to this information are debated in literature and have a focus on, for example, how well single parameters are identified and whether insight is gained on parameter inter-dependencies. By such information the weaknesses of the manual Trial and Error calibration procedure must be overcome. Automated calibration procedures mostly are applied to CRR model simulations while applications to PBRR are very scarce. The review therefore also focussed on the issue whether such calibration procedures could be applied to PBRR models and whether calibration could be achieved when multiple state variables are selected for calibration. In the literature such applications are propagated

and often are referred to as multi-objective model calibration. For this thesis it is decided that an automated calibration technique should be applied that allows multi-objective model calibration through the use of multiple state variables. Further specific requirements are that specific information on parameter dependencies and parameter identifiability must become available.

Maximum likelihood estimation

After reviewing the approaches it is decided to select the geo-statistical based MLE procedure. Applications of the MLE procedure allows for model calibration by use of multiple hydrological state variables that are of a different kind and order and that all can be combined in a single objective function. The geo-statistical approach yields specific information on a) parameter sensitivity through a sensitivity matrix called the Jacobian matrix, b) parameter inter-dependencies through parameter covariance and correlation matrices and c) how well parameters are identified through eigen-value and eigen-vector matrices. Although in literature procedures are advocated that yield such information, such applications in the field of PBRR modelling are very limited. A limitation of the procedure is that it aims at finding the most optimal and single best parameter set thus ignoring any uncertainty that must be associated with the optimised parameter values.

Case study of the Troy basin

For this thesis software based on the MLE procedure is provided through PEST that is combined with the Flowsim model approach. A catchment model is developed for the Troy basin of 1.6 ha that is situated in the state of Idaho, USA. This basin is selected after an extensive search for a catchment that allows for the application of multi-objective model calibration by use of channel flow observations and groundwater piezometer observations. Other specific requirements are that information on the subsurface and land surface had to be available for the three-dimensional modelling of topography and subsurface. For the Troy basin detailed field studies already were executed by researchers of UI and detailed descriptions of topography, land use and soil type and layer distributions already were available. Also time series on precipitation, evaporation, temperature, groundwater piezometers and channel flow discharges were available, this for the winter period of

1999. Researchers of UI made the database of the Troy basin available for this thesis.

With respect to the short observation period of the time series, it was not possible to make simulations covering extensive periods but instead single events had to be selected. This selection has taken considerable time since it proved to be difficult to find a time period where non-freezing conditions prevailed and where snowmelt did not effect the channel flow hydrograph. Also, and partly due to freezing conditions, time series of channel flow observation often were incomplete and unfortunately recordings were not taken continuously in time. Selected time series of channel flow were incomplete and observation gabs existed that have manually been filled. With respect to the groundwater system, 102 piezometers are installed in the catchment and observations are taken twice a day. Analysis of these time series learned that only a relatively small number of piezometers could be identified that, to some extent, express the dynamic groundwater flow behaviour that underlies the theory of the saturation overland flow mechanism. For a number of piezometers it was concluded that they mal-functioned while a number of piezometer did not show clear responses to rainfall. The final selection of piezometers to be used for model calibration is made on the criterion that, when assembled to represent a cross section along a hill slope, they, to some extent characterise the dynamic groundwater behaviour that underlies the theory of the saturation overland flow mechanism. In the piezometer hydrographs, however, clear exfiltration periods could not be identified.

By the fact that only single events could be simulated, an additional problem came into play that dealt about the simulation of initial model conditions. While in runoff modelling normally a warm-up period is selected to simulate initial model conditions, now a different procedure had to be applied. A subsurface model initialisation procedure based on the Topmodel approach is developed that allows the simulation of the water table depth for the saturated subsurface and the simulation of a 3 dimensional soil moisture distribution over the cells of the unsaturated zone model. For this thesis the ISMC-model is developed that is described in Appendix C. For simulations by the ISMC-model approach, the entire piezometer network is used where only piezometers are ignored that mal-functioned.

Simulation cases

For this thesis 10 simulations are executed of which 2 are non-calibrated simulations and 8 are simulations with automated model calibration by MLE. Simulations are executed for two models of the Troy catchment where only the initial soil moisture condition differed and thus any other input data figure such as rainfall and model parameters remained similar. Model calibration is performed for the two models where for each model four calibration sets with state information are defined. For single objective model calibration, two sets are defined that only have piezometer observations while one set only has channel discharge observations. For multi-objective model calibration one set is defined that has piezometer observations as well as channel discharge observations. To each of the two models these four sets are applied. Optimised model parameters for all eight cases are the saturated hydraulic conductivity and the porosity for the three model layers. Although for all eight cases single best and optimised parameter values are estimated, all sets are different and for some parameters significant differences exist. Also the simulated channel flow hydrograph for each case differs and thus for each case a slightly different catchment runoff behaviour is simulated. Hydrographs mainly differed with respect to the simulated peak discharge as well as the shape of the recession limb. Simulation results in general are not satisfying, particularly for multi-objective model calibration. Sound conclusions on the applicability of the MLE are not formulated since too many factors that have significant effect on the results are not properly defined. Such factors are for example the reliability of the selected data set and the appropriateness of the designed model concept of Flowsim. Also effect of the initial model condition on the simulation results is not clear although it appeared that selected initial conditions have a major effect on the simulation results.

By comparison of the parameter correlation matrices it has become apparent that parameter dependencies change subject to a) the selected set of hydrological state observations used for model calibration and b) the simulated initial condition. While the degree of the correlations changes, also the plus or minus sign change for some parameter correlations. By comparison of the eigen-vectors matrices, it also has become apparent that dominance's of single parameters in the eigen-vectors change. Such changes imply that different parameter combinations dominate the model calibration for the various cases and

thus it is concluded that the simulated catchment response mode, as expressed by model calculated counterparts of the selected state variables, has a major effect on these simulation results. Clearly, such response modes change over time and over the model domain during and, as well as, for the different simulation cases. A pre-requisite for the use of time series of observations for model calibration is that time series are accurate and reliable. After extensive analysis of the large database of the Troy basin it is concluded that available time series must be exercised with care. Particularly for the automated model calibration cases where only piezometer observations are used this has become apparent. For these cases significant deviations exist between simulated and observed channel flow hydrographs and thus the real world catchment response through the use of groundwater piezometers is not well represented. This implies that either the model structure of Flowsim has major weaknesses or that selected time series are inaccurate and unreliable.

Event based modelling

After reviewing all the simulation results it is concluded that event based rainfall-runoff simulation by a PBRR model approach is too complex to be successful. By such approach too many generic modelling issues and aspects come into play that easily cause model performance to become unsatisfactory. First of all, runoff production simulation requires a computer code that is able to simulate the dominating flow and meteorological processes of the hydrological cycle. Computer codes thus are very complex in terms of the number of flow algorithms and the simulation of mass exchanges between the various algorithms. Algorithms must be developed for many flow processes such as infiltration, percolation, saturated subsurface flow, overland flow while mass exchanges between algorithms also must be allowed for. Each flow equation must be parameterised that results in a parameterised catchment model that must be interpreted as a gross simplification of the real world system. Such models allow for the simulation of the catchment runoff behaviour, albeit it is still in a simplistic manner as compared to the complexity of the real world catchment runoff behaviour. In any model, processes are simulated at either much larger or smaller spatial and temporal scales than the process scales. Although any real world model simplification results in a reduction of required

model input data, such reduction by far is not significant enough to reduce the input data-requirements to a level that data can be made available through measurements at required spatial and temporal model scales. Therefore, for any model always a trade-off can be defined between the (too) limited data availability and the exactness and correctness of the model input data.

Input data requirements

Input data values always represent averaged values that are integrated over the scales of the model calculation units. Examples of required data types are geometrical data to represent the land surface and sub-surface, physiographic and topographic data to parameterise all model equations and meteorological data to simulate meteorological stresses at the boundaries of the catchment model. Moreover, meteorological stresses that must be interpreted as a surface boundary fluxes only are observed at specific time moments and at specific locations. Representative data also is required to simulate flow boundary conditions of the groundwater system although groundwater flow across topographic divides and to the deeper groundwater water system is very difficult to observe. The accurate simulation of each of these features becomes even more significant when runoff behaviour must be simulated for only a very short period of time such as is the case in event based model simulations. Generally speaking, the smaller the time and space scales such processes must be simulated, the more a model must be able to simulate the highly dynamic and non-linear flow behaviour by which runoff is generated. It is evident that the 'data requirement - data availability' paradox becomes apparent here.

The biggest problem in PBRR modelling, however, deals with the simulation of the initial model condition. For each sub-model such condition must be defined and thus at the onset of the model simulation, for each sub-model hydrological states across the model domains must be defined. Particularly in event-based modelling this feature is of great importance since a 'warm-up' period, as commonly applied in continuous stream flow simulation models, is not defined. Over the length of the warm-up period, meteorological stresses are entered into the model to tune the model in such manner that all hydrological states are simulated correctly at the onset of the actual simulation. The length of such a period cannot be defined a-priori but is subject to the system to

be modelled but generally ranges between 0.5 and 5 years. Defining such warm-up period in event based modelling is not possible and therefore other procedures must be selected and developed to simulate such condition. In this thesis the ISMC-model is developed to deal with this problem and by this approach the initial condition of the saturated and unsaturated sub-surface models are simulated. For model simulations with the ISMC-model approach, also model parameters and time series of state observations are required to simulate the initial conditions. Clearly, also here all modelling features come into play and any simulation result must be questioned how accurate simulations are in representing the real world behaviour. With respect to the event based Flowsim simulations, any applied initial condition will yield a different model result since a unique hydrological state distribution across the model domains yields a unique flow pattern in terms of discharges and flow directions. Understanding all these issues causes that event based PBRR modelling at this stage of research still is too complex. The reviews as well as the MLE simulation results generated for this thesis support this conclusion. Although parameter optimisation has not failed for any of the eight cases, the simulation results from the non-calibrated cases can be improved as well as all cases were automated calibration is applied.

Recommendations

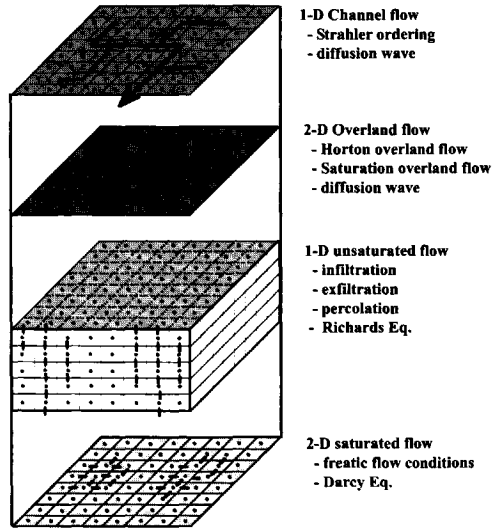
A first recommendation with respect to this thesis work is to repeat MLE simulations on a different catchment for which a reliable data set is available. In the selection of a catchment, more emphasis must be laid upon the availability of reliable time series as compared to the data on subsurface catchment characteristics. This since model performance is evaluated by means of an objective function in which observed and simulated hydrological states are compared and residual errors are calculated.

A second recommendation is that MLE also must be tested in CRR modelling. In CRR approaches, calibration issues like parameter identifiability and parameter dependencies also are apparent as shown in automated calibration by the MOCOM-UA algorithm while the model approaches generally are far less complex than PBRR model approaches. By use of CRR model approaches the 'added value' of MLE to runoff modelling may become more pronounced.

A third recommendation is that for automated calibration procedures comparative research must be performed. For such research, few runoff codes with increasing complexity must be selected for which selected automated calibration procedures are applied. By such research it must become clear which approaches are the most advantageous and promising and also what approaches must be rejected. For such judgement objective guidelines must be set.

Appendix A

Mathematics of Flowsim



I Rainfall and Evaporation model

In the modelling approach of Flowsim, spatial interpolation techniques are used to simulate the spatial distribution of rainfall and evaporation over a grid layer. By interpolation, an estimate of such depth at any grid element is generated by field data that is observed by gauging stations of a measuring network. Techniques used for estimations are called 'interpolation' schemes'. In the following theoretical and mathematical aspects of such techniques are presented.

A large variety of schemes is available for interpolating randomly scattered point observations in an area. With respect to spatial interpolation, all interpolation techniques make assumptions with regard to the possible behaviour of the process to be simulated. From a hydrological point of view, caution must be exercised about the likely accuracy of any interpolation scheme since the validity of a scheme has to be seen against the (extreme) variability caused by non-linearity of the processes under study. Temporal and spatial processes of rainfall generally are much smaller than the process scales of evaporation and as such interpolation of rainfall observation compared to evaporation observations becomes less complicated. For estimation of point observations, 'local' and 'global' techniques are available. By local estimation techniques, the value at an unknown point is estimated based on the known values within the small neighbourhood of this point. Global techniques try to find a model that incorporates all the measurements and principally take into account the large scale spatial variability. This as contrasted to local techniques that mainly use local information to make estimates at non-measured locations. Most techniques consider the distance from the sample to the point being estimated as a weighing factor in their estimation. By doing so, the underlying assumption is that data measured near the point of interpolation are likely to be in more correspondence with the value to be estimated. In science a range of techniques are developed to decide on:

- the method the 'weight' has to be defined, and
- the effect each weight should have in the interpolation scheme.

¹ Interpolation is the process of transferring information from measuring points into space.

A rational framework dealing with spatial variability and uncertainty on the behaviour of phenomena is provided by the theory of random functions.

I.1 Random function theory

By a random function, the structured and random character of a 'Regionalized Variable' (REV²) is expressed simultaneously. In the rainfall model, a REV represents the rainfall depth at a pre-defined location for a certain period of time. A rainfall depth is gauged at, or estimated for any unknown location. In the random function theory, mathematical tools for the estimation of a REV are available. Although a random function model does not describe the full spatial behaviour of the rainfall, the model is able to represent the spatial distribution of the rainfall depth. Restrictions to reliability mainly are due to the number of measurements in relation to the, often, complex behaviour of the phenomenon.

For characterising a rainfall field, in this study the first two statistical moments are used. The first moment of a random field is expressed by the mean while the variance, the covariance or the semi-variance expresses the second moment. Subject to the stationarity of the rainfall field, the second moment is defined.

The mean or the expected value of the random field $z(x)$ is defined as:

$$E[z(x)] = m(x) \tag{A.1}$$

For characterising the dispersion around the expected value of the random variable z , three-second order moments are available in geostatistics:

- the variance:

$$\sigma(x)^2 = \text{Var}[z(x)] = E\{[z(x) - m(x)]^2\} \tag{A.2}$$

- the covariance:

$$C(x_1, x_2) = E\{[z(x_1) - m(x_1)][z(x_2) - m(x_2)]\} \tag{A.3}$$

- the semi-variance:

$$\gamma(x_1, x_2) = \frac{1}{2} E\{[z(x_1) - m(x_2)]^2\} \tag{A.4}$$

² A REV is described by a function, which gives at any point x the unique value of the property z being studied; $z(x)$. Applying a set of point measurements, a spatially distributed random function model can be made.

Stationarity of a random field

For characterising the spatial variability of a rainfall/evaporation field the stationarity of the process is defined first. A process is assumed strictly stationary if a random function describing this process is invariant under translation. Weaker forms of stationarity are the first-order stationarity, the second-order stationarity and the intrinsic stationarity.

First-order stationarity

If the random field is characterised by a constant mean value over the spatial domain, the average value of $z(x_i) - z(x_j)$ is zero. By first-order stationarity an expression of the first moment, the mean, is defined which expected value is constant and independent of x .

$$E[z(x) - z(x+h)] = 0 \quad [\text{A.5}]$$

Second-order stationarity

When z fluctuates in space around a given mean m , without a definite trend in any direction, the mean and the variance are the same everywhere. The covariance $C(h)$ between the process at points x_i and x_j is independent of the individual locations x_i and x_j but only dependent on the lag vector h where $h = x_i - x_j$.

$$E[\{z(x) - m\}\{z(x+h) - m\}] = C(h) \quad [\text{A.6}]$$

The stationarity of the covariance presumes the existence of variance that is finite and independent of x . If h tends to zero then the covariance, $C(0)$, approaches the variance of the random variable z :

$$E[\{z(x) - m\}^2] = \text{Var}[z(x)] = C(0) \quad [\text{A.7}]$$

The semi-variance has to be stationary:

$$\gamma(x, x+h) = \gamma(h) = \frac{1}{2} E[\{z(x) - z(x+h)\}^2] \quad [\text{A.8}]$$

The semi-variance is a measure of the similarity, on average, between points a given distance, h , apart.

Under second-order stationary conditions the relation between the variance, covariance and semi-variance makes one of the parameters superfluous.

The semi-variance is rewritten as:

$$\gamma(h) = \frac{1}{2} E\left[\{z(x) - m - z(x+h) - m\}^2\right] \tag{A.9}$$

$$\gamma(h) = \frac{1}{2} \left\{ E\left[\{z(x) - m\}^2\right] + [z(x+h) - m]^2 - 2E\left[\{z(x) - m\}\{z(x+h) - m\}\right] \right\} \tag{A.10}$$

or

$$\gamma(h) = \frac{1}{2} \left\{ \text{Var}[\{z(x)\}] + \text{Var}[z(x+h)] - 2\text{Cov}[z(x), z(x+h)] \right\} \tag{A.11}$$

Table A.1: Statistical parameters as subject to the process stationarity.

Statistical parameter	First-order stationarity	Second-order stationarity	Intrinsic stationarity
Mean	m	m	m(h)
Variance	-	$E\left[\{z(x) - m\}^2\right]$	$E\left[\{z(x) - m\}^2\right]$
Covariance	-	$E\left[\{z(x) - m\}\{z(x+h) - m\}\right]$	-
Semi-variance	-	$\frac{1}{2} E\left[\{z(x) - z(x+h)\}^2\right]$	$\frac{1}{2} E\left[\{z(x) - z(x+h)\}^2\right]$

Intrinsic stationarity

When the rainfall field is assumed to be intrinsic stationary, the mean m of the rainfall field is unknown. The intrinsic hypothesis (Matheron, 1989) requires stationarity for the increments of z(x) only. While the expected value of the difference z(x)-z(x+h) may be zero, the expected value of the square of this difference is not necessarily zero. By the intrinsic hypothesis, a consistent set of assumptions can be made weaker than second-order stationarity.

A random process z(x) satisfies the intrinsic hypothesis if the first-order differences z(x_i) - z(x_j) are stationary in the mean and the variance:

$$E[z(x) - z(x+h)] = m(h) \tag{A.12}$$

$$E[\{z(x) - z(x+h)\}^2] = \text{Var}[z(x) - z(x+h)] = 2\gamma(h) \tag{A.13}$$

In the second-order stationary case, C(0) is bounded, constant, and independent of x, so γ(h) is finite and dependent on h. Second-order stationarity automatically implies intrinsic properties. Under intrinsic stationarity only the first-order differences of z(x) have finite variances.

The variance of $z(x)$ itself may well be infinite, in which case the phenomena would not be stationary to the second order.

$$\text{Var}[z(x)] \neq \text{Var}[z(x+h)] \quad [\text{A.14}]$$

When considering intrinsic stationarity, only a semi-variance can be defined:

$$\gamma(h) = \frac{1}{2} E\left[\{z(x) - z(x+h)\}^2\right] \quad [\text{A.15}]$$

Semi-variance

Matheron [1989] defines the function γ as a semi-variogram in which one-half of the spatial variance $\text{Var}[z(x)-z(x+h)]$ is presented as function of distance. An estimation of the semi-variance with the existing data can be made. From n measurements z_i , it is possible to build $n(n-1)/2$ combinations of measurements, with locations x_i and x_j . Each pair is associated with a distance vector $h = x_i - x_j$. The pairs are grouped in a number of distance classes in order to have a significant number of pairs in each class. The mean value of the semi-variance of all pairs in a distance class, h_i , is estimated by half the spatial variance $\text{var}[z(x)-z(x+h)]$ divided by the n_i possible pairs of observations in that class.

The spatial variability of a rainfall field can be viewed when the mean semi-variance of the different distance lag classes, $\gamma(h_i)$, is plotted against the mean distance of that class. The non-parametric estimator is:

$$\gamma(h) = \frac{1}{2n(h)} \sum_{i=1}^{n(h)} \{z(x_i) - z(x_i+h)\}^2 \quad [\text{A.16}]$$

where:

$\gamma(h)$ = estimated semi-variance for the distance classes h

$z(x_i)$ = measured values at x_i

$z(x_i+h)$ = measured values within a distance class h

$n(h)$ = amount of pairs in the distance class h .

The experimental semi-variance shows the expected difference in value of two points against its distance. Kitanidis [1993] gives some guidelines to obtain a reasonable semi-variance:

- use three to six intervals,
- make sure you have at least ten pairs in each interval,
- include more points at distances where the differences between calculated semi-variances are larger. Especially for large values of h there may be significant differences between semi-variances calculated from different subsets of data.

The idealised curves are defined as simple mathematical functions that relate γ to h . Generally the semi-variance is an increasing function of the distance. In a stationary medium, however, the rate of increase minimises to zero. The distance at which the maximum semi-variance, also called the 'sill', C , is reached is called the 'range', a , of the phenomenon. The range characterises the zone of spatial dependency of the data.

I.2 Stationary semi variogram models

In hydrology very often the spherical fit is used, its equation is given by:

$$\gamma(h) = C_0 + C \left\{ \frac{3}{2} \cdot \frac{h}{a} - \frac{1}{2} \left(\frac{h}{a} \right)^3 \right\} \quad \text{for } 0 < h < a \quad [\text{A.17}]$$

$$\gamma(h) = C_0 + C \quad \text{for } h > a \quad [\text{A.18}]$$

Where:

C_0 = the nugget variance

C = the range of variance.

The nugget effect is a spatial un-correlated noise term caused by random measurement errors and small-scale variability (variability over a distance smaller than the distance between neighbouring observation points).

The nugget variance consists of the variance caused by measurement errors, σ_{ME}^2 , and the variance of the micro-scale process, σ_{MS}^2 :

$$C_0 = \sigma_{ME}^2 + \sigma_{MS}^2 \quad [\text{A.19}]$$

The least square method very often is used to estimate the parameters of the semi-variance from the experimental semi-variance. The problem consists in estimating the parameters of the semi-variance when adjusting a model of the semi-variance to an experimental semi-variance.

I.3 Estimation techniques

Estimation by Distance Weighing

The values at the unmeasured points are estimated by a weighted mean based on measured values of different sample points within a certain area. The weights assigned to the measured data points depend on a distance function. Delfiner and Delhomme [1973] make the following comment with regard to distance weighting schemes:

'Clearly, no general rule can be derived from experiment on particular data and point configurations. Consequently, the choice of a distance weighting function is more or less a matter of personal belief, of tradition or of confidence in the device of influential authorities'.

Distance weighting schemes suffer from arbitrariness in the selection of interpolation parameters, also they do not cope well with clustered data. In hydrology, mostly the Inverse Distance method is used in which the estimation weights are inversely proportional to the distances. The weights in the distance function may be raised to a higher power to increase the effect of the distance weighting function. Inverse distance squared, however, is most commonly used:

$$Z^*(x_0) = \sum_{i=1}^n \lambda_i \times Z(x_i) \quad [\text{A.20}]$$

$$\lambda_i = \frac{1/d_{ij}^2}{\sum_{j=1}^n 1/d_{ij}^2} \quad \text{for } i = 1, 2, \dots, n.$$

where d_{ij} is the distance between the sample point x_i and the point to be estimated x_j .

A characteristic of this equation is that the higher the distance weighting power, the more swift the decline in weight becomes; sample points further away will have less effect on the estimation value. For a higher distance weighting power (>3), an estimate will become in more correspondence with the value of the nearest sample point. For simulating rainfall distributions, in general, it can be said that the higher the spatial variability the higher the power must be in the distance function. Convective rainfall events must be simulated by a distance function to the power 2 or 3 while depression events must be simulated by a distance function with the power 1 or 2. It also is recommended to

apply higher power distance functions when temporal distributions have to be simulated with high gauging resolutions. Annual rainfall and evaporation distributions mostly are simulated by linear distance functions. Interpolations by the inverse distance method give the best simulation results when the sampling points are spatially distributed in a homogeneous manner although the method does not cope well with clustered data. In general, clustered data have a significant negative effect on simulation results. By usage of Distance Weighing functions, no assumption is made with regard to the type of stationarity of the process that underlies the estimation.

Estimation by Kriging

By the Kriging technique a class of interpolators is denoted based on a stochastic approach. The general formulation of the theory is provided by Matheron [1969, 1970], and is named after D.R. Krige. A unique advantage of the Kriging interpolation method is its ability to quantify the reliability of prediction, to provide an estimate plus a confidence interval.

The objective of Kriging is to find the best linear unbiased estimate of a linear function of field $z(u)$. We will emphasise the estimate P_e of the true mean area precipitation P_t . The qualifiers of the estimate are defined as (after Bras and Iturbe, 1984)

Linearity: The estimator P_e is formed from a linear combination of the observed values

$$P_e = \sum_{i=1}^n \lambda_i \cdot z(u_i) \quad [A.21]$$

where λ_i , $i = 1, \dots, n$ are a set of weights to be optimised according to the criterion for "best" estimator.

Unbiasedness. This condition requires that the expected value of the estimator P_e is equal to the expected value of the true mean area precipitation P_t .

$$E[P_e] = E[P_t] \quad [A.22]$$

Best criterion: The estimator is considered 'best' if it gives the smallest estimation variance. The estimation variance, also called the mean square error is defined as

$$\sigma_p^2 = E[(P_t - P_e)^2] = \text{var}[P_t - P_e] \quad [A.23]$$

Very important for Kriging is the extent of stationarity of the process. Today many different Kriging³ algorithms are developed depending on the scope of work.

Central in these algorithms is that the variable 'z' is decomposed into three continuous parts: a structural component, a purely random effect and locally dependent errors. By Kriging techniques, the estimate, the estimation error and the error variance in the estimation process are calculated.

Estimate

If x denotes a point in space and $Z(x)$ is a function of x which is known in the n observation points x_1, x_2, \dots, x_n , then an estimate $Z^*(x_0)$ of $Z(x_0)$ at any location can be made by:

$$Z^*_{(x_0)} = \sum_{i=1}^n \lambda_i \times Z_{(x_i)} \quad [\text{A.24}]$$

This estimate is obtained by a linear combination of the observed values, multiplied by a weight λ_i for each of the observation points.

Estimation error

The difference between the estimate value $Z^*_{(x_0)}$ and the true value $Z_{(x_0)}$ for any set of weights is called the estimation error ϵ_{est} . If e.g. the weight on the closest observation is one, and all other weights are zero, then the value of the closest observation $Z_{(x_i)}$ would be used as the estimator $Z^*_{(x_0)}$ of $Z_{(x_0)}$. The estimation error becomes:

$$\epsilon_{\text{est}} = Z^*_{(x_0)} - Z_{(x_0)} = Z_{(x_i)} - Z_{(x_0)} \quad [\text{A.25}]$$

If there is no trend (i.e. the stationary hypothesis holds) then $Z^*_{(x_0)}$ is an unbiased estimate of $Z_{(x_0)}$, the expected value of the difference between the estimated and true value will be zero:

$$E[Z^*_{(x_0)} - Z_{(x_0)}] = 0 \Leftrightarrow E[Z^*_{(x_0)}] = E[Z_{(x_0)}] \quad [\text{A.26}]$$

³ Simple Kriging (Matheron, 1963) Ordinary Kriging (Matheron, 1971); Universal Kriging (Matheron, 1969); Random Kriging (Serra and Marechal, 1970); Disjunctive Kriging (Matheron, 1973); Co-Kriging (David, 1977); Factorial Kriging (Matheron, 1982); Dual Kriging (Galli et al., 1984); Positive Kriging (Barnes and Johnson, 1984); Detrending Kriging (Chua and Bras, 1980).

Error variance

The error variance, also called the estimation variance, of this difference, ϵ_{est} , is not zero: it is the mean of the squared difference. In the general case with the estimated point being a linear combination of values 1, 2, ..., n, Eq. [A.24], the error variance is as follows:

$$\sigma^2 = E[Z_{(x_0)}^* - Z_{(x_0)}]^2 \quad [\text{A.27}]$$

$$\sigma^2 = E\left[\left(\sum_{i=1}^n \lambda_i Z_{(x_i)}\right)\left(\sum_{j=1}^n \lambda_j Z_{(x_j)}\right)\right] - 2E[\lambda_i Z_{(x_i)} Z_{(x_0)}] + E[Z_{(x_0)}^2] \quad [\text{A.28}]$$

$$\sigma^2 = \sum_{i=1}^n \sum_{j=1}^n \lambda_i \lambda_j E[Z_{(x_i)} Z_{(x_j)}] - 2 \sum_{i=1}^n \lambda_i E[Z_{(x_i)} Z_{(x_0)}] + E[Z_{(x_0)}^2] \quad [\text{A.29}]$$

Each observation contributes a different proportion to the total estimation variance of $Z_{(x_0)}$. There are an infinite number of ways in which the weights are allocated, and each will produce a different estimation variance. Among these, at least one combination of weights must produce a minimum estimation variance. It is this combination that Kriging seeks to find. If the covariance function; the semi-variance or the covariance is known, the weights λ_i can be calculated. In case spatial distributed rainfall and evaporation maps are required for catchments of regional or larger scale, the ordinary Kriging is applied to perform the spatial interpolation.

Ordinary Kriging

In ordinary Kriging the variable to be estimated has a constant but unknown mean where all variation is statistical by second-order stationarity or intrinsic stationarity and where the covariance function can be defined without any underlying trend. Ordinary Kriging refers to the following model assumption:

$$Z_{(x)} = m + \alpha_{(x)} \quad [\text{A.30}]$$

where m denotes the unknown stationary mean. The expected value of the error at any particular location often is referred to as the bias.

Implementing the unbiasedness condition yields:

$$E[Z_{(x_0)}^*] = E[Z_{(x_0)}] \quad [\text{A.31}]$$

When substituting Eq. [A.2.3] we can write:

$$E\left[\sum_{i=1}^n \lambda_i * Z_{(xi)}\right] = E[Z_{(x0)}] = m \quad [A.32]$$

with the first constraint:

$$\sum_{i=1}^n \lambda_i = 1 \quad [A.33]$$

Unbiasedness is guaranteed because the coefficients sum to 1.

The second constraint is that the error variance is minimal. The weights λ_i have to be solved with the constraint that the error variance is minimal:

$$E[Z^*_{(x0)}] = E[Z_{(x0)}] = \sum_{i=1}^n \sum_{j=1}^n \lambda_i \lambda_j E[Z_{(xi)} Z_{(xj)}] - 2 \sum_{i=1}^n \lambda_i E[Z_{(xi)} Z_{(x0)}] + E[Z^2_{(x0)}] \quad [A.34]$$

This equation can be rewritten where the first term of Eq. [A.34] is the covariance between $z(x_i)$ and $z(x_j)$:

$$E[Z_{(xi)} Z_{(xj)}] = C_{(xi,xj)} \quad [A.35]$$

the second term of Eq. [A.34] is the covariance between $z(x_i)$ and $z(x_0)$

$$E[Z_{(xi)} Z_{(x0)}] = C_{(xi,x0)} \quad [A.36]$$

the third term of Eq. [A.34] is the covariance of $z(x_0)$ with itself and is equal to the variance of $z(x_0)$. Assuming that all the random variables have the same variance, the third term can be expressed as σ_v^2 or $C_{(0)}$.

Combining these three terms again the following expression holds for the error variance:

$$\sigma^2 = \sum_{i=1}^n \sum_{j=1}^n \lambda_i \lambda_j C_{(xi,xj)} - 2 \sum_{i=1}^n \lambda_i C_{(xi,x0)} + \sigma_v^2 \quad [A.37]$$

To find the set of weights that will give the minimum mean square error, Eq. [A.37] is minimised subject to constraint Eq. [A.33]. This is accomplished through the technique of Lagrangian multipliers that minimises $L_{(\lambda_i, \mu)}$:

$$L_{(\lambda_i, \mu)} = \frac{1}{2} E\left[\left(Z^*_{(x0)} - Z_{(x0)}\right)^2\right] - \mu \left(\sum_j \lambda_j - 1\right) \quad [A.38]$$

where:

μ = the Lagrangian multiplier.

The optimal parameters satisfy:

$$\sum_{j=1}^n \lambda_j C_{(x_i, x_j)} - \mu = C_{(x_0, x_i)} \quad i = 1, 2, \dots, n \tag{A.39}$$

$$\sum_{i=1}^n \lambda_j = 1$$

where:

$C_{(x_i, x_j)}$ = the covariance of Z between the sampling points,

$C_{(x_0, x_i)}$ = the covariance between the sampling points x_i and the estimated point x_0 .

In this method the weights are selected on the basis of the spatial structure of the phenomenon.

The same solutions in terms of semi-variances give:

$$\sum_{j=1}^n \lambda_j \gamma_{(x_i, x_j)} - \mu = \gamma_{(x_0, x_i)} \quad i = 1, 2, \dots, n \tag{A.40}$$

$$\sum_{i=1}^n \lambda_j = 1$$

where:

$\gamma_{(x_i, x_j)}$ = the semi-variance of Z between the sampling points,

$\gamma_{(x_0, x_i)}$ = the semi-variance between the sampling points x_i and the estimated point x_0 .

These formulas can be shown in a matrix:

$$\begin{bmatrix} \gamma_{(x_1, x_1)} & \gamma_{(x_1, x_2)} & \dots & \gamma_{(x_1, x_n)} & 1 \\ \gamma_{(x_2, x_1)} & \gamma_{(x_2, x_2)} & \dots & \gamma_{(x_2, x_3)} & 1 \\ \dots & \dots & \dots & \dots & \dots \\ \gamma_{(x_n, x_1)} & \gamma_{(x_n, x_2)} & & \gamma_{(x_n, x_n)} & 1 \\ 1 & 1 & 1 & 1 & 0 \end{bmatrix} \times \begin{bmatrix} \lambda_1 \\ \lambda_2 \\ \dots \\ \lambda_n \\ \mu \end{bmatrix} = \begin{bmatrix} \gamma_{(x_0, x_1)} \\ \gamma_{(x_0, x_2)} \\ \dots \\ \gamma_{(x_0, x_n)} \\ 1 \end{bmatrix} \tag{A.41}$$

With the solutions of the weights the error variance is found on the reliability of the interpolation:

$$\sigma_{k(x_0)}^2 = E\left[\left(Z_{(x_0)}^* - Z_{(x_0)}\right)^2\right] = \sum_{j=1}^n \lambda_j \gamma_{(x_0, x_j)} + \mu \quad [A.42]$$

or, in case the chosen model is second-order stationary:

$$\sigma_{k(x_0)}^2 = E\left[\left(Z_{(x_0)}^* - Z_{(x_0)}\right)^2\right] = C_{(0)} - \sum_{j=1}^n \lambda_j \gamma_{(x_0, x_j)} + \mu \quad [A.43]$$

The estimation error variance, σ_k^2 , can be viewed as depending exclusively on the number and the locations of the rain gauges. Therefore σ_k^2 is an efficient tool for solving network optimisation problems such as the optimal choice of measurement locations. It must be emphasised that σ_k^2 is not the variance of the actual real spatial estimation error but a simulation error that represents a theoretical measure of the relative accuracy of the various estimates. For estimating the value of the non-visited point Eq. [A.24] is applicable.

Remarks

When n is large, it is a formidable task to get the results of an interpolation. But since λ_j decreases as the distance between x_0 and x_i increases most points far from x_0 can be omitted from the calculation without serious consequences. Another reason for limiting the area is that the variogram is best known for small values of h and becomes less accurate as h increases. In this case one speaks of a moving neighbourhood. When using the Kriging interpolation method, it is very important to make an accurate semi-variogram since the accuracy of Kriged estimates depend mostly on the goodness of the computed semi-variogram, which is the most critical part of the Kriging technique.

The calculations made with Kriging are mostly done with software-packages among such as GEO-EAS, GEOSTAT and Surfer.

II Overland flow model

A DEM of the catchment is required for simulation of overland flow in a distributed manner. Figure A.1 presents the spatial discretisation of a catchment surface by a raster grid where grid elements are indexed by a

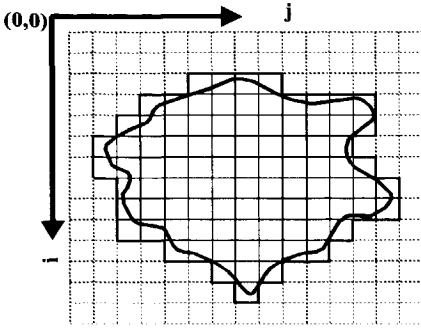


Figure A.1: Simulation of the catchment shape by a raster grid.

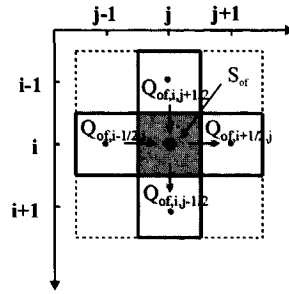


Figure A.2: 5-Point calculation scheme.

j, i grid co-ordinate system. All grid elements of the DEM are rectangular, uniform and thus of equal size. In order to simulate the catchment shape and size, a catchment boundary file overlies the DEM to differentiate 'active' elements from 'in-active' elements. Active elements make up the catchment while inactive elements are ignored in any model simulation.

For the simulation of overland flow a 2 dimensional calculation scheme is developed. The overland flow model requires the use of a DEM and a grid layer indicating the boundary grid elements at the catchment divide. At these elements a no-flow boundary condition is implement. For any active element and for all calculation time steps, the conservation equation of mass is solved that has the general form:

$$w \frac{\partial h_{of}}{\partial t} + \frac{\partial Q_{of,x}}{\partial x} + \frac{\partial Q_{of,y}}{\partial y} - S_{of} = 0 \tag{A.44}$$

where

- w = width of flow [L]
- h_{of} = thickness of water layer at land surface [L]
- $Q_{of,x}$ = overland flow discharge in x direction [L³ T⁻¹]
- $Q_{of,y}$ = overland flow discharge in y direction [L³ T⁻¹]
- t = time [T]
- S_{of} = sink/source term overland flow model [L² T⁻¹]
- x, y = horizontal Cartesian co-ordinates [L].

For solving Eq. [A.44] the 5-point calculation scheme of figure A.2 is applied. For all grid elements the water depth is simulated by considering the water flows from the orthogonal connected grid elements and the

sink/source term, S_{of} . Rewriting Eq. [A.44] in finite difference form yields:

$$w \frac{h_{of,j,i}^{t+1} - h_{of,j,i}^t}{\Delta t} = \frac{Q_{of,j-1/2,i} - Q_{of,j+1/2,i}}{x_{j+1/2,i} - x_{j-1/2,i}} + \frac{Q_{of,j,i-1/2} - Q_{of,j,i+1/2}}{y_{j,i+1/2} - y_{j,i-1/2}} - S_{of} \quad [A.45]$$

In x direction the width b becomes equal to $y_{j,i+1/2} - y_{j,i-1/2}$ (i.e. Δy) while in y direction b becomes equal to $x_{j,i+1/2} - x_{j,i-1/2}$. (i.e. Δx). Rewriting Eq. [A.45] for h_{of} at location i,j for time instant $t+1$ and with consideration of the previous statement, the following expression is developed:

$$h_{of,j,i}^{t+1} = h_{of,j,i}^t + \left(Q_{of,j-1/2,i} - Q_{of,j+1/2,i} + Q_{of,j,i-1/2} - Q_{of,j,i+1/2} \right) \frac{\Delta t}{A} + S_{of} \frac{\Delta t}{A} \quad [A.46]$$

where

$Q_{of,j-1/2,i}$	= overland flow discharge at from left grid element	$[L^3 T^{-1}]$
$Q_{of,j+1/2,i}$	= overland flow discharge from right grid element	$[L^3 T^{-1}]$
$Q_{of,j,i-1/2}$	= overland flow discharge from upper grid element	$[L^3 T^{-1}]$
$Q_{of,j,i+1/2}$	= overland flow discharge from lower grid element	$[L^3 T^{-1}]$
Δt	= time increment	$[T]$
A	= surface area grid element (i.e. $\Delta x \cdot \Delta y$)	$[L^2]$
S_{of}	= sink/source term overland flow model	$[L^3 T^{-1}]$.

This equation constitutes the governing equation by which the overland flow water depth at any grid element is simulated. For the simulation of the overland flow discharges $Q_{j-1/2,i}$, $Q_{j+1/2,i}$, $Q_{j,i-1/2}$, and $Q_{j,i+1/2}$, the Strickler-Manning hydraulic resistance equation [A.47] is used:

$$Q = k_m \cdot b \cdot \sqrt{i} \cdot R^{2/3} h \quad [A.47]$$

where

Q	= discharge	$[L^3 T^{-1}]$
b	= width of grid element	$[L]$
i	= energy gradient line	$[-]$
R	= hydraulic radius	$[L]$
h	= water depth	$[L]$
k_m	= reciproke of the Manning resistance coefficient	$[L^{1/3} T^{-1}]$.

In the overland flow model only sheet flow is considered. By approximation the hydraulic radius, R , so becomes equal to the overland flow water depth, h_{of} :

$$Q_{of,x} = k_m \cdot b \cdot \sqrt{i_{sl,x}} \cdot h_{of}^{2/3} \cdot h_{of} \tag{A.48}$$

For the overland flow model a mixed calculation scheme⁴ is developed. In this scheme the linear part of the overland flow water depth, h_{of} , in Eq. [A.48] is solved by implicit calculation while the non-linear part, $h_{of}^{2/3}$, is solved by explicit calculation. The reciproke of the Manning coefficient, k_m the slope gradient of the DEM in x-direction, $i_{sl,x}$, arc model parameters that remain constant over time. For the overland flow discharges $Q_{of,j+1/2,i}$, $Q_{of,j-1/2,i}$, $Q_{of,j,i+1/2}$ and $Q_{of,j,i-1/2}$, the set of equations [A.49] is developed.

For the reciproke of the Manning resistance coefficient, k_m , the average is taken for two connected grid elements in the direction of flow. The slope gradient in x and y direction is defined by the hydraulic gradient of connected elements. For the water depths a factor is assigned to the water depths of two neighbouring grid elements to weigh water depths for discharge calculations.

$$\begin{aligned}
 Q_{j+1/2,i} &= \frac{k_{j+1,i} + k_{j,i}}{2} \cdot b \cdot \sqrt{\frac{h_{j+1,i} + z_{j+1,i} + h_{j,i} + z_{j,i}}{x_{j+1,i} - x_{j,i}}} \cdot \left(\frac{1}{2}\right)^{5/3} \cdot \\
 &\quad \left((2-\zeta)h_{j+1,i} + \zeta h_{j,i}\right)^{2/3} \cdot \left((2-\zeta)h_{j+1,i} + \zeta h_{j,i}\right) \\
 Q_{j-1/2,i} &= \frac{k_{j-1,i} + k_{j,i}}{2} \cdot b \cdot \sqrt{\frac{h_{j-1,i} + z_{j-1,i} + h_{j,i} + z_{j,i}}{x_{j-1,i} - x_{j,i}}} \cdot \left(\frac{1}{2}\right)^{5/3} \cdot \\
 &\quad \left((2-\zeta)h_{j-1,i} + \zeta h_{j,i}\right)^{2/3} \cdot \left((2-\zeta)h_{j-1,i} + \zeta h_{j,i}\right) \\
 Q_{j,i+1/2} &= \frac{k_{j,i+1} + k_{j,i}}{2} \cdot b \cdot \sqrt{\frac{h_{j,i+1} + z_{j,i+1} + h_{j,i} + z_{j,i}}{y_{j,i+1} - y_{j,i}}} \cdot \left(\frac{1}{2}\right)^{5/3} \cdot \\
 &\quad \left((2-\zeta)h_{j,i+1} + \zeta h_{j,i}\right)^{2/3} \cdot \left((2-\zeta)h_{j,i+1} + \zeta h_{j,i}\right) \\
 Q_{j,i-1/2} &= \frac{k_{j,i-1} + k_{j,i}}{2} \cdot b \cdot \sqrt{\frac{h_{j,i-1} + z_{j,i-1} + h_{j,i} + z_{j,i}}{y_{j,i-1} - y_{j,i}}} \cdot \left(\frac{1}{2}\right)^{5/3} \cdot \\
 &\quad \left((2-\zeta)h_{j,i-1} + \zeta h_{j,i}\right)^{2/3} \cdot \left((2-\zeta)h_{j,i-1} + \zeta h_{j,i}\right)
 \end{aligned} \tag{A.49}$$

⁴ During the coding, preliminary simulation results showed that a forward in time calculation scheme was not suitable due to reasons of numerical instability.

In any simulation, the water depth of the upstream grid element gets assigned the value $(2-\zeta)$ while the water depth of the downstream grid element gets assigned the value ζ . In the descriptions of Eq.[A.49], it is assumed that the grid element with indexes i,j always is the lower of the two connected elements. Therefore, in the formulations of Eq.[A.49], the weighing factor ζ is assigned to the grid element with index i,j . In any calculation, the computer code is able to define the appropriate weighing factor by analysing the DEM slope gradients of connected grid elements. By substitution of the Stickler-Manning equations Eq.[A.49] for the flow discharges in Eq.[A.46] and by calculating the sink/source term due to rainfall, infiltration and/or exfiltration, a general expression is obtained for simulation of the water depth h at time instant $t+1$. In the numerical model the effects of rainfall, evaporation, infiltration and exfiltration on the overland flow water depth are defined preceding the overland flow simulation in the subsequently the rainfall, evaporation and groundwater flow models.

For reasons of convenience in the formulation of the numerical model and also for programme coding it is assumed that the grid element with indexes i,j is the lowest grid element. So for calculating the thickness of the water layer at the land surface, all four overland flow discharges $Q_{j,i-1/2}$, $Q_{j+1/2,i}$, $Q_{j,i-1/2}$, and $Q_{j,i+1/2}$, contribute to the new water level. The water depths $h_{i,j}$ at time instant $t+1$ are calculated by

$$h_{j,i}^{t+1} = h_{j,i}^t + (c_{j,i} \left((2-\zeta)h_{j-1,i}^{t+1} + \zeta h_{j,i}^{t+1} \right)) + (b_{j,i} \left((2-\zeta)h_{j+1,i}^{t+1} + \zeta h_{j,i}^{t+1} \right)) + (d_{j,i} \left((2-\zeta)h_{j,i+1}^{t+1} + \zeta h_{j,i}^{t+1} \right)) + (e_{j,i} \left((2-\zeta)h_{j,i-1}^{t+1} + \zeta h_{j,i}^{t+1} \right)) \quad [A.50]$$

where

$$b_{j,i} = \left(\frac{1}{2} \right)^{5/3} \cdot \frac{(k_{j+1,i} + k_{j,i})}{2} \cdot b \cdot \frac{i_{j,i}}{\sqrt{i_{j,i}}} \cdot \left((2-\zeta)h_{j+1,i}^t + \zeta h_{j,i}^t \right)^{2/3} \cdot \frac{\Delta t}{A}$$

$$c_{j,i} = \left(\frac{1}{2} \right)^{5/3} \cdot \frac{(k_{j-1,i} + k_{j,i})}{2} \cdot b \cdot \frac{i_{j,i}}{\sqrt{i_{j,i}}} \cdot \left((2-\zeta)h_{j-1,i}^t + \zeta h_{j,i}^t \right)^{2/3} \cdot \frac{\Delta t}{A}$$

$$d_{j,i} = \left(\frac{1}{2} \right)^{5/3} \cdot \frac{(k_{j,i+1} + k_{j,i})}{2} \cdot b \cdot \frac{i_{j,i}}{\sqrt{i_{j,i}}} \cdot \left((2-\zeta)h_{j,i+1}^t + \zeta h_{j,i}^t \right)^{2/3} \cdot \frac{\Delta t}{A}$$

$$e_{j,i} = \left(\frac{1}{2} \right)^{5/3} \cdot \frac{(k_{j,i-1} + k_{j,i})}{2} \cdot b \cdot \frac{i_{j,i}}{\sqrt{i_{j,i}}} \cdot \left((2-\zeta)h_{j,i-1}^t + \zeta h_{j,i}^t \right)^{2/3} \cdot \frac{\Delta t}{A} \quad [A.51]$$

When rewriting Eq.[II.7] this gives a coefficient equation:

$$\begin{aligned}
 & a_{j,i} h_{j,i}^{t+1} + (b_{j,i} ((2 - \zeta) h_{j+1,i}^{t+1})) + (c_{j,i} ((2 - \zeta) h_{j-1,i}^{t+1})) + \\
 & (d_{j,i} ((2 - \zeta) h_{j,i+1}^{t+1})) + (e_{j,i} ((2 - \zeta) h_{j,i-1}^{t+1})) + f_{j,i}^t = 0
 \end{aligned}
 \tag{A.52}$$

where

$$\begin{aligned}
 a_{j,i} &= (-1 + \zeta b_{j,i} + \zeta c_{j,i} + \zeta d_{j,i} + \zeta e_{j,i}) \\
 f_{j,i}^t &= h_{j,i}^t
 \end{aligned}$$

Eq.[A.52] presents the general flow equation in case the grid element (i,j) has the lowest elevation for the 4 orthogonal connected grid elements. As stated, the weighing factors between the connecting elements will change subject to the direction of flow.

In the programme code of Flowsim, the ADI method (Peaceman and Rachford, 1955) is selected to solve the set of equations for the overland flow model. By the ADI method, differential equations for simulation of overland flow are partly solved in an implicit manner. The ADI method is applied to single grid elements and follows the general description:

$$(I + \alpha_p H) h^{(2p+1)} = (I - \alpha_p V) h^{(2p)} + \alpha_p f
 \tag{A.53}$$

$$(I + \alpha_p V) h^{(2p+2)} = (I - \alpha_p H) h^{(2p+1)} + \alpha_p f
 \tag{A.54}$$

where

- I = unit matrix
- h = vector variable
- α_p = iteration constant
- p = the number of the iteration step
- H = horizontal part of coefficient matrix
- V = vertical part of coefficient matrix
- f = vector variable

In matrix notation Eq.[A.52] is expressed by:

$$Ah^{t+1} + f = 0
 \tag{A.55}$$

By dividing the coefficient matrix in a vertical and a horizontal part, the variable h^{t+1} is solved implicitly. By Eq.[A.55] the main diagonal of unknown coefficient matrix A has positive values where A is divided in a horizontal part, H_A , and a vertical part, V_A .

$$H_A h^{t+1} + V_A h^{t+1} + f = 0
 \tag{A.56}$$

Also coefficient $a_{j,i}$ of Eq.[A.52] is divided in a coefficient for the horizontal part, $aH_{j,i}$, and a coefficient for the vertical part, $aV_{j,i}$.

$$aH_{j,i} = -\frac{1}{2} + (\zeta b_{j,i} + \zeta c_{j,i}) \quad [A.57]$$

$$aV_{j,i} = -\frac{1}{2} + (\zeta d_{j,i} + \zeta e_{j,i}) \quad [A.58]$$

Rewriting Eq.[A.52] in matrix notation of the form of Eq.[A.56] and by substitution of Eq.[A.57] and Eq.[A.58] for H_A and V_A , respectively, the general matrix equation for calculating overland flow becomes:

$$[aH_{j,i}(2-\zeta)b_{j,i}(2-\zeta)c_{j,i}] \begin{bmatrix} h_{j,i}^{t+1} \\ h_{j+1,i}^{t+1} \\ h_{j-1,i}^{t+1} \end{bmatrix} + [aV_{j,i}(2-\zeta)d_{j,i}(2-\zeta)e_{j,i}] \begin{bmatrix} h_{j,i}^{t+1} \\ h_{j,i+1}^{t+1} \\ h_{j,i-1}^{t+1} \end{bmatrix} + f_{j,i} = 0 \quad [A.59]$$

Implementing the Peaceman Rachford procedure

Rewriting Eq.[A.59] by implementing the Peaceman-Rachford Eq's.[A.53] and [A.54] gives respectively:

$$h_{j,i}^{2p+1} - \alpha_p \left([aH_{j,i}(2-\zeta)b_{j,i}(2-\zeta)c_{j,i}] \begin{bmatrix} h_{j,i}^{2p+1} \\ h_{j+1,i}^{2p+1} \\ h_{j-1,i}^{2p+1} \end{bmatrix} \right) = \quad [A.60]$$

$$h_{j,i}^{2p} + \alpha_p \left([aV_{j,i}(2-\zeta)d_{j,i}(2-\zeta)e_{j,i}] \begin{bmatrix} h_{j,i}^{2p} \\ h_{j,i+1}^{2p} \\ h_{j,i-1}^{2p} \end{bmatrix} + f_{j,i} \right)$$

and

$$h_{j,i}^{2p+2} - \alpha_p \left([aV_{j,i}(2-\zeta)d_{j,i}(2-\zeta)e_{j,i}] \begin{bmatrix} h_{j,i}^{2p+2} \\ h_{j,i+1}^{2p+2} \\ h_{j,i-1}^{2p+2} \end{bmatrix} \right) = \quad [A.61]$$

$$h_{j,i}^{2p+1} + \alpha_p \left([aH_{j,i}(2-\zeta)b_{j,i}(2-\zeta)c_{j,i}] \begin{bmatrix} h_{j,i}^{2p+1} \\ h_{j+1,i}^{2p+1} \\ h_{j-1,i}^{2p+1} \end{bmatrix} + f_{j,i} \right)$$

To solve Equations [A.60] and [A.61] a double sweep procedure is applied. In this procedure a horizontal forward sweep, a horizontal backward sweep, a vertical forward sweep and a vertical backward sweep are defined. By the horizontal forward sweep the explicit coefficients in horizontal perspective are defined by considering the water depths of the previous time step. In the horizontal backward sweep the new water depths are calculated. By the vertical forward sweep the vertical coefficients are calculated by considering the water depth of the horizontal backward sweep while by the vertical backward sweep the water depth for time instant $t = t+1$ are calculated. The final water depth for time instant $t = t+1$ is defined through iteration. In the following the coefficients are defined for the orthogonal connected elements.

These coefficients reduce to zero when grid elements become dry or when a grid boundary element is simulated. For both flow conditions a no-flow boundary condition is introduced into the calculation scheme.

Horizontal forward sweep

By the right hand side of Eq.[A.60], the equation parameters of Eq.[A.48] and the water depth, $h_{j,i}$, $h_{j,i+1}$, $h_{j,i-1}$, at time instant $t = t$ are defined:

$$x_{j,i} = h_{j,i}^{2p} + \alpha_p \left(\left[aV_{j,i}(2-\zeta)d_{j,i}(2-\zeta)e_{j,i} \begin{bmatrix} h_{j,i}^{2p} \\ h_{j,i+1}^{2p} \\ h_{j,i-1}^{2p} \end{bmatrix} + f_{j,i} \right] \right) \tag{A.62}$$

By substitution of $x_{j,i}$ of Eq.[A.62] for the right hand side of Eq.[A.60] the following expression is obtained:

$$h_{j,i}^{2p+1} - \alpha_p \left(\left[aH_{j,i}(2-\zeta)b_{j,i}(2-\zeta)c_{j,i} \begin{bmatrix} h_{j,i}^{2p+1} \\ h_{j+1,i}^{2p+1} \\ h_{j-1,i}^{2p+1} \end{bmatrix} \right] \right) = x_{j,i} \tag{A.63}$$

Rewriting Eq.[A.63] for $x_{j,i} / -\alpha_p$ gives

$$-\frac{x_{j,i}}{\alpha_p} = \left[\left(aH_{j,i} - \frac{1}{\alpha_p} \right) (2-\zeta)b_{j,i}(2-\zeta)c_{j,i} \begin{bmatrix} h_{j,i}^{2p+1} \\ h_{j+1,i}^{2p+1} \\ h_{j-1,i}^{2p+1} \end{bmatrix} \right] \tag{A.64}$$

For solving Eq.[A.64] the water depth $h_{j,i}$, is expressed by the double sweep equation:

$$h_{j,i} = \alpha_{j,i} h_{j+1,i} + \beta_{j,i} \quad [A.65]$$

For the forward horizontal sweep, the coefficients $\alpha_{j,i}$ and $\beta_{j,i}$ are defined when Eq.[A.65] is expressed for $h_{j-1,i}$:

$$h_{j-1,i} = \alpha_{j-1,i} h_{j,i} + \beta_{j-1,i} \quad [A.66]$$

and when Eq.[A.66] is substituted in Eq.[A.64]:

$$\begin{aligned} -\frac{x_{j,i}}{\alpha_p} = & \left(aH_{j,i} - \frac{1}{\alpha_p} \right) h_{j,i}^{2p+1} + (2-\zeta)b_{j,i} h_{j+1,i}^{2p+1} + \\ & (2-\zeta)c_{j,i} (\alpha_{j-1,i} h_{j,i} + \beta_{j-1,i})^{2p+1} \end{aligned} \quad [A.67]$$

When rewriting Eq.[A.67] for $h_{j,i}^{2p+1}$ gives:

$$\begin{aligned} h_{j,i}^{2p+1} = & -\frac{(2-\zeta)b_{j,i}}{\left(aH_{j,i} - \frac{1}{\alpha_p} \right) + (2-\zeta)c_{j,i}\alpha_{j-1,i}} h_{j+1,i}^{2p+1} - \\ & \frac{(2-\zeta)c_{j,i}\beta_{j-1,i} + \frac{x_{j,i}}{\alpha_p}}{\left(aH_{j,i} - \frac{1}{\alpha_p} \right) + (2-\zeta)c_{j,i}\alpha_{j-1,i}} \end{aligned} \quad [A.68]$$

where

$$\alpha_{j,i} = -\frac{(2-\zeta)b_{j,i}}{\left(aH_{j,i} - \frac{1}{\alpha_p} \right) + (2-\zeta)c_{j,i}\alpha_{j-1,i}} \quad [A.69]$$

$$\beta_{j,i} = -\frac{(2-\zeta)c_{j,i}\beta_{j-1,i} + \frac{x_{j,i}}{\alpha_p}}{\left(aH_{j,i} - \frac{1}{\alpha_p} \right) + (2-\zeta)c_{j,i}\alpha_{j-1,i}} \quad [A.70]$$

For $j = 2$.to. $n-1$ all values for $\alpha_{j,i}$ and $\beta_{j,i}$ are defined by Eq.[A.69] and Eq. [A.70] respectively. At the watershed boundary with $j = 1$ or $j = n$, the coefficients $\alpha_{j,i}$ and $\beta_{j,i}$ are defined by the boundary condition.

Horizontal backward sweep

By Eq.[A.68] the overland flow depth, $h_{j,i}^{2p+1}$ is calculated by the horizontal backward sweep. $h_{j,i}^{2p+1}$ Now is calculated by the subsequent substitution of the water depth $h_{j+1,i}^{2p+1}$ at grid element with index $j+1,i$. By implementing the no-flow boundary condition at element $j = n$, the overland flow water depths are defined. Based on Eq.[A.68] all overland flow water depth for $j = n$ to 1 are calculated by:

$$h_{j,i}^{2p+1} = \alpha_{j,i} h_{j+1,i}^{2p+1} + \beta_{j,i} \tag{A.71}$$

Vertical forward sweep

By considering the water levels of Eq.[A.71], the right hand side of Eq.[A.61] is calculated:

$$y_{j,i} = h_{j,i}^{2p+1} + \alpha_p \left(\begin{bmatrix} aH_{j,i}(2-\zeta)b_{j,i}(2-\zeta)c_{j,i} & \begin{bmatrix} h_{j,i}^{2p+1} \\ h_{j+1,i}^{2p+1} \\ h_{j-1,i}^{2p+1} \end{bmatrix} \end{bmatrix} + f_{j,i} \right) \tag{A.72}$$

when rewriting Eq.[A.72] for $y_{j,i} / -\alpha_p$ this yields

$$-\frac{y_{j,i}}{\alpha_p} = \left[\begin{bmatrix} aV_{j,i} - \frac{1}{\alpha_p} (2-\zeta)d_{j,i}(2-\zeta)e_{j,i} & \begin{bmatrix} h_{j,i}^{2p+2} \\ h_{j+1,i}^{2p+2} \\ h_{j,i-1}^{2p+1} \end{bmatrix} \end{bmatrix} \right) \tag{A.73}$$

For solving Eq.[A.73] by a double sweep is the water depth $h_{j,i}^{2p+2}$ expressed by:

$$h_{j,i}^{2p+2} = \alpha_{j,i} h_{j+1,i}^{2p+2} + \beta_{j,i} \tag{A.74}$$

Analogous to the procedure of calculating the coefficients $\alpha_{j,i}$ and $\beta_{j,i}$ by the horizontal forward sweep, the coefficients $\alpha_{j,i}$ and $\beta_{j,i}$ of Eq.[A.74] is calculated by Eq's.[A.75] and [A.76]:

$$\alpha_{j,i} = - \frac{(2-\zeta)d_{j,i}}{\left(aV_{j,i} - \frac{1}{\alpha_p} \right) + (2-\zeta)e_{j,i}\alpha_{j,i-1}} \tag{A.75}$$

$$\beta_{j,i} = - \frac{(2 - \zeta)e_{j,i}\beta_{j,i-1} + \frac{y_{j,i}}{\alpha_p}}{\left(aV_{j,i} - \frac{1}{\alpha_p} \right) + (2 - \zeta)e_{j,i}\alpha_{j,i-1}} \quad [A.76]$$

For $i = 2$ to $m-1$ all values for $\alpha_{j,i}$ and $\beta_{j,i}$ can be defined by Eq. [A.75] and Eq. [A.76] respectively. At the watershed boundary $\alpha_{j,i}$ and $\beta_{j,i}$ must be defined by the boundary condition. For $i = 2$ to $m-1$ all values for $\alpha_{j,i}$ and $\beta_{j,i}$ are defined when $\alpha_{j,i}$ and $\beta_{j,i}$ for $i = 1$ and $i = m$ are defined. This by implementing a no-flow boundary condition. The overland flow depths as defined by the horizontal backward sweep are substituted in Eq. [A.72].

Vertical backward sweep

By the calculated $\alpha_{j,i}$ and $\beta_{j,i}$ the corresponding values of $h_{j,i}^{2P+2}$ are calculated by the backward sweep of Eq. [A.74]:

$$h_{j,i}^{2P+2} = \alpha_{j,i} h_{j,i+1}^{2P+2} + \beta_{j,i}$$

Calculation of the coefficients $\alpha_{j,i}$ and $\beta_{j,i}$ for boundary elements

By analysis of the DEM, all grid elements are labelled by use of a GIS to indicate whether grid elements are active or inactive during model simulations. Grid elements outside the catchment boundary are in-active and labelled '0' while all other grid elements are active and labelled by a value ranging from 1 to 17. The labelling of a grid element is according to the scheme of figure A.3. The code represents a type of flow element and is required by the numerical code. Boundary elements are active grid elements that are neighboured by any element with code '0'. For the boundary elements the coefficients $\alpha_{j,i}$ and $\beta_{j,i}$ reduce subject to the connected elements with a no-flow boundary flow condition. In the numerical scheme, a no-flow boundary condition is also simulated in case the overland flow water depth reduces to zero. For such elements the flow of water out of an element is not possible and thus, mathematically, should be treated as a boundary element.

For grid elements in j direction three types of no-flow conditions are defined. For each flow condition the values of $\alpha_{j,i}$ and $\beta_{j,i}$ are defined for the double sweep equation Eq. [A.65]:

$$h_{j,i} = \alpha_{j,i} h_{j+1,i} + \beta_{j,i}$$

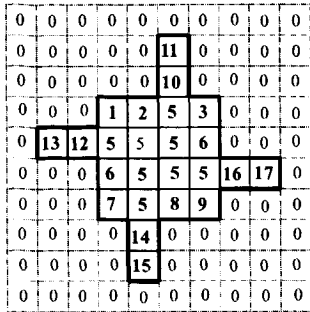
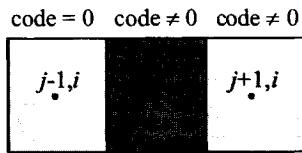


Figure A.3: Labelling of grid elements.

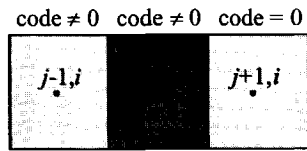
No-flow type I: $c_{j,i} = 0$



$$\alpha_{j,i} = - \frac{(2-\zeta)b_{j,i}}{\left(aH_{j,i} - \frac{1}{\alpha_p} \right)} \quad [A.77]$$

$$\beta_{j,i} = - \frac{\frac{x_{j,i}}{\alpha_p}}{\left(aH_{j,i} - \frac{1}{\alpha_p} \right)} \quad [A.78]$$

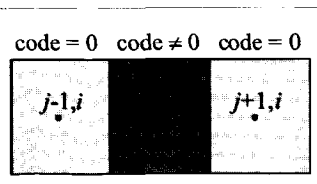
No-flow type II: $b_{j,i} = 0$



$$\alpha_{j,i} = 0 \quad [A.79]$$

$$\beta_{j,i} = - \frac{(2-\zeta)c_{j,i}\beta_{j-1,i} + \frac{x_{j,i}}{\alpha_p}}{\left(aH_{j,i} - \frac{1}{\alpha_p} \right) + (2-\zeta)c_{j,i}\alpha_{j-1,i}} \quad [A.80]$$

No-flow type III: $b_{j,i} = 0, c_{j,i} = 0$



$$\alpha_{j,i} = 0 \quad [A.81]$$

$$\beta_{j,i} = - \frac{\frac{x_{j,i}}{\alpha_p}}{\left(aH_{j,i} - \frac{1}{\alpha_p} \right)} \quad [A.82]$$

For grid elements in i direction also three types of no-flow conditions are defined. For each type the values of $\alpha_{j,i}$ and $\beta_{j,i}$ are defined for the double sweep equation Eq. [A.65]:

$$h_{j,i} = \alpha_{j,i} h_{j,i+1} + \beta_{j,i}$$

No-flow type IV: $e_{j,i} = 0$

code $\neq 0$	$j, i-1$
code $\neq 0$	
code = 0	$j, i+1$

$$\alpha_{j,i} = - \frac{(2-\zeta)d_{j,i}}{\left(aV_{j,i} - \frac{1}{\alpha_p} \right)} \quad [A.83]$$

$$\beta_{j,i} = - \frac{\frac{y_{j,i}}{\alpha_p}}{\left(aV_{j,i} - \frac{1}{\alpha_p} \right)} \quad [A.84]$$

No-flow type V: $d_{j,i} = 0$

code = 0	$j, i-1$
code $\neq 0$	
code $\neq 0$	$j, i+1$

$$\alpha_{j,i} = 0 \quad [A.85]$$

$$\beta_{j,i} = - \frac{(2-\zeta)e_{j,i}\beta_{j,i-1} + \frac{y_{j,i}}{\alpha_p}}{\left(aV_{j,i} - \frac{1}{\alpha_p} \right) + (2-\zeta)e_{j,i}\alpha_{j,i-1}} \quad [A.86]$$

No-flow type VI: $d_{j,i} = 0, e_{j,i} = 0$

code = 0	$j, i-1$
code $\neq 0$	
code = 0	$j, i+1$

$$\alpha_{j,i} = 0 \quad [A.87]$$

$$\beta_{j,i} = - \frac{\frac{y_{j,i}}{\alpha_p}}{\left(aV_{j,i} - \frac{1}{\alpha_p} \right)} \quad [A.88]$$

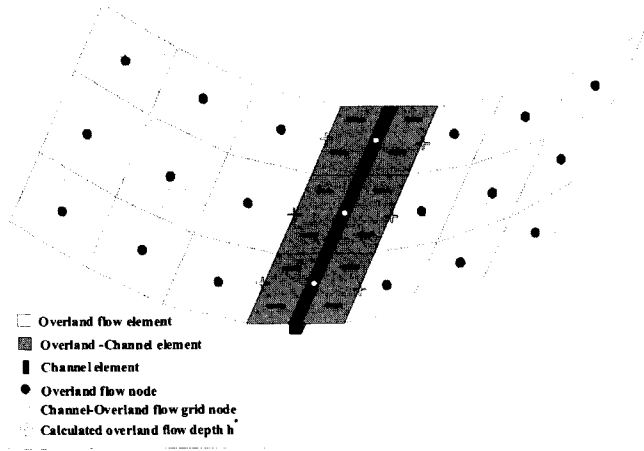


Figure A.4: Simulating overland flow runoff into the channel.

Mass exchange Overland flow - Channel flow models

During model simulations, overland flow runoff into the channel model is simulated when a channel element is present in an element of the overland flow model (see figure A.4). In the overland flow model mass exchange is simulated through a sink term while in the channel flow model a source term is simulated. For each overland flow-channel flow element such sink/source term is simulated. The effect of the sink term of the overland flow model is calculated within the implicit calculation scheme. The magnitude of the sink term is defined by a 1-dimensional Strickler-Manning flow Eq.[A.94] and is simulated at the scale of an overland flow element.

Water transport towards the river is simulated by:

$$Q_{j+1/2,i}^s = k_{j,i} \cdot b \cdot \sqrt{\frac{z_{j+1/2,i} + h_{j+1,i}^* - z_{j,i} - h_{j,i}^*}{x_{j+1,i} - x_{j,i}}} \cdot \left(\frac{h_{j+1,i}^t + h_{j,i}^t}{2} \right)^{2/3} \cdot (h_{j,i}^*) \quad [A.89]$$

$$Q_{j-1/2,i}^s = k_{j,i} \cdot b \cdot \sqrt{\frac{z_{j,i} + h_{j,i}^* - z_{j-1/2,i} - h_{j-1,i}^*}{x_{j,i} - x_{j-1,i}}} \cdot \left(\frac{h_{j-1,i}^t + h_{j,i}^t}{2} \right)^{2/3} \cdot (h_{j,i}^*)$$

where

$$Q_{j+1/2,i}^s = \text{Overland inflow from cell fraction } (j+1/2,i) \quad [L^3 T^{-1}]$$

$$Q_{j-1/2,i}^s = \text{Overland inflow from cell fraction } (j-1/2,i) \quad [L^3 T^{-1}]$$

Equations are solved for the intermediate iteration steps t^* and require the use of the updated overland flow water depth of the preceding horizontal or vertical backward iteration step h^* . The magnitude of the sink term $S_{j,i}^*$ of the overland flow model is defined by:

$$S_{j,i}^* = (Q_{j+1/2,i}^s + Q_{j-1/2,i}^s) \frac{\Delta t}{A} \quad [A.90]$$

where

$S_{j,i}^*$ = Overland flow sink term at grid element (j,i) [L]

Δt = time increment [T]

A = surface area grid element (i.e. $\Delta x \cdot \Delta y$) [L²]

During model simulation, for the first horizontal forward iteration step, $h_{j,i}^t$ is used in Eq.[A.62]. In the succeeding backward step a new overland flow depth $h_{j,i}^*$ is calculated through:

$$h_{j,i}^* = \frac{h_{j,i}^t}{1 + \frac{S_{j,i}^*}{h_{j,i}^t}} \quad [A.91]$$

and is used in the succeeding vertical forward step of Eq.[A.72]. In the following vertical backward step a new water depth $h_{j,i}^{t+1}$ is calculated by use of the updated $h_{j,i}^*$ and the sink term $S_{j,i}^*$:

$$h_{j,i}^{t+1} = \frac{h_{j,i}^*}{1 + \frac{S_{j,i}^*}{h_{j,i}^*}} \quad [A.92]$$

The effect of the source term of the channel flow model on the channel flow water depth is defined in an explicit manner in a sense that prior to channel flow routing the water depths are increased by the source term. In case of a flood condition (i.e. the hydraulic heads of overland flow and channel flow models are higher than the DEM-elevation) the simulated sink/ source term are reduced in such a manner that hydraulic heads of the overland flow model and channel flow model become equally high. As such the hydraulic head of the channel flow model cannot become higher than the hydraulic head of the overland flow model and flooding of the overland-channel flow element is simulated

III Unsaturated subsurface flow model

For simulation of unsaturated flow, the spatial discretisation of the DEM is adapted. Spatial discretisation in vertical direction is achieved by usage of multiple model layers. To each grid cell of a subsurface model layer a variable depth is assigned that, when multiplied, by the size of the element gives a cell volume. By the applied discretisation, the subsurface is described in a full three-dimensional perspective. Water storage per cell is simulated by the model algorithm of the unsaturated subsurface flow model. Water flow in the unsaturated subsurface is simulated by a 1-dimensional model approach.

The applied conservation equation of mass reads:

$$\frac{\partial \theta}{\partial t} + \frac{\partial q_{sf,z}}{\partial z} + S_{sf} = 0 \tag{A.93}$$

where

- θ = soil water content [-]
- t = time instant [T]
- $q_{sf,z}$ = specific discharge unsaturated flow in z direction [L T⁻¹]
- z = elevation head [L]
- S_{sf} = sink/source term subsurface flow model [T⁻¹].

While the momentum equation reads:

$$q_{sf,z} = -k(\theta) \left(\frac{\partial h(\theta)}{\partial z} + 1 \right) \tag{A.94}$$

where

- $q_{sf,z}$ = specific discharge subsurface flow in z direction [L T⁻¹]
- $h(\theta)$ = pressure head subject to θ [L]
- $k(\theta)$ = hydraulic conductivity subject to θ [L T⁻¹]
- z = elevation head [L].

Both the pressure head and the hydraulic conductivity are functions of the soil water content. In the model approach, the reference level is chosen at the bottom of the model domain while the momentum Eq.[A.94] is solved in upward direction.

The flow equation of the unsaturated flow model is obtained through substitution of the momentum equation [A.94] in the continuity of mass Eq.[A.93].

$$\frac{\partial \theta}{\partial t} + \frac{\partial \left(-k(\theta) \left(\frac{\partial h(\theta)}{\partial z} + 1 \right) \right)}{\partial z} + S_{sf} = 0 \quad [A.95]$$

In describing the flow of water, the use of the pressure head has the advantage that the pressure head remains continuous at the boundaries between the layers. The use of Eq. [A.95] has the advantage that for the entire flow region both the saturated flow and partially saturated flow is described. (Feddes et al., 1988).

By substitution of the momentum Eq. [A.94] for $q_{sf,z}$ in the continuity Eq. [A.93] and when rewriting $\partial \theta / \partial t$ for $\partial h(\theta) / \partial t$, Richards flow equation (Richards, 1931) is obtained for describing water flow in unsaturated flow conditions:

$$\frac{\partial h(\theta)}{\partial t} = \frac{1}{C(h(\theta))} \frac{\partial}{\partial z} \left[k(h(\theta)) \left(\frac{\partial h(\theta)}{\partial z} + 1 \right) \right] + \frac{S_{sf}}{C(h(\theta))} \quad [A.96]$$

where

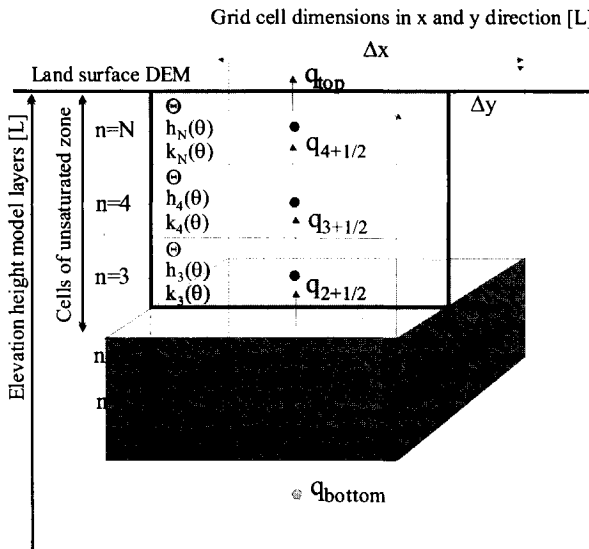
$C(h(\theta))$ = soil water capacity (i.e. $\partial \theta / \partial h$) [L⁻¹]

S_{sf} = sink/source term unsaturated subsurface [T⁻¹].

In Eq. [A.96] the pressure head $h(\theta)$ is the dependent state variable. In rainfall-runoff modelling the soil water content is the dependent state variable since the generation of the saturation overland flow is closely related to the soil water storage condition. Changes in water storage in the unsaturated subsurface are due to infiltration, percolation, capillary rise and saturated flow. When groundwater table depths change over time in a simulation, the volume of soil water in the unsaturated zone changes and a redistribution of soil water storage is simulated. This redistribution is calculated by the unsaturated flow Eq. [A.95].

In the mathematical model, the continuity equation [A.93] is discretised in the vertical flow direction. An index n is added to the horizontal indexes i, j in order to geo-reference the cell in the column of subsurface cells. The index n , ranges from 1 to N and represents the centre of a grid cell at which the nodal points are placed (see Figure A.5).

When the sink/source term, S_{sf} , is set to zero then Eq. [A.93] in discretised form reads:



Reference level $z=0$

Figure A.5: Schematised representation of the unsaturated flow model.

$$\frac{\theta_n^{t+1} - \theta_n^t}{\Delta t} + \left(\frac{q_{n+1/2}^t - q_{n-1/2}^t}{z_{n+1/2} - z_{n-1/2}} \right) = 0 \quad [A.97]$$

where

- θ_n^{t+1} = soil water content at nodal point n at time instant $t+1$ [-]
- θ_n^t = soil water content at nodal point n at time instant t [-]
- $q_{n+1/2}^t$ = specific discharge at point $n+1/2$ and time instant t [L T⁻¹]
- $q_{n-1/2}^t$ = specific discharge at point $n-1/2$ and time instant t [L T⁻¹]
- $z_{n+1/2}$ = layer elevation at point $n+1/2$ [L]
- $z_{n-1/2}$ = layer elevation at point $n-1/2$ [L]
- Δt = time increment [T].

For the soil water content at time instant $t+1$ this gives

$$\theta_n^{t+1} = \theta_n^t + (q_{n-1/2}^t - q_{n+1/2}^t) \frac{\Delta t}{z_{n+1/2} - z_{n-1/2}} \quad [A.98]$$

The momentum Eq.[A.94] in discretised form for $q_{n+1/2}$ is expressed by:

$$q_{n+1/2} = -\frac{k_{n+1}(\theta) + k_n(\theta)}{2} \left(\frac{h_{n+1}(\theta) - h_n(\theta)}{z_{n+1} - z_n} + 1 \right) \quad [A.99]$$

while for $q_{n-1/2}$ this equation changes to:

$$q_{n-1/2} = -\frac{k_n(\theta) + k_{n-1}(\theta)}{2} \left(\frac{h_n(\theta) - h_{n-1}(\theta)}{z_n - z_{n-1}} + 1 \right) \quad [A.100]$$

where

z_n = layer elevation at nodal point n [L]

z_{n+1} = layer elevation at nodal point n+1 [L]

z_{n-1} = layer elevation at nodal point n-1 [L].

By substitution of Eq.'s [A.99] and [A.100] for $q_{n+1/2}$ and $q_{n-1/2}$ of Eq.[A.98], the following expression is obtained:

$$\theta_n^{t+1} = \theta_n^t + \left(\left(-\frac{k_n(\theta) + k_{n-1}(\theta)}{2} \left(\frac{h_n(\theta) - h_{n-1}(\theta)}{z_n - z_{n-1}} + 1 \right) \right) - \left(-\frac{k_{n+1}(\theta) + k_n(\theta)}{2} \left(\frac{h_{n+1}(\theta) - h_n(\theta)}{z_{n+1} + z_n} + 1 \right) \right) \right) \frac{\Delta t}{z_{n+1/2} - z_{n-1/2}} \quad [A.101]$$

The soil water content θ_n^{t+1} becomes the dependent state variable, where the index t+1 indicates the time instant. In figure A.6 a schematic of the model approach is presented.

Equation [A.101] makes up the flow equation of the subsurface flow algorithm. This equation is solved by an explicit calculation scheme. By Eq.[A.101] the processes of infiltration, percolation and capillary rise are simulated. By q_{top} and q_{bottom} the water inflow and outflow of the unsaturated zone is calculated that act as boundary flow conditions for the sub-model.

Boundary conditions and model interactions.

By the inflow discharge q_{top} the process of infiltration at the overland flow model is simulated while, if activated, by q_{bottom} a head dependent flow boundary is simulated. Mostly, however, q_{bottom} is set to zero and thus a no-flow boundary is implemented. The rise and drop of the groundwater table and possible exfiltration as caused by saturated groundwater flow are simulated through updating the total soil water storage in the column of grid cell. Changes in water table depths are simulated subject to the change in the water volume stored in the

subsurface column. If all cells of a subsurface column become saturated, groundwater starts to exfiltrate since the hydraulic head of the water exceeds the DEM-elevation height.

For simulation of q_{top} , the potential infiltration rate q_{inf} is defined first. In the model approach it is assumed that the pressure head becomes zero in case a thin water layer is present at the land surface due to rainfall or a saturated exfiltration front. By such assumption the momentum Eq.[A.99] then reduces to:

$$q_{inf} = -k_s \left(\frac{-h_N}{z_{ls} - z_N} + 1 \right) \tag{A.102}$$

where

- k_s = hydraulic conductivity in saturated conditions [L T⁻¹]
- h_N = the pressure head of the subsurface top layer [L]
- z_{ls} = elevation of the land surface [L]
- z_N = layer elevation of nodal point N [L].

If by rainfall a water layer develops at the land surface, this water layer will partly or completely infiltrate as subject to the infiltration capacity. If the potential infiltration capacity $q_{inf} \times \Delta t$ is larger than or equal to the thickness of the water layer h_{of} , then q_{top} is set to become equal to the actual infiltration rate and is defined by:

$$q_{top} = \frac{h_{of}}{\Delta t} \tag{A.103}$$

The actual infiltration depth over Δt is equal to h_{of} . It is obvious that q_{top} reduces to zero in case the depth of the water layer becomes zero. In case the thickness of the water layer h_{of} is larger than the actual infiltration $q_{inf} \times \Delta t$, then the infiltration is equal to the potential infiltration (i.e. $q_{inf} = q_{top}$) and a new water layer at the land surface is defined by:

$$h_{of}^{new} = h_{of}^{old} - (q_{top} \times \Delta t) \tag{A.104}$$

For all elements of the top layer (i.e. $n=N$) the soil water content is defined by:

$$\theta_N^{t+1} = \theta_N^t + (q_{N-1/2} + q_{top}) \frac{\Delta t}{\Delta z} \tag{A.105}$$

For simulation of q_{bottom} the following equation is applied:

$$q_{\text{bottom}} = -\left(\frac{k_n(\theta) + k_s}{2}\right) \left(\frac{h_n(\theta) - h_{\text{wt}}}{z_n - z_{\text{wt}}} + 1\right) \quad [\text{A.106}]$$

where

k_s = hydraulic conductivity in saturated conditions [L T⁻¹]

$k_n(\theta)$ = hydraulic conductivity in highest unsaturated cell [L T⁻¹]

$h_n(\theta)$ = pressure head in highest unsaturated cell of soil column [L]

h_{wt} = pressure head at groundwater water table [L]

z_{wt} = elevation height of the groundwater table [L]

z_n = elevation height of highest unsaturated cell [L].

Since the pressure head at the groundwater table is equal to zero,

Eq.[A.106] changes to

$$q_{\text{bottom}} = -\left(\frac{k_n(\theta) + k_s}{2}\right) \left(\frac{h_n(\theta)}{z_n - z_{\text{wt}}} + 1\right) \quad [\text{A.107}]$$

For all elements of the bottom layer ($n=1$) the soil water content is updated by:

$$\theta_n^{t+1} = \theta_n^t + (q_{\text{bottom}} - q_{n+1/2}) \frac{\Delta t}{\Delta z} \quad [\text{A.108}]$$

Soil water content, pressure head and hydraulic conductivity

The use of the hydraulic conductivity and pressure head as function of water content, requires information on the soil characteristic curves $k(\theta) - \theta$ and $h_m(\theta) - \theta$. For simulation of these curves the Van Genuchten relations [1980] are implemented that define the hydraulic conductivity and the pressure head as a function of the effective soil water content. Effective means that only a part of the water contents contributes to the flow processes. The effective water content, θ_e , is expressed by

$$\theta_e = \frac{\theta - \theta_r}{\eta - \theta_r} \quad [\text{A.109}]$$

where

θ = soil water content [-]

θ_r = residual soil water content [-]

η = porosity [-].

The relation between the effective soil water content and the hydraulic head, $h(\theta)$, is expressed by (Van Genuchten, 1980):

$$\theta_e = \left[\frac{1}{1 + (h(\theta)\alpha)^n} \right]^m \tag{A.110}$$

When rewriting Eq.[A.110] for $h(\theta)$ and after substitution of Eq.[A.109] for θ_e this gives:

$$h_m = \frac{1}{\alpha} \left[-1 + \left(\frac{\theta - \theta_r}{\eta - \theta_r} \right)^{\frac{1}{m}} \right]^n \tag{A.111}$$

where

- α = constant [L⁻¹]
- m = constant [-]
- n = constant [-].

The constant α is comparable to the so-called bubbling pressure head ψ_b . at which air starts to escape form the soil matrix by wetting of the soil. The values of ψ_b may be obtained through for example the use of pedo-transfer functions. The values of ψ_b generally range from 0 to -50 cm and are subject to the soil type.

The relation between the saturated and unsaturated hydraulic conductivity has the form (Van Genuchten, 1980):

$$\frac{k(\theta)}{k_s} = \left(\frac{\theta - \theta_r}{\eta - \theta_r} \right)^{\frac{1}{2}} \left[1 - \left(1 - \left(\frac{\theta - \theta_r}{\eta - \theta_r} \right)^{\frac{1}{m}} \right)^m \right]^2 \tag{A.112}$$

where

- θ = soil water content [-]
- θ_r = residual soil water content [-]
- $k(\theta)$ = hydraulic conductivity as function of θ [L T⁻¹]
- k_s = hydraulic conductivity in saturated conditions [L T⁻¹]
- $h_m(\theta)$ = pressure head as function of the soil water content [L].

The constants m and n are defined as follows:

$$n = \lambda + 1 \quad \text{and} \quad m = \frac{\lambda}{\lambda + 1} \tag{A.113}$$

The value of λ can either be defined through laboratory experiments or model calibration or can be defined based on the use of pedo-transfer functions such as developed by e.g. Rawls and Brakensiek [1985]:

$$\lambda = \exp \left(\begin{array}{l} -0.7842831+0.0177544.S-1.062498.\eta-0.00005304.S^2- \\ 0.00273493.C^2+1.11134946.\eta^2-0.03088295.S.\eta+ \\ 0.00026587.S^2.\eta^2-0.00610522.C^2.\eta^2-0.00000235.S^2.C+ \\ 0.00798746.C^2-0.00674491.\eta^2.C \end{array} \right) \quad [A.114]$$

where

S = percentage sand

C = percentage clay

η = porosity of the soil

By the flow equation [A.101] the soil water content is updated per calculation time step and per grid element of the unsaturated zone model. In case this content exceeds the available storage volume, an element is saturated. In the computer code an element is saturated in case the calculated soil water content θ_n becomes larger than the phreatic storage coefficient. Since only phreatic flow conditions are considered, the storage coefficient is equal to the porosity η_n . For any grid cell, the water volume that exceeds the storage volume is added to the unsaturated grid cell that overlays the saturated cell. Water will remain at the land surface in case the infiltration depth exceeds the storage depth of the unsaturated top cell.

IV Saturated subsurface flow model

For simulation of saturated subsurface flow, a model approach similar to the overland flow model is applied. Water flow is simulated in two-dimensional perspective by use of a conservation equations of mass and momentum. Saturated flow is simulated in a single grid layer where the applied discretisation of the DEM is adapted. In vertical perspective the saturated thickness is lumped into one aggregated cell. In the model approach only saturated flow in phreatic flow conditions is simulated and, as such, in terms of runoff contributions, only rapid groundwater flow in shallow systems is simulated.

The conservation equation of mass reads:

$$S \frac{\partial h_{h,wt}}{\partial t} + \frac{\partial q_{sf,x}}{\partial x} + \frac{\partial q_{sf,y}}{\partial y} = S_{sf} \quad [A.115]$$

where:

S	= storage coefficient	[-]
$h_{h,wt}$	= hydraulic head of groundwater table	[L]
t	= time instant	[T]
$q_{sf,x}$	= specific discharge saturated flow in x direction	[L ² T ⁻¹]
$q_{sf,y}$	= specific discharge saturated flow in y direction	[L ² T ⁻¹]
S_{sf}	= sink/source term saturated flow	[L T ⁻¹]
x,y	= Cartesian space co-ordinates	[L].

while the Darcy flow equation of motion is used for quantifying the specific discharges:

$$q_{sf} = -k_s h_{sat} \frac{dh_h}{dl} \quad [A.116]$$

where

q_{sf}	= specific discharge saturated flow	[L ² T ⁻¹]
k_s	= saturated hydraulic conductivity	[L T ⁻¹]
h_{sat}	= thickness of saturated zone	[L]
h_h	= hydraulic head	[L]
l	= distance in direction of flow	[L].

Hydraulic head

For any simulation time step and preceding the simulation of saturated subsurface flow, the hydraulic head as driving force for saturated flow is calculated. Such force is defined by use of a saturated subsurface layer thickness that is simulated in the column of cells in the combined unsaturated-saturated subsurface model approach. The saturated thickness is defined by summing the thicknesses of saturated cells and an equivalent unsaturated zone water thickness in which the effect of the saturation degree on saturated flow is considered. By extensive model test, such approach proved to be effective in order to accommodate for the effects partially saturated cells must have on saturated groundwater flow. For any unsaturated cell a threshold value for the soil moisture content is defined above which the soil moisture content contributes to

the calculation of the 'effective' saturated zone thickness. The threshold moisture content is defined according to;

$$\lim\theta = \theta_r + \text{coeff}(\eta - \theta_r) \quad [\text{A.117}]$$

where

$\lim\theta$ = threshold value for moisture content

θ_r = residual moisture content

coeff = threshold coefficient $0 < \text{coeff} < 1$

η = porosity.

In case the actual moisture content exceeds the threshold value $\lim\theta$, the saturated zone thickness and thus the 'effective' water table height increases according to

$$\Delta\text{wtb} = (\theta - \theta_r)\Delta z_n \quad [\text{A.118}]$$

The water table height is defined by adding this height to the water table of the fully saturated cells. The hydraulic head as driving force in the saturated flow model now is set by adding the total water table height to the elevation height of the model bottom. This bottom height on its turn is simulated by subtracting the total soil layer depth from the DEM element heights.

Saturated subsurface flow is simulated by an explicit numerical calculation scheme based on Eq.[A.117].

Numerical approach

The flow equation is obtained by substitution of the expression of $q_{gf,x}$ and $q_{gf,y}$ in [A.115]. For quantification of the saturated flow discharges of $q_{gf,x}$ and $q_{gf,y}$, the expression of Eq.[A.116] is followed. The flow equation [A.115] is solved in two directions and, after discretisation, the inflow and outflow discharges to each grid cell are calculated. This conservation of mass equation in discretised form reads:

$$S \frac{h_{h(j,i)}^{t+1} - h_{h(j,i)}^t}{\Delta t} + \left(\frac{q_{gf(j+1/2,i)}^t - q_{gf(j-1/2,i)}^t}{x_{(j+1/2,i)} - x_{(j-1/2,i)}} \right) + \left(\frac{q_{gf(j,i+1/2)}^t - q_{gf(j,i-1/2)}^t}{y_{(j,i+1/2)} - y_{(j,i-1/2)}} \right) = S_{gf} \quad [\text{A.119}]$$

that, after rewriting for the dependant variable $h_{h(j,i)}^{t+1}$, yields:

$$h_{h(j,i)}^{t+1} = h_{h(j,i)}^t + \left(\frac{q_{gf(j-1/2,i)}^t - q_{gf(j+1/2,i)}^t}{x_{(j+1/2,i)} - x_{(j-1/2,i)}} \right) + \left(\frac{q_{gf(j,i-1/2)}^t - q_{gf(j,i+1/2)}^t}{y_{(j,i+1/2)} - y_{(j,i-1/2)}} \right) + S_{gf} \frac{\Delta t}{S} \quad [\text{A.120}]$$

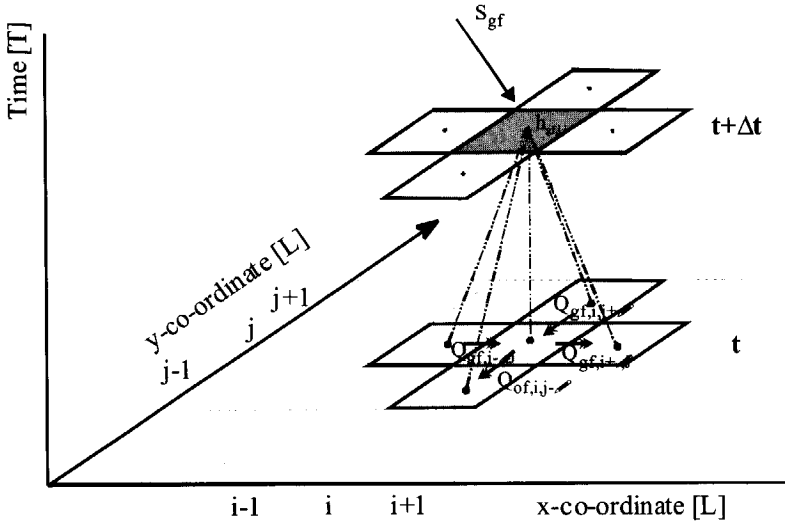


Figure A.6: Schematic representation of the finite difference scheme of the saturated flow algorithm.

where

- $h_{h(j,i)}^{t+1}$ = hydraulic head at cell j,i and at time instant $t+1$ [L]
- $h_{h(j,i)}^t$ = hydraulic head at cell j,i and at time instant t [L]
- $q_{gf(j-1/2,i)}^t$ = specific discharge saturated flow at $j-1/2,i$ [$L^2 T^{-1}$]
- $q_{gf(j+1/2,i)}^t$ = specific discharge saturated flow at $j+1/2,i$ [$L^2 T^{-1}$]
- $q_{gf(j,i+1/2)}^t$ = specific discharge saturated flow at $j,i+1/2$ [$L^2 T^{-1}$]
- $q_{gf(j,i-1/2)}^t$ = specific discharge saturated flow at $j,i-1/2$ [$L^2 T^{-1}$]
- S_{gf} = sink/source term saturated flow [$L T^{-1}$]
- S = storage coefficient [-].

A schematic of the finite difference scheme of the numerical flow model is presented in figure A.6.

In the subsurface flow model the hydraulic head $h_{h(j,i)}^{t+1}$ is defined by means of Eq.[A.116] that makes use of the hydraulic head $h_{h(j,i)}^t$ and the specific discharges of the orthogonal connected grid cells for time instant t . This scheme thus is characterised as fully explicit.

The specific flow discharges $q_{gf,j+1/2,i}$, $q_{gf,j-1/2,i}$, $q_{gf,j,i+1/2}$ and $q_{gf,j,i-1/2}$ are defined over the effective saturated zone thickness of the flow model while the spatial subsurface discretisation of the soil column of grid cells is disregarded. In this approach, the saturated subsurface flow is simulated over an aggregated column of saturated cells while calculation nodes in a column are replaced by a single calculation node. For the aggregated cells, averaged values of the model parameters are required. The transmissivity over an effective saturated column is defined over the cells that are entirely saturated and the top cells that is partly saturated:

$$\overline{k_{s(j,i)}h_{h(j,i)}} = \sum_{n=1}^{n_{sat}} k_{s(j,i,n)} \cdot \Delta z_{(j,i,n)} \quad [A.121]$$

where

$$\begin{aligned} \overline{k_{s(j,i)}h_{h(j,i)}} &= \text{average transmissivity for aggregated cell } j,i & [L T^{-2}] \\ k_{s(j,i,n)} &= \text{saturated hydraulic conductivity at cell } j,i,n & [L T^{-1}] \\ \Delta z_{(j,i,n)} &= \text{layer thickness of cell } j,i,n & [L] \\ n_{sat} &= \text{lowest unsaturated cell in column} & [-]. \end{aligned}$$

The depth of the saturated flow profile is bounded by the bottom of the model and the calculated hydraulic head in each column of grid cells.

The Darcy flow equation [A.116] is discretised as follows:

$$\begin{aligned} q_{gf(j+1/2,i)}^t &= - \left(\frac{k_{s(j,i)} \cdot h_{h(j,i)}^t + k_{s(j+1,i)} \cdot h_{h(j+1,i)}^t}{2} \right) \cdot \frac{h_{h(j+1,i)}^t - h_{h(j,i)}^t}{x_{(j+1,i)} - x_{(j,i)}} \\ q_{gf(j-1/2,i)}^t &= - \left(\frac{k_{s(j,i)} \cdot h_{h(j,i)}^t + k_{s(j-1,i)} \cdot h_{h(j-1,i)}^t}{2} \right) \cdot \frac{h_{h(j,i)}^t - h_{h(j-1,i)}^t}{x_{(j,i)} - x_{(j-1,i)}} \\ q_{gf(j,i+1/2)}^t &= - \left(\frac{k_{s(j,i)} \cdot h_{h(j,i)}^t + k_{s(j,i+1)} \cdot h_{h(j,i+1)}^t}{2} \right) \cdot \frac{h_{h(j,i+1)}^t - h_{h(j,i)}^t}{x_{(j,i+1)} - x_{(j,i)}} \\ q_{gf(j,i-1/2)}^t &= - \left(\frac{k_{s(j,i)} \cdot h_{h(j,i)}^t + k_{s(j,i-1)} \cdot h_{h(j,i-1)}^t}{2} \right) \cdot \frac{h_{h(j,i)}^t - h_{h(j,i-1)}^t}{x_{(j,i)} - x_{(j,i-1)}} \end{aligned} \quad [A.122]$$

In figure A.7 a schematic for the simulation of saturated flow is presented. Saturated cells of a column are aggregated into one cell and inflow and outflow from the cell is simulated at the interface between connected aggregated cells. Although the schematic suggests that the top and bottom of the model domain are flat, in the mathematical model the

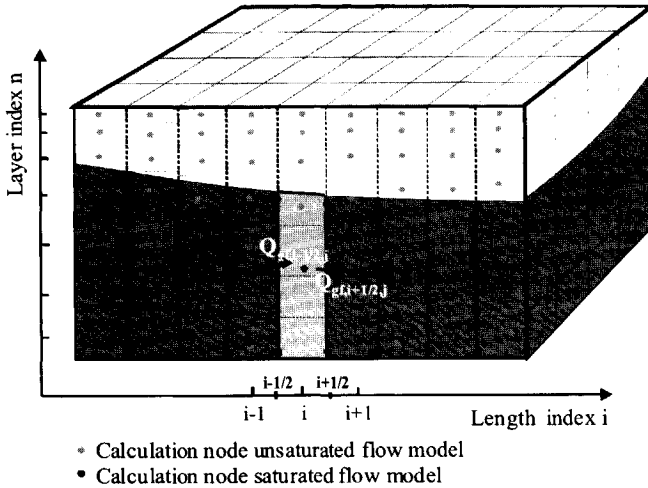


Figure A.7: Schematic of aggregated grid cells and saturated flow simulation.

grid cell elevations differ. The top layer represents the elevation heights of the DEM and the bottom represents the hydrological base of the model.

The saturated flow in the model effects the soil water storage in the unsaturated zone by updating the saturated flow volume over the aggregated cells. At the end of a calculation time step also the soil water storage of the unsaturated zone cells is updated and water must be added to, or subtracted from the total volume of stored water. A soil water redistribution procedure is developed and is termed the corrector procedure. In this procedure the change of the water volume is redistributed over the grid cells of the unsaturated soil cells. In case saturated flow causes a decrease of the water stored in any column, water is subtracted from any unsaturated cell where the decrease of soil moisture is proportional to the saturation degree. When the filling of a cell is simulated, all water is added to the lowest unsaturated cell in the column of subsurface cells. By such approach, an updated soil moisture distribution is simulated when compared to the soil water distribution as calculated prior to the saturated flow. The updated distribution is used in the succeeding simulation time step of the unsaturated zone model. In case over-saturation of the top cell takes place, subsurface water will exfiltrate at the land surface. By this exfiltration the overland flow water

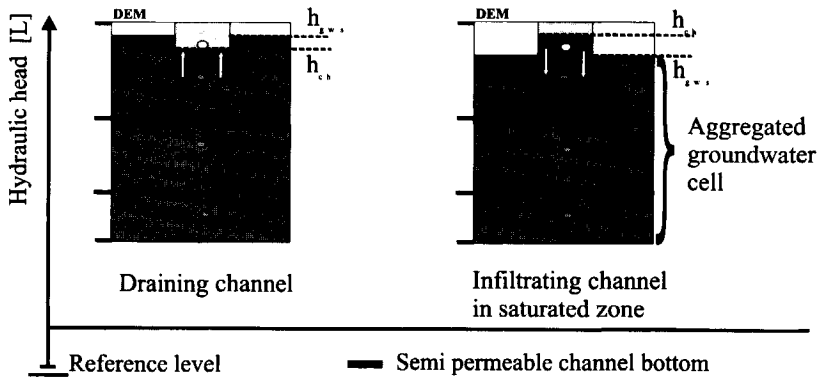


Figure A.8: Schematic of mass exchange in the saturated subsurface by channel-groundwater system interaction.

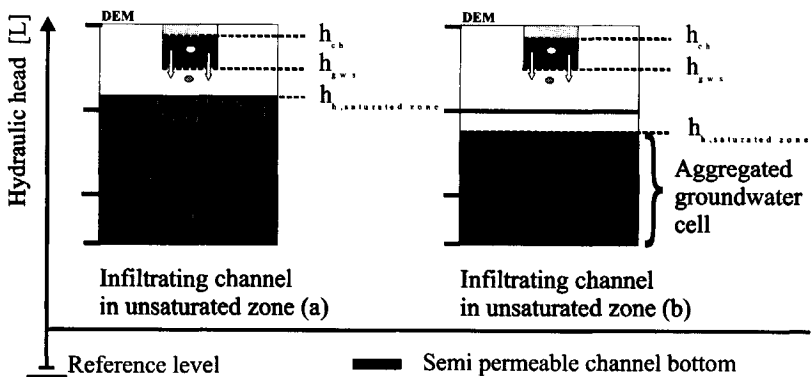


Figure A.9: Schematic of mass exchange in the unsaturated subsurface by channel-groundwater system interaction.

depth is updated at the end of the simulation time step and is used in Eq's [A.46] and [A.49] at the beginning of the succeeding time step.

Interactions between the groundwater flow and channel flow models are simulated by a head dependent boundary condition commonly known as the Cauchy boundary condition. Exchange fluxes are simulated for every time step and are subject to the hydraulic head of the groundwater flow model and the hydraulic head of the channel flow model. In figure's A.8 and A.9 schematics are presented for the simulation of mass exchange between the subsurface and channel flow models for draining and infiltrating channels. Mass exchanges in the model approach is

obstructed by use of an hydraulic resistance value, C , that represents the combined effect of the entry resistance of water to flow through the channel bottom and the radial flow resistance that, in real world systems, is observed near the channel bottom. The hydraulic resistance value is calculated by the quotient of the thickness of channel bottom and the vertical hydraulic conductivity of the channel bottom.

Mass exchange between the channel flow - saturated subsurface flow model is simulated by:

$$q_{\text{ch,gws}}^{t+1} = \frac{h_{\text{ch}(j,i)}^t - h_{\text{gws}(j,i)}^{t+1}}{C} \quad [\text{A.123}]$$

where

$$\begin{aligned} q_{\text{ch,gws}}^{t+1} &= \text{exchange flux channel - saturated flow model} & [\text{L T}^{-1}] \\ h_{\text{ch}(j,i)}^t &= \text{hydraulic head of channel flow model at element } j,i & [\text{L}] \\ h_{\text{gws}(j,i)}^{t+1} &= \text{hydraulic head of saturated flow model at cell } j,i & [\text{L}] \\ C &= \text{hydraulic resistance at channel bottom} & [\text{T}]. \end{aligned}$$

Exchange volumes are quantified by multiplication of $q_{\text{ch,gws}}$ with the cross sectional flow area of the channel bottom. The exchange volumes are added or subtracted from the aggregated saturated subsurface cell via the sink/source term S_{gf} . In case over-saturation of the top cell occurs, water will exfiltrate at the land surface. The Cauchy type boundary condition Eq. [A.123] also is applied to flow situations where the channel flow model is disconnected from the saturated subsurface due to the presence of an unsaturated grid cell underneath the channel cell. A schematic of the channel flow infiltration model in unsaturated flow conditions is presented in figure A.9.

In both infiltration situations the hydraulic head of the groundwater system is fixed at the elevation height of the channel bottom in order to prevent the simulation of unrealistic high seepage fluxes. The exchange volume is added to the specific subsurface element at which the channel bottom is simulated.

V Channel flow model

For the routing of runoff water in the channel network a one-dimensional flow model is developed. In the model approach, the DEM

is adapted and serves for the geometrical projection of the channel network layout in a model grid layer. By such approach an exact simulation of the real world network layout is not possible since channel flow grid elements are geo-referenced by the resolution of the DEM. Also, the numerical model is solved in orthogonal connected grid elements only and the accurate geometric simulation of the channel layout is restricted further. The channel network system is subdivided in channel segments and channel flow grid elements that, when combined, make up a segment. Segments may be connected to multiple upstream and/or downstream segments and the structure of the connected segments make up the entire channel network. Figure A.10 presents an example of a channel layout network system as simulated by the flow model.

Channel flow routing within the entire channel network system is achieved through the simulation of water movement from head-water elements downstream to the catchment outlet element. Within each segment water is routed from the inflow (or headwater element) to the outflow element while each outflow element is connected to an inflow element of the down-stream segment. One inflow element thus may be connected to two outflow elements when channel segments merge and both segments contribute to the downstream flow discharge.

The groundwater flow model, the unsaturated zone model and the overland flow model are linked through the DEM. The DEM is used for spatial discretisation and for geo-referencing the calculation nodes of each of the model sub-domains.

For the simulation of water transport the conservation equation of mass and the Strickler-Manning hydraulic resistance equation are applied. The one-dimensional conservation of mass equation reads:

$$\frac{\partial h_{ch}}{\partial t} + \frac{\partial q_{ch}}{\partial l} - S_{ch} = 0 \quad [A.124]$$

where

h_{ch}	= water depth channel flow	[L]
t	= time	[T]
q_{ch}	= specific discharge channel flow	[L ² T ⁻¹]
S_{ch}	= sink/source term channel flow model	[L T ⁻¹]
l	= spatial co-ordinate in direction of flow	[L].

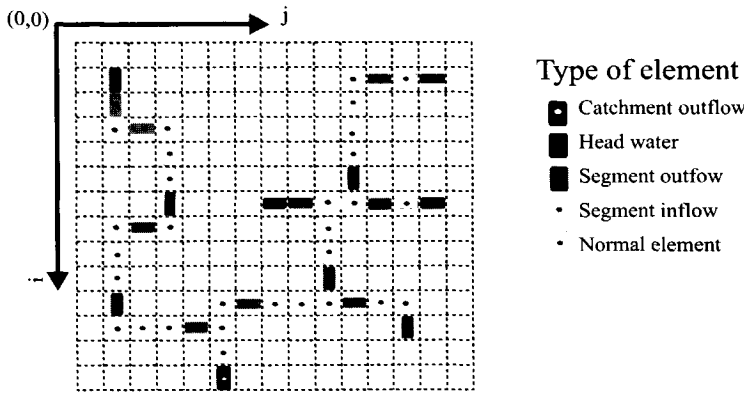


Figure A.10: Geometric representation of channel network layout.

while the channel flow discharges are calculated by the Strickler-Manning equation:

$$Q_{ch} = k_m \cdot A_{ch} \cdot R^{2/3} i^{1/2} \tag{A.125}$$

where

- Q_{ch} = discharge [L³ T⁻¹]
- k_m = reciprocal of Manning resistance coefficient [L^{1/3} T²]
- A_{ch} = wetted cross sectional area [L²]
- R = hydraulic radius [L]
- i = energy gradient line [-]

In the numerical approach, both equations are discretised in time and space over the model domain. The conservation equation of mass is discretised and solved for each grid element and specific discharges are simulated at the boundary of the upstream and downstream elements. Discretisation of Eq. [A.126] over a channel flow grid element gives the following expression:

$$\frac{h_{ch,j}^{t+1} - h_{ch,j}^t}{\Delta t} = \left(\frac{q_{j-1/2} - q_{j+1/2}}{x_{j+1/2} - x_{j-1/2}} \right) + S_{ch} \tag{A.126}$$

or, when rewriting for water depth, $h_{ch,j}^{t+1}$, this gives:

$$h_{ch,j}^{t+1} = h_{ch,j}^t + \left(\frac{q_{j-1/2} - q_{j+1/2}}{x_{j+1/2} - x_{j-1/2}} \right) \Delta t + S_{ch} \Delta t \tag{A.127}$$

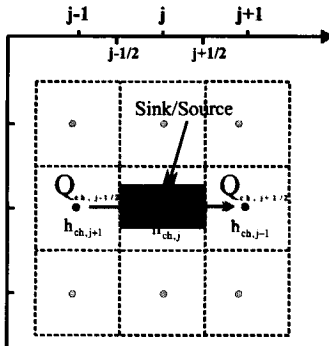


Figure A.11: 3-Point calculation scheme

where

$q_{j-1/2}$ = specific channel flow discharge from upstream element [$L^2 T^{-1}$]

$q_{j+1/2}$ = specific channel flow discharge to downstream element [$L^2 T^{-1}$]

Δt = time increment [T]

S_{ch} = sink/source term channel flow model [$L T^{-1}$].

By the sink/source term, S_{ch} , runoff contributions from overland flow and groundwater flow are simulated and channel flow water depths are updated. These depths are used in the channel flow routing algorithm and are used to update the channel flow water depth at the end of the simulation time step $t+\Delta t$.

For quantification of the specific channel flow discharges of Eq. [A.127], discharges are defined by the Strickler-Manning equation [A.125] and are divided by the cross sectional flow area of the channel elements. Eq. [A.127] now becomes:

$$h_{ch,j}^{t+1} = h_{ch,j}^t + \left(\frac{Q_{j-1/2} - Q_{j+1/2}}{x_{j+1/2} - x_{j-1/2}} \right) \frac{\Delta t}{A_{ch}} + S_{ch} \Delta t \quad [A.128]$$

For solving this equation a three-point calculation scheme is developed. For all grid elements the water depths are simulated by considering the inflow and outflow from the upstream and downstream grid elements respectively, and the runoff contributions as simulated by the sink/source term. In figure A.11, a schematic about this calculation scheme is presented.

In Flowsim only rectangular cross-sectional flow areas are considered where cross sectional flow areas are quantified by multiplication of the width of the channel section, b_{ch} , by the water layer depth h_{ch} . In this approach the hydraulic radius, R , is equal to $b_{ch}/(2+b_{ch}/h)$.

For $Q_{j+1/2}$ and $Q_{j-1/2}$, the following expressions of the Strickler-Manning equation [A.125] are developed:

$$Q_{j+1/2} = k_{m,j+1/2} \cdot b \cdot \sqrt{i_{j+1/2}} \cdot \left(\frac{b}{2 + \frac{2b}{\zeta h_{j+1}^t + (2-\zeta)h_j^t}} \right)^{2/3} \left(\frac{\zeta h_{j+1}^{t+1} + (2-\zeta)h_j^{t+1}}{2} \right) \quad [A.129]$$

$$Q_{j-1/2} = k_{m,j-1/2} \cdot b \cdot \sqrt{i_{j-1/2}} \cdot \left(\frac{b}{2 + \frac{2b}{(2-\zeta)\zeta h_{j-1}^t + \zeta h_j^t}} \right)^{2/3} \left(\frac{(2-\zeta)h_{j-1}^{t+1} + \zeta h_j^{t+1}}{2} \right) \quad [A.130]$$

where the gradients $i_{j+1/2}$ and $i_{j-1/2}$ represent hydraulic gradients. By substitution of $Q_{j+1/2}$ and $Q_{j-1/2}$ from Eq.[A.129] and Eq.[A.130] in Eq.[A.128] and when ignoring the sink/source terms S_{ch} this yields:

$$h_j^{t+1} = h_j^t + (c_j((2-\zeta)h_{j-1}^{t+1} + \zeta h_j^{t+1})) - (b_j(\zeta h_{j+1}^{t+1} + (2-\zeta)h_j^{t+1})) \quad [A.131]$$

where

$$b_j = k_{m,j+1/2} \cdot b \cdot \frac{i_{j+1/2}}{\sqrt{i_{j+1/2}}} \cdot \left(\frac{b}{2 + \frac{2b}{\zeta h_{j+1}^t + (2-\zeta)h_j^t}} \right)^{2/3} \cdot \frac{\Delta t}{A_{ch}} \cdot \frac{1}{2} \quad [A.132]$$

$$c_j = k_{m,j-1/2} \cdot b \cdot \frac{i_{j-1/2}}{\sqrt{i_{j-1/2}}} \cdot \left(\frac{b}{2 + \frac{2b}{(2-\zeta)\zeta h_{j-1}^t + \zeta h_j^t}} \right)^{2/3} \cdot \frac{\Delta t}{A_{ch}} \cdot \frac{1}{2}$$

and where i_j is the hydraulic slope gradient.

After rewriting Eq.[A.131] this gives

$$a_j h_j^{t+1} - b_j \zeta h_{j+1}^{t+1} + c_j (2-\zeta) h_{j-1}^{t+1} + d_j = 0 \quad [A.133]$$

where

$$a_j = (-1 - (2 - \zeta)b_j + \zeta c_j) \quad [\text{A.134}]$$

$$d_j = h_j^t \quad [\text{A.135}]$$

For solving Eq.[A.133] a double sweep algorithm similar as to the overland flow model is introduced.

Implementing the double sweep algorithm

The general double sweep equation reads:

$$h_j^{t+1} = \alpha_j h_{j+1}^{t+1} + \beta_j \quad [\text{A.136}]$$

while in the notation for h_{j-1} this gives:

$$h_{j-1}^{t+1} = \alpha_{j-1} h_j^{t+1} + \beta_{j-1} \quad [\text{A.137}]$$

After substitution of the expression of h_{j-1}^{t+1} from Eq.[A.137] in

Eq.[A.133] and when rewriting this equation for h_j^{t+1} the general form of the double sweep equation [A.136] is obtained where α_j and β_j are defined by Eq.[A.139] and Eq.[A.140]:

$$h_j^{t+1} = \frac{\zeta b_j}{(2 - \zeta)c_j \alpha_{j-1} + a_j} h_{j+1}^{t+1} + \left(\frac{-(2 - \zeta)c_j \beta_{j-1} - d_j}{(2 - \zeta)c_j \alpha_{j-1} + a_j} \right) \quad [\text{A.138}]$$

$$\alpha_j = \frac{\zeta b_j}{(2 - \zeta)c_j \alpha_{j-1} + a_j} \quad [\text{A.139}]$$

$$\beta_j = -\frac{(2 - \zeta)c_j \beta_{j-1} + d_j}{(2 - \zeta)c_j \alpha_{j-1} + a_j} \quad [\text{A.140}]$$

It is obvious that both the inflow and outflow are simulated. When elements 'fall dry' during a model calculation time step, the coefficients are reduced subject to the flow condition. Specific flow conditions relate to the inflow and outflow discharges of an elements and conditions defined are; $Q_{j+1/2} = 0$ and $Q_{j-1/2} > 0$; $Q_{j+1/2} > 0$ and $Q_{j-1/2} = 0$; $Q_{j+1/2} = 0$ and $Q_{j-1/2} = 0$. In the following the appropriate expressions for the double sweep coefficients α_j and β_j are given.

Calculation of the double sweep coefficients α_j and β_j for zero flow conditions

Boundary grid elements are marked by the code number '0' and correspond to the code as applied in the overland flow model. In figure I.2 the use of code numbers is explained.

No-flow type I: $Q_{j-1/2} = 0 \Rightarrow c_j = 0$

<table border="0" style="width: 100%; text-align: center;"> <tr> <td>code = 0</td> <td>code ≠ 0</td> <td>code ≠ 0</td> </tr> <tr> <td style="border: 1px solid black; width: 30px; height: 30px;">j-1</td> <td style="background-color: black; width: 30px; height: 30px;"></td> <td style="border: 1px solid black; width: 30px; height: 30px;">j+1</td> </tr> </table>	code = 0	code ≠ 0	code ≠ 0	j-1		j+1	$\alpha_j = \frac{\zeta b_j}{a_j}$	[A.141]
code = 0	code ≠ 0	code ≠ 0						
j-1		j+1						

$\beta_j = -\frac{d_j}{a_j}$	[A.142]
------------------------------	---------

No-flow type II: $Q_{j+1/2} = 0 \Rightarrow b_j = 0$

<table border="0" style="width: 100%; text-align: center;"> <tr> <td>code ≠ 0</td> <td>code ≠ 0</td> <td>code = 0</td> </tr> <tr> <td style="border: 1px solid black; width: 30px; height: 30px;">j-1</td> <td style="background-color: black; width: 30px; height: 30px;"></td> <td style="border: 1px solid black; width: 30px; height: 30px;">j+1</td> </tr> </table>	code ≠ 0	code ≠ 0	code = 0	j-1		j+1	$\alpha_j = 0$	[A.143]
code ≠ 0	code ≠ 0	code = 0						
j-1		j+1						

$\beta_j = -\frac{(2-\zeta)c_j\beta_{j-1} + d_j}{(2-\zeta)c_j\alpha_{j-1} + a_j}$	[A.144]
---	---------

No-flow type III: $Q_{j-1/2} = 0$ and $Q_{j+1/2} = 0 \Rightarrow b_j = 0, c_j = 0$

<table border="0" style="width: 100%; text-align: center;"> <tr> <td>code = 0</td> <td>code ≠ 0</td> <td>code = 0</td> </tr> <tr> <td style="border: 1px solid black; width: 30px; height: 30px;">j-1</td> <td style="background-color: black; width: 30px; height: 30px;"></td> <td style="border: 1px solid black; width: 30px; height: 30px;">j+1</td> </tr> </table>	code = 0	code ≠ 0	code = 0	j-1		j+1	$\alpha_j = 0$	[A.145]
code = 0	code ≠ 0	code = 0						
j-1		j+1						

$\beta_j = h_j'$	[A.146]
------------------	---------

Segment connectivity by inflow and outflow elements

Segments are connected by the inflow and outflow elements. In a segment such elements are defined when the spatial orientation of a segment changes direction within the two-dimensional grid or when two segments come together at a confluence element to form a single segment. Since the mathematical model only is able to simulated channel flow in one direction (i.e. either j-direction or i-direction), a separate procedure is developed to transfer channel discharges from one (or two)

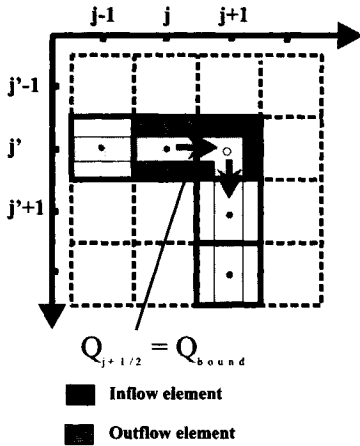


Figure A.12: Schematic of perpendicular connected segments.

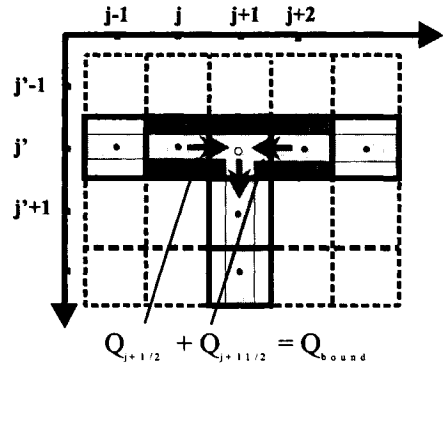


Figure A.13: Schematic of segment connectivity at confluences.

segments into the downstream segment. In the figures A.12 and A.13 two schematics are presented for flow situations of perpendicular connected segments and confluences of two segments.

Inflow element

At the inflow elements the channel flow depth is simulated by the inflow from the upstream segment(s). Each inflow element so makes up the first element of a segment and water flow out of the element is simulated by the procedure described above. The inflow to these elements is simulated by use of a sink/source term approximation. Calculated discharges at the boundary between the outflow and inflow elements are converted to a channel flow water depth and added to the water depth of the inflow elements as defined at time instant t . This procedure is applied to perpendicular connected segments and to confluence elements. Such inflow is termed the boundary inflow, Q_{bound} that, as shown in figure A.12, is equal to $Q_{j+1/2}$ while boundary inflow that is shown in figure A.13 is equal to $Q_{j+1/2} + Q_{j+11/2}$. The change of the water depth at the inflow element due to Q_{bound} now is updated through simple calculus; Q_{bound} is divided by ch_{area} that is defined by multiplying b_{ch} with the grid size.

By the sink/source term of an inflow element also the overland flow and groundwater inflow are simulated. The procedure to simulate the change

of the water depth at an inflow element prior to the simulation of the outflow now becomes:

$$\Delta h_j = h_{\text{sink/source}}^{\Delta t} + h_{\text{qBound}}^{\Delta t} \tag{A.147}$$

Outflow element

The outflow discharge at the outflow elements also is simulated by a double sweep procedure that is based on the same procedure as applied to the normal elements of a segment. The procedure requires a small modification since the outflow element becomes the end element of the upstream segment and so this makes that the inflow element is part of the downstream segment. For simulation of the outflow discharge, hence the hydraulic gradient at the outflow boundary is not known. Therefore for each outflow element an imaginary grid element is added to the segment and the bottom slope gradient at the outflow boundary is set to be equal to the gradient at the inflow boundary. For the calculation of the outflow discharge the water depths of the last two elements are used and so a water depth at the imaginary element is not required. For the outflow and normal elements various inflow and outflow situations are defined. The double sweep coefficients are defined in the following manner.

The continuity equation for an outflow element with index J reads:

$$h_j^{t+1} = h_j^t + (Q_{j-1/2}^t - Q_{j+1/2}^t) \frac{\Delta t}{A_{ch}} \tag{A.148}$$

After substitution of Eq.[A.130] for $Q_{j-1/2}^t$ in Eq.[A.148] and after rewriting this gives

$$a_j h_j^{t+1} - k_j Q_{j+1/2}^t + c_j (2 - \zeta) h_{j-1}^{t+1} + d_j = 0 \tag{A.149}$$

where

$$a_j = (-1 + \zeta c_j^t) \tag{A.150}$$

$$k_j = \frac{\Delta t}{A_{ch}} \tag{A.151}$$

$$d_j = h_j^t \tag{A.152}$$

where c_j follows the expression from Eq.[A.132]. For any end point, $Q_{j+1/2}^t$ is defined by:

$$Q_{j+1/2}^i = k_m b \sqrt{i_{j-1/2}} \left(\frac{b}{2 + \frac{b}{h_j^i}} \right)^{2/3} h_j^{i+1} \tag{A.153}$$

The coefficients α_j and β_j in the double sweep equation [A.138] are now defined. The double sweep equation for $j = J$ reads

$$h_j^{i+1} = \alpha_j h_{j+1}^{i+1} + \beta_j \tag{A.154}$$

while for

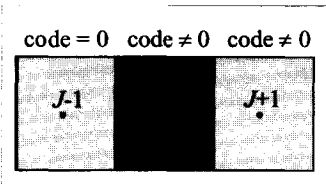
$$h_{j-1}^{i+1} = \alpha_{j-1} h_j^{i+1} + \beta_{j-1} \tag{A.155}$$

After substitutions of this equation for h_{j-1}^{i+1} in Eq. [A.26] and A.[153] for $Q_{j+1/2}^i$ in Eq.[26] the following expression for h_j^{i+1} is obtained:

$$h_j^{i+1} = \frac{-(2-\zeta)c_j \beta_{j-1} - d_j}{-k_j \left(k_m b \sqrt{i_{j-1/2}} \left(\frac{b}{2 + \frac{b}{h_j^i}} \right)^{2/3} \right) + (2-\zeta)c_j \alpha_{j-1} + a_j} \tag{A.156}$$

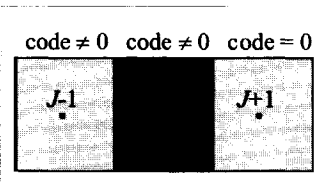
Both inflow and outflow are simulated. When implementing the flow conditions I to III Eq.[A.156] changes to

No-flow type I: $Q_{j-1/2} = 0 \Rightarrow c_j = 0$



$$h_j^{i+1} = \frac{-d_j}{-k_j \left(k_m b \sqrt{i_{j-1/2}} \left(\frac{b}{2 + \frac{b}{h_j^i}} \right)^{2/3} \right) + a_j} \tag{A.157}$$

No-flow type II: $Q_{j+1/2} = 0$



$$h_j^{i+1} = \frac{-(2-\zeta)c_j \beta_{j-1} - d_j}{(2-\zeta)c_j \alpha_{j-1} + a_j} \tag{A.158}$$

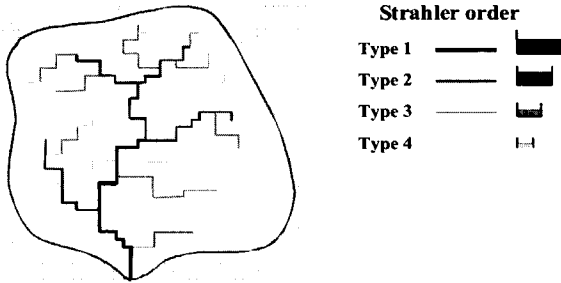


Figure A.14: Channel shape and geometry by the Strahler order network approximation.

No-flow type III: $Q_{j-1/2} = 0$ and $Q_{j+1/2} = 0 \Rightarrow c_j = 0$

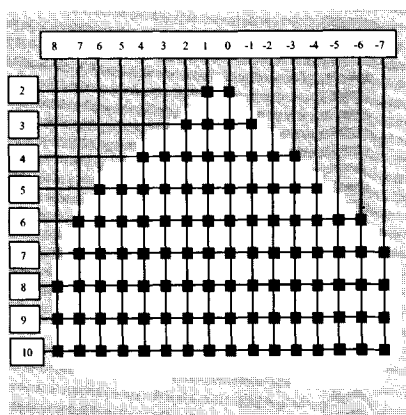
code = 0	code ≠ 0	code = 0	$h_j^{t+1} = \frac{-d_j}{a_j}$	[A.159]
$J-1$		$J+1$		

Channel network geometry

For the simulation of the channel network layout a Strahler-ordering scheme is adapted. Segments of the channel network system are indexed by a Strahler-order number and segments are indexed by the modeller. For each Strahler-order, similar channel shape geometries and Strickler-Manning roughness coefficients are defined. The hydraulic resistance value, C , (Eq. [A.121]) for the simulation of channel flow - groundwater flow interactions are defined per grid elements and so vary may over a channel segment. In the model only prismatic channel shapes are considered. By such approach, it is obvious that gross simplifications are introduced into the model. For parameterisation of the channel flow model, such simplifications cause a significant reduction of the parameter demand although it must be kept in mind that such simplification may have pronounced effects on the routing of runoff volumes in the channel flow model. In figure A.14 a schematic on the implementation of the Strahler ordering scheme is presented.

Appendix B

Analyses Troy data set



I Groundwater

For model calibration, time series of observed water table depth are selected from the data set that has been made available for this thesis by UI. For the subsurface, the data set comprised time series of observations for 144 piezometers from which 102 are located within the catchment (figure B.1) Analyses focussed on the winter period of 1999 since piezometers and sensors of the network had been checked by the UI in 1998.

For each piezometer researchers at UI have compared manual observations of the water table depth with sensor observations of automated data loggers. By this comparison a number of piezometers could be rejected for further analysis due to malfunction and observation inconsistencies and are indicated by a red label in figure B.3. It also was revealed that a number of piezometers had been installed at a depth above the fragipan instead of at the fragipan. Such piezometers also are considered as inappropriate for further use and are indicated by a purple label.

The objective of further analyses it to identify a number of piezometers that can be used for model calibration. Piezometers must have trustworthy time series and reliable readings in a sense that the depth of the groundwater table clearly must respond to rainfall events and groundwater flow across the catchment. An ensemble data set of observation time series must be selected in which the observed groundwater behaviour clearly supports the theory of the saturation overland flow mechanism.

The first analysis dealt with visual interpretation of the observation time series. For each piezometer a groundwater hydrograph is produced and analysed. In figure B.2 groundwater hydrographs for each piezometer are shown and represent the depth of the groundwater table below the land surface. A positive value for the water table depth indicates a water layer at the land surface. It is observed that a number of piezometers have readings with water layers at the land surface of 10 cm. or more. Although researchers of UI have observed water at the land surface, water depths were only shallow. Therefore, in the analyses, piezometers with readings of water layers at the land surface of 10 cm. or more are

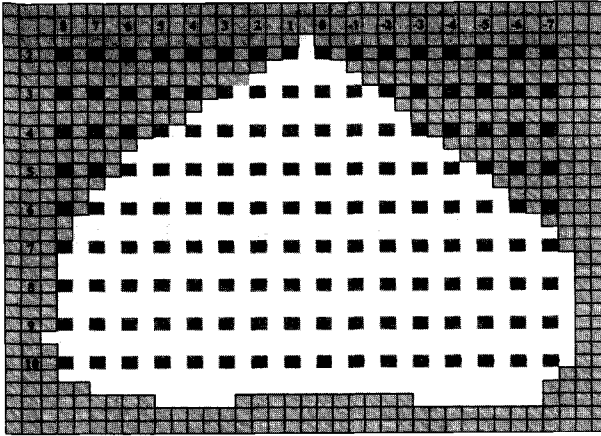


Figure B.1: *Piezometer network of the Troy area.*

rejected and classified as unreliable. As such piezometers 7.6, 7.7, 6.9, 5.5, 4.4, 4.5, 3.5, 3.8, 3.10 and 0.2 are disregarded for further analyses.

The second analyses focussed on whether characteristics of the groundwater flow behavior that underlies the saturation overland flow mechanism could be identified in an ensemble of piezometer time series. For such analyses a number of piezometers are combined in a sub-data set by making cross sections along the catchment. In total seven cross sections are constructed that are indicated in figure B.3.

For each cross section the water table distribution along the hill slopes is created for 5 consecutive days, from February 27 till March 3, at 12.00 A.M. This time period follows a short period with extreme rainfall as indicated in figure B.11. On February 28 and March 1st, 17 mm. and 16 mm. of rainfall is recorded respectively, while on February 27 and on March 2nd and 3rd no rainfall was recorded. The hydrological state of the catchment therefore is characterised as very wet were saturation overland flow most likely is generated.

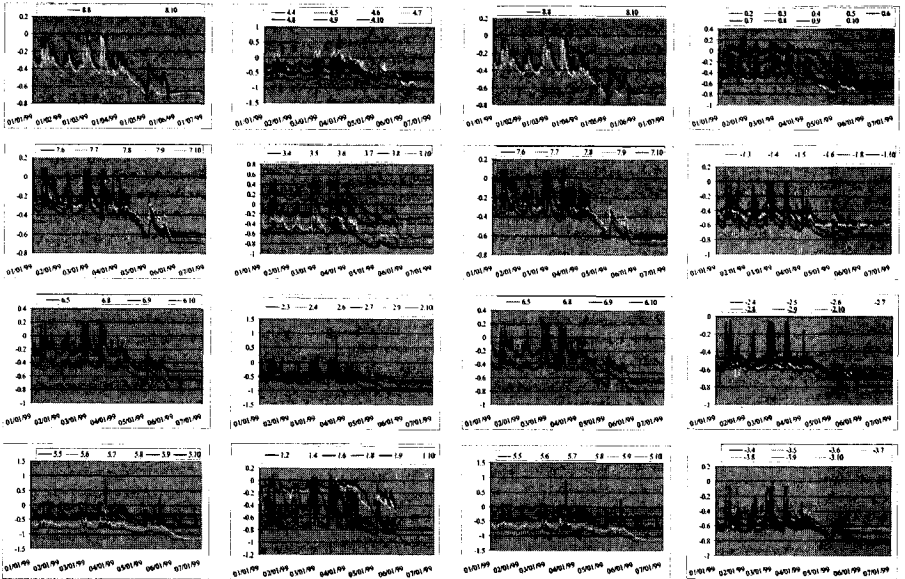


Figure B.2: Ground water table hydrographs for each grid column of piezometers.

For the time series to be selected for model calibration it is a prerequisite that the groundwater fluctuations that cause exfiltration and generation of saturation overland flow is reflected in the time series of selected piezometers along the cross sections. In the following, each of the cross sections is discussed and a selection is made for piezometers to be used in the model calibration.

For each cross section three graphs are made and are presented in the figures B.4 through B.11. In these figures, the first graph represents the hill slope elevation and the water table depth with respect to the datum of the catchment (i.e. the lowest point of the Troy area). This graph gives specific information of the shape of the hill slope and the location of each piezometer on the hill slope. In the second graph, water tables are drawn for the 5 consecutive time steps. For each piezometer the water table level below the land surface and the water tables across the hill slope are drawn. These graphs give specific information on whether exfiltration and saturation overland is generated during and shortly after the rainfall events of February 28 and March 1. Such observations also should be consistent with water table depths as observed in the upper sections of the hill slopes. In these figures the depth of the fragipan is

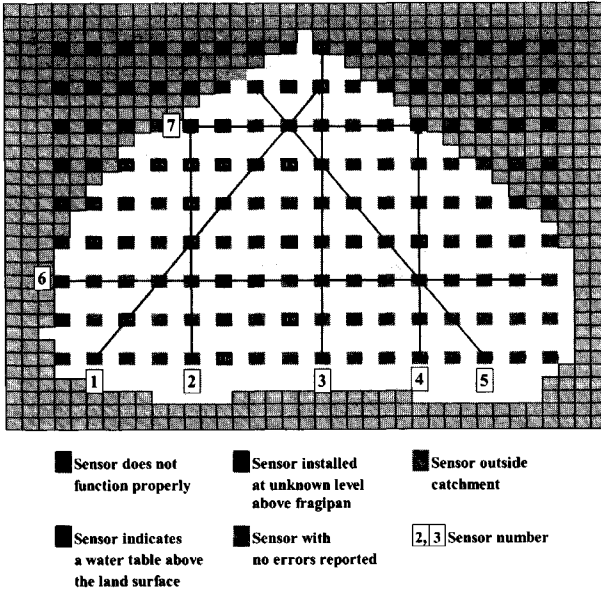


Figure B.3: Selected cross sections of piezometers along the catchment.

added in order to evaluate the water table depth with respect to the fragipan. The third graph presents the response of the water table to precipitation. Graphs are constructed for the month of February and March and give specific information on the groundwater fluctuations as observed in each piezometer. In the graphs it can be observed whether a) exfiltration will occur, b) the groundwater depth along the cross section is deepest at catchment boundary and shallowest at the channel with a gradual decrease of depth and c) the theory of saturation overland flow generation in the catchment is supported by the field data.

During the analyses it was revealed that the observation network is of (very) poor quality and (very) unreliable. The cause of this is due to the manner the network is installed. During installation of the piezometers, the fragipan depth is measured at each piezometer location and this depth serves as the elevation reference for the observation time series of the individual piezometers. As such, piezometer levels are gauged with respect to the bottom of the piezometer and thus the time series of observations are referenced to the fragipan depth. During the analyses it proved that the fragipan depth was poorly defined. Within the cross sections relatively large differences in the fragipan height are observed

and are not in correspondence with fluvial and geomorphologic hill slope considerations. In the second set of graphs it is observed that the shape of the fragipan dominates the water table distribution along a cross section. In the third set of graphs this phenomenon shows up when piezometer hydrographs are compared. Observations of the time series often are separated by a constant water depth. A 'deep' fragipan shows 'deep' water table levels while a 'shallow' fragipan shows 'shallow' water table levels below the land surface. A clear example of this phenomenon is given by comparison of piezometers 0.5 and -2.7 in section 5. For obtaining a more reliable network, each piezometer must be re-surveyed were the top of the piezometer is defined with respect to the datum. Observations then must be made with respect to the top of the piezometer.

Cross section 1

In cross section 1, piezometer with ID 7.10, 5.8, 3.6 and 1.4 are analysed that are located at 0, 36, 72 and 106 m. respectively in the cross section. For the very wet period February 23 and March 1, piezometer 1.4 shows the smallest water table fluctuation, 7.10 shows the largest fluctuations while 5.8 shows fluctuations in between. It is surprising that at the end of February all piezometers have water table depths close to, or even at, the land surface. This, however, only is expected for 1.4. It also is observed that, after rainfall ceased, the up-slope area rapidly depletes while at the lower section the drainage volumes from the up-slope area cause a much slower depletion. Time series of 3.6 and 5.8 are classified as unreliable since water levels are out of a realistic observation range. For 3.6, levels generally are too low while for 5.8 levels are too high. The cause of the errors most likely is that the depth of the fragipan, and so the depth of the piezometer, is wrongly defined.

Cross section 2

In cross section 2, piezometers 4.6 and 4.7 are ignored from analyses since they are classified as unreliable by researchers of UI. In the analyses for this thesis, 4.5 and 4.6 are ignored since sensors failed during the wet periods. As such only 4.8, 4.9 and 4.10 are used that are located at 0, 15 and 30 m. in the cross section. Piezometer 4.8 shows the smallest water table fluctuation with water tables up to the land surface. Time series from 4.9 and 4.10 show rapid responses to rainfall while at inter-storm periods a rapid depletion of the (up-slope) groundwater

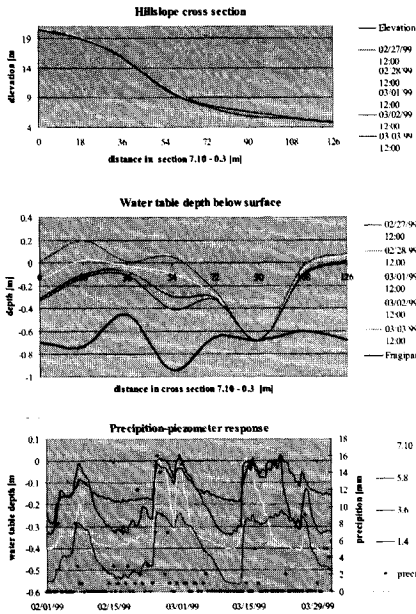


Figure B.4: Graphs of cross section 1.

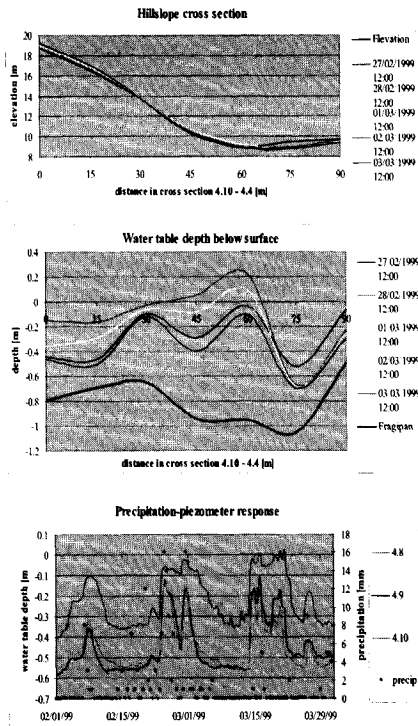


Figure B.5: Graphs of cross section 2.

system is observed. A groundwater rise to the land surface is not shown in the figure for the heavy rain event in the second half of February. When comparing piezometers 4.9 and 4.10 to 7.10 and 5.8 in cross section 1, it is uncertain which readings are reliable. Although a groundwater table rise up to the land surface is clearly observed in 7.10 and in 5.8, this is not observed in 4.9 and 4.10. For 4.8 it is surprising that only very little depletion takes place in between rainfall events. The same behaviour, however, also is shown in 5.8 in cross section 1. It is preliminary concluded that 4.9 and 4.10 are suitable for model calibration. Further comparisons to other piezometers, however, are required to be more conclusive.

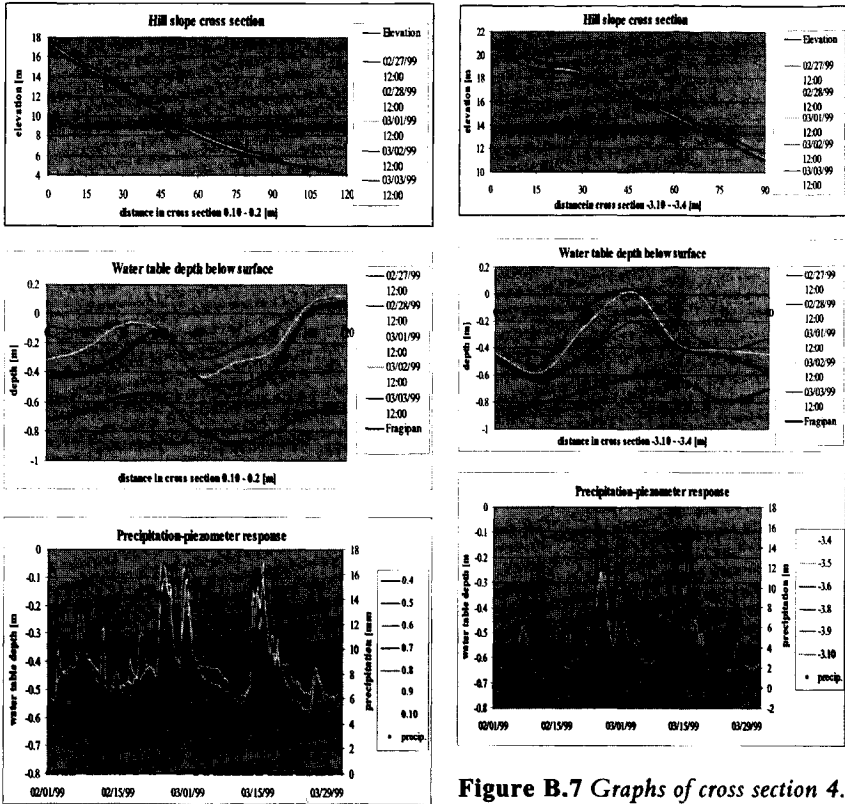


Figure B.7 Graphs of cross section 4.

Figure B.6: Graphs of cross section 3.

Cross section 3

In cross section 3, 0.2 and 0.3 are classified as unreliable by the conclusions of previous analyses. At first, 0.6 is rejected since fluctuations are not in range with the other piezometers. Regarding the position of 0.7 on the hill slope, this also shows uncertain water table levels. Water level fluctuations are too small and, generally, water levels are too high. Fluctuations in 0.10 and 0.9 have great similarity with those of 4.9 and 4.10 in cross section 2. The rapid response to rainfall and the rapid depletion is observed in all four piezometers and also the water table depth below the surface shows similarities. 0.8 Shows water table depths that are smallest for the whole cross section and as such are not realistic. 0.5 On the contrary shows deepest water table depths that, considering its location on the hill slope, also must be questioned. It is

concluded that 0.4, 0.9 and 0.10 are the most reliable in cross section 3 and possibly suitable for use in model calibration.

Cross section 4

Piezometers -3.10, -3.9 and -3.5 show great similarity in water level fluctuations that are considered relatively small. -3.9 Shows water levels that generally are 20 cm lower than piezometers -3.10 and -3.5.

Piezometers -3.4, -3.6 and -3.8 show much larger fluctuations and more rapid responses to rainfall. Hydrographs from -3.4 and -3.8 show great similarity although graphs, approximately, differ some 35-40 cm. in depth. Piezometer -3.4 is positioned near the catchment boundary while -3.8 is positioned at the middle section of the hill slope.

Conclusions on reliability of time series are difficult to make. When assuming that -3.8 is correct than it is unexpected that -3.6 has lower peak levels since the up-slope area from -3.6 is much larger than -3.8. For the same reason it also is expected that -3.10 must have deeper water levels than -3.9. It is surprising that, in an explanatory sense, -3.10 and -3.9 do not match with time series of up-slope piezometers of other cross sections. For -3.5 it is unexpected that fluctuations are smaller than -3.4. The overall conclusion is that all piezometers of this cross section must be exercised with care. Based on physical reasoning, the two most reliable piezometers likely are -3.4 and -3.6.

Cross section 5

Groundwater levels in 0.5 are unrealistically low as compared to 1.4 and -1.6. Piezometer 1.4 is located near by the channel and, as such, shows very shallow groundwater levels while -1.6 is located at the middle hill slope and shows rapid response to rainfall and a gradual depletion of the subsurface. By physical reasoning, such depletion is expected at -1.6 and also groundwater levels are at, relatively, shallow depth. -5.10 Shows rapid responses to rainfall and also rapid depletions of the subsurface. Compared to -4.9, piezometer -5.10 shows much smaller water table fluctuations for, in particular, periods of heavy precipitation. -2.7 and -3.8 shows great similarity for groundwater level fluctuations as well as for the water table depth. Both piezometers show hydrographs that very well could be explained by physical reasoning. The theory underlying the mechanism of saturation overland flow generation is observed in

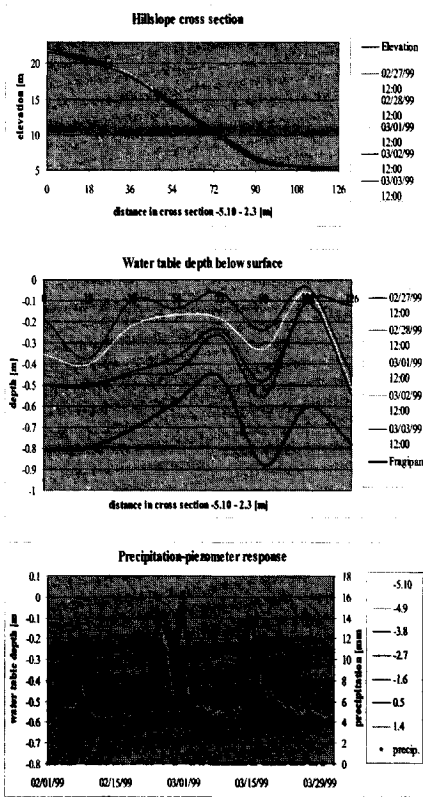


Figure B.8: Graphs of cross section 5.

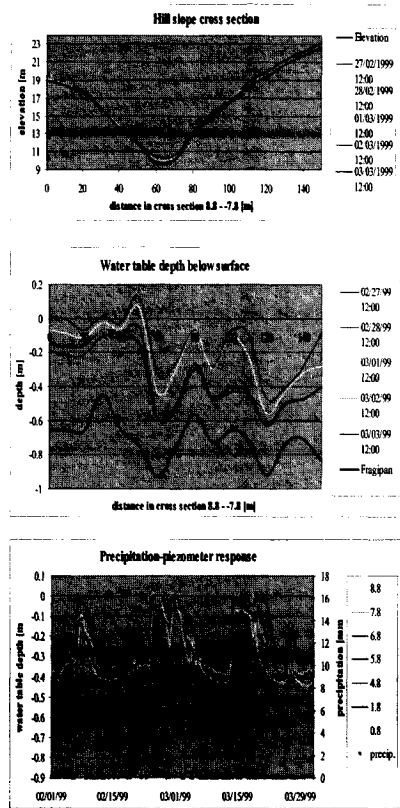


Figure B.9: Graphs of cross section 6a.

this cross section. It is concluded that 1.4, -1.6, -3.8, -2.7 and -5.10 are the most reliable and are suitable for use in model calibration.

Cross section 6a

In this cross section 2.8 and 3.8 already are rejected by previous analyses. High groundwater table levels in 8.8, 5.8 and 4.8 should, potentially, generate overland flow. Such overland flow generation, however, is not realistic for 8.8, 7.8, 5.8 and 4.8. This since 8.8 is at the up-slope catchment boundary and since the up-slope areas for 7.8, 5.8 and 4.8 are relatively small. In the theory of the saturation overland flow mechanism such water table rise can only be explained in the vicinity of the channel where the up-slope groundwater flow system is largest.

All four piezometers therefore are rejected. Piezometers 0.8 and 6.8 show similar groundwater table behaviour although 0.8 shows more rapid groundwater depletion. Regarding the locations of 6.8 and 0.8 on the hill slope cross section this is unexpected. To be conclusive on the reliability of 0.8 or 6.8 for use in model calibration is difficult.

Cross section 6b

Piezometer -1.8 is rejected since high water table levels are not observed but readings are probably caused by a failure of the sensor. All other piezometers show rapid responses to rainfall and also rapid depletions of the subsurface. Hydrographs also show great similarity and only differences are shown with respect to observed water table levels.

Regarding the upslope piezometers -5.8, -6.8 and -7.8, it is surprising that -7.8 records higher water levels than -6.8 while this piezometer has higher water levels than -5.8. Based on physical reasoning the opposite behavior should be observed in the series. Comparing -3.8 to -2.8 at the middle hill slope section, it is observed that water levels in -2.8 are gradually higher than in -3.8.

The same behavior is observed by comparing -2.8 to 0.8. All three piezometers show similar responses to rainfall and also subsurface depletion occurs rapidly without any storage delays. Considering the size of the up-slope area the rapid depletion is expected and 0.8, -2.8 and -3.8 therefore show time series that are suitable for use in model calibration. Regarding the analyses in cross section 6a, piezometer 0.8 is the most uncertain.

Cross section 7

In this cross section the piezometers -4.4, 3.4 and 2.4 are rejected by previous analyses. All piezometers show rapid responses to rainfall with highest water levels in piezometer at the bottom section of the hill slope. Piezometer 1.4 is situated near the channel and shows high water levels for the entire period. Regarding the series of 5 piezometers, only the time series of 0.4 shows unexpected groundwater behavior. Piezometer -3.4 at the catchment boundary shows the deepest water levels and the least fluctuation compared to -2.4 and -1.4. Hydrographs from these piezometers have higher water table levels while the water table itself generally is at shallower depth. Also the depletion of the subsurface shows an increasing delay when moving from the upslope piezometer

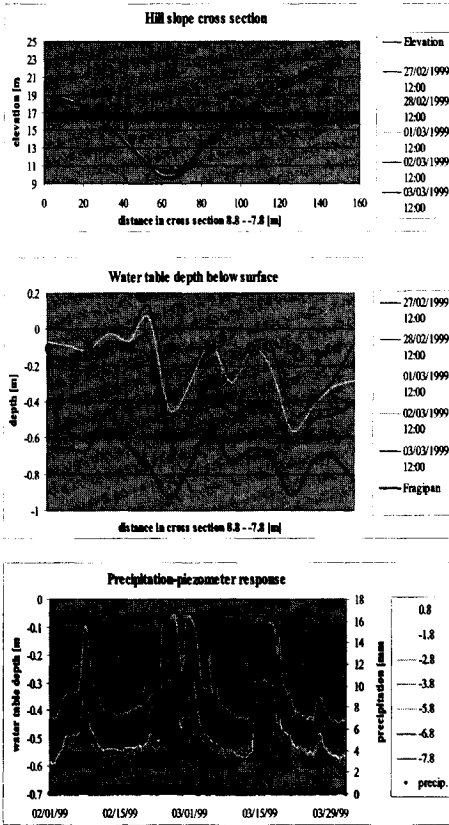


Figure B.10: Graphs of cross section 6b.

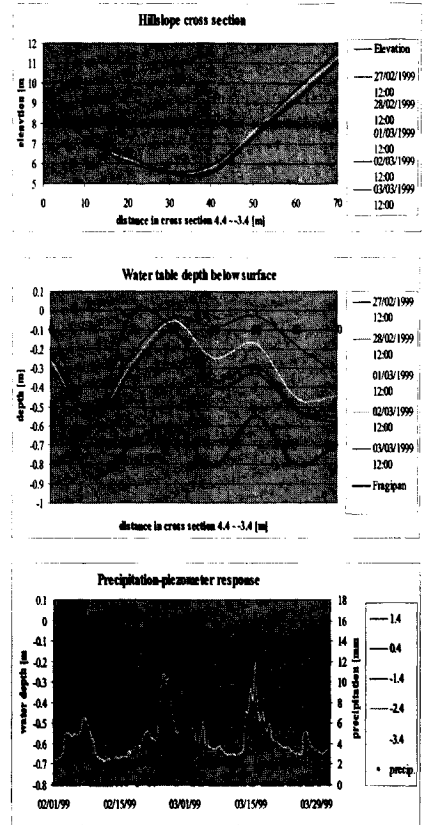


Figure B.11: Graphs of cross section 7.

-3.4 to the downslope piezometer -1.4. It is concluded that the groundwater behavior shown in this cross section supports the theory of the saturation overland flow mechanism. Observed water table fluctuations, the depth of the water table along the hill slope cross section and observed time delays in the subsurface depletion process support the theory. It is therefore concluded that 1.4, -1.4 -2.4 and -3.4 are suitable for model calibration.

The final and overall conclusion is that piezometers 4.8, 4.9, 4.10, 1.4, 0.9, 0.10, -1.4, -1.6, -2.4, -2.7, -2.8, -3.4, -3.6, -3.8 and -5.10 could be used for model calibration although clear saturation overland flow periods cannot be identified. Most piezometers are selected since, when combined, they show consistent dynamic groundwater flow behaviour of

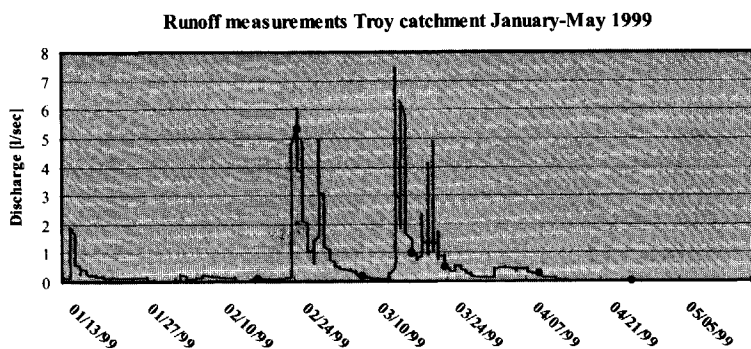


Figure B.12: Runoff records Troy catchment for the period January-May 1999.

the rapid rise of the water table towards the channel reaches. Unfortunately such rise up to the land surface is only observed by few piezometers.

II Rainfall-runoff

For analyses of the precipitation-runoff records the period January-May 1999 is selected. Runoff measurements in the Troy basin started at January 13, 1999 by a Thomson weir equipped with an automated data logger. Runoff recordings are available at regular time intervals of 15 min for the month of January till May 1999 and the observed hydrograph is presented in figure B.12. Peak flow discharges up to 7 l/sec are observed at the end of February and the second half of March while base flow discharges are at the order of 0.1 l/sec. At the end of May, base flow is not observed any more as there is no groundwater drainage into the channel. In the figure automated measurements are indicated by purple dots while manual measurements are indicated by red dots. These measurements serve for calibration purposes of the flume.

The observation records clearly show that the catchment rapidly responds to rainfall and also that depletion of the shallow subsurface rapidly takes place. By the recession curves that follow the peak flows, it is shown that within a few days after rainfall ceases flow discharges reduce to less than 0.5 l/sec.

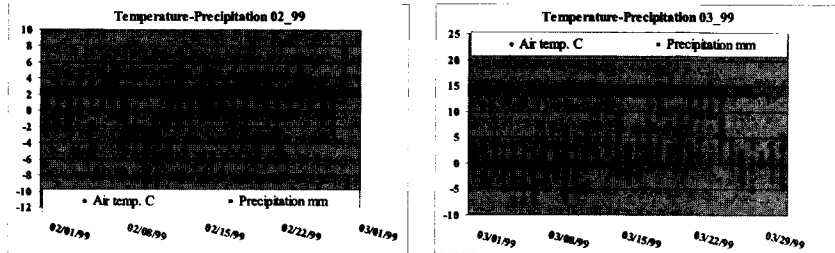


Figure B.13: *Temperature-precipitation relation for the month February/March 1999.*

By analyses of the time series it appeared that many observation gabs existed. In general, for low flow discharges only few readings were made while for periods of peak flow small gabs exist. Larger gabs even existed in recession curve recordings that, to a large extent, are due to the freezing of water in the flume as caused by the low air temperatures. Analyses of the air temperature records showed that for the entire period January-May 1999 significant periods of freezing conditions existed in the catchment. For some periods it is observed that air temperatures are above zero during day-time while temperatures drop below zero during night-time. During freezing conditions, the data recorder has made discharge recordings at a constant value or, in some cases, recordings fail and a discharge value of zero is recorded.

For the month of February and March 1999, temperature-precipitation records are presented in figure B.13. Both temperature and precipitation are observed at hourly base that, when combined, clearly show whether precipitation is as rainfall or snowfall. For analyses of the rainfall-runoff relation it is necessary to identify the meteorological circumstances that caused the runoff. For the runoff peaks shown in figure B.12 it appears that the runoff peak at the end of February primarily is caused by rainfall. Although during the night air-temperature measurements are below zero, it most likely is that any snow depth will melt immediately at the land surface. Soil temperature readings in the catchment at 10, 20 and 50 cm. depth in the subsurface have indicated that any freezing of the subsurface did not occur and that infiltration of rainfall and /or wet snow as such was not hampered.

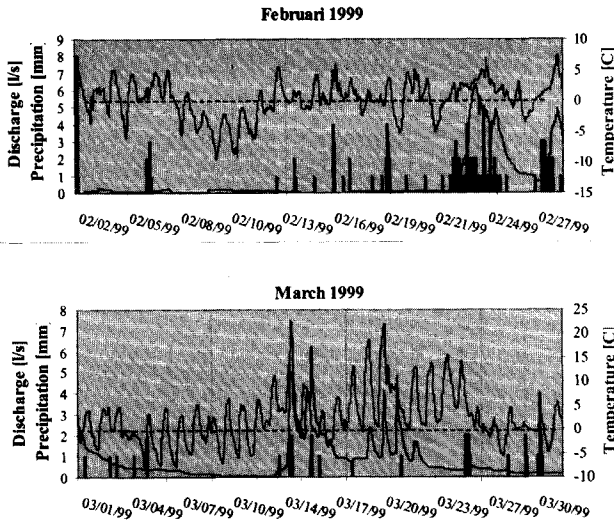


Figure B.14: *Precipitation –runoff-temperature relation for the month of February and March 1999. Precipitation depths are added for time intervals of 15 minutes.*

For the second peak flow at early March it is not clear what has caused the high discharges. While the peak flow discharge is even higher than the peak flow discharge of the first storm period, a significant long period with precipitation prior to the peak flow is not recorded. For both month the precipitation–runoff–temperature relation is graphically presented in figure B.14. It is observed that at February 21 a storm period starts that causes the development of a peak flow discharge at February 23. Analyses whether precipitation is as rainfall or snowfall are not conclusive. For the period prior to the event, it is observed that runoff observations are at a constant level without any response to the precipitation.

Precipitation therefore most likely is in the form of snowfall that remains at the land surface due to the low air temperature. At February 21 the air temperature starts to rise above zero and runoff is generated by rainfall as well as by snowmelt. At February 27 a new, but smaller peak flow discharge are observed that is due to rainfall only. For this storm period (i.e. period I) as well as a second storm period (i.e. period II) in March, the precipitation–runoff–temperature relations are given in

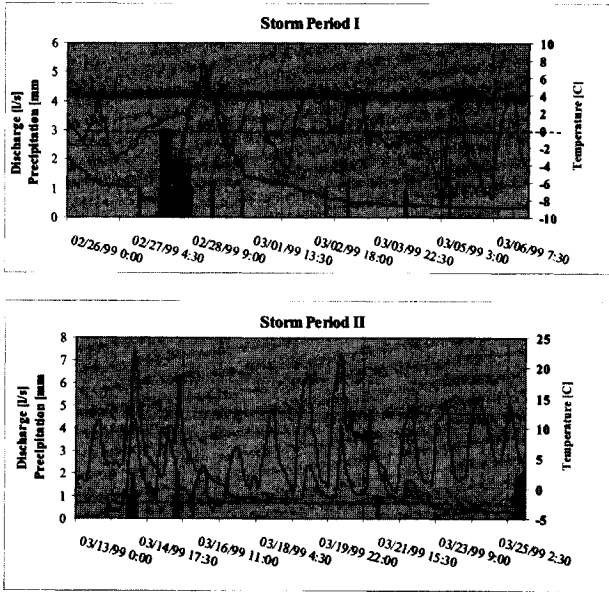


Figure B.15: *Precipitation-runoff-temperature relation for the two isolated storm periods.*

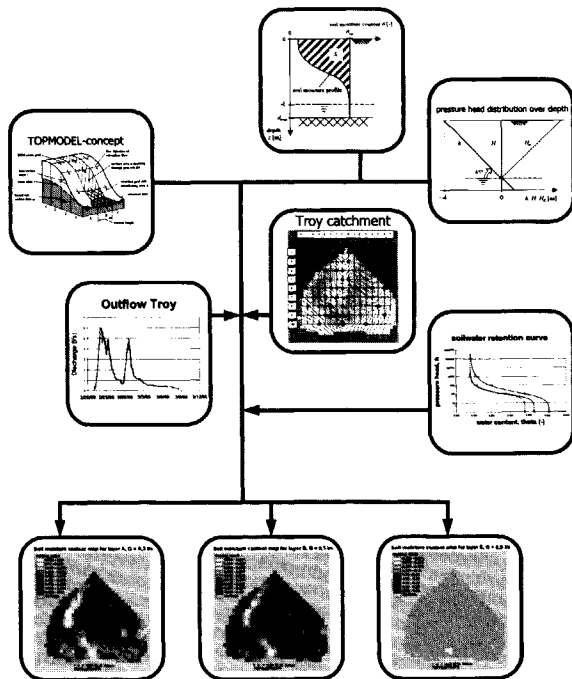
Figure B.15. Prior to period I, a constant channel flow discharge is observed. This constant discharge is due to the freezing of the weir and water discharge is not observed as such. At the first rainfall event the temperature has risen again above zero and a small part of the recession is observed. The heavy rainfall period at February 21 rapidly generates runoff. By the piezometer network analysis it is concluded that most likely saturation overland flow will be generated. The runoff volume thus is due to groundwater-river interaction and saturation overland flow. The peak discharge is reached shortly after rainfall ceases. The rapid depletion is observed at similar time span as the rainfall period and is followed by two recession periods with constant depletion rates. For storm period II the rainfall-runoff relation is less clearly defined. In this period two major runoff event are observed at March 13-14 and smaller runoff events at March 19-22. For the latter event, precipitation records show that precipitation is not observed prior to the peak flows. All 4 runoff peaks however follow periods of high day temperatures assuming that runoff is due to snowmelt. For the first two observed runoff peaks

the precipitation-runoff relation also is questionable. Compared to the runoff peaks as observed in the first period, peak runoff rates are much higher although the rainfall period is much smaller and the total rainfall depth is much smaller. The two runoff peaks however follow periods of rainfall. The precipitation-runoff-temperature relation as presented in figure B.14 shows that extensive precipitation periods did not occur between March 1 and 13 although the temperature record show day-time temperatures above zero. It therefore is concluded that the precipitation-runoff records are unreliable and that a unique rainfall-runoff relation cannot be defined. This conclusion is especially valid for the storm period II as shown in figure B.15 although, clearly, also the reliability of the data records underlying the rainfall-runoff relation as observed for the first period is uncertain.

To select a time series of channel flow discharges for the model calibration, the runoff event of the event of storm period I in figure B.15 is selected. For this event a clear catchment response to the rainfall input is observed in the channel flow record as well as in the piezometer records.

Appendix C

Initial Soil Moisture Content



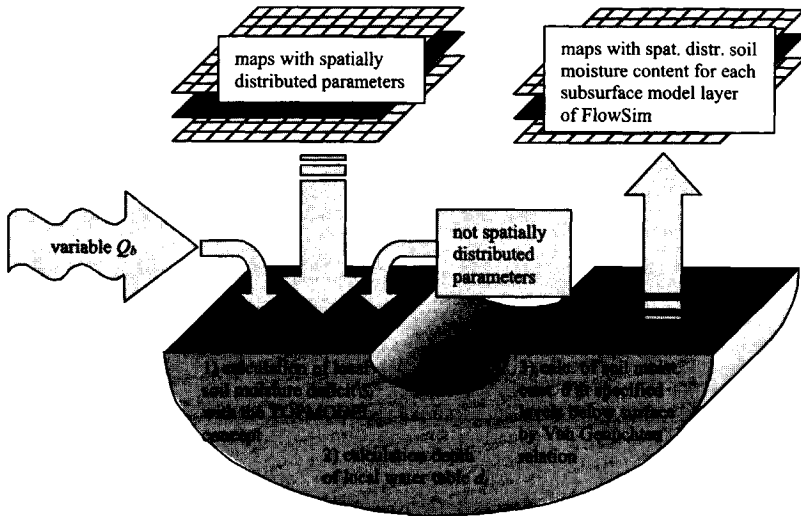


Figure C.1: Schematic of the ISMC model approach (Pilot, 2002)

For the simulation of the initial soil moisture contents in Flowsim, a pre-processing tool termed the Initial Soil Moisture Content (ISMC) model is developed by Pilot [2002] in close co-operation with the author. In this Appendix only a general description about the approach is presented, for an extensive description reference is made to Pilot [2002].

The ISMC-model approach is partly based on the Topmodel approach as introduced by Beven and Kirkby [1979]. Ever since its introduction this approach is widely applied in rainfall-runoff simulation and descriptions are presented by Sivapalan et al. [1987], [Quinn et al., 1991], Troch et al. [1993a and b], Rowan et al. [1994], Ambroise et al. [1996], Moore & Thompson [1996], Seibert et al. [1997], Lamb et al. [1997], among others. Such description will not be repeated here but only the subsurface model approach of the Topmodel approach will be elaborated on since this is adopted in the work of Pilot [2002]. In the Topmodel approach, soil moisture deficits are simulated for single storage cells that represent an entire soil column underlying a DEM element. At the core of the ISMC model this storage deficit is redistributed over the grid cells of the Flowsim model layers. A schematic of the calculation procedure is shown in figure C.1 and is further discussed here.

Subsurface storage concept

In the Topmodel approach, groundwater storage is simulated by non-linear water storages S_i across the spatially distributed model domain. For each soil column underlying a DEM grid element such store is defined from which groundwater is added and discharged through a 1-dimensional groundwater flow equation. The simplest form to describe water depletion from the non-linear store is expressed by an exponential depletion function:

$$q_b = q_0 \exp(S_i/\lambda) \quad [C.1]$$

where

$$q_0 = \text{discharge when store is fully saturated} \quad [m \text{ s}^{-1}]$$

$$q_b = \text{discharge} \quad [m \text{ s}^{-1}]$$

$$S_i = \text{local store depth} \quad [m]$$

$$\lambda = \text{scale factor.} \quad [m].$$

It is noted that positive values of S_i represent a soil moisture surplus in store i while negative values represent a deficit as compared to average soil column saturation. In the following description each store in the Topmodel is referred to as a grid cell of the distributed model domain.

Subsurface flow

In the approach is only saturated groundwater flow considered. Such flow across the grid cells is described by a Darcy type model approximation where it is assumed that, volumetrically, groundwater flow is a function of the up-slope contributing area and the area average recharge rate R :

$$q_i = a_i R \quad [C.2]$$

where

$$q_i = \text{groundwater flow through grid cell } i \quad [L^2 T^{-1}]$$

$$a_i = \text{up-slope area per unit elevation contour length} \quad [L]$$

$$R = \text{catchment average and spatially uniform recharge rate} \quad [L T^{-1}].$$

To describe groundwater flow through grid cell i , phreatic flow conditions are assumed and a Darcy type flow equation is applied:

$$q_i = T_i \frac{dh_h}{dx} \quad [C.3]$$

where

$$\begin{aligned} T_i &= \text{transmissivity in grid cell } i && [L^2 T^{-1}] \\ h_h &= \text{hydraulic head of groundwater table} && [L] \\ x &= \text{distance in flow direction} && [L]. \end{aligned}$$

For the hydraulic gradient it is assumed that steady state conditions prevail and that the hydraulic gradient of the groundwater table in grid cell i can be approximated by the local land surface slope gradient, $\tan\beta_i$, of the DEM

$$\frac{dh_h}{dx} = \tan\beta_i \quad [C.4]$$

where

$$\tan\beta_i = \text{local land surface slope gradient} \quad [-].$$

The transmissivity is equal to the product of the saturated hydraulic conductivity and the dept of the saturated flow profile. In the Topmodel approach the transmissivity is maximum when the storage deficit has reduced to zero and becomes smaller when the soil moisture deficit increases. Consequently the transmissivity T_i is described by the product of the maximum transmissivity $T_{o,i}$ of grid cell i and a scaling function that is subject to the soil moisture deficit.

$$T_i = T_{o,i} \cdot \chi(S_i) \quad [C.5]$$

where

$$\begin{aligned} T_i &= \text{actual transmissivity at grid cell } i && [L^2 T^{-1}] \\ T_{o,i} &= \text{maximum transmissivity of grid cell } i && [L^2 T^{-1}] \\ \chi(S_i) &= \text{scaling factor subject to } S_i && [-]. \end{aligned}$$

For describing the transmissivity distribution in a soil column various approaches are known. Beven [1982] states that the transmissivity in the subsurface can be described by an exponential transmissivity profile while Ambrose et al. [1996] also consider parabolic and linear profiles. In these profiles (see Figure C.2) the distribution of the saturated hydraulic conductivity in a soil column is described by exponential, parabolic and linear approximations. In the approximation of the exponential and parabolic profiles it is assumed that the decrease is due to soil compaction.

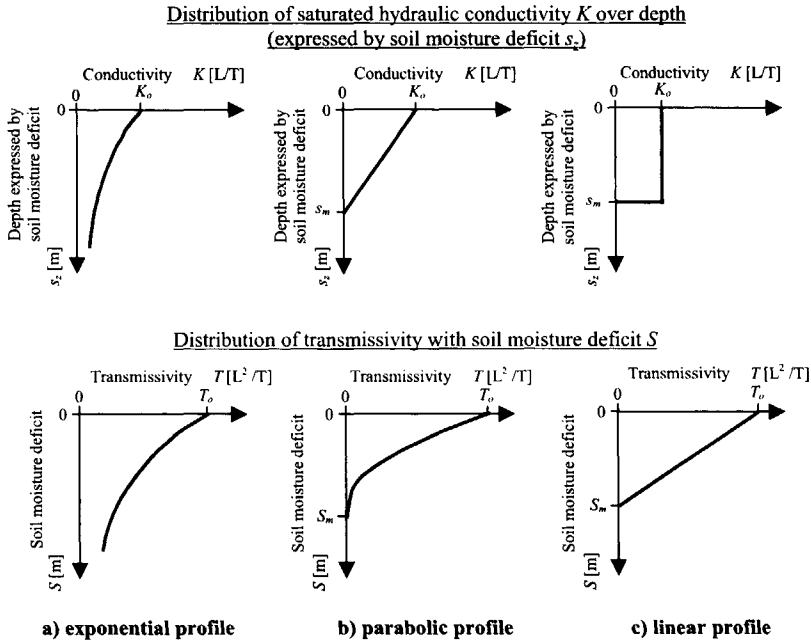


Figure C.2: Schematic showing the saturated hydraulic conductivity and the transmissivity as function of the storage deficit (Ambrose et al., 1996).

For describing the distribution of the saturated hydraulic conductivity and the transmissivity over depth the following expressions are developed (Ambrose et al., 1996):

Exponential	parabolic	Linear	
$K_{s,i}(z) = K_{o,i} \exp\left(-\frac{S_z}{m_i}\right)$	$K_{s,i}(z) = K_{o,i} \left(1 - \frac{S_z}{S_{m,i}}\right)$	$K_{s,i}(z) = K_{o,i}$ for $0 \leq S_z \leq S_{m,i}$	[C.6]

$T_i(S_i) = T_{o,i} \exp\left(-\frac{S_i}{m_i}\right)$	$T_i(S_i) = T_{o,i} \left(1 - \frac{S_i}{S_{m,i}}\right)^2$	$T_i(S_i) = T_{o,i} \left(1 - \frac{S_i}{S_{m,i}}\right)$	[C.7]
--	---	---	-------

where:

- $K_{s,i}(z)$ = saturated hydraulic conductivity as function of s [L T⁻¹]
- $K_{o,i}$ = saturated hydraulic conductivity when $S_i = 0$ [L T⁻¹]
- S_z = depth z expressed by the soil moisture storage deficit [L]
- m_i = rate of exponential decrease of K_s with S [L]
- $S_{m,i}$ = maximum local soil moisture storage deficit [L].

For defining the saturated hydraulic conductivity for a grid cell, the soil moisture deficit is used as depth indicator in stead of using a metric depth scale. A large deficit is indicative for a relatively deep water table and thus, in case of an exponential or parabolic distribution, a small $K_{s,i}$ value. In the expressions of the transmissivity it is assumed that $K_{s,i}$ is integrated over the thickness of the saturated subsurface. A schematic of Eq's [C.6] and [C.7] is shown in figure C.1. Extensive descriptions about the approaches are presented in Sivapalan et al. [1987], Wolock [1995b], Ambroise et al., [1996], Moore & Thompson [1996], Beven [1997] and Pilot [2002].

To simulate groundwater flow at any grid cell the following expressions are developed by combining Eq's [C.7], [C.3] and [C.4]:

<i>Exponential</i>	<i>parabolic</i>	<i>Linear</i>
$q_i = T_{o,i} \exp\left(-\frac{S_i}{m_i}\right) \tan\beta_i$	$q_i = T_{o,i} \left(1 - \frac{S_i}{S_{m,i}}\right)^2 \tan\beta_i$	$q_i = T_{o,i} \left(1 - \frac{S_i}{S_{m,i}}\right) \tan\beta_i$

 [C.8]

After introducing the relative local soil moisture deficit δ_i this gives

<i>Exponential</i>	<i>parabolic</i>	<i>linear</i>
$q_i = T_{o,i} \exp(-\delta_i) \tan\beta_i$	$q_i = T_{o,i} (1 - \delta_i)^2 \tan\beta_i$	$q_i = T_{o,i} (1 - \delta_i) \tan\beta_i$

 [C.9]

where

<i>exponential</i>	<i>parabolic</i>	<i>linear</i>
$\delta_i = S_i/m_i$	$\delta_i = S_i/S_{m,i}$	$\delta_i = S_i/S_{m,i}$

Combining Eq's [C.1] and [C.10] and when rewriting for S_i an expression is obtained in which the local soil moisture deficit becomes a function of the topographic index, $a_i/\tan\beta_i$, the selected transmissivity profile, $T_{o,i}$, the local maximum soil moisture storage deficit, $S_{m,i}$, and the recharge rate, R :

<i>Exponential</i>	<i>parabolic</i>	<i>Linear</i>
$S_i = m_i - \ln\left(\frac{a_i R}{T_{o,i} \tan\beta_i}\right)$	$S_i = S_{m,i} \left(1 - \sqrt{\frac{a_i R}{T_{o,i} \tan\beta_i}}\right)$	$S_i = S_{m,i} \left(1 - \frac{a_i R}{T_{o,i} \tan\beta_i}\right)$

 [C.10]

In the approach it is assumed that for the recharge rate, R , the catchment average recharge rate must be substituted that is obtained when Eq.[C.10] is rewritten for R :

$$\begin{array}{ccc}
 \text{Exponential} & \text{parabolic} & \text{Linear} \\
 -\ln(R) = \delta_i + \ln\left(\frac{a_i}{T_{o,i} \tan \beta_i}\right) & \sqrt{R} = \left(1 - \frac{S_i}{S_{m,i}}\right) \sqrt{\frac{T_{o,i} \tan \beta_i}{a_i}} & R = \left(1 - \frac{S_i}{S_{m,i}}\right) \frac{T_{o,i} \tan \beta_i}{a_i}
 \end{array} \quad [C.11]$$

In resemblance to the expressions of Eq.[C10] the catchment average soil moisture store deficits can be defined. Such values are obtained through space integration of Eq.[C10]:

$$\begin{array}{l}
 \text{exponential: } \bar{S}_i = \frac{1}{A} \int_A \left\{ -m_i \left(\ln\left(\frac{a_i}{T_{o,i} \tan \beta_i}\right) + \ln(R) \right) \right\} dA \\
 \text{parabolic: } \bar{S}_i = \frac{1}{A} \int_A \left(S_{m,i} - S_{m,i} \sqrt{\frac{a_i}{T_{o,i} \tan \beta_i}} \sqrt{R} \right) dA \\
 \text{linear: } \bar{S}_i = \frac{1}{A} \int_A \left(S_{m,i} - S_{m,i} \frac{a_i}{T_{o,i} \tan \beta_i} R \right) dA
 \end{array} \quad [C.12]$$

Substitution of integrated values for m_i and S_m in Eq.[C12] yields:

$$\begin{array}{l}
 \text{exponential: } \bar{S}_i = \frac{1}{A} \int_A -m_i \ln\left(\frac{a_i}{T_{o,i} \tan \beta_i}\right) dA + \bar{m}_i \frac{1}{A} \int_A -\ln(R) dA \\
 \text{parabolic: } \bar{S}_i = \bar{S}_{m,i} - \frac{1}{A} \int_A S_{m,i} \sqrt{\frac{a_i}{T_{o,i} \tan \beta_i}} dA \cdot \frac{1}{A} \int_A \sqrt{R} dA \\
 \text{linear: } \bar{S}_i = \bar{S}_{m,i} - \frac{1}{A} \int_A S_{m,i} \frac{a_i}{T_{o,i} \tan \beta_i} dA \cdot \frac{1}{A} \int_A R dA
 \end{array} \quad [C.13]$$

By substitution of the catchment average topographic index and the catchment average recharge rate of Eq. [C.11] this results in:

$$\begin{array}{l}
 \text{exponential: } \bar{S}_i = -\bar{m}_i \ln\left(\frac{a_i}{T_{o,i} \tan \beta_i}\right) + \bar{m}_i \left(\frac{S_i}{m_i} + \frac{m_i \ln\left(\frac{a_i}{T_{o,i} \tan \beta_i}\right)}{m_i} \right) \\
 \text{parabolic: } \bar{S}_i = \bar{S}_{m,i} - S_{m,i} \sqrt{\frac{a_i}{T_{o,i} \tan \beta_i}} (S_{m,i} - S_i) \frac{1}{S_{m,i} \sqrt{\frac{a_i}{T_{o,i} \tan \beta_i}}}
 \end{array} \quad [C.14]$$

$$\text{linear: } \bar{S}_i = \bar{S}_{m,i} - \left(S_{m,i} \frac{a_i}{T_{o,i} \tan \beta_i} \right) (S_{m,i} - S_i) \frac{1}{S_{m,i} \frac{a_i}{T_{o,i} \tan \beta_i}}$$

In the Topmodel approach it is assumed that the base flow can be calculated by an exponential subsurface depletion function:

<i>exponential</i>	<i>parabolic</i>	<i>linear</i>	
$Q_b = Q_o \exp\left(-\frac{\bar{S}_i}{m_i}\right)$	$Q_b = Q_o \left(1 - \frac{\bar{S}_i}{S_{m,i}}\right)^2$	$Q_b = Q_o \left(1 - \frac{\bar{S}_i}{S_{m,i}}\right)$	[C.15]

where Q_o is the channel flow discharge when the relative catchment averaged soil moisture store deficit = 0. Q_o follows the expressions:

<i>exponential</i>	<i>Parabolic</i>	<i>Linear</i>
$Q_o = A \exp\left(-\frac{m_i \ln\left(\frac{a_i}{T_{o,i} \tan \beta_i}\right)}{m_i}\right)$	$Q_o = A \frac{(S_{m,i})^2}{\left(S_{m,i} \sqrt{\frac{a_i}{T_{o,i} \tan \beta_i}}\right)^2}$	$Q_o = A \frac{\bar{S}_{m,i}}{\left(S_{m,i} \frac{a_i}{T_{o,i} \tan \beta_i}\right)}$

The expression of the local soil moisture storage deficit now is obtained by combining Eq's [C.14] and [C.15] and by rearranging:

$$\text{exponential: } S_i = m_i \left[\frac{m_i \ln\left(\frac{a_i}{T_{o,i} \tan \beta_i}\right)}{m_i} - \frac{m_i \ln\left(\frac{a_i}{T_{o,i} \tan \beta_i}\right)}{m_i} - \ln\left(\frac{Q_b}{Q_o}\right) \right]$$

$$\text{parabolic: } S_i = S_{m,i} - \bar{S}_{m,i} \frac{S_{m,i} \sqrt{\frac{a_i}{T_{o,i} \tan \beta_i}}}{S_{m,i} \sqrt{\frac{a_i}{T_{o,i} \tan \beta_i}}} \sqrt{\frac{Q_b}{Q_o}} \quad [C.16]$$

$$\text{linear: } S_i = S_{m,i} - \bar{S}_{m,i} \frac{S_{m,i} \frac{a_i}{T_{o,i} \tan \beta_i}}{\left(S_{m,i} \frac{a_i}{T_{o,i} \tan \beta_i}\right)} \frac{Q_b}{Q_o}$$

As can be concluded from Eq.[C.16] the local soil moisture deficit is a function of the base flow discharge, the topographic index, the local and catchment averaged maximum storage deficit and the selected transmissivity profile. In the ISMC approach, Eq.[C.16] is at the core of the mathematical model and is used to simulate the local soil moisture deficit at grid cells across the DEM grid layer. By applying spatially variant values for the selected soil moisture profile and topographic indexes the approach of [Pilot 2002] differs from previous approaches by e.g. Sivapalan et al. [1987], [Quinn et al., 1991], Wolock [1995b], Ambroise et al., [1996], Moore & Thompson [1996], Seibert et al. [1997], Lamb et al. [1997].

Redistribution of S_i and calculation of θ

Since the local soil moisture deficit represents a lumped value for the water store underlying a DEM grid element, such deficit must be redistributed across the cells that make up a column of grid cells of the subsurface flow model of Flowsim. In such manner the outcome of ISMC forms the initial soil moisture condition for the 3-dimensional subsurface model domain of Flowsim.

In the redistribution scheme the local soil moisture deficit S_i is converted into a water table depth, d_i , for any column of grid cells. Given the fixed value of S_i , and based on mass conservation considerations, the calculated water table depth is subject to the soil moisture distribution in the subsurface. In Flowsim the Van Genuchten relations are selected to simulate the soil characteristic curves and thus these relations also are selected in the ISMC approach to describe the soil moisture distribution across a column of grid cells. By an iteration procedure the value of S_i is matched to a soil moisture deficit value for a column as defined by the Van Genuchten relation, $S_{i,VG}$. In this procedure the calculated water table depth is updated until a satisfactory match is obtained and thus the soil water storage deficit volumes $S_{i,VG} \approx S_i$. In the following this procedure will be explained.

Through the Van Genuchten relation any soil moisture content θ is uniquely related to a given pressure head. With respect to the pressure head distribution over depth it is assumed that the entire soil profile is at field capacity. Combining the assumed distribution of the pressure head over depth and the soil characteristic relation $h - \theta$, it is possible to estimate a soil moisture profile for any given d_i .

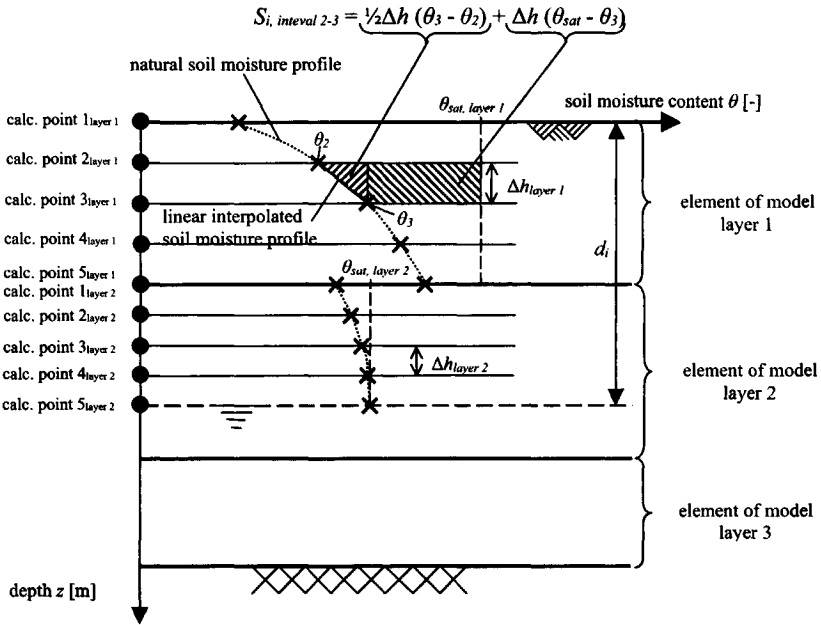


Figure C.3: Schematic of the calculation of $S_{i, VG}$ in a subsurface column. In this example the model exists of three subsurface model layers, each with different characteristics. The water table is at depth d_i below the land surface. In each point is θ calculated and across these points the deficit is integrated. The grid cell of the third layer is situated below the water table and the soil moisture content is equal to the saturated soil moisture content. (Pilot, 2002)

For the simulation of the subsurface geometry, the discretisation method of Flowsim is adapted where for each DEM grid element a column of grid cells of varying depth is simulated. In the ISMC approach, however, every unsaturated element is once more subdivided by a number of calculation points. These points are located at the top and bottom of the grid cells and at places equally distributed in between these points. In the element at which the water table is situated are calculation points not equally distributed but distributed between the water table elevation and the top of the element. By this approach the lowest calculation point always corresponds to the water table elevation. Figure C.3 shows a diagram with three model layers.

The soil moisture deficit is defined as the saturated soil moisture content minus the actual soil moisture content, $\theta_s - \theta$. In the code the calculation

procedure is implemented in several steps. The code starts with the calculation of the value of h of the highest calculation point in the highest element, after which the actual soil moisture content θ is defined through the Van Genuchten relation. Then these two calculation steps are repeated for the calculation point below the previous one. Next step is the calculation of the deficit over the interval between these two points. In figure C.3 also the principle of the deficit calculation between the points 2-3 in the top layer is shown. Between both points $\theta_s - \theta$ is integrated over depth by applying a linear interpolation function for the actual soil moisture content. The calculated deficit is added to the total deficit of the column. These steps are repeated for the calculation point within a grid cell after which the procedure is repeated for the following grid cell. The calculation procedure terminates when the water table is reached. The soil moisture deficit over the entire column, $S_{i,VG}$, then is summed and compared to S_i as simulated by the Topmodel approach. The accuracy of the match thus also depends on the number of calculation points that, in the ISMC computer code, can be pre-selected.

Three specific cases that do not require the calculation of $S_{i,VG}$ are the following:

1. If $Q_b = 0 \text{ m}^3/\text{s}$ and the modeller has chosen to apply the exponential transmissivity profile then $\ln(0)$ and thus S_i cannot be defined. For such cases the depth to the water table d_i is equal to its maximum $d_{\max,i}$ that is the total depth of the subsurface model layers.
2. If $S_i \leq 0 \text{ m}$. the grid cell is saturated and thus $d_i = 0 \text{ m}$.
3. If $S_i \geq S_{m,i,VG}$ the code assigns the value of $d_{\max,i}$ to d_i .

The iteration procedure is based on minimisation of the objective function value by least root square estimation:

- A new value for d_i is defined based on :

$$d_{i,1} = d_{i,0} \sqrt{\frac{S_i}{S_{i,VG,0}}} \quad [C.17]$$

Start values for the iteration are: $d_{i,0} = d_{\max,i}$ and $S_{i,VG,0} = S_{m,i,VG}$.

- The previous step results in $d_{i,1} = d_{i,0}$ when $S_{i,VG,0} = S_i$. Therefore the code exits the iteration procedure when

$$\sqrt{(d_{i,1} - d_{i,0})^2} \leq 0.0000001 \quad [C.18]$$

Based on this simple iteration procedure the ISMC computer code quickly calculates the value of d_i for which the soil moisture deficit under field capacity conditions is equal to S_i . The soil moisture content $\theta_{i,layer}$ of every Flowsim subsurface grid cell can now be defined by summing the soil moisture contents within the calculation points of a grid cell. For a grid cell that is situated below the water table $\theta_{i,layer} = \theta_{i,sat,layer}$ becomes valid. For cells of unsaturated soil profile the total moisture content $\theta_{i,ayer}$ is defined by:

$$\theta_{i,layer} = \frac{1}{n-1} \left(\frac{1}{2} \theta_1 + \theta_2 + \dots \dots + \theta_{n-1} + \frac{1}{2} \theta_n \right) \quad [C.19]$$

where

- $\theta_{i,layer}$ = average soil moisture content of subsurface element [-]
 θ_j = soil moisture content in calculation point i [-]
 n = number of calculation points in one element.

The calculation points 1 and n are located at the top and bottom boundary of the element and are $\frac{1}{2}$ the height of the other calculation points in a grid cell. For the grid element in which the water table is situated equation, C.20 also is applied where the saturated soil moisture contents are applied to point that fall within the saturated cell domain.

The ISMC model is extensively tested for various combinations of parameter input data that are the selected transmissivity profile, the values for S_m or m and T_o and the base flow discharge value. Also a selection can be made whether the spatially distributed parameter are variant or invariant. Simulation results and a model sensitivity analyses are described by Pilot [2002]. For this thesis only two model simulations are considered that serve as the initial soil moisture condition for Flowsim. The output of these two simulations are also shown in section 6.3 and represent a relatively 'dry' and 'wet' initial soil moisture condition. Case I is obtained by $Mc=9b$ with $S_m=0.34$, $T_o=0.52$ and $Q_b=0.42$ while Case II is calculated by $Mc=8b$ applying the following parameters values. $Mc=8b$, $S_m=0.5$, $T_o=5$, $Q_b=0.65$.

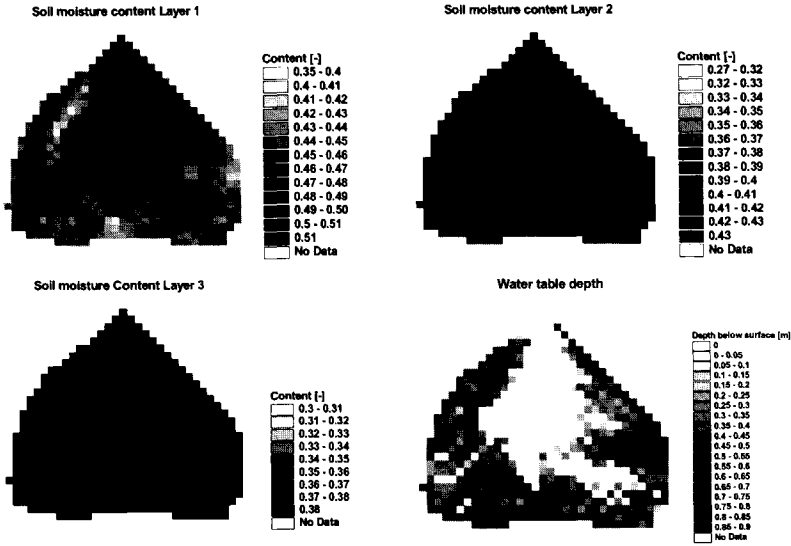


Figure C.4a: Soil moisture distribution Case 1.

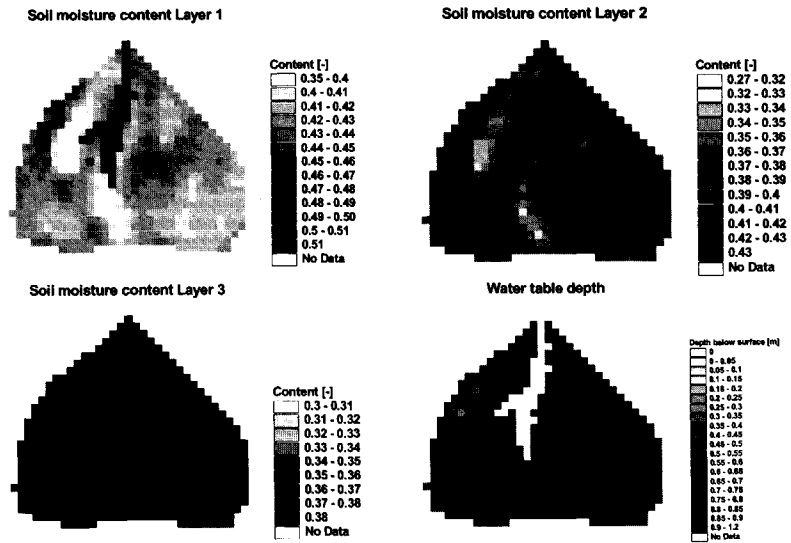


Figure C.4b: Soil moisture distribution Case 2.

In this appendix the simulation results of MLE are presented. For the eight cases graphical output from the PEST-software is shown and discussed. Graphical output deals about output graphs such as the parameter value evolution over the number of optimisation step, the residual vs. observed values, matrices of the parameter co-variances, correlations and eigen-vectors and about histograms such as the Jacobian and eigen-values. Detailed mathematical analysis of these output data for all eight cases are not presented here but instead the analysis are much more focussed on a comparison of the model result for the eight cases.

With respect to the output data a number of conclusions are drawn. The most important conclusion is that the application of the MLE by PEST-software is able to optimise parameter values for each of the selected cases. Optimised parameter values for the eight cases however show a, relatively, wide value range as shown in table 6.6. Optimised values are subject to the selected state variables that are used for calibration (see tables 6.4a,b; 6.5) and also are subject to the selected initial soil moisture condition as shown in figures 6.16a,b. In figure 6.18a the observed channel flow hydrograph is compared to the simulated hydrograph of the two cases where parameter values are not optimised. In figure 6.18b the observed channel flow hydrograph is compared to the simulated hydrograph of the eight parameter-optimisation cases. By this figure it is clear that for none of the optimisation cases the hydrographs match well with the observed hydrograph. Such matching is best for the cases Ch_1 and Ch_2 in which only observations of the channel discharges are applied to the calibration. For both cases the peak runoff rate is underestimated while the recession limb of the hydrograph is overestimated. Case Ch_1 represents the 'wet' initial soil moisture condition and shows that the size of the saturation overland flow area as simulated prior to the Flowsim simulation has a much more pronounced effect on the simulated hydrograph as compared to case Ch_2. Also, the recession period is much longer as compared to the field observation. This suggests that observations of the peak flow discharge have a more pronounced effect on the parameter optimisation as compared to observations of the recession limb and base flow. Compared to the non-optimised cases Case_1 and Case_2 it proves that the simulated recession limb is significantly affected by the observations of the channel flow discharges that are applied to the calibration. Recession in both non-optimised cases is rapid and in more correspondence with the field

observations. With respect to the optimised values of the hydraulic conductivity for the eight cases, these are highest for Case Ch_1 and second highest for Case Ch_2. These comparatively high values cause that groundwater flow from the up-slope areas to the down-slope area is relatively rapid and that soil saturation near the channel advances over a relatively short period of time.

With respect to PEST output, significant differences are observed. Through the Jacobian matrix it is concluded that parameter sensitivity with respect to the observed channel discharges differs. For case Ch_2 it is observed that the model is sensitive to all 9 parameters. For both cases it is shown that the model sensitivity towards the porosity dominates the optimisation and also that, generally speaking, observations of the rising limb have a more pronounced effect on the parameter optimisation. Analysis of the residuals show that calculated counterparts for observed channel flow discharges for most observations are lower. This also is shown in figure 6.17. With respect to the covariance, the correlation coefficient and the eigen-vector - eigen-values matrices, also here differences are observed. Through the covariance and correlation matrices it is shown that the spatial dependencies between parameters change, particularly for the porosity of all three layers. In case Ch_1, the parameters por2 and por3 (i.e. porosity of layer 2 and 3) are positively correlated while in case Ch_2 these are negatively correlated. Also, parameters por1 and por3 in case Ch_1 are negatively correlated while the opposite is observed for case Ch_2. By the size of the symbols the magnitude of the correlation coefficients is expressed. By comparison of both cases it becomes apparent that the correlation coefficients change significantly.

With respect to the eigen-vector and eigen-value analysis also a significantly different output is shown. Besides the fact that eigen-vectors are dominated by different model parameters also eigen-vectors are differently composed. Since only the initial soil moisture condition was changed for both cases, any of the described difference must be attributed to this condition as entered to the model. By the change of the initial condition, a dissimilar saturated zone groundwater flow behavior is simulated resulting in a change of the available storage volume of the subsurface layers and the size of the saturation overland flow source area. By this reasoning, it is concluded that different parameter combinations dominate the automated calibration procedure as subject

to the initial condition. Hence, general conclusions on parameter inter-dependencies and parameter identifiability are difficult to formulate.

Also for the cases ChGws_1 and ChGws_2 in which channel discharge observations are combined with piezometer observations, only conclusions with respect to the specific cases can be drawn. An important conclusion based on the Jacobian matrices is that for both cases the piezometer observations dominate the parameter optimisation and that observations of the channel flow discharges hardly have an effect on the optimised parameter values. This dominance could possibly be explained by the fact that all observations are equally weighted in the optimisation although the magnitude of discharge values is much smaller compared to the piezometer observation values. The Jacobian matrices of both cases shown small differences compared to the Jacobian matrices for the cases Gws_1b and Gws_2b respectively. In the latter cases the same piezometer observations are used for model calibration while observations of the channel flow discharges are excluded. The optimised parameter values for the cases ChGws_1 and Gws_1b and the cases ChGws_2 and Gws_2b only show very small differences while the calculated channel flow hydrographs for these respective cases mostly overlap. As such similar conclusions can be drawn for the cases ChGws_1 and Gws_1b and cases ChGws_2 and Gws_2b.

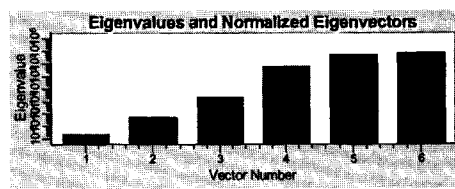
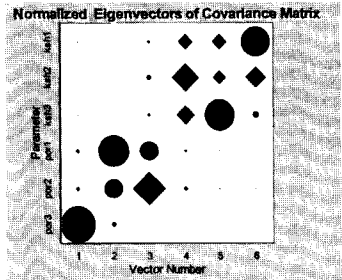
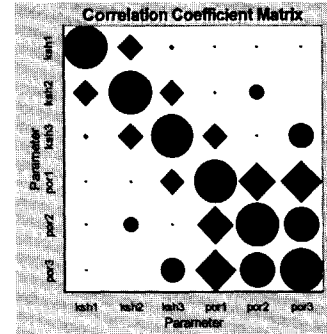
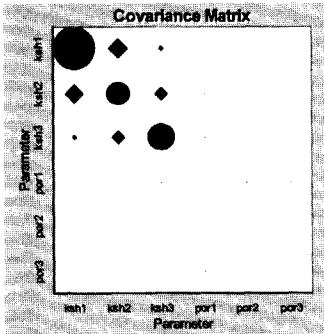
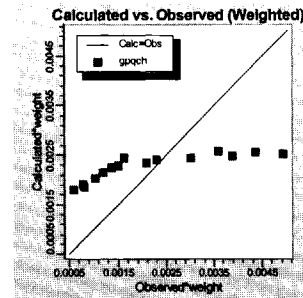
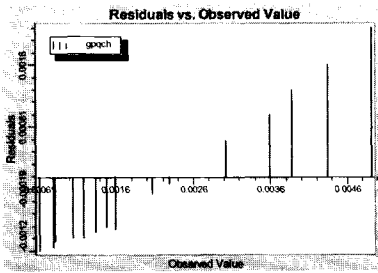
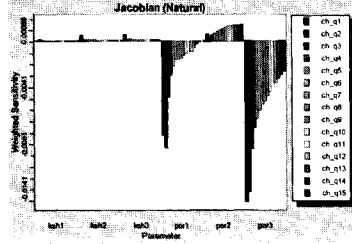
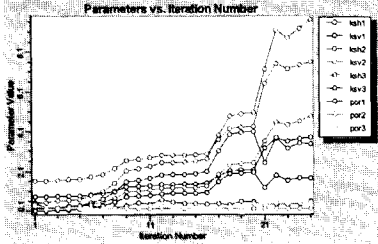
With respect to the cases Gws_1b and Gws_2b only the initial soil moisture content differs and any change in model outcome must be related to the entered initial condition. In table 6.6 significant differences are observed in the optimised parameter values. Saturated hydraulic conductivity values as well as porosity values differ although optimised values lie within the same order of magnitude. The Jacobian matrix shows similar model sensitivities towards the same parameters. Also the graphs of Calculated vs. Observed values show a similar pattern. Differences in model results, however, are observed in the covariance - correlation matrices and the eigen-value eigen-vector matrices. The parameter structure by means of the correlation matrix shows significant differences. In case Gws_1b the saturated hydraulic conductivity shows significant correlation to other hydraulic conductivities while such dependency towards the porosity is much smaller. Also the mutual correlations are much smaller while correlation coefficients for case Gws_2b generally are much smaller compared to case Gws_1b. It is surprising that the plus and minus signs (i.e. red circle and blue diamond

respectively) of some parameter correlations change between cases. Compared to the real world catchment characteristics such result is unexpected. With respect to the eigen-value and eigen-vector matrices also some differences occur. In the eigen-vector matrix the dominance of single parameters changes and thus parameters are not consistently identified but are subject to the initial soil moisture condition. Clearly this condition has a large effect on the groundwater table depth within columns of subsurface cells. By this depth the groundwater flow behaviour is effected and thus the change of the water table depth throughout the simulation. Following this reasoning it is obvious that different parameter combinations come in effect during a simulation and as such different optimised parameter values are calculated. Contradictory to this reasoning, the fact remains that large differences in the residual errors are not observed.

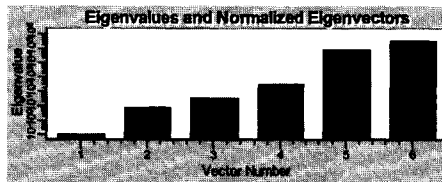
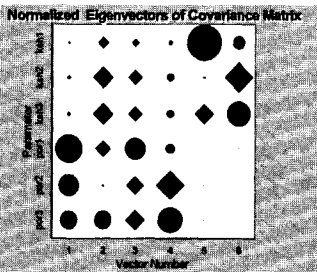
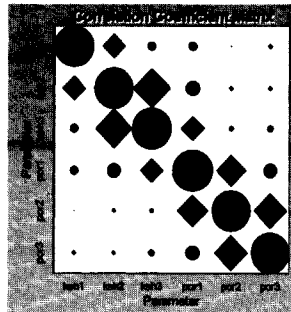
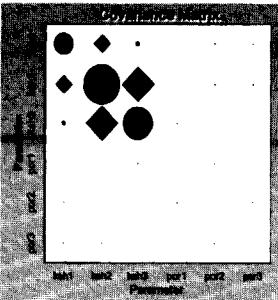
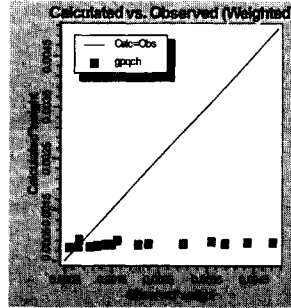
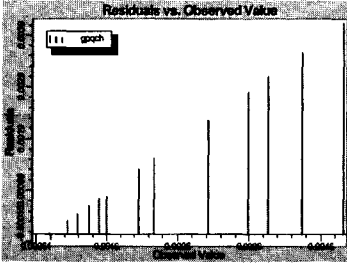
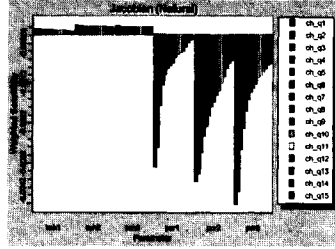
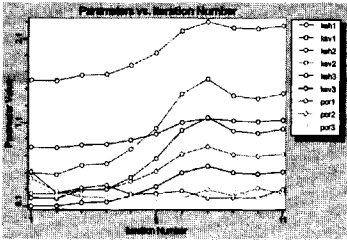
When comparing the results of cases Gws_1a and Gws_2a it is observed that also for these cases differences occur. With respect to the residuals, in case Gws_2a few outliers are observed. A comparison of both Jacobian matrices also shows some differences. In case Gws_2a model sensitivity towards parameters is much more pronounced. With respect to the previously mentioned outliers, such outliers in the Jacobian matrix are not observed at the end of the simulation. Observations with respect to the correlation and covariance matrices are similar to those made for the cases Gws_1b and Gws_2b. Besides the fact that the magnitude of the parameter dependency in terms of correlations change for both cases, also the plus and minus sign change for some parameters. Correlations for case Gws_1a generally are lower as compared to case Gws_2a and are not in correspondence with the observations for the cases Gws_1b and Gws_2b. Also the eigen-value and eigen-vector matrices show some differences. In the normalized eigen-vector matrices, parameters are not equally identified. Particular for the eigen-vectors with the lowest eigen-values differences show up while such difference are not shown for vectors 4, 5 and 6. For these vectors, however, the sign changes for some parameters. By a comparison of model results of all four cases in which only piezometer observations are used for model calibration it becomes evident that model result are diverse. General conclusions on parameter dependencies through the calculation of parameter correlation matrices are difficult to formulate. Such conclusion(s) on parameter identifiability as based on the eigen-value and eigen-vector matrices also are difficult to

make. It is however concluded that porosity values dominate the eigenvectors and thus porosity values are better identified than hydraulic conductivity values. Also, porosity values of the deeper and thus fully saturated subsurface layers (i.e. por_2 and por_3) are better identified compared to the porosity of the top layer.

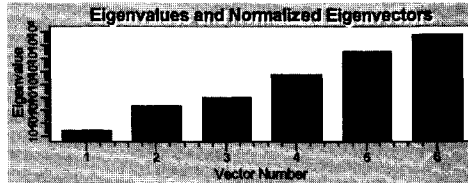
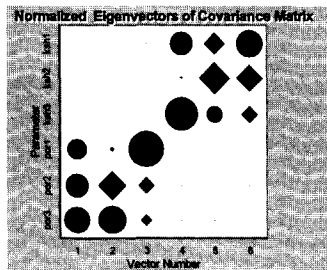
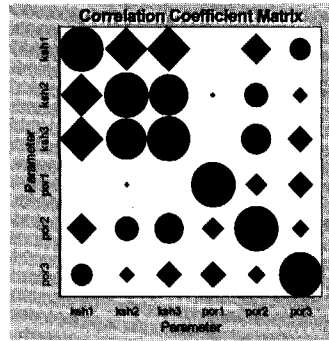
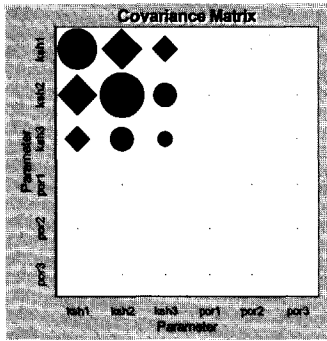
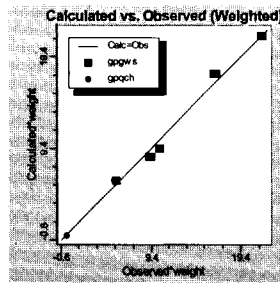
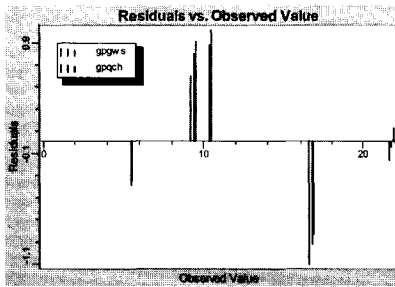
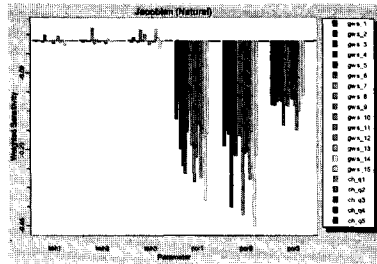
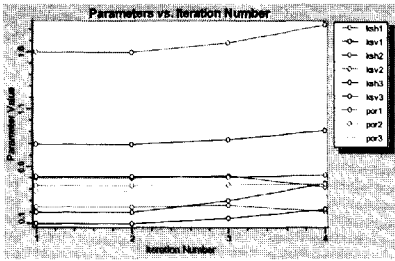
Case Ch_1



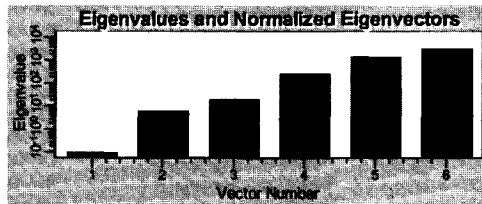
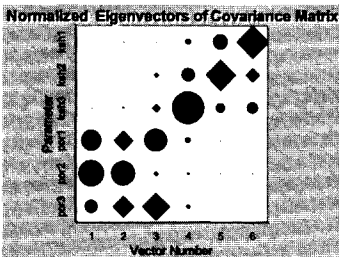
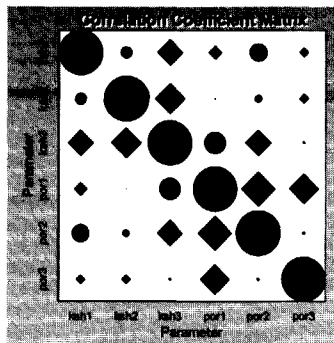
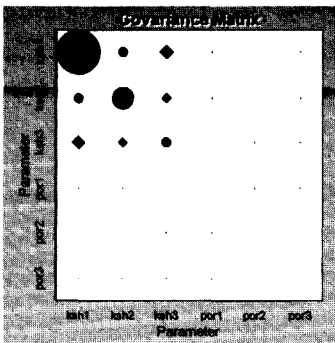
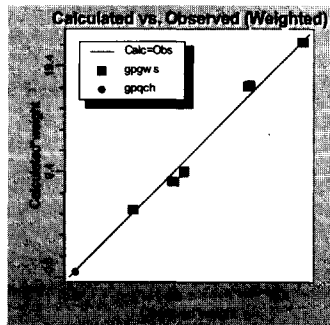
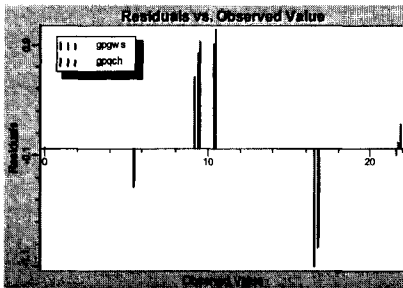
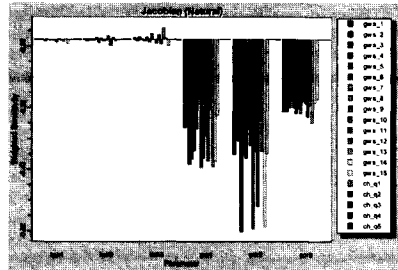
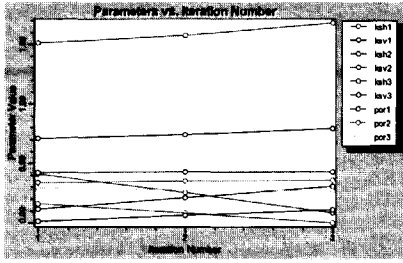
Case Ch_2



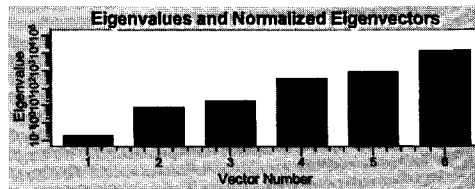
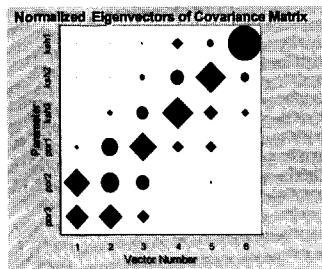
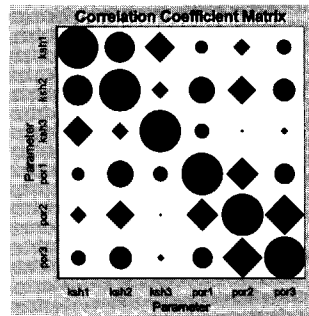
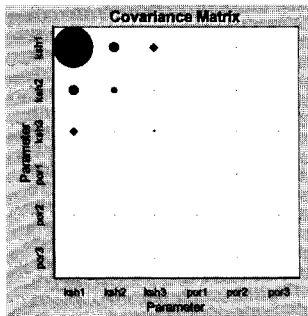
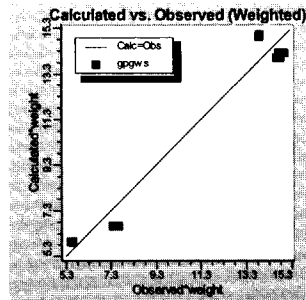
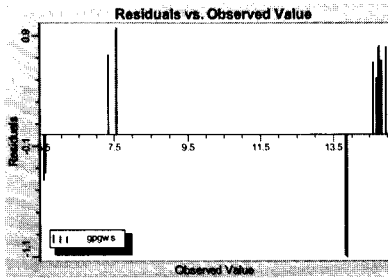
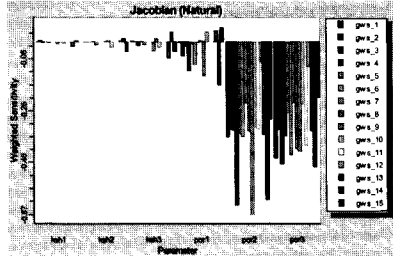
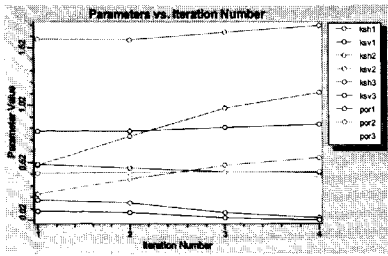
Case ChGws_1



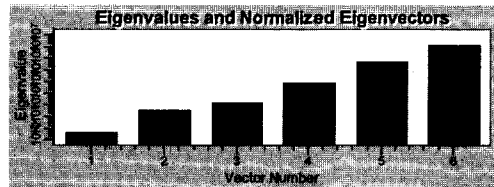
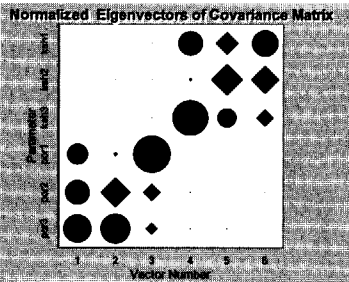
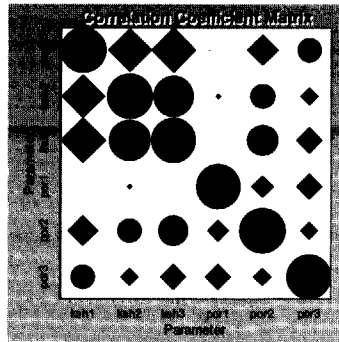
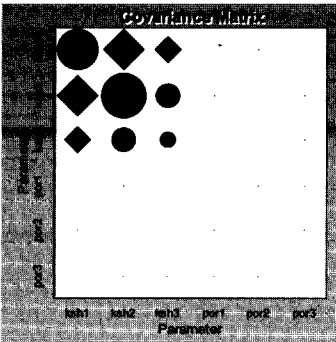
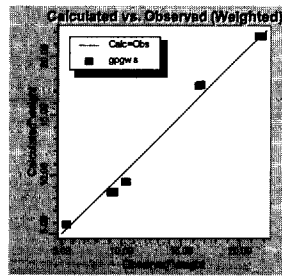
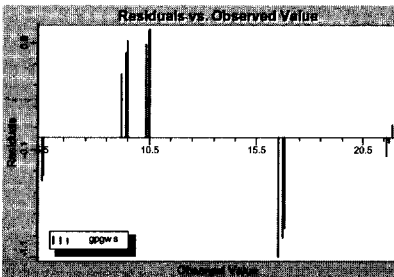
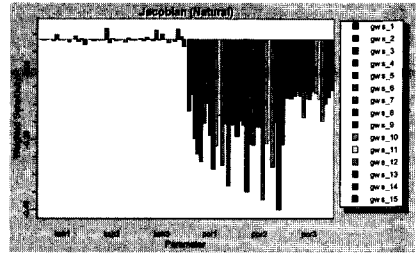
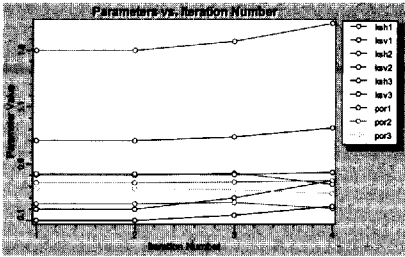
Case ChGws_2



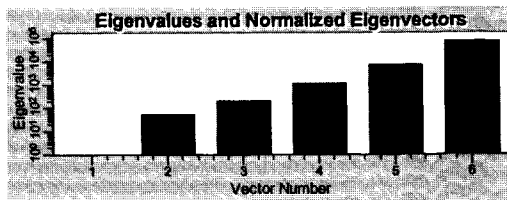
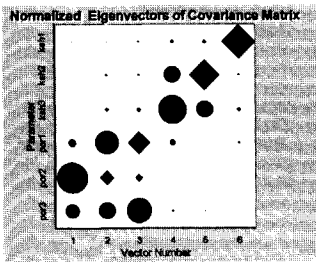
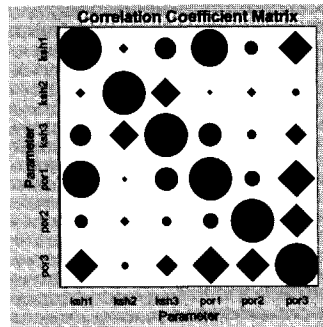
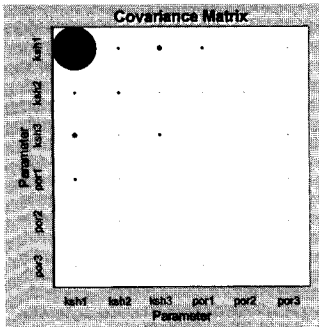
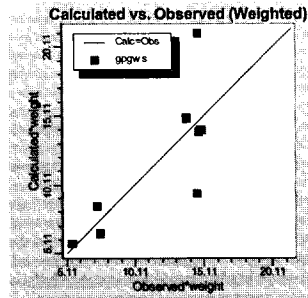
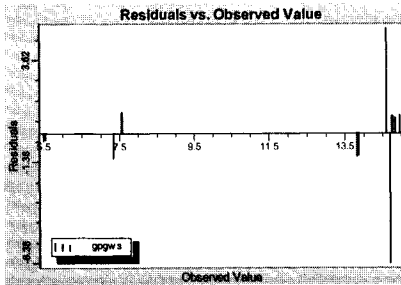
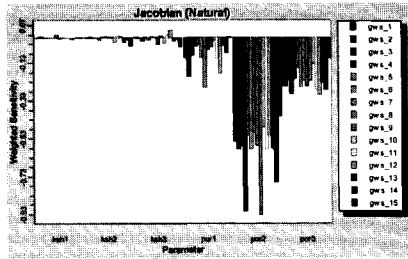
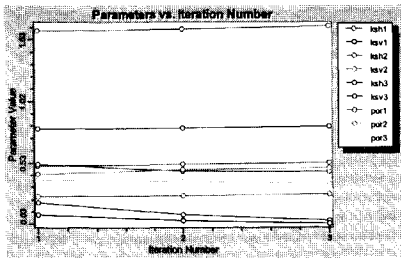
Case Gws_1a



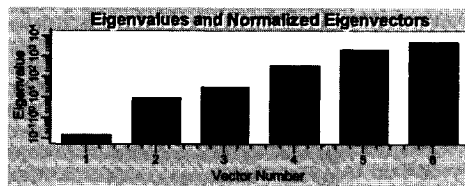
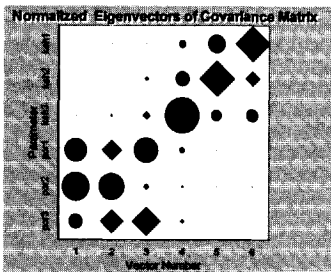
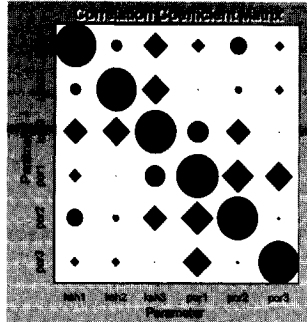
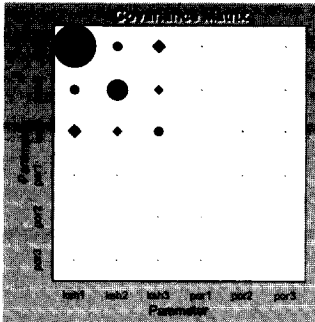
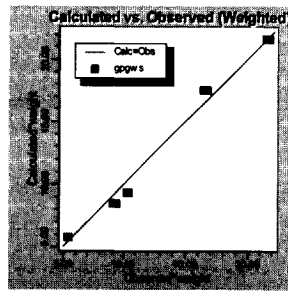
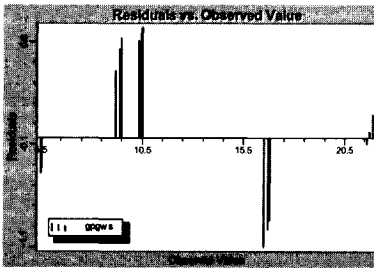
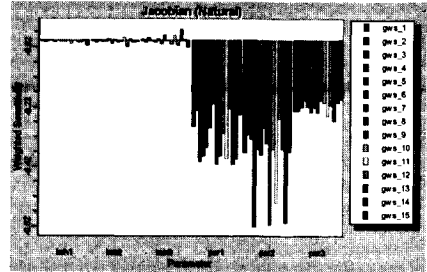
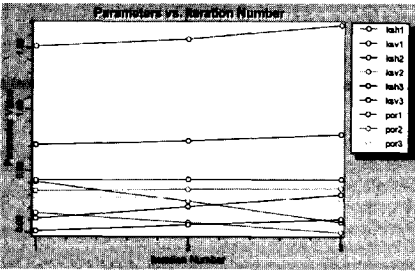
Case Gws_1b



Case Gws_2a



Case Gws_2b



Inverse modelling of the rainfall-runoff relation. A multi objective model calibration approach.

Summary

Introduction

The objective of rainfall-runoff modelling generally is to simulate, predict or forecast the hydrograph at the catchment outlet. For such simulation many model approaches are developed that range in complexity from very simple to very complex. Model design and development has been an important research topic for many decades although only during the past decade the development of a small number of distributed physically-based model approaches is reported. The development was initiated by expectations and presumptions that runoff production mechanisms could be simulated in a consistent and detailed manner by model algorithms that are based on conservation equations of mass and momentum. For a number of reasons that are described in the literature review of Chapter 3 such approaches have great difficulties to meet the performance expectations. It proved that simulation of the complex real world runoff behaviour at desired temporal and spatial scales is very problematic. Model approaches require very extensive model input data and are difficult to calibrate in a reliable and trustworthy manner. Moreover, model performance often is not satisfactory and modelling must be associated with uncertainty. For these reasons approaches often are rejected. To increase the model performance less complex and more parsimonious model approaches are required and model calibration procedures must be improved that help to overcome the issue of the high performance uncertainty (Chapter 5).

The main research topic of this thesis is to improve physically-based distributed modelling of the hydrologic catchment behaviour under meteorological conditions that cause the generation of saturation overland flow. To achieve this objective, extensive literature reviews are completed on the runoff production mechanisms, physically-based runoff modelling approaches and automated model calibration procedures. Also a theoretical description of the Flowsim model

approach that is designed, developed and coded for this thesis is presented (Chapter 4). A case study on automated model calibration by Maximum Likelihood Estimation is presented in Chapter 6.

Runoff hydrology

Based on extensive field research during the seventies, an understanding based on physical reasoning is gained on hydrologic catchment behaviour that causes extreme runoff discharges. An important runoff mechanism described by Dunne [1978] is the Saturation overland flow mechanism. In this mechanism, overland flow is generated in response to rainfall in case a soil column becomes fully saturated due to a (rapid) groundwater table rise. As the groundwater table intersects the land surface exfiltration and consequently saturation overland flow is observed. The rise of the groundwater table is due to a number of subsurface flow processes that are observed in Darcian and non-Darcian flow conditions. The dominant flow process that causes the rapid water table rise is lateral groundwater flow from upslope areas (Dunne, 1978). In Chapter 3 it is described that soil saturation mostly is observed near channel areas at lower elevations in the catchment where saturated areas vary in width in response to rainfall. The expansion and contraction of the overland flow source areas is characterised as a highly dynamic and a non-linear phenomenon (Kirkby, 1988) that is a function of physiographic, geologic and meteorological catchment conditions. In distributed PBRR modelling such behaviour is simulated by some a priori defined model approach.

Physically-based model approaches

For simulating the saturation overland flow mechanism in a physically realistic and consistent manner, distributed model approaches must be applied that have conservation equations of mass and momentum at the core of the model algorithms. Such algorithms are developed for flow processes at the land surface, the saturated and unsaturated subsurface and the channel system. Additionally, spatial and temporal meteorological forcing is simulated.

In Chapter 3 four physically-based distributed model approaches are reviewed and compared. It proved that model approaches differ significantly with respect to the selected model concept, mathematical

model and model input requirements. Based on conclusion from the review, the model concept of Flowsim is designed and is presented in Chapter 4 and further described in Appendix A. In the model concept, a catchment is partitioned in multiple grid layers while the discretisation of the Digital Elevation Model (DEM) is adapted to each of the grid layers. All DEM grid elements in horizontal plane (i.e. x-y perspective) are squared and of equal size while for the subsurface grid cells the third space dimension (i.e. depth) is added. For each grid cell a specific thickness is defined and hence a three-dimensional subsurface model domain is constructed.

For simulating overland flow a two-dimensional sheet flow model as based on the diffusion wave is selected. Subsurface flow processes are described for Darcian (matrix) flow conditions only. For the unsaturated subsurface a one-dimensional multi-layer flow model based on Richards equation (Richards, 1931) is developed. For simulating saturated subsurface flow a two-dimensional groundwater flow model as based on Boussinesq equation is developed. For channel flow a one-dimensional flow model is developed based on the diffusion wave equation. In the approach interactions and mass exchanges between model algorithms are simulated as well.

In Chapter 3 it is described that model performance of the reviewed model approaches generally is not satisfactory. Specific explanations for this poor performance have to do with complexity of the approaches and the issue of model uncertainty. In any model approach uncertainty is introduced due to incompleteness of the selected model concept and the lack of adequate catchment data to represent real world characteristics at appropriate spatial scales. Such data relate to topography, subsurface, meteorology but also to hydrologic state variables that must be simulated. Data collection and simulation at appropriate scales often is not possible and also in this thesis it is concluded that scale issues hamper model simulations. To overcome some of these issues simplifying assumptions are introduced in the model approaches.

All catchment characteristics, initial model conditions and meteorological model input for example are averaged and lumped at the spatial scale of the grid elements although field observations of these data types mostly are taken at the much smaller point scale. Also within the spatial scales of model grid elements and grid cells multiple processes

are observed in the real world. These processes cannot be simulated realistically at appropriate process scales and its detailed simulation is ignored. Only dominant processes are simulated and model algorithms are parameterised accordingly. In this procedure any spatial variability at small scales is ignored and averaged and grid effective parameter values are defined. These parameter values cannot be defined prior to a model simulation but are optimised through model calibration that is described in Chapter 5.

Model calibration

Each of the reviewed PBRR model approaches in Chapter 3 is calibrated by the Trial and Error procedure. This procedure however has major limitations and is rejected from further application (Chapter 5). A very important limitation for example is that it is difficult to determine when the best parameter set has been reached. This aspect and aspects relating to parameter uniqueness, parameter identifiability and parameter dependencies is accommodated for in automated optimisation procedures. These procedures are propagated in this thesis. Procedures reviewed in Chapter 5 are the Bayesian procedure GLUE, the single and multi-objective evolutionary procedure MOCOM-UA, the geo-statistically based MLE procedure and a novel procedure based on the use of ANNs. In distributed PBRR modelling (very) little attention has been paid towards the use of any of these procedures. Procedures primarily are applied to conceptual rainfall-runoff model approaches.

For the case study in Chapter 6, the MLE procedure is selected that has the Gauss Marquardt Levenberg algorithm at the core of the optimisation algorithm. The procedure is selected since quantitative statistical information on spatial dependencies of parameters becomes available through a parameter correlation matrix while information on parameter identifiability by means of eigen vector- eigen value matrixes becomes available. Such information does not come available in any of the other procedures. A second important advantage is that models can be calibrated for multiple state variables such as piezometer and channel flow data that are of a different kind and order. A major restriction of the procedure is that, based on the applied software, it not (yet) possible is to quantify the effects of parameter uncertainty on model output.

The MLE procedure is coupled to the Flowsim model approach and is applied to the Troy catchment in Idaho (USA). This research basin of size 1.6 ha. is selected since a large data base was made available for this thesis by the university of Idaho. In Chapter 6 it is described that eight calibration cases are defined and that these cases are compared to two non-calibrated cases. Selected cases differ with respect to the initial model condition and the model calibration data set. For simulations, two initial subsurface model conditions are defined that are used as model input. Conditions are defined by the ISMC model approach that is developed for this thesis by Pilot [2002] and that is described in Appendix C. Two cases are calibrated on channel flow discharges, four are calibrated on piezometer observations and two are calibrated on channel flow and piezometer observations. During the research it proved that calibration cases based on piezometer observations were poorest while those with channel flow observations were best. The reason for the poor performance of the piezometer cases to a large extent is due to the poor quality of the piezometer time series. Clear and extensive periods where saturation overland flow is generated could not be identified although, based on the observed channel flow hydrograph, such period should be observable. Models thus are calibrated in such manner that global optimum of the objective function response surface is found for to low piezometer levels. Another cause of poor performance may be that the model concept of Flowsim is inadequate although this cannot be concluded directly from the simulation results. After analysis of the channel flow hydrographs it appeared that simulations are significantly influenced by the entered initial condition in the subsurface models. While automated calibration is achieved by similar state variable sets, output by the selected initial conditions differed significantly. The effect of the initial conditions is most pronounced for the two non-calibrated cases.

After automated model calibration by MLE all optimised parameter values represent realistic values that are not out of range as compared to field obtained values that are available. Also the parameter correlation matrices, the Jacobian matrix and the eigen value-eigen vector matrices are defined. For each case different optimised parameter values as well as matrices are found. Based on physical reasoning this is not surprising. For each case, (slightly) different but unique hydrologic state distributions across the model domain and over the simulation period is

simulated. Flow pattern in terms of discharges and flow directions differ accordingly during the simulations. Hence the Jacobian matrix that is interpreted as a model sensitivity matrix changes and consequently all additional MLE model output changes.

Conclusions

In this thesis it is concluded that event based rainfall-runoff simulation by distributed PBRR model approaches is too complex to be successful. This since many generic modelling issues come into play that easily cause that model performance becomes unsatisfactory. Clear conclusions on usefulness of the MLE in PBRR modelling are not formulated although for each case the parameter optimisation is achieved (Chapter 6). Its use in multi-objective model calibration, however, remains very attractive. The fact that parameter uncertainty is not expressed in the model outcome is regarded a limitation (Chapter 5). To be more conclusive, simulation cases must be repeated when more reliable time series of observations are available. Sensitivity test after weighting single observations in the objective function also must be performed. This aspect of calibration is ignored in this thesis. The MLE procedure also should be coupled to other, more parsimonious, model approaches and be applied to other catchments.

Inverse modellering van de regen-afvoer relatie. Een multi objectieve modelkalibratie benadering.

Samenvatting

Introductie

De doelstelling van regen-afvoer modellering is in het algemeen het simuleren en voorspellen van de afvoerhydrograaf op het uitstroompunt van een stroomgebied. Voor een dergelijke simulatie zijn meerdere modelbenaderingen ontwikkeld die in complexiteit verschillen van simpel tot complex. Modelontwerp en ontwikkeling zijn gedurende vele decades belangrijke onderwerpen van wetenschappelijke onderzoek geweest maar pas gedurende de afgelopen decade is de ontwikkeling van een beperk aantal complexe, gedistribueerde, fysisch gebaseerde modelbenaderingen gerapporteerd. Deze ontwikkeling is op gang gekomen door hoge verwachtingen en veronderstellingen dat afvoerproductie-mechanismen gesimuleerd konden worden op een consistente en gedetailleerde wijze met modelalgoritmen die gebaseerd zijn op behoudswetten van massa en beweging. Om een aantal redenen die beschreven staan in de literatuurstudie van Hoofdstuk 3, zijn er met deze benaderingen grote problemen om te voldoen aan de hoge verwachtingen. Het is gebleken dat het simuleren van het complexe regen-afvoer gedrag in een stroomgebied op gewenste tijd- en ruimteschalen problematisch is. Bij model-benaderingen bestaat een grote behoefte aan modelinvoergegevens en zijn moeilijk te kalibreren. Modelgedrag is vaak niet naar tevredenheid en modellen moeten geassocieerd worden met onzekerheid. Om deze redenen worden deze modelbenaderingen vaak afgewezen. Om het modelgedrag te verbeteren zijn minder complexe modelbenaderingen benodigd met een relatief lage behoefte aan modelinvoergegevens. Ook moet de methode van modelkalibratie verbeterd worden om modelonzekerheid te kunnen verlagen. (Hoofdstuk 5).

Het hoofddoel van onderzoek van deze thesis is het verbeteren van fysisch gebaseerde, gedistribueerde modellering van het stroomgebiedafvoergedrag onder meteorologische condities die het

ontstaan van verzadigde overland stroming veroorzaken. Om deze doelstelling te bereiken zijn uitvoerige literatuurstudies uitgevoerd naar mechanismen van afvoerproductie, naar fysisch gebaseerde afvoerbenaderingen en naar methoden van automatisch modelkalibratie. Ook is de Flowsim modelbenadering ontworpen, ontwikkeld en gecodeerd voor deze thesis en is een theoretische beschrijving hiervan opgenomen in Hoofdstuk 4. Een casestudie van automatische modelkalibratie op basis van "Maximum Likelihood Estimation" is beschreven in Hoofdstuk 6.

Afvoerhydrologie

Gebaseerd op uitvoerig veldonderzoek gedurende de zeventiger jaren is op basis van fysisch begrip inzicht ontstaan in hydrologisch stroomgebiedgedrag waardoor extreme afvoeren ontstaan. Een belangrijk afvoermechanisme dat beschreven is door Dunne [1978] is het verzadigde overland mechanisme. In dit mechanisme wordt overland stroming ontwikkeld in een stroomgebied indien een bodemkolom volledig verzadigd raakt door een (snelle) stijging van de grondwaterspiegel. Als de grondwaterspiegel het maaiveld raakt zal exfiltratie en vervolgens verzadigde overland stroming ontstaan. De stijging van de grondwaterspiegel is het gevolg van een aantal ondergrondse stroomprocessen die waargenomen worden in "Darcian" en "non-Darcian" stroomcondities. Het dominerende stroomproces waardoor de snelle grondwaterspiegelstijging wordt veroorzaakt is laterale grondwaterstroming van bovenstroomse gebieden (Dunne, 1978). In Hoofdstuk 3 is beschreven dat bodemverzadiging vaak waargenomen wordt langs kanaaltjes in de lagere delen van een stroomgebied waarbij verzadigde zones in breedte variëren. De groei en samentrekking van deze brongebieden van verzadigde overland stroming is een hoog dynamisch en niet-lineair fenomeen (Kirkby, 1988) en is een functie van fysiografische, geologische, en meteorologische stroomgebiedcondities. In gedistribueerde fysische gebaseerd regen-afvoer modellering is dit gedrag gesimuleerd bij een *a priori* vastgelegde modelbenadering.

Fysisch gebaseerde modelbenaderingen

Voor simulatie van het verzadigde overland mechanisme op een fysisch realistische en consistente manier, moeten gedistribueerde modelbenaderingen toegepast worden met modelalgoritmen die gebaseerd zijn op behoudswetten van massa en momenten. Algoritmen moeten toegepast worden voor overland stroomprocessen aan het landoppervlak, voor processen in de verzadigde en onverzadigde ondergrond en watertransport in het riviersysteem. Aanvullend moeten regen en verdamping gesimuleerd worden als een ruimtelijk en tijdsafhankelijk fenomenen.

In Hoofdstuk 3 zijn vier fysisch gebaseerde, gedistribueerde modelbenaderingen bestudeerd en vergeleken. Hieruit is voortgekomen dat modelbenaderingen duidelijk anders zijn ten aanzien van het ontwikkelde modelconcept, het mathematisch model en modelinvoer. Gebaseerd op de conclusies van de modelvergelijking is het modelconcept van Flowsim ontworpen zoals gepresenteerd in Hoofdstuk 4 en beschreven in Appendix A. In het modelconcept is een stroomgebied opgesplitst in meerdere gridlagen waarbij de discretisatie van het digitale hoogtemodel is overgenomen in elke gridlaag. Alle gridelementen van het digitale hoogtemodel in het horizontale vlak (x-y perspectief) zijn vierkant en van gelijke grootte waarbij voor de ondergrondse gridcellen de derde ruimtedimensie (i.e. diepte) is toegevoegd. Voor elke gridcel is een specifieke dikte bepaald en een volledig drie-dimensionaal modeldomein is op deze wijze geconstrueerd.

Voor simulatie van overland stroming is een twee-dimensionaal stroommodel ontwikkeld gebaseerd op de diffusiegolfvergelijking. Hierbij is verondersteld dat waterstroming plaatsvindt als een dunne, vlakdekkende waterlaag over het landoppervlak. Ondergrondse stroomprocessen zijn beschreven voor "Darcy" stroomcondities. Voor de onverzadigde ondergrond is een één-dimensionaal meerlagen stroommodel ontwikkeld dat gebaseerd is op de Richards vergelijking (Richards, 1931). Voor simulatie van verzadigde ondergrondse stroming is een twee-dimensionaal grondwaterstroommodel ontwikkeld gebaseerd op de Boussinesq vergelijking. Voor kanaalstroming is een één-dimensionaal stroommodel ontwikkeld gebaseerd op de diffusiegolfvergelijking. In de benadering zijn ook modelinteracties en massa-uitwisselingen tussen submodellen gesimuleerd.

In Hoofdstuk 3 is beschreven dat het modelgedrag van de onderzochte modelbenaderingen over het algemeen niet bevredigend is. Specifieke verklaringen voor dit onbevredigende gedrag zijn de complexiteit van de benaderingen en modelonzekerheid. In elke modelbenadering is onzekerheid geïntroduceerd doordat modelconcepten onvolledig zijn en door het tekort aan adequate data om stroomgebiedkarakteristieken op juiste ruimtelijke schalen in het model weer te geven. Data hebben betrekking op topografie, op de ondergrond, op meteorologie maar ook op hydrologische toestandvariabelen die gesimuleerd moeten worden. Dataverzameling en simulatie op juiste schalen is vaak niet mogelijk en ook in deze thesis is geconcludeerd dat schaalproblemen modelsimulaties beperken. Om over een aantal van deze beperkingen heen te stappen zijn simplificerende aannames geïntroduceerd in de modelbenaderingen.

Alle stroomgebiedkarakteristieken, initiële modelcondities en meteorologische modelinvoer worden bijvoorbeeld gemiddeld over de schaal van de gridelementen alhoewel veldwaarnemingen van deze data typen meestal op een veel kleinere puntschaal worden genomen. Ook binnen de ruimtelijke schalen van gridelementen en gridcellen worden in de echte wereld meerdere processen waargenomen. Deze processen kunnen niet op realistische wijze op de meest toegeëigende ruimteschaal gesimuleerd worden en gedetailleerde simulatie wordt daarom veelal genegeerd. Alleen dominante processen worden gesimuleerd en modelalgoritmen worden geparаметeriseerd om deze processen te simuleren. In deze procedure is elke ruimtelijke variabiliteit op kleine schaal genegeerd en gemiddelde en grid-effectieve parameterwaarden worden bepaald. Deze parameterwaarden kunnen niet op voorhand bepaald worden maar moeten geoptimaliseerd worden door modelkalibratie zoals beschreven in Hoofdstuk 5.

Modelkalibratie

Elk van de besproken fysisch gebaseerde neerslag-afvoer modellen in Hoofdstuk 3 is gekalibreerd met de "Trial and Error" procedure. Deze procedure heeft grote beperkingen en wordt afgewezen voor verdere toepassing (Hoofdstuk 5). Een belangrijke beperking bijvoorbeeld is dat het moeilijk te bepalen is of, gedurende de modelkalibratie, de beste parameterset bepaald is. In dit aspect en aspecten die gerelateerd zijn aan parameter-uniciteit, parameter-identificeerbaarheid en parameter-afhankelijkheid wordt in voorzien door automatische parameter

optimalisatie procedures. Deze procedures worden aanbevolen in deze thesis. Procedures gereviewd in Hoofdstuk 5 zijn de "Bayesian" procedure GLUE, de enkele en multi-objectieve evolutionaire procedure MOCOM-UA, de geostatistisch gebaseerde MLE procedure en een vernieuwende procedure gebaseerd op het gebruik van ANNs. In gedistribueerde fysische gebaseerde regen-afvoer modellering is (erg) weinig aandacht besteed aan het gebruik van deze procedures. Procedures zijn hoofdzakelijk toegepast in conceptuele regen-afvoer model benaderingen.

Voor de case studie in Hoofdstuk 6 is de MLE procedure geselecteerd die het Gauss Marquardt Levenberg algoritme hanteert als optimalisatie algoritme. De procedure is geselecteerd omdat kwantitatieve statistische informatie verkregen wordt over ruimtelijke afhankelijkheid van parameters door een parameter correlatie matrix terwijl ook informatie over parameter identificeerbaarheid door middel van "eigen vector-eigen value" matrices verkregen wordt. Deze informatie wordt niet verkregen in elk van de andere procedures. Een tweede belangrijk voordeel is dat modellen gekalibreerd kunnen worden op meerdere toestandvariabelen als grondwaterstijghoogten en rivierafvoer data die van een andere samenstelling en omvang zijn. Een grote beperking van de procedure is dat, op basis van de gehanteerde software voor deze thesis, het nog niet mogelijk is om effecten van parameter onzekerheid te kwantificeren op modeluitvoer.

De MLE procedure is gekoppeld aan de Flowsim modelbenadering en is toegepast op het Troy stroomgebied in Idaho (USA). Dit research stroomgebied met een grootte van 1.6 ha. is geselecteerd omdat voor de thesis een grote database beschikbaar kon worden gemaakt door de University van Idaho. In Hoofdstuk 6 is beschreven dat acht kalibratie cases gedefinieerd zijn en dat deze cases vergeleken worden met twee niet-gekalibreerde cases. Geselecteerde cases verschillen wat betreft de initiële modelconditie en modelkalibratie dataset. Voor simulaties zijn twee initiële bodemvochtcondities bepaald en gebruikt als modelinvoer. Conditie zijn berekend met de ISMC modelbenadering die voor deze thesis ontwikkeld is en die beschreven is in Appendix C. Twee cases zijn gekalibreerd op rivierafvoeren, vier zijn gekalibreerd op grondwaterstijghoogten en twee zijn gekalibreerd op waarnemingen van rivierafvoeren en grondwaterstijghoogten. Gedurende het onderzoek is gebleken dat kalibratie cases met grondwaterstijghoogten het minst

nauwkeurig zijn terwijl die met kanaalafvoeren waarnemingen het meest nauwkeurig zijn. De reden voor de matige resultaten voor, met name, de grondwaterstijghoogten cases wordt voor een belangrijk deel toegeschreven aan de matige kwaliteit van tijdseries van de grondwaterstijghoogten. Duidelijk en langdurige periode met verzadigde overland stroming konden niet geïdentificeerd worden alhoewel, gebaseerd op analyse van de rivierafvoer-hydrograaf, zulke perioden wel waarneembaar zouden moeten zijn. Modellen zijn gekalibreerd op een dusdanige wijze dat het globale optimum van de doelfunctie response oppervlak gevonden is voor feitelijk te lage grondwaterstijghoogten. Een andere reden voor het matige resultaten kan zijn dat het modelconcept niet adequaat is alhoewel dit niet direct geconcludeerd kan worden uit de simulatieresultaten. Na analyse van de afvoerhydrograaf is gebleken dat simulaties significant beïnvloed zijn door de ingevoerde initiële bodemvochtconditie. Terwijl automatische kalibratie bereikt is met gelijke sets van toestandvariabelen, is modeluitvoer voor de geselecteerde initiële condities significant anders. Effecten van initiële condities zijn het duidelijkste waarneembaar voor de twee niet gekalibreerde cases.

Na kalibratie met MLE, hebben alle geoptimaliseerde parameters realistische waarden die in overeenstemming zijn met waarden van beschikbare veldwaarnemingen. Ook de parameter correlatie matrices, de Jacobian matrix en de "eigen value-eigen vector" matrices zijn bepaald. Voor elke case zijn verschillen in geoptimaliseerde parameterwaarden alsmede matrices gevonden. Gebaseerd op fysisch inzicht is dit niet verrassend. Voor elke case is een iets andere ruimtelijke verdelingen van toestandvariabelen gesimuleerd. Stroompatronen in termen van debieten en stroomrichtingen verschillen daarom ook gedurende de simulaties. Als gevolg daarvan verandert de Jacobian matrix, die geïnterpreteerd is als een model gevoeligheidsmatrix en, en alle daarvan afgeleide MLE model uitvoer.

Conclusies

In deze thesis is geconcludeerd dat event gebaseerde regen-afvoer simulatie met gedistribueerde PBRR modelbenaderingen te complex is om succesvol te zijn. Dit omdat te veel generieke modelleeraspecten een rol spelen die gemakkelijk veroorzaken dat modelgedrag onbevredigend is. Eenduidige conclusies over toepasbaarheid van MLE in PBRR

modellering zijn niet geformuleerd alhoewel parameter optimalisatie wel is bereikt voor elke optimalisatie case (Hoofdstuk 6). De toepasbaarheid in multi-objectieve modelkalibratie blijft echter aantrekkelijk. Het feit dat parameteronzekerheid niet tot uitdrukking komt in modeluitvoer wordt gezien als een beperking. (Hoofdstuk 5). Om meer eenduidige conclusies te kunnen trekken moeten simulaties cases herhaald worden met meer betrouwbare tijdseries van waarnemingen. Gevoeligheidstesten naar het toepassen van wegingsfactoren voor individuele waarnemingen in de doelfuncties moeten ook uitgevoerd worden. Dit aspect van kalibratie heeft geen aandacht gehad in deze thesis. De MLE procedure moet ook gekoppeld worden aan meer spaarzame model benadering en moet toegepast worden in meerdere stroomgebieden.

References

- Aarts, L., and Van der Veer, p., 2001a. Neural network method for solving partial differential equations *Neural Processing Letters* 14(3), p. 261-271
- Aarts, L., and Van der Veer, p., 2001b. Solving systems of first order linear differential equations by a neural network method. In: *Computational Science - ICCS 2001*, part II, p. 181 - 188.
- Abbott, M.B., Bathurst, J.C., Cunge, J.A., O'Connell, P.E. and Rasmussen, J., 1986a. An introduction to the European Hydrological System - Système Hydrologique Européen, "SHE", 1. History and philosophy of a physically-based, distributed modelling system. *Journal of Hydrology*, No.87, p.45-59.
- Abbott, M.B., Bathurst, J.C., Cunge, J.A., O'Connell, P.E. and Rasmussen, J., 1986b. An introduction to the European Hydrological System - Système Hydrologique Européen, "SHE", 2. Structure of a physically-based, distributed modelling system. *Journal of Hydrology*, No.87, p.61-77.
- Akan, O.A., and Yen, B.C., 1981. Mathematical model of shallow water flow over porous media. *Journal of Hydraulics Division*, American Society of Civil Engineers, Vol.107, p.479-494.
- Ambroise, B., Perrin, J.L., and Reutenauer, 1995. Multi criterion validation of a semi-distributed conceptual model of the water cycle in Fecht catchment (Vosges massif, France), *Water Resources Research*, Vol. 31, No. 6, p.1467-1481.
- Amerman, C.R., and McGuinness, J.L., 1967. Plot and small watershed runoff: its relation to larger areas. *Trans.Amer.Soc.Agric.Engrs.*, 10(4) p.464-466.
- Anderman, E.R., Hill, M.C., and Pocter, E.P., 1996. Two-dimensional advective transport in groundwater flow parameter estimation, *Groundwater*, Vol.34, No.6, p.1001-1009.
- Anderson, M.P. & Woessner, W.W. 1992. *Applied groundwater modeling*. Simulation of flow and advective transport. Academy Press, Inc., San Diego. 381 p.
- ASCE, 2000., Artificial neural networks in hydrology. 1: Preliminary concepts. *J. of Hydrologic Engineering*, Vol. 5, No., 2. P. 115-123.
- Bastin, G., Lorent, B., Duqué, C. and Gevers, M., 1984. Optimal estimation of the average areal rainfall and optimal selection of rain gauge locations, *Water Resources Research*, Vol.20, No.4, p.463-470.
- Bates, P.B., and De Roo, A.P.J., 2000. A simple raster-based model for flood inundation simulation. *Journal of Hydrology*, Vol. 236, p.54-77.
- Bathurst, J.C., 1986a. Physically-based, distributed modelling system of an upland catchment using the Système Hydrologique Européen. *Journal of Hydrology*, No.87, p.79-102.
- Bathurst, J.C., 1986b. Sensitivity analysis of the Système Hydrologique Européen in an upland catchment. *Journal of Hydrology*, No.87, p.102-123.
- Beasley, D.B, Huggins, L.F, and Monke, E.J., 1980. ANSWERS: A Model for Watershed Planning. *Transactions of the ASAE.*, Vol.23, No.4. p.938-944.

- Beasley, D.B. and Huggins, L.F., 1982. ANSWERS - Users manual. U.S. EPA-905/9-82-001, Chicago, IL, 54p.
- Belmans, C., Wesseling, J.G. and Feddes, R., 1982. Simulation model of the water balance of a cropped soil. Swatre. *Journal of Hydrology*, Vol. 63, p. 271-286.
- Bergström, S., and Forsman, A. 1973. Development of a conceptual deterministic rainfall-runoff model. *Nordic Hydrology*, Vol. 4, No. 3.
- Bergström, S., 1976. Development and Application of a Conceptual Runoff Model for Scandinavian Watersheds. SMHI Report RHO7
- Bergström, S and Graham, L.P., 1998. On the scale problem in hydrological modelling. *Journal of Hydrology*, Vol. 211, p.253-265.
- Betson, R.P., 1964. 'What is watershed runoff?' *Journal of Geophys Research* Vol.69(B), p.1541-1552.
- Betson, R.P. and Marius, J.B., 1969. 'Source areas of storm runoff'. *Water Resources Research*, Vol.5, No.3, p.574-582.
- Beven, K., 1979. On the generalized kinematic routing method. *Water Resources Research*, Vol.15, No.5, p.1419-1424.
- Beven, K., 1981. Kinematic Subsurface Stormflow. *Water Resources Research*, Vol.17, No.5, p.1419-1424.
- Beven, K., 1982. On subsurface storm flow, an analysis of response times. *Hydrol. Sci. J.*, Vol.27, p.505-521.
- Beven, K., 1984. Infiltration into a class of vertically non-uniform soils. *Hydrol. Sci. J.*, Vol.29(4), p.425-434.
- Beven, K., 1985. Distributed models. In *Hydrological forecasting*, edited by M.G. Anderson and T.P. Burt, p.405-435, John Wiley and Sons, Chichester.
- Beven, K., 1989a. Changing ideas in Hydrology - The Case of Physically-Based Models. *Journal of Hydrology*, No.105 p.157-172.
- Beven, K., 1989b. Interflow. In *Unsaturated Flow in Hydrological Modelling*, edited by H.J. Morel-Seytoux, D.Reidel, Dordrecht.
- Beven, K., 1991a. Infiltration, soil moisture and unsaturated flow. In *Recent Advances in the Modelling of Hydrologic Systems*. edited by Bowles, D.S. and O'Connell P.E., p.137-151, Kluwer Academic Publishers, Netherlands.
- Beven, K., 1991b. Scale considerations. In *Recent Advances in the Modelling of Hydrologic Systems*. edited by Bowles, D.S. and O'Connell, P.E., p.357-371, Kluwer Academic Publishers, Netherlands.
- Beven, K., 1993a. Estimating transport parameters at the grid scale: on the value of a single measurement. *Journal of Hydrology*, Vol. 143, p.109-123.
- Beven, K., 1993b. Prophecy, reality and uncertainty in distributed hydrological modelling. *Advances in Water Resources*, Vol. 16, p.41-51.
- Beven, K.J., 1996. A discussion of distributed hydrological modelling. In: Abbott, M.B., Refsgaard, J.C.(Eds.), *Distributed Hydrological Modelling*. Kluwer Academic, p.255-278.
- Beven, K.J., 1996. Response to Comments on "A discussion of distributed hydrological modelling" by Refsgaard, J.C. et al. In: Abbott, M.B., Refsgaard, J.C.(Eds.), *Distributed Hydrological Modelling*. Kluwer Academic, p.289-295.

- Beven, K and Binley, 1992. The future of of distributed models: model calibration and uncertainty prediction, *Hydrological Processes*, Vol.6, p.279-298.
- Beven, K.L., Calver, A., and Morris, E.M., 1987. The Institute of hydrology distributed model. Report No.98, Inst.of.Hydrology, Wallingford, U.K.
- Beven, K., and Germann, P.F., 1981. Water flow in macro pores. *Journal of Soil Science*. Vol.32, p.15-29.
- Beven, K., and Germann, P.F., 1982. Macro pores and water flow in soils. *Water Resources Research*, Vol.18, p.1311-1325.
- Beven, K.J. and Kirkby, M.J., 1979. A physically based, variable contributing area model of basin hydrology. *Hydrol.Sci.Bull.* Vol.24, No.1, p.43-69.
- Beven, K., and Kirkby, M.J., 1993. *Channel network hydrology*. by John Wiley & Sons Ltd. Baffins Lane, Chichester, West Sussex. p.99-128.
- Beven, K.J., Kirkby, M.J., Schoffield, N., and Tagg, A., 1984. Testing a physically-based flood forecasting model (TOPMODEL) for three U.K. catchments. *Journal of Hydrology*, No.69, p.119-143.
- Beven, K. and Wood, E.F., 1983. Catchment Geomorphology and the Dynamics of Runoff Contributing Areas. *Journal of Hydrology* Vol.65, p.139-158.
- Beven, K.J., Wood, E.F., and Sivapalan, M., 1988. On hydrological heterogeneity: Catchment morphology and catchment response. *Journal of Hydrology* Vol.100, p.353-375.
- Bierkens, M.F.P., 1995. Opschaling van geohydrologische eigenschappen: van meetschaal tot regionale schaal. In: Onzekerheid in grondwatermodellering; Verslag van de lezingendag in Ede. p.25-45.
- Binley, A.M., and Beven, K.J., 1991. Physically base modelling of catchment hydrology: a likelihood approach to reducing predictive uncertainty. In Computer modelling in the environmental sciences, editors D.G.Farmer and M.J.Rycroft, Clarendon Press, Oxford, UK, p.75-88.
- Blöschl, G, and Sivapalan, M., 1995. Scale issues in hydrological modelling: a review; in: *Hydrological Processes*, Vol. 9, p. 251-290.
- Blum, A., 1992. Neural networks in C++; An object oriented framework for building connectionist systems. John Wiley and Sons, Inc., USA.
- Bonnell, M. and Gilmour, D.A., 1978. The development of overland flow in a tropical rainforest catchment. *Journal of Hydrology* Vol.39, p.365-382.
- Bogardi, J.J., 1991. Actual Problems in Surface Water Hydrology An Overview. Symposium IHE, Delft.
- Boomgaard., M.E. en Petter., R. 1993. Theorie en handlcidingen behorende bij het oppervlakteafvoer model Dagudo2. MSC Thesis, TU-delft, sectie Hydrologie en Waterhuishouding.
- Bowles, D.S. and O'Connell, P.E., 1991. Recent Advances in the Modelling of Hydrologic Systems. *NATO ASI Series; Serie C: Mathematical and Physical Sciences*-Vol.345.
- Bradford, P.W., Rawls, W.J., Brakensiek, D.L. and Wight, J.R., 1990. Predicting Runoff From Rangeland Catchments: A Comparison of Two Models. *Water Resources Research*, Vol.26, No.10, p.2401-2410.

- Brakensiek, D.L. 1967. Kinematic flood routing. *Trans. ASAE*, No.10, p340-343.
- Bras, R.L. and Ignacio Rodríguez-Iturbe., 1984. *Random Function and Hydrology*. pp.559.
- Bras, R.L., 1990. *Hydrology: an introduction to hydrological science*. Addison-Wesley Publishing Company, pp. 643.
- Bronstert, A., 1999. Capabilities and limitations of detailed hillslope hydrological modelling. *Hydrological processes*, Vol. 13, p.21-48.
- Bronstert, A., and Plate, E., 1996. Ein physikalisch begründetes hydrologisches modell für hänge und kleine einzugsgebiete, *Wasserwirtschaft*, Vol. 86, p.318-323.
- Bronstert, A., and Plate, E., 1997. Modelling of runoff generation and soil moisture dynamics for hillslopes and micro-catchments. *Journal of Hydrology*, Vol.198, p.177-195.
- Burnash, R.J.C., Ferral, R.L., and R.A. McGuire., 1973 A generalized streamflow simulation system, conceptual modelling for digital computers, United States of Commerce, National weather service, State of California, Dept. of Water Resources, USA.
- Burrough, P.A., 1986. Principles of Geographical Information Systems for Land Resources Assessment. Monographs on Soil and Resources Survey No.12. Varendon Press, Oxford. *An Introduction to Geographical Information Systems*. pp.287.
- Burrough, P.A., 1987. The "State of the art" of spatial variation studies in soil and water - C.H.O. No.18. The Hague p.11-28.
- Burt, T.P. 1986. Runoff processes and solutional denudation rates on humid temperate hillslopes. In Trudgill, S.T. (ed), *Solute Processes* John Wiley, Chichester, p. 193-250.
- Brooks, R.H., and Corey, A.T., 1964. Hydraulic properties of porous media. *Hydrol.Pap.* Vol. 3, pp.27. Colo.Stat Univ. Fort Collins.
- Brutsaert, W.F., 1971. A functional iteration technique for solving the Richards equation applied to two-dimensional infiltration problems. *Water Resources Research*, Vol.7, No.6, p.1583-1596.
- Cabral, M.C., Bras, R.L., Tarboton, D. and Entekhabi, D., 1990. A distributed physically based rainfall-runoff model incorporating topography for real-time flood forecasting. Ralph M. Parsons laboratory, Hydrology and water resource systems, Report Number 332.
- Cabral, C., Garrote, L., Bras, R.L., and Entekhabi, D., 1992. A kinematic model of infiltration and runoff generation in layered and sloped soils, *Adv. in Water Resources*, Vol. 15, p.311-324.
- Calver, A, 1988. Calibration, sensitivity and validation of a physically based rainfall-runoff model, *Journal of Hydrology*, Vol.103, p.102-115.
- Campbell, G.S., 1974. A simple method for determining unsaturated conductivity from moisture retention data. *Soil Science*, Vol.117, p.311-314.
- Carrera, J., and S.P. Neuman, "Estimation of Aquifer Parameters under Transient and Steady State Conditions: 1. Maximum Likelihood Method Incorporating Prior Information", *Water Resources Research*, 22(2), p.199-210, 1986.

- Chorley, R.J., 1978. The hillslope hydrological cycle. In *Hillslope hydrology* edited by M.J. Kirkby. p.1-42, Wiley, London.
- Chow, Ven Te, (ed), 1964. *Handbook of applied hydrology*. McGraw-Hill, New York.
- Chow, V.T., Maidment, D.R., and Mays, L.W., 1988. *Applied Hydrology*. Mc-Graw-Hill, New York, p.572.
- Clarke, R.T., 1973. A review of some mathematical models used in hydrology, with observations on their calibration and use. *Journal of Hydrology*, Vol.19, p. 1-20.
- Clarke, R.C., 1994. *Statistical modelling in hydrology*, John Wiley, New York.
- Corradini, C., 1985. Analysis of the effects of orography on surface rainfall by a parameterized numerical model. *Journal of Hydrology*, Vol.77, p.19-30.
- Corradini, C. and Singh, V.P., 1985. Effect of spatial variability of effective rainfall on direct runoff by a geomorphologic approach. *Journal of Hydrology*, Vol.81, p.27-43.
- Correia, F.N., and Matias, P., 1991. Omega: Impact of spatial variability of infiltration parameters on catchment response. In *Recent Advances in the Modelling of Hydrologic Systems*. edited by Bowles, D.S. and O'Connell P.E., p.407-441, Kluwer Academic Publishers, Netherlands.
- Costa-Cabral, M.C. and Burges, S.J., Digital elevation model networks (DEMON): A model of flow over hillslopes for computation of contributing and dispersal areas, *Water Resources Research*, Vol.30, No.6, p.1681-1692.
- Crawford, N.H., and R.K. Linsley. Digital simulation in hydrology; Stanford watershed model IV. Tech.Rep. 39. Dept.of Civ. Eng., Stanford University, Stanford, California.
- Cundy, W.T. and Tento, S.W., 1985. Solution to the kinematic wave approach to overland flow routing with rainfall excess given by Philip's equation. *Water Resources Research*, Vol.21, No.8, p.1132-1140.
- Cunningham, A.B. and Sinclair, P.J., 1979. Application and analysis of a coupled surface and groundwater model. *Journal of Hydrology*, Vol.43, p.129-148.
- Dam, J.C. van, 1987. Lecture Notes Some Deterministic Models for the Rainfall-Runoff Relation.
- Dam, J.C., and Feddes, R.A., 2000. Numerical simulation of infiltration, evaporation and shallow groundwater levels with the Richards equation, *Journal of Hydrology*, Vol.233, p.72-85.
- Danish Hydraulic Institute, 1993. MIKE SHE - Release 5.1, Water movement module; A short Description pp. 34.
- Delhomme, J.P., 1978. Kriging in the Hydrosiences. *Advances in Water Resources* Vol.1, No.5, p.251-266.
- Delhomme, J.P., 1979. Spatial variability and uncertainty in groundwater flow parameters: a geostatistical approach. *Water Resources Research*, Vol.15, No.2, p.269-280
- Duan, Q., 1991. A global optimization strategy for efficient and effective calibration of hydrologic models. Ph.D thesis, Dep. of Hydrol. and Water Resour., Univ., of Ariz., Tucson.

- Duan, Q., Gupta, V.K., and Sorooshian, S., 1992. Effective and efficient global optimisation of conceptual rainfall-runoff models. *Water Resources Research*, Vol.28, No.4, p.1015-1031
- Duan, Q., Gupta, V.K., and Sorooshian, S., 1993. A Shuffled complex evolution approach for effective and efficient global minimisation. *Journal of Optimisation Theory and Applications*, Vol.76, No.3, p.1015-1031
- Duan, Q., Sorooshian, S., and Gupta, V.K., 1994. Optimal use of the SCE-UA global optimisation method for calibrating watershed models. *Journal of Hydrology*, Vol.158, p.265-284.
- Dunne, T., 1969. Runoff production in a humid area. Ph.D dissertation, The Johns Hopkins Univ., Baltimore, Maryland.
- Dunne, T., 1978. Field studies of hillslope flow processes. in *Hillslope hydrology* edited by M.J. Kirkby. p.227-294. Wiley, London.
- Dunne, T., 1983. Relation of Field Studies and Modelling in the Prediction of Storm Runoff. *Journal of Hydrology*, Vol.65, p.25-48.
- Dunne, T., and Black, R.D., 1970a. An experimental investigation of runoff production in permeable soils. *Water Resources Research*, Vol.6, p.478-490.
- Dunne, T., and Black, R.D., 1970b. Partial area contributions to storm runoff in a small New England watershed. *Water Resources Research*, Vol.6, p.1296-1311.
- Dunne, T., Moore, T.R. and Taylor, C.H., (1975). Recognition and prediction of runoff producing zones in humid regions. *Hydrol.Sci.Bull.*, Vol.20, p.305-327.
- Engman, E.T., 1986. Roughness coefficients for routing surface runoff. *Journal of irrigation and drainage engineering* Vol.112, No.1, p.39-53
- Fairfield, J. and Leymarie, P., 1991. Drainage Networks from Grid Digital Elevation Models. *Water Resources Research*, Vol.27, No.5, p.709-717.
- Fausett, L., [1994]. Fundamentals of neural networks: architectures, algorithms and applications. Prentice-Hall International, Inc., USA.
- Feddes, R.A., Kowalik, P., Kolinska-malinka, K., and Zaradny, H., 1976. Simulation of field water uptake by plants using a soil water dependent root extraction function. *Journal of Hydrology*, Vol.31, p.13-26.
- Feddes, R.A., Menenti, M., Kabat, P. and Bastiaansen, W.G.M., 1993. Is large scale inverse modelling of unsaturated flow with areal average evaporation and surface soil moisture as estimated from remote sensing feasible? *Journal of Hydrology*, Vol.143, p.125-152.
- Franks, S., Ginceste, P., Beven, K., and Merot, P., 1996. On constraining the predictions of distributed models: the incorporation of fuzzy estimates of saturated areas into the calibration process *Water Resources Research*, Vol.34, No.4, p.787-797
- Freeze, R.A., 1969. The mechanism of natural groundwater recharge and discharge 1. One-dimensional, vertical, unsteady, unsaturated flow above a recharging or discharging groundwater flow system. *Water Resources Research*, Vol.5, No.1, p.153-171.
- Freeze, R.A., 1971. Three-dimensional, transient, saturated-unsaturated flow in a groundwater basin. *Water Resources Research*, Vol.7, No.2, p.347-366.

- Freeze, R.A., 1972a. Role of Subsurface Flow in Generating Surface Runoff 1. Base Flow Contributions to Channel Flow. *Water Resources Research*, Vol.8, No.3, p.609-623.
- Freeze, R.A., 1972b. Role of Subsurface Flow in Generating Surface Runoff 2. Upstream Source Areas. *Water Resources Research*, Vol.8, No.5, p.1272-1283.
- Freeze, R.A., 1978. Mathematical models in hillslope hydrology. in *Hillslope hydrology* edited by M.J. Kirkby. p.227-294. Wiley, London.
- Freeze, R.A., 1980. A stochastic-conceptual Analysis of Rainfall-Runoff Processes on a Hillslope. *Water Resources Research*, Vol.16, No.2, p.391-408.
- Freeze, R.A., and Harlan, R.L., 1969. Blueprint for a physically based digitally-simulated hydrologic response model. *Journal of Hydrology*, Vol.9, p.237-258.
- French, M.N. Krajewski, W.F., and Cuykendall, R.R., 1992. Rainfall forecasting in space and time using a neural network, *Journal of Hydrology*, Vol.137, p.1-31.
- Garrote, L.G. and Bras, R.K., 1995a. A distributed model for real-time flood forecasting using digital elevation models. *Journal of Hydrology*, Vol.167, p.279-306.
- Garrote, L.G. and Bras, R.K., 1995b. An integrated software environment for real-time use of a distributed hydrological model, *Journal of Hydrology*, Vol.167, p.307-326.
- Germann, P.F., 1990. Macro pores and hydrologic hillslope processes, in *Process studies in hillslope hydrology*, edited by A.G. Anderson and T.P. Burt. John Wiley, New York, p.327-367.
- Goodrich, D.C., 1990. Geometric simplifications of a distributed rainfall-runoff model over a large range of basin scales, Ph.D. thesis. Univ. of Aroz. Tucson, USA, pp.361.
- Goodrich, D.C., and D.A. Woolhiser, 1994. Comment on 'Physically based hydrologic modelling 1, A terrain based model for investigative purposes' by Grayson, R.B., Moore, I.D. and T.A. McMahon. *Water Resources Research*, Vol.30, No.3, p.845-849.
- Grayson, R.B., Moore, I.D. and T.A. McMahon, 1992a. Physically based hydrologic modelling 1. A terrain based model for investigative purposes. *Water Resources Research*, Vol.28, No.10, p.2639-2658.
- Grayson, R.B., Moore, I.D. and T.A. McMahon, 1992b. Physically based hydrologic modelling 2. Is the concept realistic. *Water Resources Research*, Vol.28, No.10, p.2659-2666.
- Green, W.H., and Ampt, G., 1911. Studies of soil physics. Part I-The flow of air and water through soils. *J. Agric. Sci.*, Vol.4, p.1-24
- Gupta, V.K., and Sorooshian, S., 1985. The relationship between data and the precision of parameter estimates of hydrologic models, *Journal of Hydrology*, Vol.81, p.57-77.
- Gupta, V.K., and Sorooshian, S., 1994. Calibration of conceptual hydrologic models; Past, present and future. In *Trends in Hydrology*, edited by Council of Scientific Research Integration., p 329-346, Research Trends, Kaihamukku, India.

- Gupta, V.K., Sorooshian, S., and Yapo P.O., 1998. Towards improved calibration of hydrologic models: Multiple and non-commensurable measures of information, *Water Resources Research*, Vol.34, No.4, p.751-763.
- Hammerstrom, D., 1993. Working with neural networks., IEEE Spectrum, p.46-53.
- Hazzanizadeh, M., and Gray, W.G., 1979. General averaging equations for multi-phase systems: 1 Averaging procedures. *Adv. Water Res.* Vol.2, p.131-144.
- Hewlett, J.D., 1961. Watershed management, Report for 1961, South-Eastern Experimental Station, US Forest Service, Asheville, North Carolina.
- Hewlett, J.D., 1982. *Principles of Forest Hydrology*, Univ. of Georgia Press, Athens, GA., USA.
- Hewlett, J.D. and Hibbert, A.R., 1963. Moisture and energy conditions within a sloping soil mass during drainage. *Journal of Geophys. Res.*, Vol.68, No.4, p.1081-1087.
- Hewlett, J.D. and Hibbert, A.R., 1967. Factors affecting the response of small watersheds to precipitation in humid areas. in *Forest hydrology* edited by W.E. Sooper and H.W. Lull, pp.275-290, Pergamon press, Oxford.
- Hill, M.C. "Methods and guidelines for effective model calibration", U.S. Geological Survey, Water-Resources Investigations report 98-4005, 1998.
- Hill, M.C., Cooley, R.L. and Pollock, D.W., 1997. A controlled experiment in groundwater flow model calibration. *Groundwater*, Vol.36, No.3, p.520-534.
- Holland, J.H., 1975. *Adaptation in Natural and Artificial Systems*. Univ. of Michigan Press, Ann Arbor.
- Hooke, R., and Jeeves, T.A., 1961. Direct search solutions of numerical and statistical problems. *J. Assoc. Comput. Mach.* Vol. 8, No, 2., p. 212-229.
- Holtan., H.N., 1961. A concept for infiltration estimates in watershed engineering, *USDA Bulletin*, p.41-51.
- Hornberger, G.M., and Boyer, E.W., 1995. Recent advances in watershed modelling. In: *Reviews of Geophysics*, supplement, American Geophysical Union, p.949-957.
- Hornik, K., Stinchcombe, and White, H., 1989. Multi layer feedforward networks and universal approximators. *Neural Netw.* Vol.2, p.359-366
- Horton, R.E., 1933. The role of infiltration in the hydrologic cycle. *Trans. Am. Geophys. Union*, No.14, p.446-460.
- Hughes, D.A., Soil moisture and runoff simulations using four catchment rainfall-runoff models. *Journal of Hydrology*, Vol.158, p.381-404.
- Ibbitt, R.P., 1972. Effect of random data errors on the parameter values for a conceptual model. *Water Resources Research*, Vol.8, No.1, p.70-78.
- Imrie, C.E., Durucan, S., and Korre, A., 2000. River flow prediction using artificial neural networks: generalisation beyond the calibration range. *Journal of Hydrology*, Vol.233, p.138-153.
- Islam, S., and Kothari, R., 2000. Artificial neural networks in remote sensing of hydrological processes. *J. Hydrologic Engng.*, ASCE, Vol. 5, No.2, P.138-144.
- Jakeman, A.J., and Hornberger, G.M., 1993. How much complexity is warranted in a rainfall-runoff model? *Water Resources Research*, Vol. 29, No. 8, p.2637-2649.

- Jensen, K.J., and Mantoglou, A., 1992. Future of distributed modelling. In: *Terrain Analysis and Distributed Modelling in Hydrology*, Edited by K.J. Beven and I.D. Moore. John Wiley & Sons.Ltd., Chichester, England, p.203-212.
- Johnston, P.R., and Pilgrim, D., 1976. Parameter optimisation for watershed models. *Water Resources Research*, Vol.12, No.3, p.477-486.
- Kabat, P., Hutjes, R.W.A., and Feddes, R.A., 1997. The scaling characteristics of soil parameters: from plot scale heterogeneity to subgrid parameterization, *Journal of Hydrology*, Vol.190, p.363-396.
- Karunanithi, N., Grenney, W.J., Whitley, D., and Bovee, K., 19994. Neural networks for river flow prediction. *J. Comput. Civil Engng.*, Vol. 8, No. 2, p. 201-220
- Kirkby, M.J., 1978. *Hillslope Hydrology*. pp.389, Wiley-Interscience, New York.
- Kirkby, M.J., 1988. Hillslope runoff processes and models. *Journal of Hydrology*, Vol.100, p.315-339.
- Kirkby, M.J., and Chorley, R.J., 1967. Throughflow, overland flow and erosion. *Bull. Intern. Assoc. Sci. Hydrology*, Vol.12, p.5-21.
- Klemeš, V., 1983. Conceptualization and scale in hydrology. *Journal of Hydrology*, Vol.65, p.1-23.
- Klemeš, V., 1986a. Operational testing of hydrological simulation models. *Hydrol.Sci.J.* Vol.31, p.13-24
- Klemeš, V., 1986b. Dilettantism in hydrology: Transition or Destiny? *Water Resources Research* Vol.22, No.9, p.177S-188S
- Knisel, W.G., 1982. CREAMS: A field scale model for chemicals runoff and erosion from agricultural management systems., USDA-Science and Education Administration, Conservation report No.26, p.643.
- Kozak, M., 1968. Determination of the runoff hydrograph on a deterministic basis using a digital computer. *IHAS Publ.80*, p138-151.
- Kruizinga, S. and Yperlaan, G.J., 1978. Spatial interpolation of daily rainfall. *Journal of Hydrology*, Vol.36, p.65-73
- Kuczera, G., 1982. On the relationship of the reliability of parameter estimates and hydrologic time series data used in calibration, *Water Resources Research* Vol.18, No.1, p.146-154.
- Kuczera, G., 1983a. Improved parameter inference in catchment models. 1. Evaluating parameter uncertainty, *Water Resources Research* Vol.19, No.5, p.1151-1162
- Kuczera, G., 1983b. Improved parameter inference in catchment models. 2. combining different kinds of hydrologic data and testing their compatibility, *Water Resources Research* Vol.19, No.5, p.1163-1172.
- Kuczera, G., 1988. On validity of first-order prediction limits for conceptual hydrological models. *Journal of Hydrology*, Vol.103, p.2292-247.
- Kuczera, G., and Mroczowski, M. 1998. Assessment of hydrologic parameter uncertainty and the worth of multi response data. *Water Resources Research* Vol.34, No.6, p.1481-1489
- Lamb, T., Beven, K., and Myrabo, S., 1998. Use of spatially distributed water table observations to constrain uncertainty in a rainfall-runoff model. *Adv. in Water Resources*, Vol.22, No.4, p.305-317.

- Lane, L.J., Schertz, D.L., Alberts, E.E., Laflen, J.M. and Lopez, V.L., 1988. The U.S. national project to develop improved erosion prediction technology to replace the USLE, IAHS Publ.174, p.475-481.
- Lee, M.T., and Delleur, J.W., 1976. A variable source area model of the rainfall runoff process based on the watershed stream network. *Water Resources Research*, Vol.12, p.1029-1036.
- Li, R.M., Simons, D.B. and Stevens, M.A., 1975. Non-linear kinematic wave approximation for water routing. *Water Resources Research*, Vol.11, p.245-252.
- Lidén, R., and Harlin, J., 2000. Analysis of conceptual rainfall-runoff modelling performance in different climates, *Journal of Hydrology*, Vol.238, p.231-247.
- Lindström, G., Johansson, B., Persson, M., Gardelin, M. and Bergström, S., 1997. Development and test of the distributed HBV-96 hydrological model. *Journal of Hydrology*, Vol.201, p.272-288.
- Lippmann, R.P., 1987. An introduction to computing with neural nets. *IEEE ASSP Mag.*, p.4-22.
- Loague, K., 1990. R-5 Revisited. Re-evaluation of a Quasi-Physically Based Rainfall-Runoff Model With Supplementary Information. *Water Resources Research*, Vol.26, No.5, p.973-987.
- Loague, K.M. and Freeze, R.A., 1985. A Comparison of rainfall-runoff modelling techniques on small upland catchments. *Water Resources Research*, Vol.21, p.229-248.
- Loague, K., and Gander, G.A., 1990. R-5 Revisited. 1, Spatial variability on a small range land catchment. *Water Resources Research*, Vol.26, No.5, p.957-971.
- Loague, K., 1992a. Soil-water content at R-5: 2. Impact of antecedent conditions on rainfall-runoff simulations. *Journal of Hydrology*, Vol.139, p.253-261.
- Loague, K., 1992b. Impact of overland flow plane characterisation on event simulations with a quasi-physically based model. *Water Resources Research*, Vol.28, p.1541-2545.
- Loague, K., 1992c. Using soil texture to estimate saturated hydraulic conductivity and the impact on rainfall-runoff simulations, *Water Resources Bulletin*, Vol.28, p.687-693.
- Loague, K., and VanderKwaak, J.E., 2002. Simulating hydrological response for the R-5 catchment: Comparison of two models and the impact of the roads. *Hydrological Processes*, Vol.16, p.1015-1032.
- Madsen, H., 2000. Automatic calibration of a conceptual rainfall-runoff model using multiple objectives. *Journal of Hydrology*, Vol.235, p.276-288.
- Maier, H.R., and Dandy, G.C., 1996. The use of artificial neural networks for the prediction of water quality parameters. *Water Resources Research*, Vol. 32, p.1013-1022
- Masters, T., 1993. *Practical Neural networks Recipes in C++*, Academic press, Inc., USA.
- Mattiah, R.S., Srinivasan, R., and Allen, P.M., 1997. Prediction of two year peak stream flow discharges using neural networks. *J. Am. Water. Res. Assoc.* Vol., 33, p. 625-630.
- McLaughlin, D., 1995. Recent developments in hydrologic data assimilation, in U.S. *National Report to International Union of Geodesy and Geophysics 1991-1994*.

- Contributions in Hydrology, Pielke, Sr. and Vogel, R.M., (eds), p.977-984, American Geophysical Union, Washington, DC.
- Mein, R.G. and Brown, B.M., 1978. Sensitivity of parameters in watershed models. *Water Resources Research*, Vol.14, No.2, p.299-303.
 - Meyerink, A.M.J., Valenzuela, C.R. and Stewart, A., 1988. The Integrated Land and Watershed Management Information System. ITC publication No.7, ITC Enschede.
 - Michaud, J. and Sorooshian, S., 1994. Comparison of simple versus complex distributed runoff models on a mid-sized semi-arid watershed, *Water Resources Research*, Vol.30, No.3. p.593-605.
 - Ministry of Public Works, 1994. Onderzoek Watersnood Maas, Hoofdrapport 'De Maas Meester'.
 - Minns, A.W., and Hall, M.J., 1996. Artificial neural networks as rainfall-runoff models. *J. Hydrol. Sci. Vol.*, 41, p.339-417.
 - Monteith, J.L., 1965. Evaporation and environment. In *State and movement of water in living organisms*, Proc. 15th Symposium Society for experimental Biology, Swansea, U.K. p.205-234, Cambridge University Press, London.
 - Moore, I.D. and Burch, G.J., 1986. Sediment transport capacity of sheet and rill flow: Application of unit stream power theory. *Water Resources Research*, Vol.22, No.8, p.1350-1360.
 - Moore, I.D., Burch, G.J., and Mackenzie, D.H. 1988. Topographic effects on the distribution of surface soil water and the location of ephemeral gullies. *Trans. ASAE*, Vol.31, No.4, p.1098-1107.
 - Moore, I.D. and G.R. Foster 1990. Hydraulics and overland flow, in *Process studies in hillslope hydrology*, edited by A.G. Anderson and T.P. Burt. John Wiley, New York, p.215-254.
 - Moore, I.D. and Grayson, R.B., 1989. Hydrologic and digital terrain modelling using vector elevation data (abstract) *Eos Trans. AGU*, Vol.70, p.1091.
 - Moore, I.D., Grayson, R.B. and Ladson A.D., 1991. Digital terrain modelling: A review of hydrological, geomorphological and biological applications, *Hydrological Processes*, Vol.5, p.3-30.
 - Moore, I.D. and Grayson, R.B., 1991. Terrain based Catchment Partitioning and Runoff Prediction Using Vector Elevation Data. *Water Resources Research*, Vol.27, No.6, p.1177-1191.
 - Moore, I.D., O'Loughlin, E.M. and Burch, G.J., 1988. A contour based topographic model for hydrological and ecological applications. *Earth Surf. Processes Landforms*, No.13, p.305-320.
 - Morel-Seytoux, H.J., 1976. Derivation of equations for rainfall infiltration. *Journal of Hydrology*, Vol.31, p.203-219.
 - Morel-Seytoux, H.J., 1988a. Recipe for simple but physically based modelling of the infiltration and local runoff processes. In *Proceedings of the Eighth Annual AGU Front Range Branch Hydrology Days*, edited by H.J. Morel-Seytoux and D.G. DeCoursey, Fort Collins, Colorado, p. 226-247.
 - Morel-Seytoux, H.J., 1988b. Equivalence between infiltration parameters in Horton and Morel-Seytoux formulae. In *Proceedings of the Eighth Annual AGU Front Range*

- Branch Hydrology Days*, edited by H.J. Morel-Seytoux and D.G. DeCoursey, Fort Collins, Colorado, p. 248-259.
- Mosley, M.P., 1979. Stream flow generation in a forested watershed, New Zealand. *Water Resources Research*, Vol.15, p.795-806.
 - Moussa, R., and Bocquillon, C., 1996. Criteria for the choice of flood-routing methods in natural channels, *Journal of hydrology*, Vol.186, p.1-30.
 - Nachabe. M.H., and Morel-Seytoux, H.J., 1995. Scaling of groundwater flow equation. *Journal of Hydrology*, Vol.164. P.345-361.
 - Nandakumar, N., and Mein, R.G., 1997. Uncertainty in rainfall-runoff model simulations and the implications for predicting the hydrologic effects of land use change. *Journal of hydrology*, Vol.192, p.211-232.
 - Nash, J.E., and Sutcliffe, J.V., 1970. River flow forecasting through conceptual models, Part 1. A discussion of principles, *Journal of Hydrology*, Vol. 10, p.282-290.
 - Nelder, J.A., and Mead, R., 1965. A simplex method for function minimisation. *Computer Journal*, Vol.7, p.308-313.
 - O'Connell, P.E., 1991. A Historical perspective. In *Recent Advances in the Modelling of Hydrologic Systems*. edited by Bowles, D.S. and O'Connell P.E., Kluwer Academic Publishers, Netherlands, p.3-30.
 - O'Connell, P.E., and Todini, E., 1996. Modelling of rainfall, flow and mass transport in hydrological systems: an overview. *Journal of Hydrology*, Vol.175, p.3-16.
 - O'Loughlin, E.M., 1986. Prediction of surface saturation in natural catchment by topographic analysis. *Water Resources Research*, Vol.22, No.5, p.794-804.
 - Onstad, C.A., 1973. Watershed flood routing using distributed parameters, in *Floods and droughts*, ed. E.S. Schulz, V.A. Koelzer, and K. Mahmood, Water Resources publication, Fort Collins, Colorado, p.418-428.
 - Onstad, C.A., and Brakensick, D.L., 1968. Watershed simulation by the stream path analogy. *Water Resources Research*, Vol.4, p.965-971.
 - Penman, H.L., 1961. Weather, plant and soil factors in hydrology. *Weather* Vol.16, p.207-219.
 - Pilgrim, D.H., Huff, D.D., and Steele T.D., 1979. Use of specific conductance and contact time relations for separating flow components in storm runoff, *Water Resources Research*, Vol.15, No.2, p.329-339.
 - Pilot. A., 2002. Modelling of the initial soil moisture distribution for the rainfall-runoff model Flowsim; Application of the topmodel-concept. MSC thesis Delft University of Technology, pp.126.
 - Pickup, G., 1977. Testing the efficiencies of algorithms and strategies for automatic calibration of rainfall-runoff models. *Hydrogeol. Sci. Bull.*, Vol.22, No.2, p.257-274.
 - Philip, J.R., 1957. The theory of infiltration, I. The infiltration equation and its solution. *Soil.Sci.*, No.83, p.345-357.
 - Price, W. L., 1987. Global optimisation algorithms for a CAD workstation. *J. Optim. Theory Appli.* Vol.55, No.1, p.133-146.
 - Quinn, P., Beven, K., Chevallier, P. and Planchon, O., 1992. The prediction of hillslope flow paths for distributed hydrological modelling using digital terrain

- models. In: *Terrain Analysis and Distributed Modelling in Hydrology*, Edited by K.J. Beven and I.D. Moore. John Wiley & Sons. Ltd., Chichester, England, p.63-83.
- Quinn, P.F. and Beven, K.J., 1993. Spatial and temporal predictions of soil moisture dynamics, runoff, variable source areas and evapotranspiration for plynlimon, mid-Wales. *Hydrological processes*, Vol.7, p.425-448.
 - Ragan, R.M., 1968. An experimental investigation of partial area contributions. *Int.Assoc. of Sci.Hydrol.* No.76, p.241-251.
 - Rawitz, E., Engman, E.T. and Cline, G.D., 1970. Use of mass balance method for examining the role of soils in controlling watershed performance. *Water Resources Research*, Vol.6, No.4, p.1115-1123.
 - Refsgaard, J.C., 1996. Terminology, modelling protocol and classification of hydrological model codes. In: Abbott, M.B., Refsgaard, J.C.(Eds.), *Distributed Hydrological Modelling*. Kluwer Academic, p.17-39.
 - Refsgaard, J.C., 1997. Parameterisation and validation of distributed hydrological models. *Journal of Hydrology*, Vol.198, p.69-97.
 - Refsgaard, J.C. and Strom, B., 1996. Construction, calibration and validation of hydrological models. In: Abbott, M.B., Refsgaard, J.C.(Eds.), *Distributed Hydrological Modelling*. Kluwer Academic, p.41-54.
 - Refsgaard, J.C., Storm, B., and Abbott, M.B., 1996. Comment on "A discussion of distributed hydrological modelling" by K. Beven. In: Abbott, M.B., Refsgaard, J.C.(Eds.), *Distributed Hydrological Modelling*. Kluwer Academic, p.279-287.
 - Richards, L.A., 1931. Capillary conduction of liquids through porous mediums. *Physics* No.1, p.318-333.
 - Rientjes, T., 1999a. Physically Based Rainfall-Runoff modelling applying a Geographical Information System. In: Communications of the Water Management and Sanitary Engineering Division Report no 83. Delft University of Technology, p.74.
 - Rientjes, T. 1999b. Description of the Physically Based Rainfall-Runoff model Flowsim. In: Communications of the Water Management and Sanitary Engineering Division Report no 84. Delft University of Technology, p.16.
 - Rientjes, T., C. van den Akker and P. van der Veer, 1999c. Improved catchment parameterisation for runoff modelling. In: Calibration and reliability in groundwater modelling. pre-Proceedings of the Modelcare'99 Conference, Zürich, Switzerland, p.635-640.
 - Rientjes, T. and Hassanisadeh, M., 1999d. Model Performance and Automated Calibration; the case of Distributed Physically Based Runoff Models, Poster presentation, AGU meeting, San Francisco p. F.415.
 - Rientjes, T. and Reggiani, P., 2001. Physically-based rainfall-runoff modelling: setbacks and solutions; Proceedings of the Int. Workshop on Runoff Generation and Implications for River Basin Modelling, Freiburg., p. 257-265. In *Freiburger Schriften zur Hydrologie (Band 13)*, Institut für Hydrologie, Universität Freiburg i.Br., ISSN 0945-1609.

- Rientjes, T., and Zaadnoordijk, W.J., 2000. Hoogwatervoorspelling: Fysich gebaseerde regen-afvoermodellering Dilemma of Déjà vu? *Stromingen*, Jaargang 6, no.1, p.33- 44.
- Rientjes, T., C. van den Akker en P. van der Veer,(1998), Een hoog(water)standje in 'Wartertovenaars, Delftse ideeën voor nog 200 jaar Rijkswaterstaat' bèta Imaginations publishers, p.190-201.
- Rogers, C.C.M., Beven, K.J., Morris, E.M., and Anderson, M.G., 1985. Sensitivity analysis, calibration and predictive uncertainty of the institute of hydrology distributed model. *Journal of Hydrology*, Vol.81, p.179-191.
- Rosenbrock, H.H., 1960. An automatic method for finding the greatest or least value of a function. *Computer Journal*, Vol.3, p.175-184.
- Rubin, J., and Steinhardt, R., 1963. Soil water relations during rain infiltration I:Theory. *Soil Sci.Soc.Am.J.*27, p.246-251.
- Rutter, A.J., Morton, A.J. and Robins, P.C., 1975. A predictive model of rainfall interception in forests II. Generalisation of the model and comparison with observations in some coniferous and hardwood stands. *J.Appl.Ecol.*, Vol.12, p.367-380.
- Rutter, A.J., Kershaw, K.A., Robins, P.C. and Morton, A.J., 1971. A predictive model of rainfall interception in forests, 1. Derivation of the model from observations in a plantation of Corsican pine. *Agric.Meteorol.*, Vol.9, p.367-384.
- Saint-Venant, Barré de., 1871. "Theory of Unsteady Water Flow, with Application to River Floods and to propagation of Tides in River Channels," *Comptus Rendus*, Vol.73, Acad. Sci., Paris, France, p.148-154, 237-240.
- Sajikumar, N., and Thandaveswara, B.S., 1999. A non-linear rainfall-runoff model using an artificial neural network, *Journal of Hydrology*, Vol.216, p.32-55.
- Savenije, H.H.G., 2001. Equifinality, a blessing in disguise? *Hydrological Processes*, Vol.15, p.2835-2838.
- Shamseldin, A.Y., 1997. Application of a neural network technique to rainfall-runoff modelling, *Journal of Hydrology*, Vol.199, p.272-294.
- Schultz, G.A., 1994. Meso-scale modelling of runoff and water balances using remote sensing and other GIS data, *Hydrological sciences*, Vol.39, No.2, p.121-142.
- Schuurmans, W., 1989. Study of Existing Hydrodynamic Flow Models; A study of the applicability of unsteady flow models in irrigation system design and management. Delft: TU Delft, Department of Civil Engineering.
- Seyfried, M.S., and Wilcox, B.P., 1995. Scale and the nature of spatial variability: field examples having implications for hydrologic modeling. *Water Resources Research*, Vol.31, No.1, p.173-184.
- Shamseldin, A.Y. 1997. Application of a neural network technique to rainfall-runoff modelling, *Journal of Hydrology*, Vol.199, p.272-294.
- Shamseldin, A.Y., and O'Connor, K.M., 1996. A nearest neighbours perturbation model for river flow forecasting, *Journal of Hydrology*, Vol.179, p.353-375.
- Sharma, M.L., G.A. Gander, and C.G. Hunt, 1980. Spatial variability of infiltration in a watershed, *Journal of Hydrology*, Vol.45, p.101-122.

- Sharma, M.L., Luxmoore, R.J., DeAngelis, R., Ward, R.C. and Yeh, G.T., 1987. Surface water flow simulated for hillslopes with spatially dependent soil hydraulic characteristics. *Water Resources Research*, Vol.28, p.1523-1530.
- Sherman, L.K., 1932. Streamflow from rainfall by unit-graph method. *Eng. News. Record. Union.*, Vol.25, p.57-65.
- Sivapalan, M., Beven, K., and Wood, E.F., 1987. On Hydrologic similarity. 2. A scaled model of storm runoff production. *Water Resources Research*, Vol.23, No.12, p.2266-2278.
- Smith, R.E., 1972. The infiltration envelope: results from a theoretical infiltrometer. *Journal of Hydrology*, Vol.17, p.1-21.
- Smith, R.E. and Hebbert, R.H.B., 1979. A Monte-Carlo analysis of the hydrological effects of spatial variability of infiltration. *Water Resources Research*, Vol.15, p.419-429.
- Smith, R.E. and Hebbert, R.H.B., 1983. Mathematical simulation of interdependent surface and subsurface hydrologic processes. *Water Resources Research*, Vol.19, p.987-1001.
- Smith, R.E., and Parlange, A., 1978. A parameter efficient hydrologic infiltration model. *Water Resources Research*, Vol.14, No.3, p.533-538.
- Smith, R.E., Goodrich, D.R, Woolhiser, D.A., and Simanton, J.R., 1994. Comment on 'Physically based hydrologic modelling 2, is the concept realistic' by Grayson, R.B., Moore, I.D. and T.A. McMahon. *Water Resources Research*, Vol.30, No.3, p.845-849.
- Sorooshian, S., 1981. Parameter estimation of rainfall-runoff models with heteroscedastic stream flow errors: The non-informative data case. *Journal of Hydrology*, Vol.52, p.127-138.
- Sorooshian, S., and Dracup, J.A., 1980. Stochastic parameter estimation procedures for hydrologic rainfall-runoff models: Correlated and heteroscedastic error cases. *Water Resources Research* Vol.16, No.2, p.430-442.
- Sorooshian, S., and Gupta, V.K., 1983. Automatic calibration of conceptual rainfall-runoff models: The question of parameter observability and uniqueness. *Water Resources Research* Vol.19, No.1, p.251-259.
- Sorooshian, S., and Gupta, V.K., 1985. The analysis of structural identifiability theory and application to conceptual rainfall-runoff models. *Water Resources Research* Vol.21, No.4, p.487-496.
- Sorooshian, S., Gupta, V.K., and Bastidas, L.A., 1998. Calibration of hydrological models using multi-objective and visualisation techniques. Final report on project proposal number EAR-9418147, Dept. of Hydr. and Water Res., University of Arizona, Tucson, AZ 85721.
- Sorooshian, S., Duan, Q., Gupta, V.K., 1993. Calibration of rainfall-runoff models: application of global optimization to the Sacramento soil moisture accounting model. *Water Resources Research* Vol.29, p.1185-1194.
- Spear, R.C., 1995. Large simulation models: calibration uniqueness and goodness of fit, paper presented at MODSIM 95: International Congress on Modelling and Simulation, Modell. and Soc. of Aust. Newcastle.

- Spear, R.C. and Hornberger, G.M., 1980. Eutrophication in Peel Inlet, II Identification for critical uncertainties via Generalised Sensitivity Analysis. *Water Resources Research*, Vol.14, p.43-49.
- Tanaka, T., Yasuhara, M., Sakai, H. and Marui, A., 1988. The hachioji experimental basin study-storm runoff processes and the mechanism of its generation, *Journal of Hydrology*, Vol.102, p.139-164.
- Takasao, T., and Shiiba, M., 1988. Incorporation of the effect of concentration of flow into the kinematic wave equations and its application to runoff system lumping. *Journal of Hydrology*, Vol.102, p.301-322.
- Tak, L.D. Vanderkwaak, J.E., and Bras, R.L. 1990. Incorporating Hillslope Effects into a Geomorphologic Instantaneous Unit Hydrograph. *Water Resources Research*, Vol.26, No.10, p.2393-2400.
- Thomas, R.G., 1973. Groundwater Models. *Irrigation and drainage*, Spec.Pap., F.A.O. No.21, U.N. Rome.
- Tisdale, T.S., Hamrick, J.M., and Yu, S.L., 1986. Kinematic wave analysis of overland flow using topography fitted coordinates. *Trans.Am. Geophys. Union*, Vol.69, No.10, p.344.
- T.N.O. Committee on hydrological research, 1987. Ruimtelijke variabiliteit van water en bodem. C.H.O. No.18.
- T.N.O. Committee on hydrological research, 1993. Schaalproblemen in de hydrologie. C.H.O. No.31.
- Tokar, A.S., and Johnsson, P.A., 1999. "Rainfall-runoff modelling using artificial neural networks". *J. Hydrologic Engrg.*, ASCE, Vol.4, No.3, p.232-239.
- Toth, E., Brath, A., and Montari, A., 2000. Comparison of short-term rainfall prediction models for real-time flood forecasting. *Journal of Hydrology*, Vol.239, p.132-147.
- Troch, P.A., Mancini, M., Paniconi, C., and Wood, E.F., 1993. Evaluation of a distributed catchment scale water balance model, *Water Resources Research*, Vol.29, p.1805-1817.
- Troch, P.A., Smith, J.A., Wood, E.F., and de Troch, F.P., 1994. Hydrologic controls of large floods in a small basin: central Appalachian case study, *Journal of Hydrology*, Vol.156, p.285-309.
- Troendle, D.A., 1985. Variable source area model. In *Hydrological forecasting*, by M.G. Anderson and T.P. Burt, (ed), p.347-403, John Wiley and Sons, Chichester.
- Tennessee Valley Authority (TVA), 1968. The Upper Bear Creek Experimental Project 1965-67. Knoxville, Tennessee, 49p.
- United States Department of Agriculture, 1980. 'CREAMS': A Field Scale Model for Chemical Runoff and Erosion for Agricultural Management Systems, USDA Conservation Research Report No.26, p.643.
- Van der Kwaak, J.E., and Loague, K., 2001. Hydrologic-response simulations for the R-5 catchment with a comprehensive physics-based model, *Water Resources Research*, Vol.37, p.999-1013.
- Vos de., N., 2003. Rainfall-Runoff modelling using artificial neural networks. Msc-thesis report at the Delft University of Technology, p. 137.

- Watermark Computing, 1994. Model Independent Parameter Estimation (PEST), Manuals by J. Doherty, L. Brebber and P. Whyte.
- Wigmosta, M.S. and Burgers, S.J., 1997. An adaptive modeling and monitoring approach to describe the hydrologic behavior of small catchments. *Journal of Hydrology*, Vol.202, p.48-77.
- Wilson, C.B., Valdes, L.B., and Rodrigues-Iturbe, I., 1979. On the influence of the spatial distribution of rainfall on storm runoff, *Water Resources Research*, Vol.15, No.2, p.321-328.
- WMO, World Meteorological Organisation, 1990. Hydrological models for water resources system design and operation. Operational hydrology report No.34. Geneva, Switzerland.
- Wolock, D.M., and Price, C.V., 1994. Effects of digital elevation model map scale and data resolution on a topography-based watershed model. *Water Resources Research*, Vol.30, No11, p.3041-3052.
- Wood, E.F., Sivapalan, M., Beven, K.J. and Band, L., 1988. Effects of spatial variability and scale with implication to hydrologic modelling. *Journal of Hydrology*, Vol.102, p.29-47.
- Woolhiser, D.A., Smith, R.E. and Goodrich, D.C., 1990. KINEROS, A Kinematic Runoff and Erosion Model: Documentation and User Manual. U.S. Department of Agriculture, Agriculture Research Service, ARS-77, 130p.
- Yapo, P.O., 1996. A multi objective global optimization algorithm with applications to calibration of hydrological models. Ph.D thesis, Dep. of Hydrol. and Water Resour., Univ., of Ariz., Tucson.
- Yapo, P.O., Gupta, H.V. and Sorooshian, S., 1996. Automatic calibration of conceptual rainfall-runoff models: sensitivity to calibration data. *Journal of Hydrology*, Vol. 181, p.23-48.
- Yapo, P.O., Gupta, H.V. and Sorooshian, S., 1998. Multi-objective global optimization for hydrologic models. *Journal of Hydrology*, Vol. 204, p.83-97.
- Young, R.A., Onstad, C.A., Bosch, D.D. and Anderson, W.P., 1987. AGNPS, Agricultural Non-Point-Source Pollution Model. A Watershed Analysis Tool, U.S. Department of Agriculture, Conservation Research Report 35, 80 p.
- Young, R.A., Onstad, C.A., Bosch, D.D. and Anderson, W.P., 1989. AGNPS, A non-point source pollution model for evaluating agricultural watersheds, *J. Soil and Water Conserv.* No.44, p.168-173.
- Zealand, C.M., Burn, D.H., and Simonovic, P., 1999. Short term streamflow forecasting using artificial neural networks, *Journal of Hydrology*, Vol. 214, p.32-48.
- Zhang, W. and Montgomery, D.R., 1994. Digital elevation model grid size, landscape representation, and hydrologic simulations, *Water Resources Research*, Vol. 30, No. 4, p.1019-1028.

Curriculum Vitae

Tom Rientjes is geboren op 2 augustus 1960 te Hengelo(O). In 1987 studeerde hij af aan de Hogere Bosbouw en Cultuurtechnische School (HBCS) te Velp in de studierichtingen Nederlandse en Tropische cultuurtechniek. Tijdens zijn opleiding is hij gedurende acht maanden werkzaam geweest bij 'the Institute of Irrigation and Salinity Research' in de staat Victoria, Australië.

Gedurende en kort na afronding van zijn studie heeft hij enkele korte dienstverbanden vervuld in de aannemerij. In 1988 is hij in dienst getreden van de Technische Universiteit Delft bij de Sectie Hydrologie. Binnen deze werkkring heeft hij zich gespecialiseerd in hydrologische modellering en hydro-informatica. Sinds 1994 doceert hij het vak Hydrologische modellen en begeleidt hij afstudeerders en promovendi.

Naast zijn eigen promotieonderzoek heeft in nauwe samenwerking met collega's een aantal meerjarige onderzoeksprojecten opgezet en uitgevoerd op het vakgebied van de neerslag-afvoermodellering. Ook was hij co-auteur van het oprichtingsdocument voor de onderzoeksschool 'Hydrologie voor Water- en Milieubeheer' en secretaris van de werkgemeenschap 'Integraal Waterbeheer'. Verder heeft hij wetenschappelijke publicaties op zijn naam staan en heeft bijdragen geleverd aan boekpublicaties.

Sinds 1 maart 2004 is hij werkzaam bij 'the International Institute for Geo-Information Science and Earth Observation (ITC)' te Enschede als universitair docent.





 **TU Delft**

Delft University of Technology



Delft University Press